

**Air quality in the Cologne Conurbation - high-resolution
spatiotemporal biomonitoring**

Inaugural-Dissertation

zur

Erlangung des Doktorgrades

der Mathematisch-Naturwissenschaftlichen Fakultät

der Universität zu Köln

vorgelegt von

Eva Lehdorff

aus Kaiserslautern

2008

Berichterstatter: Prof. Dr. Lorenz Schwark

Prof. Dr. Yaping Shao

Tag der letzten mündlichen Prüfung: 20.05.2008

Abstract

Atmospheric quality assessment for the Greater Cologne Conurbation, NW-Germany, has been conducted by pine needle (*Pinus nigra*) biomonitoring at high spatiotemporal resolution of 71 samples per 3600 km². Prior to analysis and interpretation of spatial variability trends, the systematic and predictable accumulation of a set of air pollutants on pine needles was verified. Air pollutants were investigated using optical determination, major and trace element concentration, enviromagnetic properties and polycyclic aromatic hydrocarbon (PAH) distribution in pine needles. The multiproxy approach allowed for substantially improved source reconciliation. On the regional scale it revealed lignite combustion in power plants to be the dominant emitter of PAH and blow-out from open pit lignite mines to dominate the fine particulate emissions. On local scale, traffic emissions in the inner city of Cologne were identified as major pollution source. Traffic emissions though difficult to separate from industrial contributions could be differentiated by trace element indicators, in particular antimony and by specific PAH, e.g. cyclopenta[cd]pyrene. Atmospheric pollution biomonitoring is of paramount importance to local population due to the increasing number of reports on detrimental health effects. In order to guide industrial and political decision makers when establishing environmental control measures, spatially highly resolved data sets of atmospheric quality are mandatory for science-based decision making. Active air quality measurements are too budget and time-intensive to build the base for such decisions. The time-integrated image of air quality derived from biomonitoring at current provides the best suited approach for regional air quality management.

Zusammenfassung

Eine Beurteilung der Luftqualität im Ballungsraum Köln, NW-Deutschland wurde mittels Anwendung eines Biomonitoringansatzes unter Verwendung von Nadeln der Schwarzkiefer (*Pinus nigra*) unter hoher raumzeitlicher Auflösung von 71 Standorten über 3600 km² durchgeführt. Vor der Analyse und Interpretation räumlicher Variationsgradienten wurde die systematische Akkumulation einer Suite von Luftschadstoffen auf Kiefernadeln verifiziert. Luftschadstoffe auf Kiefernadeln wurden analysiert unter der Anwendung optischer Methoden, Haupt- und Spurenelementverteilungen, umweltmagnetischer Eigenschaften und der jeweiligen PAH-Signaturen. Der gewählte Multiproxy-Ansatz ermöglichte eine substantiell verbesserte Quellenzuweisung der Luftschadstoffe. Auf regionaler Ebene wurde die PAH-Emission aus der Verbrennung von Braunkohle zur Stromerzeugung als dominanter Prozess identifiziert, während die Belastung durch Feinstäube in der Region von Auswehungen aus Braunkohletagebauen geprägt war. Auf lokaler Ebene wurden in der Innenstadt Kölns Verkehrsemissionen als Hauptquelle der Luftverunreinigung identifiziert. Verkehrsemissionen lassen sich nur schwer von denen der Industrie trennen, konnten aber von diesen auf der Basis von Spurenelementindikatoren, präferentiell der Antimonkonzentration, oder anhand diagnostischer PAH wie Cyclopenta[c,d]pyren unterschieden werden. Das Biomonitoring atmosphärischer Schadstoffe ist infolge der zunehmenden Berichte über Gesundheitsschädigungen für die lokale Bevölkerung von entscheidender Bedeutung. Um industriellen und politischen Entscheidungsträgern eine Grundlage für die Etablierung von Massnahmen zur Luftqualitätsverbesserung zur Verfügung zu stellen, sind raumzeitlich hochauflösende Datensätze für eine wissenschaftliche Entscheidungsfindung unverzichtbar. Aktive Luftqualitätsanalysen sind zu zeit- und kostenintensiv, um eine Basis solcher Entscheidungen zu bilden. Die zeitintegrierende und damit hochrepräsentative Luftqualitätsanalyse über Biomonitoring bildet zur Zeit den bestgeeignetsten Ansatz für regionales Luftmanagement.

Contents

1	Introduction	3
1.1	Problem definition	3
1.2	Aims and scope	4
1.3	State of the art	5
1.4	Study area	6
1.4.1	Topography	6
1.4.2	Climate	6
1.4.3	Soil	7
1.4.4	Land use and emission scenarios	7
2	Pollutant accumulation on <i>Pinus nigra</i> needles	9
2.1	Accumulation histories of magnetic particles	9
2.1.1	Sampling methods	10
2.1.2	Analytical Methods	11
2.1.3	Results	13
2.1.4	Discussion	20
2.1.5	Conclusions	25
2.2	Accumulation histories of major and trace elements	26
2.2.1	Sampling methods	27
2.2.2	Analytical Methods	27
2.2.3	Results	28
2.2.4	Discussion	32
2.2.5	Conclusions	38
2.3	Accumulation history of airborne phenanthrene derivatives	39
2.3.1	Sampling	42
2.3.2	Analytical Methods	42
2.3.3	Results	43
2.3.4	Discussion	47
2.3.5	Conclusions	53
3	Cologne City - local-scale biomonitoring	54
3.1	Cologne City air quality - optical and magnetic properties	54
3.1.1	Sampling	55
3.1.2	Analytical methods	57
3.1.3	Results	58
3.1.4	Discussion	63
3.1.5	Conclusions	66
3.2	Cologne City air quality - major and trace elements	67
3.2.1	Sampling	69
3.2.2	Analytical methods	69
3.2.3	Results and discussion	70
3.2.4	Summary and Conclusions	78
3.3	Cologne City air quality - polycyclic aromatic hydrocarbons (PAH) . .	78
3.3.1	Sampling	79

3.3.2	Methods	80
3.3.3	Results and discussion	81
3.3.4	Summary and Conclusions	91
4	Cologne Conurbation - regional-scale biomonitoring	94
4.1	Cologne Conurbation air quality - enviromagnetic proxies	94
4.1.1	Sampling	94
4.1.2	Analytical methods	95
4.1.3	Results	95
4.1.4	Discussion	97
4.1.5	Conclusion	100
4.2	Cologne Conurbation air quality - major and trace elements	101
4.2.1	Sampling methods	101
4.2.2	Analytical methods	101
4.2.3	Results	102
4.2.4	Discussion	105
4.2.5	Conclusions	116
4.3	Cologne Conurbation air quality - parent PAH	117
4.3.1	Sampling	117
4.3.2	Analytical methods	118
4.3.3	Results	119
4.3.4	Discussion	125
4.3.5	Conclusions	137
4.4	Cologne Conurbation air quality - parent and alkylated three-ring PAH	138
4.4.1	Sampling	139
4.4.2	Analytical methods	139
4.4.3	Results and Discussion	140
4.4.4	Conclusions	146
4.5	Cologne Conurbation air quality - a synthesis	146
4.5.1	Sampling and Analysis	147
4.5.2	Results	147
4.5.3	Discussion	152
4.5.4	Conclusion	159
5	Synthesis and outlook	160
	Appendix	212

List of Figures

1	Topography and soils of the Cologne Conurbation.	6
2	Land use and emission characteristics of the Cologne Conurbation.	7
3	Land use and locations of temporally-resolved sample set in the Cologne Conurbation	10
4	Biplots of physiological versus enviromagnetic properties.	14
5	Electron microprobe scan of needle surface.	15
6	Mineral and grain size diagnostic enviromagnetic parameters	16
7	Magnetic concentration parameters on pine needles in the Cologne Conurbation	18
8	Temporal accumulation trends of magnetic parameters.	19
9	Variations of enviromagnetic grain size and oxidation parameters versus time.	21
10	Schematic diagram displaying hypothetical end-member grain size distribution curves	24
11	Element concentrations of <i>Pinus nigra</i> needles versus exposure time.	29
12	Element enrichment factors for summer and winter samples.	32
13	Element enrichment factors of pine needles versus exposure time.	33
14	Identification of dimethylphenanthrenes	43
15	PAH-3 concentrations versus needle exposure time.	48
16	Phenanthrenes ratios versus needle exposure time.	51
17	Land use and sampling sites in Cologne City.	56
18	SEM and microprobe analysis of pine needle surfaces.	57
19	Sample treatment: cleaning with water and organic solvents.	60
20	Correlation of iron and magnetite concentration of pine needles.	60
21	High temperature susceptibility curve.	61
22	Magnetic properties of pine needles in Cologne City.	62
23	Grain-size effects on susceptibility and ARM analysis.	63
24	Seasonal changes in enviromagnetic properties of needles.	64
25	Enviromagnetic isopleths maps of Cologne City, I	65
26	Enviromagnetic isopleths maps of Cologne City, II	66
27	Trace element concentration ranges of pine needles in Cologne City.	70
28	Trace element and sulfur concentrations of pine needles in Cologne City.	72
29	Seasonal variations of elements on a pine in Cologne City.	74
30	Annual variations of elements in pine needles in the Dübener Heath, NE-Germany.	75
31	Biplots of traffic pollution proxy iron against lead, cadmium and zinc.	76
32	Isopleths maps of Cd and Pb in Cologne City	77
33	Generalized model of PAH transportation and deposition.	80
34	SEM scans of <i>Pinus nigra</i> needle surfaces.	82
35	Seasonal variation in wax and PAH content of pine needles.	83
36	Relation between wax content and total PAH load of pine needles.	86
37	PAH distribution profiles of pine and spruce needles.	88
38	Bivariate plots of selected PAH ratios.	89
39	Correlation of a magnetic concentration parameter to pyrene.	90

40	Isopleths maps of PAH concentrations and isomer ratios in Cologne City.	92
41	Enviromagnetic properties on pine needles in the Cologne Conurbation.	97
42	Isopleths maps of enviromagnetic proxies in the Cologne Conurbation.	99
43	Element enrichment (EF) on pine needles in the Cologne Conurbation.	105
44	Elements of geogenic origin in the Cologne Conurbation.	108
45	Elements attributed to local geogenic sources and mineralic input.	109
46	Elements attributed to traffic emissions.	112
47	Elements attributed to industrial emissions.	113
48	Elements attributed to municipal waste incineration.	115
49	Accumulation trends of PAH on pine needles in the Cologne Conurbation.	126
50	Isopleths maps of PAH on pine needles in the Cologne Conurbation.	128
51	Spatial distribution of Ip, BeP, BbjFla, Py, BaA, and CpedPy in the Cologne Conurbation.	130
52	Trends of PAH ratios versus time of needle exposure.	134
53	Bivariate plots of source indicative PAH.	136
54	Isopleths maps of PAH ratios.	137
55	Locations, emission characteristics and spatial analyses of PAH-3 in the Cologne Conurbation.	142
56	Biplots of selected phenanthrenes concentrations.	143
57	Bivariate plots of PAH, elements and enviromagnetic proxies.	151
58	Pollutant distribution characteristic for urban emissions.	154
59	Pollutant distribution characteristic for lignite combustion and geogenic dust.	156
60	Pollutant distribution characteristic for waste incineration and industrial emissions.	158
61	Molecular structure of parent and alkylated PAH	191
62	Land use and emission characteristics of the Cologne Conurbation (transparency).	218

List of Tables

1	Emission scenarios in the Cologne Conurbation	11
2	Statistical analyses of enviromagnetic parameters	12
3	Spearman's rank correlation of enviromagnetic and plant physiological parameters.	13
4	Weighted means of element concentrations on pine needles.	30
5	Kruskal-Wallis- <i>H</i> test for major and trace elements.	30
6	Element enrichment factors.	31
7	Factor analyses of major and trace element EFs.	35
8	Physico-chemical properties of PAH-3.	41
9	Statistics of PAH accumulation on pines.	45
10	Linear regression parameters for PAH-3 versus time.	45
11	Compilation of trace element data for pine needles.	71
12	Compilation of PAH biomonitoring data for pine needles.	85

13	Source diagnostic potential of enviromagnetic biomonitoring in the Cologne Conurbation	100
14	Element loads on pine needles in the Cologne Conurbation.	102
15	Factor analyses of element loads on pine needles in the Cologne Conurbation.	104
16	Sources for major and trace elements in the Cologne Conurbation.	116
17	Abbreviations and classification of PAH.	118
18	Statistics of PAH accumulation on pine needles.	120
19	PAH median concentrations on pine needles in the Cologne Conurbation.	121
20	Factor analysis of PAH concentrations on pine needles in the Cologne Conurbation.	131
21	Source diagnostic potential of PAH biomonitoring in the Cologne Conurbation.	138
22	Factor analysis of PAH-3 concentrations on pine needles.	140
23	Source diagnostic compounds and proxies established on pine needles in the Cologne Conurbation.	148
24	Spearman 's rank correlation of organic, inorganic and enviromagnetic air quality proxies.	150
25	Abbreviations	190
26	Enviromagnetic and physiological parameters, temporal study, I	192
27	Enviromagnetic and physiological parameters, temporal study, II	193
28	Enviromagnetic and physiological parameters, temporal study, III	194
29	Averaged magnetic properties for sampling sites	195
30	Mean, medians and standard deviation of magnetic properties	196
31	Enviromagnetic and physiological parameters for each needle cohort	197
32	Major and trace element concentrations temporal study	198
33	Enrichment factors (EF), temporal study	199
34	Concentration of 3-ring PAH on pine needles, temporal study	200
35	Enviromagnetic parameters on pine needles in the Cologne Conurbation.	201
36	Major and trace element concentrations and enrichment factors (EF) on pine needles in the Cologne Conurbation (data sheet 1-10).	202
37	Major and trace elements in the Cologne Conurbation, II	203
38	Major and trace elements in the Cologne Conurbation, III	204
39	Major and trace elements in the Cologne Conurbation, IV	205
40	Major and trace elements in the Cologne Conurbation, V	206
41	Major and trace elements in the Cologne Conurbation, VI	207
42	Major and trace elements in the Cologne Conurbation, VII	208
43	Major and trace elements in the Cologne Conurbation, VIII	209
44	Major and trace elements in the Cologne Conurbation, IX	210
45	Major and trace elements in the Cologne Conurbation, X	211
46	Parent PAH on pine needles of different age needle age, sheet I.	212
47	Parent PAH on pine needles of different age needle age, sheet II.	213
48	Parent PAH in <i>Pinus nigra</i> needles of the Cologne Conurbation, I.	214
49	Parent PAH in <i>Pinus nigra</i> needles of the Cologne Conurbation, II.	215
50	Three-ring PAH in <i>Pinus nigra</i> needles of the Cologne Conurbation, I.	216
51	Three-ring PAH in <i>Pinus nigra</i> needles of the Cologne Conurbation, II.	217

1 Introduction

1.1 Problem definition

Air is regarded an essential commodity, mandatory for all human beings and its composition and changes thereof will globally affect the entire system Earth. Increasing awareness of this fundamental role of the atmosphere for mankind is well documented by the broad public interest in global or climate change issues [99]. The attention paid to global-scale atmospheric quality issues, however, should not lead to neglecting air quality problems occurring on national or even smaller scale levels. Despite its elemental function for human life, air quality today is under threat on local and regional scales and thus deserves monitoring and protection. This study aims at a comprehensive characterisation of air quality in the Cologne area of NW-Germany using two different scaling approaches, a local and a regional level of investigation. A need for action to improve air quality was perceived in the 1960s by the public and by political organization that lead to world-wide legislative engagement. International conventions on transboundary atmospheric pollutant transport were established in 1979. In Germany the regulation of traffic and industrial emissions started in 1976, mainly with a focus on sulphur and nitrogen oxides which lead to "acid rain" and its detrimental effects on vegetation and human health. A further major incentive of that time was directed towards minimization of traffic related lead emission that ultimately lead to a complete lead-additive ban for petrol. Several German and other national actions were followed by EU-wide directives in the 1980s. Today, many European cities actively regulate traffic, to keep urban air within limits set in particular for fine particulates. This goal often can only be met by restricting traffic density, i.e. issuing driving bans in total or for selected vehicle types. In Germany citizens can hold their cities responsible for air quality, as supported by a legislative decision in 2007 [219]. However, environmental regulations only focus on the monitoring and reduction of a small set of pollutants that firstly are known to have the most severe health effects. Secondly, however, pollutants subjected to monitoring often are selected based on the easiness of, mostly continuous, analytical measurement thus neglecting compounds of adverse health effects that can only be determined using more sophisticated, time-consuming and costly techniques.

Despite of these shortcomings, active monitoring methods have been established that are cost-intensive and require continuous maintenance. Because of the high associated costs, monitoring is often spatially limited to regions of known high anthropogenic emissions, e.g. inner city streets with high traffic density or municipal waste incinerator sites. The advantage of active air sampling lies in the detection of absolute concentrations of pollutants in air. Exposure to such concentrations can be directly transformed into risk assessment for human health. The atmosphere comprises an extremely dynamic system characterized by sudden but mostly temporally limited occurrences of peak values that can only be detected by such active air measurements on a scale level of minutes or hours. Due to the massive efforts required and for budgetary reasons, permanent and spatially highly-resolved monitoring of atmospheric quality using active air sampling, however, is prohibited and alternative approaches have been developed and partly implemented. One major approach is the numerical modelling of atmo-

spheric pollution [107], a technique mainly successful for prediction of behaviour of atmospheric gases. A second approach utilizes the advantages of passive sampling of atmospheric pollutants. The cost-effective passive samplers bear the potential for high spatial resolution in combination with acquisition of time-integrated pollution signals, covering exposure periods of days to months or even years. In particular, the use of bioreceptors as air quality indicators has an unlimited spatial potential, covering pollution episodes that are reflecting a long-time exposure of citizens to the surrounding environment. European environmental organizations and the United States Environmental Protection Agency have designed lists of priority pollutants, building the base for environmental regulations referred to as EPA list and the EFSA list. Until now monitoring standards are based on the EPA list, but an expansion is highly recommended. Today, toxicity equivalence factors (TEF) are used to classify health affecting pollutants. In the case of the potentially carcinogenic compound class of polycyclic aromatic hydrocarbons (PAH), the lead compound benzo[a]pyrene was assigned a TEF value of 1, to which other components are normalized. This approach is superior to simple concentration analyses as for example the PAH dibenz[a,h]pyrene was assigned a TEF = 10. Though the PAH chrysene reveals a TEF of only 0.01, its methylated analogue 5-methylchrysene is given a TEF of 1.0, equivalent to the toxicity and carcinogenicity of benzo[a]pyrene [238]. The use of TEF thus allows establishing more adequate risk exposure assessments.

1.2 Aims and scope

This atmospheric quality study was conducted on two scale levels, a local one covering the City of Cologne, and a regional one, compassing the Greater Cologne Conurbation, comprising 3600 km². Both areas are subject to multiple emission sources. The study is based on a spatially high resolved biomonitoring set, to investigate long-term average air quality. A multi-proxy analysis of organic and inorganic pollutants and particulate matter fractions (PM₁₀, PM_{2.5}) is employed comprising compounds included in the US EPA list and additional pollutants with high source characteristic potential and high TEF [24]. Needles from robust and evergreen *Pinus nigra* trees were chosen as bioreceptors due to the high spatial availability in the Greater Cologne Conurbation. At first, the study addresses the systematic accumulation behaviour of pollutants on *Pinus nigra* needles. This is followed by a detailed description of pollutant dispersal and sources in i) Cologne City, an area of heterogeneous urban emission mixes, and ii) the Greater Cologne Conurbation with additional and spatially differentiated emission sources. Reliable source identification and allocation for various pollutants was based on three different approaches: i) statistical treatment, in particular factor analyses to unravel contribution from different sources, ii) relation of pollutant patterns to known specific emitters, and iii) construction of isopleths maps for pollutant concentration or diagnostic pollutant ratios using a GIS-software. The suite of atmospheric pollution indicators included in the investigation scheme encompasses environmental-magnetic properties, major and trace element composition, and concentrations of polycyclic aromatic hydrocarbons on pine needles. The combination of independent air quality indicators in conjunction with spatial high-resolution biomonitoring provides a powerful tool for identification of problem areas, potential emitters, and dispersal pathways of

atmospheric pollutants in a time-integrative manner that can serve the public, politicians, and industrial decision makers to improve environmental health regulation.

1.3 State of the art

The scientific record of air pollution considering fine to ultrafine particulate matter (PM₁₀, PM_{2.5}), major and trace elements, and pollution with carcinogenic organics started in the 1980s [77, 229, 198, 178]. Pollutant capture and analysis was mostly achieved by high volume active air sampling, allowing for a sampling of PM and associated material on filters of specific diameter (PM₁₀, PM_{2.5}) or a direct analysis of pollutants in the gas phase, often in real-time mode employing spectroscopic methods. For a minimization of maintenance and purchasing costs, and a simultaneously rising potential of a spatially high resolved documentation of pollutant dispersal, passive sampling devices and biomonitoring techniques were established [11, 185]. Often lichens and mosses have been used as bioreceptor for air pollutants, but they are relatively sensitive to environmental stress and do not appear in heavily polluted areas [11]. Thus, less sensitive plants were investigated for their use as bioindicators. A biomonitoring approach considering pollutant uptake via the food chain concentrates on the analyses of vegetables [61, 142], and is mainly focussed on heavy metal deposition and uptake. Several studies deal with pollutant uptake of plants, being of critical importance for mobile and essential trace elements [11, 142] and volatile (VOC) or semi-volatile organic compounds [233, 149, 105, 266]. As a result several uptake models were established covering equilibrium conditions preferentially for gaseous pollutants, a two-compartment model and models based on bidirectional exchange between vegetation and atmosphere including active participation of the vegetation [105, 266]. Uptake and atmospheric concentration of semivolatile organic pollutants utilizing coniferous trees was investigated with a special emphasis on source characterisation [77, 231, 233, 115]. Nevertheless, most of the PAH studies are based on the US-EPA list comprising 16 PAH, but miss most toxic and source indicative compounds [168, 56]. Methylated PAH and attributed parent compounds, e.g. phenanthrenes are highly recommended for source differentiation purposes [15] as well as the application of source indicative ratios between single PAH [287]. Enviromagnetic biomonitoring approaches first aimed at a recognition of coal fired power plants [58] and then considered monitoring of high traffic areas [91, 223, 160, 161, 156, 147, 137, 222, 284], coal power plants [74], and industrial emissions [103]. In general, major efforts in biomonitoring of urban pollution was done in Asia [66, 240], Italy [5, 44, 127, 133, 156], Spain [148, 136], and Poland [153, 154, 63]. In Sweden, Finland, and UK, large-scale studies covering transects from heavy pollutant sources to remote areas of about several 100 km were conducted [249, 200, 241]. The dispersal of gaseous pollutants can be effectively approached by modelling as previously shown for the Cologne Conurbation by Bruecher et al. [26]. In contrast spatial distribution patterns of particle-bound and particulate PAH and major and trace elements can only be achieved via high resolution sampling and subsequent spatial interpolation. Nevertheless, spatial mapping is rarely utilized in pollutant dispersal studies [82, 5, 156, 34], and often compensated by transect studies or factor analysis [249, 200, 241, 51].

1.4 Study area

All pine needle samples were collected in Cologne City and the surrounding Greater Cologne Conurbation (GCC). Most important issues for a biomonitoring study are climatic conditions in terms of pollutant dispersal, deposition and plant physiological aspects, e.g. water availability and substrate. Details that are of importance in the discussion of pollutant sources and dispersal are described where needed in the following chapters. An transparency overlay, provided in the appendix (Fig. 62) shows simplified attributes of the GCC, that are of highest importance for the analysis of air quality.

1.4.1 Topography

The Greater Cologne Conurbation is located in the Lower Rhine Embayment in the north-western part of Germany. The valley of the river Rhine is the most striking morphological feature of the GCC, building out flatly decreasing gravel terrasses into a relatively plain areal to the north-west. Cologne City in the central study area lies on average 50 m a.s.l (Fig. 1). The southern most part of the GCC is tangent to the Eifel mountains with highest elevations of approximately 300 m. To the east the Bergisches Land, part of the Rhenic Massif reaches heights up to 200 m in the sampling area. The Rhine Valley is parted from the plain Zuelpicher Boerde through a local upheaval, the Ville Ridge, tending NW-SE in the central GCC with maximum elevations of 130 m above sea level (Fig. 1). From east to west following river systems occur besides the Rhine. The river Rur drains the SE Eifel mountains and runs north through the town Dueren, parallel the Erft drains the Zuelpicher Boerde in northern direction. In the east the Sieg cuts a relatively steep valley into the Rhenic Massif opening out into the Rhine south of Cologne City.

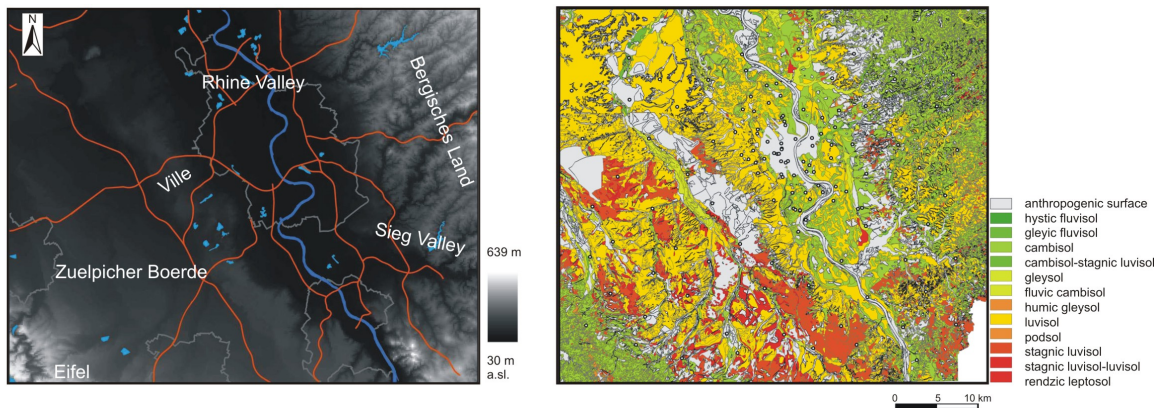


Figure 1: a) Morphological features of the Cologne Conurbation and local designations, highways were provided for orientation, b) dominant soil types in the Cologne Conurbation.

1.4.2 Climate

Meteorological data of the Greater Cologne Conurbation is provided by the Deutsche Wetterdienst (DWD). For interpretation of time-integrated pollutant signals on pine needles in the study area, a yearly average value calculated from 1961 to 1990 is

considered to be sufficient to represent the climatic conditions in the GCC. Thus, precipitation given for 18 weather stations in the region is shown to be highest in the eastern Bergisches Land (1000 mm a^{-1}), followed by the Rhine Valley with about 800 mm a^{-1} and lowest precipitation in the western Zuelpicher Boerde ($600\text{-}700 \text{ mm a}^{-1}$). Temperature data reveals on average $10.5 \text{ }^\circ\text{C}$ for the urbanized Rhine Valley and approximately $1 \text{ }^\circ\text{C}$ less in the adjacent areas. Prevailing wind directions in the Greater Cologne Conurbation follow morphological patterns. Thus, the Rhine Valley with cities Bonn, Cologne and Leverkusen are mostly affected by NW-winds, whereas the eastern Rhine Valley and the rise of the Bergisches Land is characterized by upcurrent winds. In the western Zuelpicher Boerde west winds are dominant [26].

1.4.3 Soil

Soils in the study area show a homogenous pattern reaching from preferentially luvisols in the west of the Rhine Valley to cambisols in the east (Fig. 1). Deposits of loess occur in the western Rhine Valley and lead to a substantial increase in soil nutrition status and agricultural land use, whereas the poorer and sandy soils of the Bergische Land are a perfect substrate for pines. About 10 % of the soils in the GCC are anthropogenic land fills, especially soils in Cologne City and former and active mining areas, which make the estimation of soil influence on biomonitoring difficult.

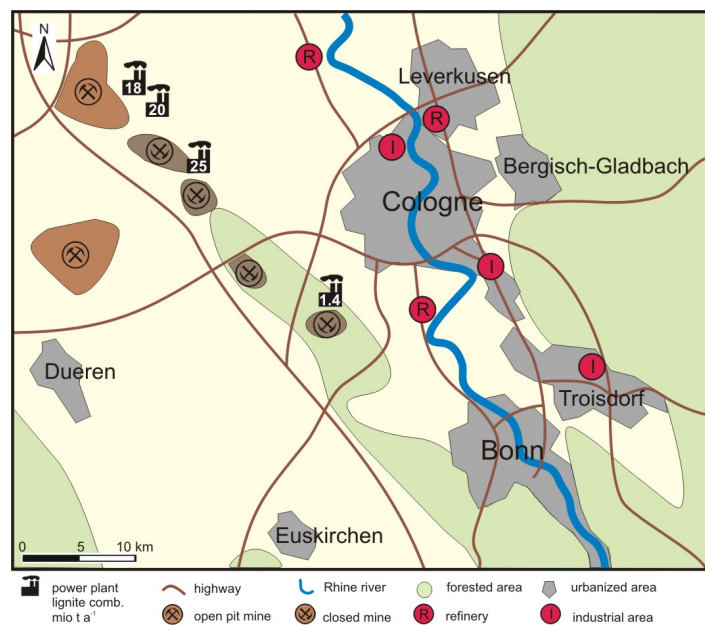


Figure 2: Land use and emission characteristics of the Cologne Conurbation, simplified according to data from CORINE landcover and the NRW Emission Register [69, 118].

1.4.4 Land use and emission scenarios

The Greater Cologne Conurbation is highly urbanized with Cologne and Bonn City having 1,300,000 citizens plus inhabitants of 8 smaller towns and rural areas. Altogether, this makes approximately 2,000,000 citizens in the GCC, contributing to air

quality with domestic heating and traffic activities. In addition, there is substantial shuttle traffic in the rush-hours into and from the highly industrialized Rhine Valley. This is reflected by a multitude of highways in the GCC, forming a nearly ubiquitous pattern with two major highways tending S-N, two E-W and a highway ring around Cologne and Bonn (Fig. 2). Major industrial complexes are found south and north of Cologne City and in the Sieg Valley. Here, large refineries, municipal waste incinerators and inorganic chemical production sites are located. Most dominant emitters are listed by the Emission Register NRW [118], above all the lignite fueled power plants (LFPP) in the north-western part of the GCC. One smaller capacity plant is lying directly west of the Cologne City limit close to a former open pit mine. The LFPP in the north-west are spatially attributed to two large open pit minings covering an area of 100 km². Waste incineration is concentrated on two major plants in the Cologne Conurbation, located in the north of Cologne and in Bonn with capacities for 590,000 t a⁻¹ and 245,000 t a⁻¹ waste, respectively. Five minor municipal waste incinerators (MWI) are situated along in the Rhine Valley. Large areas in the south-west are used as agricultural crop lands, the former lignite area in the Ville Ridge is now characterized by successful forest recultivation zones and the eastern Bergisches Land shows predominantly forested zones (Fig. 2).

2 Pollutant accumulation on *Pinus nigra* needles

The use of vegetation surfaces as biomonitors for air quality is dependent on the plants ability of pollutant uptake and capture. Therefore, it is important to take a closer look at the *Pinus nigra* surface properties and the properties of the investigated pollutants before an interpretation of air quality can be approached.

Thus, a detailed analysis of pollutant accumulation is done in this chapter, using electron microscopy for needle surface analysis, enviromagnetic methods for estimation of ultrafine and fine particulate matter loads (PM_{0.1}, PM_{2.5}, PM₁₀), and analysis of deposition and uptake of organic gaseous and particle-bound polycyclic aromatic hydrocarbons (PAH) and inorganic major and trace elements. A systematic accumulation is here shown on a temporally resolved data set based on consequent needle generations covering a time-span of 4 years.

2.1 Accumulation histories of magnetic particles

It is now well established that particulate matter (PM) in urban air contribute significantly to adverse health effects [190, 274, 256]. The European Community (EC) and authorities of the World Health Organisation (WHO) have consequently developed strategies for monitoring and reducing particulate matter in urban air [49, 50, 275]. Ultrafine ($< 0.1 \mu\text{m}$, PM_{0.1}) and aggregate ($< 1 \mu\text{m}$, PM_{1.0}) particulates are proven to have worse health effects than fine ($< 2.5 \mu\text{m}$, PM_{2.5}) materials [87, 276].

Particulate matter sampling can be achieved by active collection onto filters, with the advantage that different size classes can be differentiated. This method is time and cost intensive and, therefore, limited with respect to highly resolved spatial monitoring or for reconstruction of past pollution trends for a given location. Environmental magnetics offer a means of PM analysis of urban air and has been applied to the study of filter-collected particulates [58, 223, 285, 160, 162, 103, 222]. Alternatively, biomonitoring, employing passive accumulation of PM on plant surfaces, has been introduced as an air quality indicator. In biomonitoring studies the spatial mapping of PM loads via environmental magnetic techniques has been shown to be rapid, non-destructive and affordable [147, 103, 156, 82, 255, 66]. Conifers were proven to be more reliable than broadleaf trees due to higher deposition velocities for fine to ultrafine particulates and higher capture efficiency [13, 62]. Seasonal broadleaved trees or grasses only yield short-lived PM accumulation histories in the order of months. Evergreen broadleaves serve as pollutant collectors for up to 3 years and allow investigating temporal distribution trends [156]. Whereas temporal variations over the vegetation period are known to strongly affect the concentration of volatile and semivolatile pollutants in plants [115, 173], effects of seasonality have not been studied for PM accumulation. Here, the accumulation histories for PM on *Pinus nigra* needles with maximum exposure of 5 years applying environmental magnetic techniques are investigated. Summer and winter samples were collected for 5 needle generations at 6 locations with different emission background in the Cologne Conurbation and adjacent rural areas. Magnetic mineral composition, concentration, and magnetic PM grain sizes can be analysed using enviromagnetic methodology. The magnetic properties are compared to needle surface structure as well as the physiologically and seasonally controlled water and wax

content. The influence of seasonal variation and of non-linear accumulation histories needs to be investigated in order to select most representative needle cohorts suitable for spatial monitoring studies. In order to verify whether the variability inherent in natural systems allows for assemblage of a representative biomonitoring data set the problem of intra-site versus inter-site variability is further addressed [222]. The results discussed in this chapter have been published by Lehndorff et al. [126].

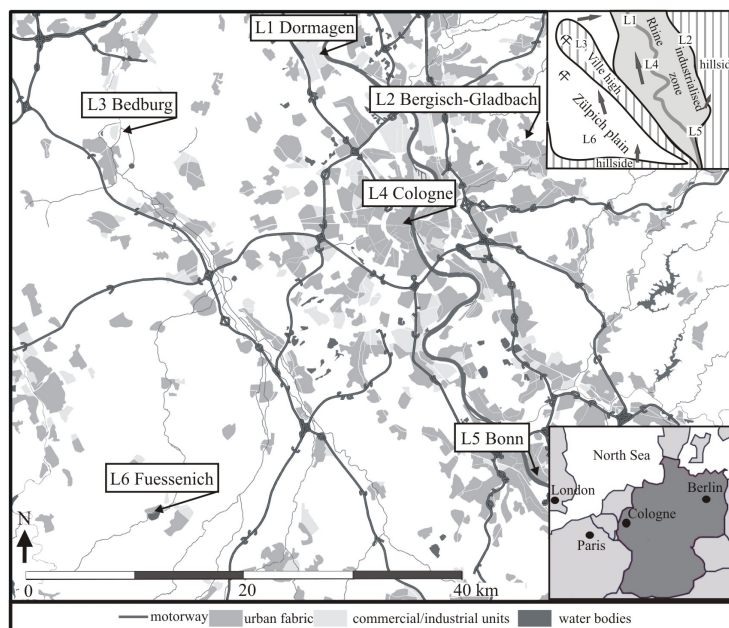


Figure 3: Simplified map of land use and traffic infrastructure with location of sampling sites. Insert at lower right depicts location of Cologne Conurbation in NW-Europe. Insert at upper right shows simplified morphology, prevailing wind directions and location of lignite mines.

2.1.1 Sampling methods

The Cologne Conurbation is situated in the western part of Germany, close to Belgium and the Netherlands (Fig. 3). Dominant morphological features generally trend NW-SE and include the Lower Rhine Valley. The adjacent slopes of the Rhenic Massif reach elevations of 200 m above sea level (a.s.l.) in the East and 300 m a.s.l. in the West. The Lower Rhine Embayment cuts a triangular plain into the Rhenic Massif with average elevations around 50 m a.s.l. in the Cologne Conurbation, flanked by the Ville Ridge (130 m a.s.l.) and the Zülpich Plain (80 m a.s.l.). The western part is characterised by mining of Tertiary lignite deposits in two open cast pits, which cover a total area of 60 km². Lignite comprises a major regional energy source, generated in three lignite fueled power plants (total capacity 10,000 MW/a). Prevailing wind directions are north-north-westerly in the South, changing to a westerly direction in the North of the Lower Rhine Embayment (Fig. 3). Principal land use includes urbanised, industrialised and rural areas (Fig. 3). An industrial corridor along the river Rhine

Location			Pine tree environment	Emission Scenario
L1	Do	Dormagen	trees in park adjacent to petrochemical plant, along Rhine River	industrial, petrochemical
L2	B-Gl	Bergisch-Gladbach	forested area at higher elevation, trees on premises of sport park	rural, forested
L3	Bb	Bedburg	small forest adjacent to power plant, lignite mine and major road	traffic, lignite mining
L4	C	Cologne	small park in center of dwelling area with high population density	traffic, industrial activity
L5	Bn	Bonn	small park in dwelling area close to Rhine River	suburban park, traffic
L6	Fu	Fuessenich	soccer ground in rural area with high agricultural intensity	rural, agriculture

Table 1: Characteristic land use and emission scenarios for sampling sites investigated.

shows the highest population and traffic density. With respect to specific emission characteristics six sites were chosen as depicted in Table 1.

All sampling sites were selected to provide pine needles with minimal influence from near point sources (particularly traffic). To best represent the local atmospheric situation, only pines fully exposed to all wind directions were chosen. Needle samples were taken from three trees per location to study the inter-site consistency of accumulated pollutants or pollutant proxies. In order to evaluate accumulation rates, needle cohorts of the past four growth periods were taken during two sampling campaigns in February and August 2004, 3 to 8 months after needle shoot respectively. This allows investigating seasonal variation in pollutant concentrations, resulting from temperature and emission changes or plant physiological reactions. Averaged needle density of the first and second needle generation of each tree was estimated against a reference, as described by the Federal Research and Training Centre for Forests, Natural Hazards and Landscape, Austria (<http://bfw.ac.at/rz/wlv.lexikon>, 2004). Samples were collected from 3 sides of a tree at 3 to 5 m height and combined to composite sample cohorts using extendable pruning shears. Needles were cut directly from the branch, at about 1 cm from the needle base and stored deep frozen prior to analyses.

2.1.2 Analytical Methods

Microscopical and microprobe analyses Needle surfaces of different age and pollution background after gold sputtering was investigated with a scanning electron microscope (CamScan44, Cambridgeshire, UK). One centimetre was cut off of the centre of three needles per sample and arranged on the sampler holder with both the abaxial and adaxial side exposed. SEM-scans allow identification of epicuticular wax structure (crystalline shape and surface wax film), needle surface properties (polluted and unpolluted stomata) and particles of diverse shape and size. Electron optical resolution was limited to a magnification of 25,000 times allowing the detailed inspection of particles to a minimum size of $\sim 1 \mu\text{m}$. For identification of the elemental composition, electron microprobe analysis was applied using a JEOL JXA-8900RL Superprobe (JEOL, Peabody, USA).

a)	H-value (n = 36)	<i>p</i>	critical H-value				
water loss	11.46	0.04298	11.07				
wax	5.77	0.32933	9.24				
χ	29.51	0.00002	25.74				
SIRM	25.40	0.00012	20.52				
ARM	18.34	0.00255	15.09				
B_{cr}	18.72	0.00217	15.09				
s-ratio	13.75	0.01727	11.07				

b) loc.	water loss	wax	χ	SIRM	ARM	B_{cr}	s-ratio
L1	13.25	2.50	23.67	24.50	27.33	20.00	12.33
L2	11.83	7.00	14.67	10.50	12.33	32.67	23.17
L3	9.67	7.50	24.33	22.33	26.67	13.00	20.50
L4	23.40	4.50	33.17	33.17	23.50	13.00	8.83
L5	19.75	7.00	10.50	11.67	8.83	22.17	28.33
L6	9.33	10.50	4.67	8.83	12.33	10.17	17.83
n	28	12	36	36	36	36	36

Table 2: Statistical analyses of pine needle populations at 6 locations by non-parametric Kruskal-Wallis- H test. a) mean ranks for parameters at individual locations, b) H -values for individual parameters ($df = 5$, $n = 6$), $p =$ asymptotic significance at a 99% confidence level. Means used for calculation are given in Table 29 in the appendix.

Magnetic analyses Environmental magnetic analyses ($n=143$) was carried out following procedures given detailed by Urbat et al., [255]. In brief, bulk magnetic susceptibility χ was measured at room temperature on a KLY-2 susceptibility bridge (noise level 4×10^{-8} ; AGICO, Czech Republic). Susceptibility gives the magnetizability of the sample and is likely to be dominated by ferrimagnetic particles. Anhysteretic Remanent Magnetization (ARM) was imparted using peak alternating fields (AF) of 100 mT, with a biasing field of 40 μ T superimposed. The ARM is interpreted as a concentration parameter and is particularly sensitive to the content of stable single domain (SSD) ferrimagnets (for magnetite these are grain sizes between 0.03 - 0.4 μ m). The Isothermal Remanent Magnetization (IRM) was imparted at progressively higher pulse fields up to 1.5 T, followed by a stepwise acquisition of the backfield curve to 0.3 Tesla. This measurement provides information about mineral composition, particle size and relative concentration of remanent magnetic particles (Saturation IRM (SIRM)). The backfield curve gives additional information about the mineral magnetic composition and grain size ranges from the calculation of the coercitivity of remanence (B_{cr}) and s-ratio ($s = [1 - (IRM_{-300mT} / SIRM)]$) after Bloemendal et al. [21]). ARM and IRM measurements were carried out using the respective in-line solenoids and pulse magnet of a three-axis DC-SQUID magnetometer (noise level 5×10^{-12} A m²; model 755R, 2G Enterprises, USA).

Organic geochemical analyses Organic solvent extraction and clean up of needle wax was applied on each needle cohort. In order to minimise analytical costs and efforts a composite sample was prepared for each needle cohort from all individual locations sampled in triplicate. Recovery of waxes also yields the polycyclic aromatic

	water loss	wax	χ	SIRM	ARM	B_{cr}	s-ratio
water loss	1						
wax	-0.35*	1					
χ	-0.34**	0.50**	1				
SIRM	-0.34**	0.52**	0.98**	1			
ARM	-0.43**	0.44**	0.88**	0.89**	1		
B_{cr}	-0.26**	0.54**	0.77**	0.76**	0.60**	1	
s-ratio	0.25**	0.05	-0.02	-0.01	-0.25**	0.03	1

Table 3: Spearman’s rank correlation coefficients ($n = 142$ for magnetic parameters, $n = 134$ for water loss, $n = 47$ for wax concentration, raw data given in Table 26 in appendix). Values are significant at * $p < 0.05$, ** $p < 0.01$.

hydrocarbons (PAH) on the pine [123] and the extraction process was optimised for full recovery of the PAH. The needle surface was extracted by accelerated solvent extraction (DIONEX ASE 200, $p=75$ bar, $T=120^\circ\text{C}$) with hot *n*-hexane:dichloromethane 99:1 (v/v). Plant waxes are insoluble in *n*-hexane at room temperature and precipitated upon cooling to form crystalline aggregates. These were separated by centrifugation and the amount determined gravimetrically. Water content of needles was determined after drying for one week in an oven (50°C).

Statistical analyses Data were analyzed statistically using SPSS 12.0 for Windows. Nonparametric analysis of variance was performed by the Kruskal-Wallis-*H* test to identify significant variations between the 6 sampling sites ($n = 36$, Table 2 and Table 29 in appendix). Normal distribution of sample populations ($n = 142$, Table 26 in appendix) was tested by the Kolmogorov-Smirnov procedure. Spearman’s rank correlation coefficients were determined to evaluate relationships among magnetic parameters (Table 3).

2.1.3 Results

Wax and water content Magnetic particles accumulate on the outer surface of pine needles and in stomatal cavities with no translocation to the needle interior or volatilisation loss reported. Generally, the amount of PM accumulated on vegetation surface is reported normalized to the dry weight of the whole needle or leaf. The amount and surface area of waxes in relation to the total needle weight varies seasonally and between locations depending on environmental factors including temperature, humidity, or wind stress. Thus, waxes are subject to ongoing degradation but are periodically renewed by the plant. Wax abrasion and dissolution may remove previously wax-embedded magnetic PM. Hence, the wax content has to be considered to properly evaluate accumulation histories for magnetic PM on pine needles.

Wax concentrations per cohort for the 6 locations increases during the first 20 months after bud break (Fig. 4a; Table 26 in appendix) and then reach equilibrium. On average 50 months old needles reveal concentrations 3 times higher than needles with a lifetime of 3 months. Mean concentrations differ depending on location with highest wax contents occurring in Bedburg and low concentrations in Bergisch-Gladbach. The

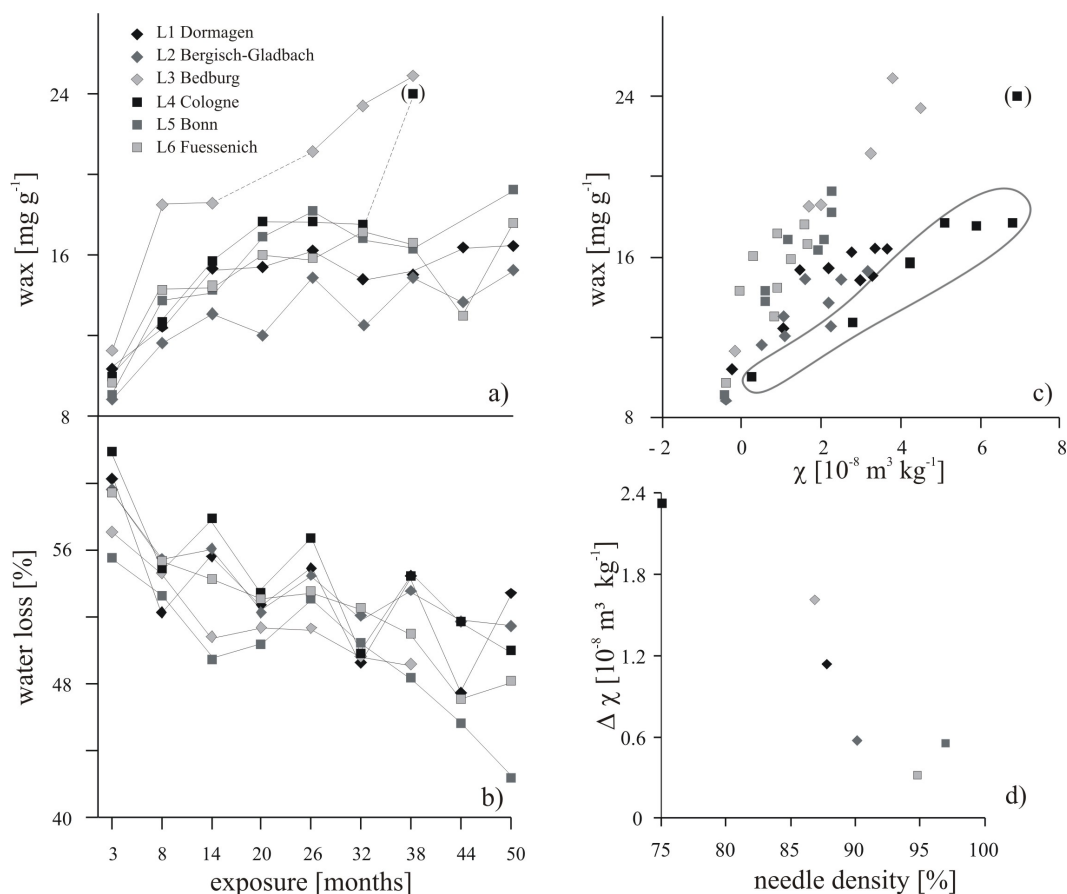


Figure 4: Physiological and environmental properties. a) wax content vs. exposure time, b) water loss vs. exposure time, c) wax content vs. magnetic susceptibility χ , samples from metropolitan Cologne grouping separately are highlighted, d) needle density vs. difference in χ determined for 2nd and 1st needle cohort, sampled in winter.

initial water content of young needles varies between 55% and 62% for the six locations (Fig. 4b) and then gradually decreases to about 50% over the next 50 months. The needle density noted for summer and winter samples is location specific (Fig. 4d) and reveals a negative correlation to the gain in susceptibility $\Delta\chi$ comparing first to second year needles (displayed as $\Delta\chi = \chi$ needle cohort 2 - 1; Fig. 4d). Cologne shows the lowest needle density for the first and second cohort but the highest increase in susceptibility for these needle generations. In contrast, rural Bonn and Fuessenich pines maintain approximately 100% needle density and correspondingly low differences in susceptibility.

PM composition, concentration and grain size For the Cologne Conurbation it is shown by electron microscopy with EDX that pine needle surface and stomatal cavities show predominantly spherical iron-bearing particles up to 2.5 μm that result from combustion processes [255]. This could be confirmed by environmental magnetic analysis indicating the presence of almost exclusively magnetite, predominantly in a size class $<2.5 \mu\text{m}$ [255]. In contrast to the previous study, the pine needles analyzed in this investigation, except for one sample, are not restricted to metropolitan Cologne

but derive from 5 locations in its vicinity (Fig. 3). Pine needles are thus expected to have been exposed to different emission scenarios and to show variable accumulation histories reflected in the magnetic PM composition.

Microscopical PM identification Needle surface investigation by SEM showed highest relative particle density and size in samples from Cologne, whereby needle wax deterioration and number of particles increased with needle age. The rural station Fuessenich revealed the lowest number of particulates on needle surfaces, whereby particles were restricted to finer grain sizes. Structural integrity of waxes was highest for needles from the Fuessenich location. In contrast to the study of pine needles from Cologne City [255], where only spherical iron particles were observed, this study also revealed the presence of irregularly shaped iron-bearing PM reaching sizes up to $30\ \mu\text{m}$ (Fig. 5). Sharp-edged particle fragments are commonly attributed to abrasion in vehicles, especially brake wear [244, 86]. Fig. 5 shows such a particle with a dimension of about $15\ \mu\text{m}$ accompanied by an iron-bearing spherulite of $2.5\ \mu\text{m}$ diameter and irregular, eventually fragmented dust particles.

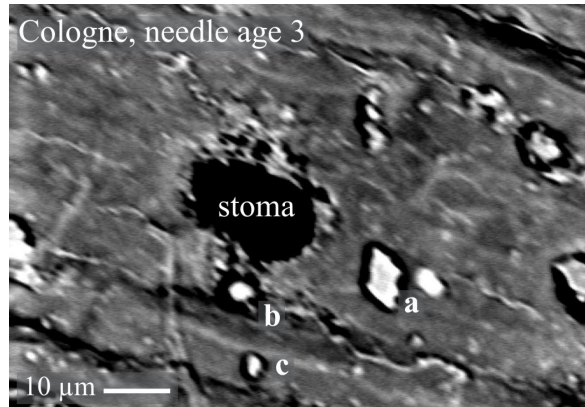


Figure 5: Electron microprobe scan of needle surface. Third year needle sample from Cologne exhibits different particles: a) sharp-edged particle $\sim 15\ \mu\text{m}$ in size, composed of Fe, Si, O, b) spherulite $\sim 2.5\ \mu\text{m}$ in diameter, composed of Fe, Si, O, Al, c) irregular shaped particle $\sim 2\ \mu\text{m}$ in diameter, composed of Si, Al, O, K.

Magnetic mineral and grain size identification Magnetic mineral composition of actively sampled PM or vegetation surfaces has previously been shown to be dominated by magnetite [160, 162, 156]. In agreement with the results from Cologne City [255] the present mineral magnetic measurements also identify magnetite (Fe_3O_4) as the dominant ferrimagnet at all locations. While the mineral magnetic parameters yield a rather uniform picture with respect to the type of the magnetic mineral, major differences in between the locations derive from varying concentrations and grain size distributions. Typical for fine grained magnetite (i.e. $<0.4\ \mu\text{m}$) the IRM acquisition curves are initially flat ($<10\ \text{mT}$) and generally approach saturation in fields of $200\ \text{mT}$ (Fig. 6a [248]). The incomplete saturation at $200\ \text{mT}$ points to a minor deviation from stoichiometric magnetite, likely due to a slight mineral oxidation. A ferrimagnetic dominance in all samples is further supported by s-ratios >0.94 (Fig. 9d). B_{cr} values

generally range from 30 - 53 mT, except for the youngest needles (3 months) having coercivities of remanence of 16 - 30 mT. Under the assumption that dominantly magnetite is present in the samples the B_{cr} values can be regarded as grain size sensitive. Note, that the B_{cr} range viewed per location is even more restricted (Fig. 9a).

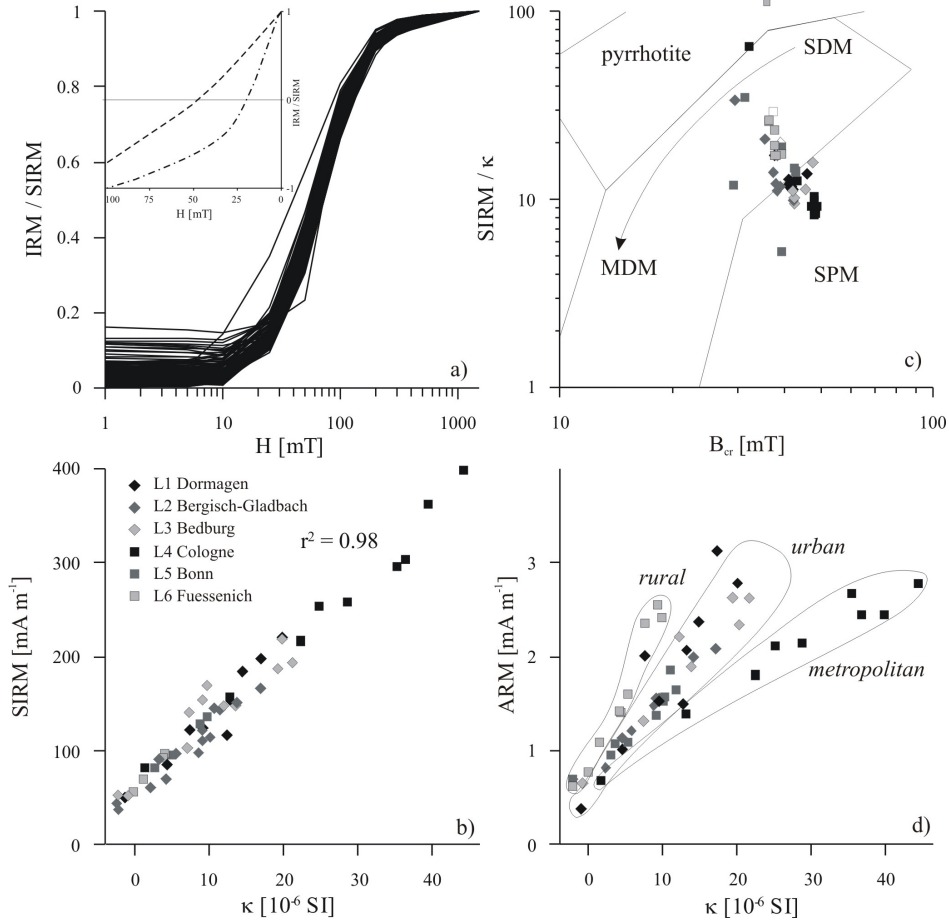


Figure 6: Mineral and grain size diagnostic enviromagnetic parameters: a) acquisition curves of IRM normalised to saturation IRM (SIRM); insert displays spread in backfield curves, only minimum and maximum B_{cr} yielding curves are shown; b) binary plot of volume magnetic susceptibility κ versus SIRM with data points coded according to location, triplicates for each needle cohort per location are averaged; c) bivariate plot for identification of magnetic minerals [187] with indication of magnetite domain status, SDM = single domain magnetite, MDM = multi domain magnetite and SPM = superparamagnetic magnetite; d) binary plot of κ versus ARM, data points can be grouped according to location and dominant emission scenario. For details see text.

From the significant linear correlation of SIRM and κ ($r^2 = 0.98$; Fig. 6; Table 3), it is inferred that the susceptibility is predominantly controlled by the amount of magnetite on the pine needles. A bivariate plot combining SIRM/ κ and B_{cr} illustrates the dominance of magnetite in the single domain grain (SDM) size range (Fig. 6c; [187]). Locations are grouped with respect to SIRM/ κ , indicating additional contributions of coarser multi domain magnetite (MDM) for the stations at Cologne, Bergisch-Gladbach and Bonn as well as finer superparamagnetic magnetite (SPM) on Bonn and Cologne

needles. Only one sample from the Fuessenich location yields an exceptionally high ratio, typical of iron sulfides like pyrrhotite. There is, however, no further supporting evidence for this notion. Samples from Cologne, Bedburg and Dormagen display SIRM/ κ lower than would be expected for magnetite grains $>0.03 \mu\text{m}$. It is concluded that κ in these samples is relatively increased over SIRM due to the admixture of ultrafine ($<0.03 \mu\text{m}$) magnetite. Such ultrafine particles (SPM) are characterised by high susceptibilities, but, do not contribute to SIRM due to their short relaxation times. Ultrafine magnetite is further supported by a comparison of ARM intensities (sensitive to SSD magnetite) and susceptibilities (Fig. 6d; [89]). Dissimilar to SIRM vs. κ the overall linear correlation for the entire data set is lost (Table 3). Instead, different slopes of linear regression lines separate the respective locations. Samples from metropolitan Cologne are characterized by relatively elevated susceptibilities, again confirming ultrafine magnetite admixtures. In contrast, rural site Fuessenich displays the opposite trend towards decreased ultrafine contributions.

Magnetic mineral concentration The concentration of magnetic PM on pine needles serves as a proxy for atmospheric particle loading in Europe [103, 156, 82] and Asia [66]. In Kathmandu a concentration range of χ in broadleaved trees of $0.01 - 54 \times 10^{-8} \text{ m}^3 \text{ kg}^{-1}$ was determined [66]. Moreno et al. [156] determined a range in χ of $0.2 - 49 \times 10^{-8} \text{ m}^3 \text{ kg}^{-1}$ on evergreen broadleaved trees. No detailed information on exposure times and composition of leaf cohorts analysed was given.

For this study, no sites with direct point source exposure (e.g. traffic) were chosen. Values for χ vary between -0.5 and $8 \times 10^{-8} \text{ m}^3 \text{ kg}^{-1}$ for the entire data set ($n=143$; Table 26 in appendix). If susceptibility is averaged using weighted contributions of every needle cohort, the range in susceptibility for a given location including summer and winter collected needles is $0.03 - 6 \times 10^{-8} \text{ m}^3 \text{ kg}^{-1}$ (Fig. 7; Table 31 in appendix). Weighting factors of $1 : 0.9 : 0.5 : 0.2$ were utilized for 4 consecutive needle generations. Highest mean concentrations were detected in Cologne, followed by Bedburg and Dormagen. The lowest concentrations were measured for Bergisch-Gladbach, Bonn and Fuessenich. In general, elevated concentrations are associated with a higher spread in total susceptibility values (Fig. 7). The ranges in the upper to lower quartile remain similar for stations Dormagen, Bergisch-Gladbach, Bonn and Fuessenich, whereas stations Bedburg and Cologne reveal broader ranges (Fig. 7). The SIRM values reveal tendencies similar to the susceptibility (Fig. 6b; Table 26 in appendix) with only slightly higher SIRM values observed for the Dormagen location (Fig. 7). When compared to χ and SIRM, the ARM shows a different distribution pattern, with enhancement for stations Dormagen and Fuessenich, contrasted by a significant decline in Cologne (Fig. 7; Table 29 in appendix). ARM data differentiate two groups, the one with lower ARM signals is represented by more rural stations in Bergisch-Gladbach, Bonn and Fuessenich, the second with higher ARM intensities includes urban locations in Dormagen, Bedburg and Cologne (Fig. 7).

Magnetic mineral accumulation history Concentration dependent parameters χ , SIRM and ARM increase with needle exposure time (Fig. 8a-c). Gradients in accumulation rate vary between locations and for χ and SIRM increase in the order Fuessenich, Bonn, Bergisch-Gladbach, Dormagen, Bedburg, and finally Cologne (Fig.

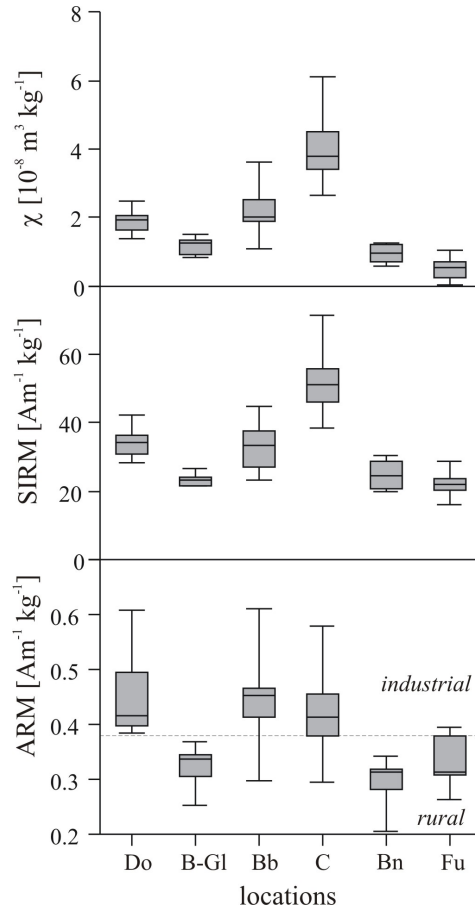


Figure 7: Ranges in magnetic concentration parameters, triplicate analyses averaged for each tree. Boxes indicate upper and lower quartile, whiskers encompass maximum and minimum values and horizontal bar gives median value. Locations: Do = Dormagen, B-Gl = Bergisch-Gladbach, Bb = Bedburg, C = Cologne, Bn = Bonn, Fu = Fuessenich. For discussion see text.

8a,b; Table 26, 31 in appendix). A deviation is noted in lower ARM intensities for Cologne and a minor enhancement for Fuessenich. This allows samples to be grouped into two clusters according to their ARM intensities (Fig. 7; Table 29 in appendix).

The increase in PM accumulation, as determined by enviromagnetic proxies is not linear but occurs at higher rates during the first 20 months followed by establishment of equilibrium concentrations after approximately 26 months. The highest PM accumulation is measured between the first two needle generations of each sampling campaign ($\Delta\chi$, Fig. 4d). Non-linear increase occurs two-fold, in a non-systematic manner, as observed for the Cologne station with strongest excursions observed for exposure months 26 and 44 (Fig. 8a,b). Systematic alternations between summer and winter collected samples occur in Bedburg and Fuessenich, whereby it is important to note the alternation pattern is directly opposed and, thus, not a function of seasonality.

Statistical results Physiological and enviromagnetic data ($n = 143$) are normally distributed as indicated by the Kolmogorov-Smirnov test (χ : $p = 0.24$; SIRM: $p = 0.4$; ARM: $p = 0.7$). Nonparametric analysis of variance by the Kruskal-Wallis- H test

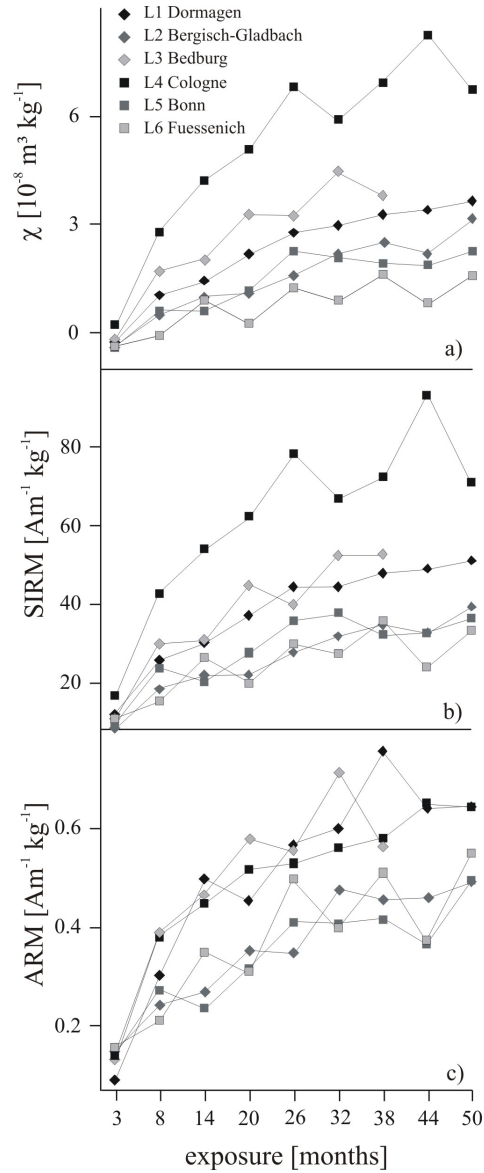


Figure 8: Accumulation curves for averaged needle cohorts analysed in triplicate. Samples representing 3, 14, 26, 38, and 50 months of exposure were taken in summer 2004, remaining samples were collected in winter season of 2004. For discussion of trends in accumulation curves see text.

is commonly used for data sets with high variability between groups [75, 222]. For all enviromagnetic parameters the test proves significant inter-site variability between locations, whereas wax and water content are close to or below the critical H -value (Table 2). Spearman's rank correlation coefficients determined to evaluate relationships among different magnetic parameters (Table 3) show significant correlation at the $p < 0.01$ level, except for wax vs. water loss with $p < 0.05$ and the s-ratio showing no significant correlation with the remaining parameters.

2.1.4 Discussion

Prior to the discussion of magnetic properties as proxies for atmospheric PM loads, seasonal variations thereof and source allocation of PM, it is required to demonstrate that the differences in magnetic properties are systematically influenced by air quality and not dependent on sampling procedures or strategies. It is of importance to interpret only those enviromagnetic signals that are clearly differentiated from the variability inherent in natural systems. The systematic variations observed in this study are above natural background variability and thus represent air quality.

Enviromagnetic techniques are most sensitive to ferromagnetic particulates and, thus, preferentially characterise the fraction of atmospheric particulates that derives from combustion processes or metallic wear and abrasion. In the presence of magnetite, needle bound minerogenic dust contributes only subordinately to the total magnetic susceptibility. Importantly, application of more sophisticated IRM and ARM techniques exclusively records combustion derived ferrimagnetic particles. These occur mainly in the PM_{2.5} fraction or as nanoparticles and, thus, have strong adverse health effects [276]. Enviromagnetic techniques, therefore, provide the “most wanted” atmospheric quality information, though they are incapable of reflecting the total suspended particle loads.

Inter- and intra-site variation At each location a pine needle composite from three trees was taken to fully represent local conditions in atmospheric particle loadings. The Kruskal-Wallis- H test proves significant inter-site variability of enviromagnetic parameters between all locations, whereas water loss and wax content are not significantly dissimilar (Table 2a). Location Fuessenich has the lowest mean rank (Table 2b) due to “a high noise” at an unpolluted background site. The box and whisker plots in figure 7 indicate that the variability at a given location is smaller than in between locations. This is confirmed by the low coefficients of variation (Table 29 in appendix) and mean ranks (Table 4b) per site.

The excellent correlation between χ and SIRM (Fig. 6b, 7; Table 3) indicates that the susceptibility almost exclusively reflects ferrimagnetic pollutant concentrations. As shown in figure 7 and Table 4, the ARM displays a pattern different from χ and SIRM. The box and whisker plots show much higher intra-site variability for stations Dormagen, Bedburg and Cologne. The larger spread at these sites is due to the twofold influence of magnetic mineral concentration as well as grain size on ARM intensities, whereas χ and SIRM are less susceptible to variation in grain size composition. This can be taken as evidence for a preferentially urban or industrial emission scenario characterised by high magnetic particle loadings dominated by fine, single domain magnetite. In contrast the Bergisch-Gladbach, Bonn and Fuessenich locations exhibit a predominantly rural particle loading with a smaller fraction of fine PM.

Accumulation processes Since vegetation surfaces constantly interact with the surrounding environment, a linear accumulation of particles with time is not to be expected. Additionally, variation in emission patterns contributes to local variability. Understanding of the accumulation behaviour of a monitored pollutant is of great importance for sampling strategy and interpretation of the acquired data. The dis-

cussion of accumulation controlling processes is based on needle cohorts sampled in winter (n=4) and summer 2004 (n=5), altogether revealing the accumulation history of 4 years for each station (Fig. 8a-c, Table 31 in appendix).

Anthropogenically induced accumulation The magnetic susceptibility of 3 months old pine needles is below zero for all locations, except Cologne, revealing a dominance of diamagnetic plant material and only a minor contribution of magnetite for the most polluted station in the city of Cologne (Fig. 8a). The continuing increase in the accumulation curve is location-specific and clearly separates every location after 20 months of needle exposure. Systematically growing differences in concentration of χ show that no saturation for particle enrichment on the needles surface is reached. Curve shapes detected by SIRM analysis are similar to χ and reveal the metropolitan station in Cologne as having the steepest accumulation rate, being higher by a factor of 4 compared to rural Fuessenich. Therefore, the concentration of SIRM and χ , for needles older than 2 years in general, is a function of cumulative and time-averaged atmospheric pollution. Additionally, ARM intensities (Fig. 8c) rise with increasing needle exposure time but reflect higher concentrations of the fine magnetic mineral fraction. The distinction between two types of atmospheric environments, one with a higher amount of small grain sizes and one with lower contributions of fine magnetite, is established after 8 to 14 months of needle exposure and remains until needle senescence.

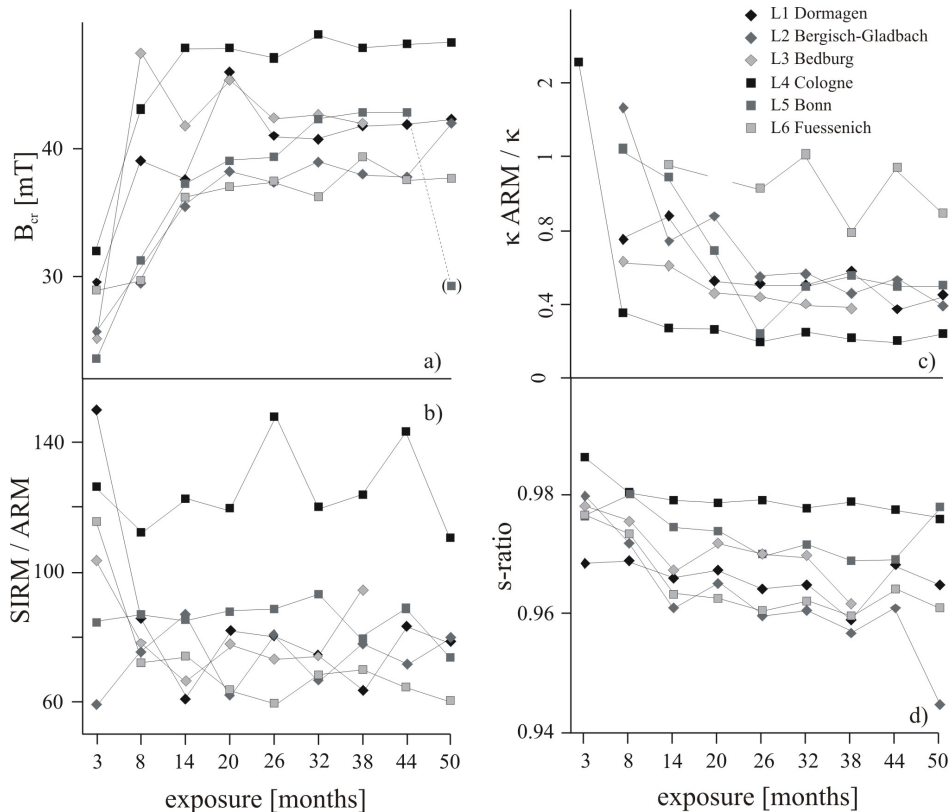


Figure 9: Variation of grain size and oxidation indicative environmental magnetic parameters versus needle exposure time, averaged for needle cohorts analysed in triplicate. Diamagnetic samples excluded in panel c).

The s-ratio emphasizes an anthropogenic induced accumulation process. Small variances from 0.95 to 0.99 (Fig. 9d) are interpreted as an increasing oxidation of the magnetite over a period of four years [113]. Although a fraction of the magnetite accumulated in the first year(s) of exposure may be removed from the needle by rain or wind abrasion, the magnetic PM is not seasonally eroded and renewed in total.

Natural accumulation factors The non-linear accumulation pattern of magnetite on pine needles is assumed to be controlled by diverse natural processes. A canopy effect, as proposed by Horstmann and MacLachlan [93], is a reasonable explanation for a lowered accumulation rate measured for consecutive needle cohorts in this study (Fig. 8a-c). Since first year needles reach an mean twig length of 20 - 30 cm, older generations are successively protected by younger cohorts scavenging most of the airborne pollutants. The needle density noted for cohort 1 and 2 is here used as a proxy for limitation of PM throughfall and shows a significant influence on particle accumulation (Fig. 4d). Additionally, magnetic investigations on trees at urban road sides show a 45 % difference between the road-facing and the road-opposing side due to the filtering capacity of the road-exposed foliage [147].

Chemical and physical alterations of vegetation surfaces also have to be considered to contribute to a loss of particles. Degradation and renewed production of epicuticular waxes, abrasion or wash-off may lead to an equilibration level of particle accumulation and degradation. As discussed by Urbat et al. [255] temperature induced seasonal decline of surface wax concentration does not influence magnetic properties of needles. In this study no reduction in wax concentration with increasing needle age was observed (Fig. 4a). As waxes are assumed to sorb magnetic PM their degradation would lead to a more effective particle abrasion. In contrast, waxes reveal an accumulation trend over four years that is comparable to the particle enrichment (Fig. 4a and Fig. 8a,b). The lack of correlation between wax amount and magnetite concentration for the locations (Fig. 4c) indicates particle accumulation is not only a function of the integrity of the epicuticular wax layer. It is important to note that needles from Cologne pines deviating from the general trend of covariance seen in figure 4c, show an exceptionally high magnetite but low epicuticular wax concentration. Covariance is assumed to result from the time dependence of both processes, i.e. wax production or particle accumulation.

As discussed by Kylin and Sjödin [115] changes in needle diameter may exert an influence on particle concentration, which is primarily a function of surface area. Water loss of pine needles investigated is supposed to reflect a decrease in needle surface area with age (Fig. 4b). The biannual changes in magnetic properties behave contrary to a reduction in water content and surface area, implying that effects of needle surface area are of minor importance.

Seasonal variation in accumulation Seasonal effects on deposition, removal or transport of PM result from natural, mainly climatic processes, as well as from changes in anthropogenic emissions [160]. Monthly resolved sampling campaigns and investigations of particulate pollutants, in general, show seasonal shifts to higher atmospheric pollution in winter [85, 252, 276, 255], due to higher traffic density and domestic heating.

A systematic change in particle load for the summer and winter sampling campaign was detected for Fuessenich and Bedburg, whereas Cologne, Dormagen, Bonn and Bergisch-Gladbach samples do not show notable variations (Fig. 6a,b). The smoother accumulation curves are interpreted as a result of a seasonally constant pollutant input characteristic for areas with high anthropogenic emissions, e.g. from traffic, domestic burning, waste incinerators, or power plants. Alternating concentration patterns measured for Fuessenich and Bedburg pines seem to be controlled by seasons, but are directly opposed and, therefore, a climatic dependence of magnetic properties can again be excluded. An alternative explanation is a seasonal difference in PM transportation distances [58, 252]. Warm air masses can carry more particles over longer times and distances and, therefore, remote areas like Fuessenich face a slightly elevated pollutant load in summer. Possible sources for long-distance transportation are power plants, to the North of the Zuelpich plain or industrialised regions in the Rhine industrial corridor (Fig. 3). In winter, Bedburg pines are exposed to higher atmospheric particle loads from the two nearby power plants. As the power plants are run at nearly constant capacity throughout the year, higher atmospheric loads in the vicinity of the power plants are preferentially due to temperature-controlled shorter PM dispersal distances.

Grain size distribution The spatial distribution of magnetic particle concentrations measured on vegetation can be used to identify potential sources and assess transport distances of PM [160, 162, 156, 255]. The locations investigated in this study can be divided into two groups based on ARM (Fig. 8c), which is highly susceptible to the presence of the specific grain size class PM_{2.5} to PM_{1.0}. More detailed information about the grain size composition of magnetite is given by the comparison of χ , SIRM and ARM data. Thus a further discrimination of the stations according to rural, urban and metropolitan pollution background can be achieved by plotting ARM versus κ (Fig. 6d). The coercitivity of remanence (B_{cr}) and ratios of SIRM/ARM, SIRM/ κ and κ ARM/ κ , if compared with needle exposure (Fig. 6c, 9a-c), reveal only one notable change in grain size. This shift occurs for the 3 months to the older needle cohorts. After 8 to 14 months of exposure the grain size spectrum remains constant at each location (Fig. 9a). The B_{cr} indicates a mean grain size value for magnetite pointing to more or smaller grains on pine needles in metropolitan Cologne than at the most rural site Fuessenich. B_{cr} values indicate an opposite grain size composition (Fig. 9b,c), with samples from Cologne displaying the highest SIRM/ARM and lowest κ ARM/ κ ratios. Samples from Fuessenich represent the lowest and highest ratios, respectively. While the low κ ARM/ κ ratios in Cologne are easily explained by the relatively high contribution of ultrafine particles (SP, <PM_{0.1}) to the susceptibility, these are of minor importance in rural Fuessenich. In contrast, the high SIRM/ARM ratios (Fig. 9b) suggest a relative increase of particles in the >PM_{2.5} fraction being most prominent in Cologne. The latter is attributed to the admixture of large multidomain grains, the largest of which have been detected by SEM to reach sizes around 30 μ m. The coarser magnetite fraction is attributed to wear debris resulting from train and tram or road traffic.

The combined interpretation of the four grain size related magnetic parameters lead to the conclusion that Cologne needles exhibit a broad spectrum of SP, SD, and MD magnetite characteristic of a grain size distribution ranging from PM_{0.1} up to PM₁₀.

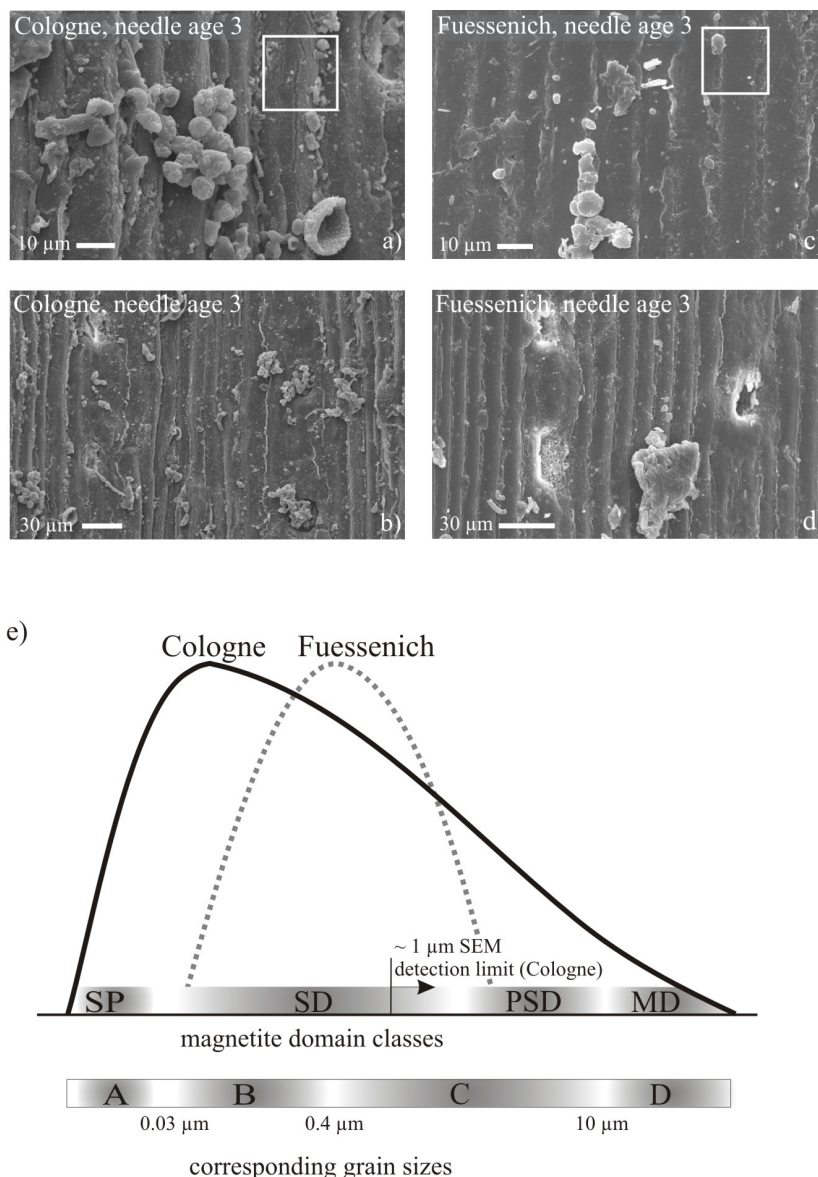


Figure 10: Grain size distribution investigated using SEM and enviromagnetic techniques: a) high and b) low resolution image of needle surface from Cologne site; c) high and d) low resolution image of needle surface from Fuessenich site; white boxes guide in assessment of fine particle density per $400 \mu\text{m}^2$; e) schematic diagram displaying hypothetical end-member grain size distribution curves for metropolitan location Cologne and rural station Fuessenich; upper bar: approximate magnetic domains for magnetite are indicated with SP = superparamagnetic, SD = single domain, PSD = pseudo single domain, MD = multi domain; lower bar: approximate corresponding grain sizes with separation of size classes by multiproxy enviromagnetics: A = χ elevated versus ARM, B = ARM high sensitivity region, C = region of IRM and χ equivalence, D = region of enhanced IRM vs. ARM.

The Fuessenich site, in contrast, is dominated by one dominant magnetite phase (PSD - SD), typical for a narrow grain size distribution <0.03 to $2.5 \mu\text{m}$. The hypothetical grain size distribution curves in figure 10e show a Gaussian particle size distribution for single-sourced location Fuessenich versus the broader and low diameter skewed

distribution for the Cologne location. The wider range and elevated contribution of nanoparticles in Cologne is attributed to the higher traffic density and low atmospheric residence time of $PM_{0.1}$. The coarser fraction noted to contribute to the Cologne particle load is related to an input from traffic associated material wear. Sharped-edged particles were identified on Cologne needle surfaces by SEM and Electron Microprobe (Fig. 5). Particulate emission from industry and power plants occurs preferentially in the SD fraction and is most prevalent in Cologne, Dormagen and Bedburg (Fig. 7; Fig. 8c).

SEM analyses support the interpretation of enviromagnetic properties, even if the microscopical methods are not suitable to reveal the presence and quantity of particles $\ll 1 \mu\text{m}$ diameter. The pronounced differences in grain size spectra between the Cologne and Fuessenich sites can be revealed by SEM. Cologne needle surfaces exhibit a high particle density (Fig. 10a,b) characterised by aggregates up to $30 \mu\text{m}$ in size and an equal abundance of fine particles. Needle surfaces at the Fuessenich site show a much lower particle density with isolated large organogenic fragments and multiple fine particles preferentially derived from anthropogenic sources (Fig. 10c,d). A synthesis of variation in atmospheric particulate grain size deciphered by application of enviromagnetic techniques is presented in a schematic diagram given in figure 10e.

2.1.5 Conclusions

The six locations studied, each characterised by a distinctive emission pattern, reveal diagnostic and consistent pine needle enviromagnetic signatures and concentrations. Triplicate analyses of needle cohorts taken at each location indicate inter-site variability exceeds intra-site variation as confirmed by statistical analyses employing the Kruskal-Wallis- H test. This is a prerequisite for selecting passive vegetation samplers with inherent natural variability for environmental biomonitoring. Accumulation histories for magnetic PM were found to be systematic and reflect exposure to environmental pollutant load. Accumulation reaches a state of equilibrium due to canopy effects and PM removal via wax degradation after 26 months of needle exposure time. For spatially resolved data sets to map air quality it is recommended to collect needles at least 8 months old or to gain composite samples spanning an exposure time of 8 months to needle senescence. Grain size distribution can be assessed via enviromagnetic techniques employing susceptibility and remanence data and combinations thereof. In contrast to optical methods, enviromagnetics allow identifying the presence and quantity of fine to ultrafine PM. The relative grain class distribution may guide source identification or allocation and differentiation of most prevalent transportation processes. Spatially and temporally highly resolved analysis of hazardous atmospheric particulates is of paramount importance. Enviromagnetic biomonitoring offers a high-resolution and cost-efficient technique for the assessment of particulate atmospheric pollution, especially by covering the most health-sensitive fine to ultrafine particle classes.

2.2 Accumulation histories of major and trace elements

Atmospheric pollution comprises a serious threat to human health and behaviour of atmospheric pollutants requires ongoing investigations [49, 256]. Processes of emission, transport and dispersal, reactivity and natural attenuation of atmospheric pollutants are investigated by laboratory experiments, modelling and study of real-world concentrations determined by active air sampling or utilization of passive samplers. Biomonitoring is a now well established technique [239] in atmospheric pollution studies and allows obtaining temporally and spatially highly resolved data in a time-integrative manner. One of the most important advantages of biomonitoring lies in the acquisition of time-integrated records of air quality, provided that the accumulation behaviour of the plant biomonitor is adequately known and understood. The accumulation behaviour of magnetic particulates in the Greater Cologne Conurbation was studied by environmental magnetic techniques previously [126], which enable the recognition of fine to ultrafine particulates. These result from high-temperature combustion processes that are of great environmental concern due to their easy respiratory uptake. The technique, however, is unsuitable for the investigation of non-magnetic particulates, which requires the analyses of a wider suite of elements in plants originating from a variety of different processes.

In general elements in plants can be attributed to biogenic, lithogenic and anthropogenic sources [11] and may be differentiated due to the following criteria: Elements exceeding the essential element concentration in pine needles may be attributed to additional uptake via soil or bedrock enriched in certain elements or to atmospheric wet and dry deposition. Source apportionment can be achieved by analyses of element concentration in soil/bedrock and plant and calculation of enrichment factors [11, 211]. Elimination of elements associated with dust particles loosely attached to the needle surface is achieved by washing in distilled water [154, 63]. Identification of anthropogenic versus lithogenic contributions or dust loadings is done by calculating enrichment of selected elements versus average dust composition using reference elements [11, 211]. Dust composition is either determined by collection of dust particles in the study area and determination of element concentrations or by using globally averaged dust elemental composition [150]. A variety of source indicator elements have been identified and the preferred mode of emission from anthropogenic activities has been compiled [179]. The knowledge that certain indicator elements are most informative for pollution studies allows a reduction in the number of critical elements to be studied.

Environmental biomonitoring frequently aims towards identification of spatial or temporal variations in critical element loads and thus requires knowledge on accumulation histories of pollutants in needles or leaves of perennial plants. Sampling of different needle cohorts and repetitive sampling over the growing season allows identifying seasonal effects, approach of equilibrium concentrations and degradation or detoxification processes. Pine needle element loadings have been studied for several needle ages and a systematic increase in element concentrations was observed for non-washed [200, 71, 212, 254] and washed samples [154, 63].

Here, a detailed pollutant accumulation study of *Pinus nigra* needles up to 5 years in age, collected separately to represent summer and winter concentrations for the

environmentally relevant elements Ba, Ca, Cd, Fe, Mo, Na, Pb, Sb, Ti, V, Zr, and rare earth elements (REE) is presented. Pines were sampled at six different locations selected according to highly different emission scenarios. Results discussed in this chapter have been published by Lehdorff and Schwark [125].

2.2.1 Sampling methods

The study area of the Greater Cologne Conurbation has been described in detail in a previous publication [126] and thus only the most important characteristics are summarized here. The six stations selected for investigating the accumulation behaviour of major and trace elements on pine needles were chosen to represent natural background and exposition towards region-specific anthropogenic emission sources (Table 1). Sample collection procedures are specified in Lehdorff et al. [126] and aimed towards exclusion of local point sources, differentiation between summer versus winter seasonal effects and recovery of maximum number of needle age classes (3-5). For analysis of major and trace elements 51 samples were obtained from the six locations studied.

2.2.2 Analytical Methods

Elemental analysis Freeze-dried needles were ground to <0.4 mm in a swing mill (Siebtechnik) prior to analytical work up. A total of 35 elements were determined by Activation Laboratories, Canada employing hot aqua regia digestion followed by high resolution inductively coupled mass spectrometry (HR-ICP-MS). The following 11 elements (Ba, Ca, Cd, Fe, Mo, Na, Pb, Sb, Ti, V, Zr) and 15 rare earth elements (Table 32 in appendix) were selected for discussion of biogenic, geogenic, and anthropogenic sources. Quality assurance was carried out by analysis of standard reference material NIST 1575a yielding the following recoveries: Ba (108%), Ca (106%), Cd (90%), Fe (106%), Na (121%), Mo (119%), and Pb (92%). Concentration values suggested for Sb and V in NIST 1575a were met with a recovery of 74% and 51%. Replicate analyses of three samples for elements Ba, Ca, Cd, Fe, Pb, Sb, V, Mo, Na, Ti, Zr, and REE gave a standard deviation <9%.

Enrichment factors The dust component of aerosols deposited on plant surfaces is quantitatively important, and although dust loads on pine needles may result from human activities like mining, the dust fraction has to be discriminated from anthropogenic and/or biogenic element contribution. This is often achieved by calculation of enrichment factors (EFs) whereby the EF usually represents the non-geogenic derived part of an element. Various types of EFs have been used in environmental monitoring [211, 253]. The most commonly applied calculation of the EF relies on the normalization of the element of interest to the geogenic background concentration:

$$EF = \frac{(C_x/C_{\text{reference element}})_{\text{biomass}}}{(C_x/C_{\text{reference element}})_{\text{geogenic background}}} \quad (1)$$

Hereby, the geogenic background may be defined as local/regional soil or bedrock [258] or as the average global dust composition [11, 86]. The latter is taken as being

equivalent to the composition of upper continental crust (UCC) or average shale as compiled in the literature [150].

Incompatible elements in UCC that are least affected by weathering, provenance and sorting during transportation are the REE, Th and Sc. Due to the often very low concentration of these elements in bioaccumulated dust, elements like Al or Si occurring at higher concentrations, have been used for normalization [11]. Concentrations of Al and Si are notably affected by biological processes in plants and soils and thus are not recommended for application as reference elements in biomonitoring [86].

Investigations by Wyttenbach et al. [283] and Tyler [253] demonstrate that REE are perfectly suitable as reference elements in biomonitoring studies due to their high incompatibility and low emission rates in anthropogenic processes. Thus, the summed REE concentrations (La, Ce, Pr, Nd, Sm, Eu, Gd, Tb, Dy, Ho, Er, Tm, Yb, Lu, and Hf) of UCC reported in McLennan [150] were employed for normalization of element concentrations.

Statistical analyses Data were analysed statistically using SPSS 12.0 for Windows. Nonparametric analysis of variance was performed by the Kruskal-Wallis- H test to identify significant variations between the 6 sampling sites ($n = 12$). Normal distribution of sample populations ($n = 51$) was tested by the Kolmogorov-Smirnov procedure. Factor analysis (FA) was based on data of separated needle ages, excluding 3 months old needles ($n = 45$). The FA was operated with following parameters: extraction method = principal component, extraction analysis = correlation matrix, rotation method = varimax.

2.2.3 Results

Element concentrations The highest total concentrations in pine needles were measured for Ca (1.5 - 12.1 g kg⁻¹) followed by Fe (32 - 350 mg kg⁻¹), Na (2 - 676 mg kg⁻¹) and Ba, Ti, Pb (0.1 - 4.5 mg kg⁻¹). Mo, Sb and REEs varied between 20 to 1000 µg kg⁻¹, and Cd and Zr only reached 5 to 300 µg kg⁻¹ (Fig. 11; Table 32 in appendix). Based on weighted average concentrations of elements for each location the highest loadings on pine needles were observed in Cologne for Fe, Na, Pb, Sb and Zr, in Bedburg for Ba, Cd, Ti, V and REE, in Bergisch-Gladbach for Ca and in Dormagen for Mo (Table 4). The variation between sites was significantly higher than within sites as demonstrated by the H values exceeding the $H_{critical}$ values of the Kruskal-Wallis- H test (Table 5a).

Concentrations of all elements except for Cd and Mo increased continuously with time of exposure (Fig. 11; Table 32 in appendix). For cadmium notably higher concentrations were determined for Bergisch-Gladbach and Bedburg (Fig. 11). Molybdenum concentrations were elevated in Dormagen and to a minor extent in Cologne. The concentration of antimony was particularly high in Cologne and the loadings of Fe, Ti, V and Zr were notably the above average of the remainder elements in Cologne and Bedburg.

Superimposed on the general increase of element loads with needle age is a trend to notable variability between summer and winter samples. This trend is most pronounced for Pb, showing diminished concentrations in winter for Fuessenich and Bergisch-

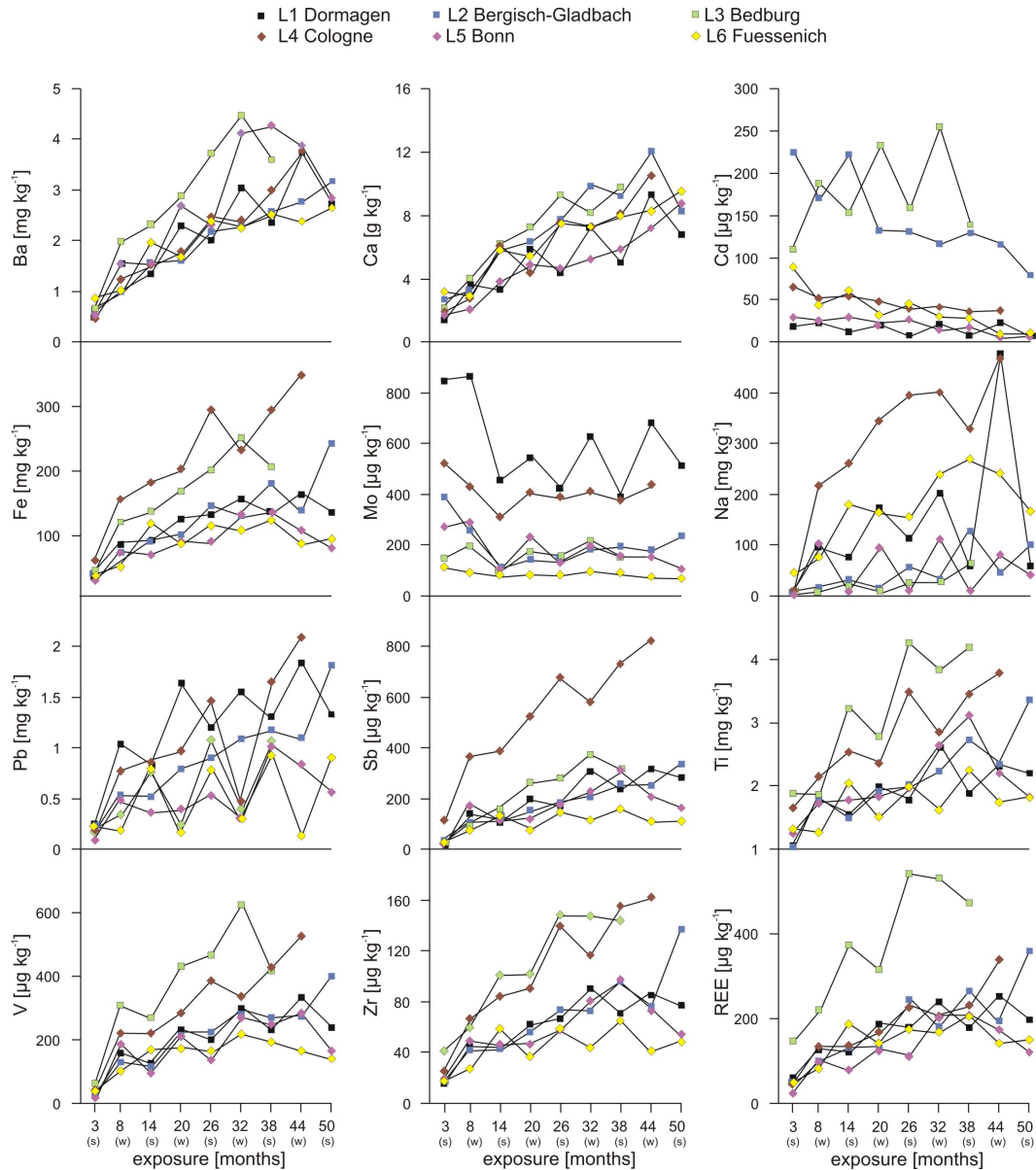


Figure 11: Element concentrations of *Pinus nigra* needles from the Greater Cologne Conurbation versus exposure time in months. Needle cohorts exposed for 3, 14, 26, 38, and 50 months were taken in summer 2004, those exposed for 8, 20, 32, and 44 months were collected in winter 2004.

Gladbach, but quite the opposite behaviour for Dormagen (Fig. 11). These opposing trends are also recorded to a minor extent for Ti, Zr and REE at locations Fuessenich and Dormagen. Furthermore, mirror images between summer and winter concentrations for elements may occur at individual stations. In Bedburg cadmium shows exceptionally high values in winter samples whereas lead reveals highest loads for summer samples (Fig. 11).

For the Bedburg location significantly above average concentrations of REE were observed, which are related to a significant dust component. In order to facilitate a comparison of element loadings on pine needles independent of geogenic dust contri-

loc.	Ba [mg/kg]	Ca [g/kg]	Cd [μ g/kg]	Fe [mg/kg]	Mo [μ g/kg]	Na [mg/kg]
L1	1.94	4.65	16.7	111	612	114
L2	1.81	6.84	154	115	198	38.8
L3	2.64	6.43	179	154	164	21.2
L4	2.00	5.99	48.3	213	416	298
L5	2.35	4.14	22.4	86.5	200	54.6
L6	1.74	5.50	46.0	87.8	91.1	152

loc.	Pb [mg/kg]	Sb [μ g/kg]	Ti [mg/kg]	V [μ g/kg]	Zr [μ g/kg]	REE [μ g/kg]
L1	1.17	175	1.84	188	56.9	156
L2	0.81	166	1.96	196	60.8	164
L3	1.93	202	2.96	354	99.4	328
L4	3.37	502	2.71	290	100	158
L5	2.09	155	1.96	168	54.2	114
L6	1.34	100	1.66	144	41.8	135

Table 4: Element concentrations shown as weighted means for each location (2 x 4-5 needle generations; $n \leq 9$; maximum concentrations in bold).

butions the absolute concentrations were normalized to upper crust concentrations.

Element enrichment factors Normalized element concentrations (EFs) are presented in Table 6 and Table 32 in the appendix. The highest EFs are noted for Fe, Na, Sb, V, and Zr at the Cologne location, followed by highest EFs for Ba, Ca, Ti, and Zr in Bonn, Mo and Pb in Dormagen, and finally Cd in Bergisch-Gladbach. Normalization to UCC notably changed the pattern of highest element loadings with Bonn not contributing a maximum for absolute element concentrations but several for EFs (Table 4 and 6). The highest EFs were determined for antimony, followed by cadmium

a)	H	p	H_{crit}	b)	H	p	H_{crit}
Ba	6.15	0.29	6.06	Ba EF	10.08	0.07	9.24
Ca	7.46	0.19	7.29	Ca EF	7.38	0.19	7.29
Cd	10.00	0.08	9.24	Cd EF	9.31	0.10	9.24
Fe	10.23	0.07	9.24	Fe EF	9.85	0.08	9.24
Mo	10.08	0.07	9.24	Mo EF	10.54	0.06	9.24
Na	8.62	0.13	7.29	Na EF	10.08	0.07	9.24
Pb	1.92	0.86	1.61	Pb EF	8.69	0.12	7.29
Sb	9.15	0.10	9.24	Sb EF	10.46	0.06	9.24
Ti	8.23	0.14	7.29	Ti EF	9.00	0.11	7.29
V	7.62	0.18	7.29	V EF	5.77	0.33	4.35
Zr	9.92	0.08	9.24	Zr EF	9.92	0.08	9.24

Table 5: Nonparametric analysis of variance performed by Kruskal-Wallis- H test for a) element concentration and b) enrichment factors ($df = 5$). H -values for all elements show that variation between locations are higher than data variability at one sampling site.

loc.	Ba	Ca	Cd	Fe	Mo	Na	Pb	Sb	Ti	V	Zr
L1	3.4	148	160	3.1	392	3.7	54	840	0.6	3.0	0.3
L2	3.1	214	1440	3.0	122	1.2	38	775	0.6	3.1	0.3
L3	2.2	95	835	2.0	50	0.3	11	454	0.4	2.7	0.2
L4	3.1	174	450	5.3	248	8.6	41	2149	0.8	4.1	0.4
L5	5.6	188	321	3.3	176	2.1	31	1029	0.9	3.5	0.4
L6	3.5	204	516	2.8	68	5.9	24	555	0.6	2.7	0.3

Table 6: Element enrichment factors versus upper continental crust given as weighted means for each location (2 x 4-5 needle generations; $n \leq 9$; maximum concentrations in bold).

with values showing a 1000-fold increase versus UCC. Enrichment by several hundred was noted for molybdenum and calcium, whereas lead was enriched versus UCC by a factor of 50. The elements Ba, Fe, Na, and V yielded minor EFs between 1 and 5. EFs of less than unity were determined for titanium and zirconium. Variability of EFs between sites was significantly higher than within sites as shown by application of the Kruskal-Wallis- H test (Table 5b).

Figure 13 shows the enrichment factors for all elements versus needle exposure time. Exclusion of the geogenic background highlights the anthropogenic pollutant load which except for sodium differs strongly from the accumulation trend observed for the concentration data (Fig. 11). In contrast to increasing absolute concentrations with exposure time, EFs for elements Ba, Ca, Fe, Na, Pb, Sb, V, and Zr remain quasi-constant over exposure time (Fig. 13). For elements Cd, Mo, and Ti a strong decrease in EFs is noted for the 3 months old needles. Inter-site variability was most pronounced for Sb, showing extreme enrichment in Cologne, whereas Ba yielded highest EFs for the Bonn location (Table 5b, Fig. 13). Iron showed extreme enrichment for the Cologne site and for Bedburg a notable depletion versus all other sites (Fig. 13). Moderate enrichment was noted for the elements cadmium in Bergisch-Gladbach, and sodium and zirconium in Cologne.

In comparison to seasonal variations in absolute element concentrations the EFs reveal enhanced variability in particular for V, Fe and Zr, but diminished changes for Ba, Ti, Mo, and Cd (Fig. 13).

Factor and regression analysis In order to discriminate source differences factor analysis was carried out using EFs leading to the definition of four groups, which explain 82% of the variance in the data set (Table 7). The first factor carries high loadings for Sb, Fe, Zr, and V, the second factor for Ba and Ti, the third for Pb and Mo and the fourth factor for Cd. The elements Ti and Na bear similar but moderate loadings on factors 1 and 2 and 1 and 4, respectively.

Within factor 1, explaining 36.5% of total variance, the element with the highest EF is Sb (Fig. 12), whereas Fe and V show only moderate to minor enrichment or in the case of Zr even a depletion versus UCC. The EF fingerprint of factor 1 reveals higher seasonal variability for Na and Fe, whereby the trends between summer and winter enrichment are opposite (Fig. 3). Factor 2 gives a notable enrichment of Ca but only moderate variability for Ba. The 3rd factor reveals notable EFs for Mo and Pb with no systematic influence of seasonal variations. The 4th factor represented exclusively by

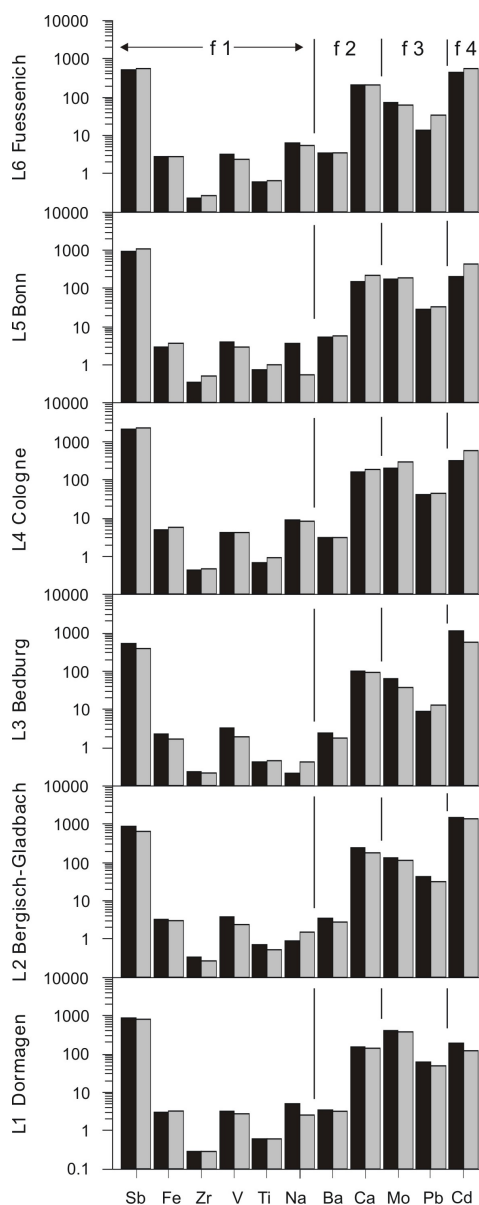


Figure 12: Element enrichment factors for summer and winter samples at each location. Elements are sorted according to their association with the four most critical loading factors obtained by factor analysis.

Cd showed very high enrichment and marked seasonal variability. Locations Dormagen, Bergisch-Gladbach and Bedburg are characterized by higher EFs for the summer, whereas higher EFs for winter were determined for Cologne, Bonn and Fuessenich (Fig. 12).

2.2.4 Discussion

Source recognition via absolute element concentrations Major and trace elements in atmospheric particles accumulating in plants can be broadly attributed to geogenic sources (Al, As, Co, Cr, Cu, Fe, Mn, Ni, Pb, Si, Sc, Th, Ti, V, and REE),

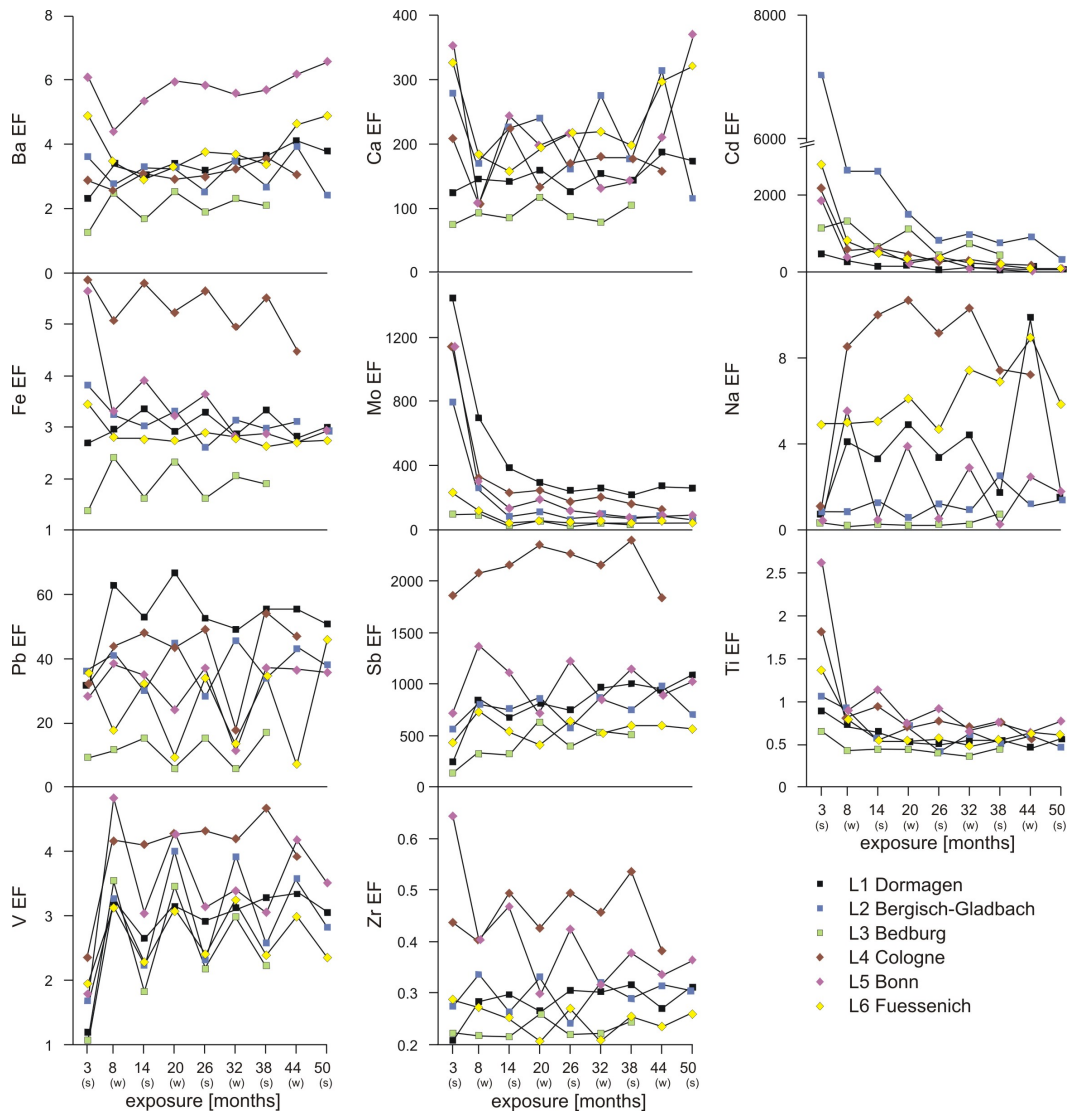


Figure 13: Element enrichment factors versus average upper continental crust composition for *Pinus nigra* needles from the Greater Cologne Conurbation versus exposure time in months. Needle cohorts exposed for 3, 14, 26, 38, and 50 months were taken in summer 2004, those exposed for 8, 20, 32, and 44 months were collected in winter 2004.

biogenic sources (Ca, K, Mo, P, Se, Zn) and anthropogenic sources (Ag, As, Cd, Cu, Hg, Mo, Ni, Pb, Se, V, Zn) as compiled by Bargagli [11]. Several elements will have to be partitioned between these groups depending on the degree of anthropogenic utilization. Particles of geogenic origin often form the nucleus for adsorbing elements of anthropogenic origin and, consequently, covariance between lithogenic and anthropogenic elements will occur [276].

The absolute concentration data point towards a strong tendency for accumulation of particulates with geogenic origin as revealed by the continuous increase in REE loads on pine needles. This is confirmed by similar behaviour of typical geogenic elements including Ti, V, Zr, and Fe (Fig. 11). The highest absolute concentrations of geogenic elements occurred at the Bedburg location, an area that is most heavily influenced by

open pit lignite mining, associated dispersal of wind-blown dust from the open mines, transport of excavated materials, mine tailings and emissions from lignite-fuelled power plants. The lithogenic dust component from mining operations was not detected by environmental magnetic techniques [126] due to the low level of susceptibility exerted by geogenic minerals when compared to combustion-derived magnetite.

Parallel concentration patterns of Ti, V, Fe, and Zr relative to REE occurred for the Cologne location (Fig. 11) but are assumed not to be exclusively of geogenic origin. For REE no increase in concentration at the Cologne site was observed.

The cadmium concentrations in Bedburg are three times higher than in Cologne and attributed to dust dissemination during mining operations. Comparably high cadmium concentrations are noted for the Bergisch-Gladbach location and here can be explained by blow-out of dust from old Pb/Zn-mine tailings and soil abundantly occurring in the Rhenic Massif. Similar Cd-loadings on pine needles have been observed for the Stolberg mining district 70 km west of the Bergisch-Gladbach location [250].

Elements typically associated with industrial or petrochemical emissions are Pb and Mo [179, 23]. Pine needles showed especially high loadings at the Dormagen site, which is surrounded by a refinery complex. Surprisingly, the concentration of vanadium, an element typically associated with refinery operations [23, 210] is not notably higher at the Dormagen site (Fig. 11).

The element lead in the past was preferably associated with traffic emissions, but due to the passing out of leaded gasoline nowadays may no longer serve as traffic indicator. Alternatively, other elements have been suggested as traffic emission markers, in particular barium [155] and antimony [41, 210]. Whereas antimony concentrations confirm the high traffic emissions at the Cologne site, as indicated by environmental magnetic results [126], the absolute concentrations of barium can not be related to traffic sources (Fig. 11).

When associated with pine needles, calcium may originate from the carbonate component of atmospheric dust particles or as essential element may be of biogenic origin. Plants and especially conifers are known to accumulate large amounts of calcium in the form of Ca-oxalate crystals [59]. In order to discriminate between these two potential major sources the differentiation of dust-derived and biogenic contribution may be achieved by discussion of enrichment factor of elements versus UCC signature.

Source recognition via enrichment factors The absolute element concentration data served to identify the importance of wind-blown dust of average crustal composition in particle accumulation on pine needles. Incompatibilities in absolute trace element distribution between locations and site-specific concentration maxima for selected elements already pointed towards other anthropogenic or biogenic sources for needle associated elements. Differentiation of such additional sources is facilitated by interpretation of enrichment factors, which after deduction of the dominant dust component enhance the signal derived from alternate sources.

Statistical treatment of data set reveals that the EFs can be allocated to 4 factors, which will here be discussed in detail.

The highest loadings on factor 1 responsible for 36.5% of variance in the data were determined for the elements Sb and Fe, followed by Zr and V. Antimony almost exclusively is related to traffic emission sources, whereas for Fe, Zr, and V multiple sources

	f 1	f 2	f 3	f 4
Sb	0.94	-0.04	0.18	-0.14
Fe	0.94	0.01	0.20	-0.08
Zr	0.88	0.22	0.23	0.04
V	0.78	0.14	0.13	-0.06
Ti	0.62	0.52	0.27	0.28
Na	0.60	-0.10	0.01	-0.60
Ba	0.06	0.91	0.06	-0.18
Ca	0.07	0.82	-0.10	0.00
Mo	0.22	-0.13	0.88	-0.06
Pb	0.23	0.11	0.85	-0.09
Cd	0.01	-0.16	-0.14	0.91
% variance	36.5	17.3	15.8	12.1

Table 7: Factor analyses of element enrichment factors performed on separate needle cohorts excluding the youngest age ($n = 45$). The FA was performed with principal components and varimax rotation. Loadings >0.75 are given in bold and the relative percentage of variance explained by each factor is indicated.

have to be considered. Normalization on UCC removes potential interference from a geogenic source, albeit small due to the low abundance of Sb in geogenic materials [150]. Antimony does not serve as an essential element for plants [11] and is not biologically enriched in needles. Elevated Sb concentrations almost exclusively derive from anthropogenic input, whereby it has only limited technical applications. Major utilization of antimony is in brake linings, which may contain 20-70 g kg⁻¹ SbS₃ [64, 244, 90] and in wheel balance weights [207]. Sb may also originate from combustion residue of gasoline and diesel fuels [95, 264].

Pine needle concentration of iron may be attributed to i) a biogenic fraction as iron is an essential element for plants, ii) lithogenic sources, which are excluded when calculating EFs, and iii) anthropogenic sources. The biogenic Fe fraction was suggested to contribute about 50-70 mg kg⁻¹ of the total iron load based on regression of Fe concentration versus the SIRM-values of pine needles in Cologne [126]. This is in agreement with the estimates of the essential element concentration in pine needles [11, 71]. The lithogenic derived iron in pine needles is recognized by the good correlation of Fe and REE concentrations (Fig. 11). A comparison of Fe concentrations and Fe enrichment factors versus exposure time (Fig. 11 and 13) reveals that the steady increase over time is removed by normalization. This indicates that accumulation of geogenic dust and anthropogenic-derived Fe proceeds at the same rate, most likely due to sorption of ultrafine Fe-spheroids to coarse dust particles. Enrichment factors for urban locations Cologne and Bonn are the highest observed in the data set and agree with a predominantly traffic-related accumulation of iron on pine needles. The traffic-derived Fe-fraction consists preferentially of ultrafine superparamagnetic magnetite particles formed during high temperature combustion processes [126].

The zirconium concentrations and EFs of pine needles behave very similar to the Fe-content. Again a notable portion derives from lithogenic dust, but normalization of Zr concentration to UCC shows that the traffic-polluted locations Cologne and Bonn show

the highest Zr-enrichment. This is attributed to zirconium from brake-wear, which may comprise up to 25 g kg^{-1} by weight [64, 135]. Enrichment factors for zirconium <1 can be attributed to a Zr-lean shale-dominated geogenic source and to the intensive sorting fractionation of zirconium [150].

The contribution of vanadium to factor 1 is notably smaller than for Sb, Fe and Zr (Table 6) and thus vanadium may originate from mixed sources but still be bearing a significant traffic signature. It is well established that V is enriched in petroleum and released from refinery operations [23] and that concentrations in asphalt paving are high [130]. The association of V with a traffic source thus results from asphalt degradation rather than from fuel emissions.

The highest loadings for titanium and sodium are noted for factor 1, thus indicating a traffic related source but the low loading values of 0.62 and 0.60 point to major contributions from other sources. The concentrations and the EFs for sodium show a marked increase for the winter samples (Fig. 11, 13) and thus a substantial proportion of the sodium loads on pine needles will originate from salt applications for deicing purposes in winter time. Sodium associated with road dust will be transferred to pine needles by enduring resuspension in the winter period. Self-detoxification and utilization of Na as essential element during the summer period induce the annual cycling of Na in traffic exposed locations. The less pronounced annual cyclicity noted for locations Cologne and Fuessenich is attributed to the application of Na-based fertilizers preferentially during the summer growth period that will enhance the overall Na-concentration and EFs.

The high loadings of titanium on factor 1 can be attributed in part to a lithogenic component as already noted for Fe and Zr. In addition Ti may derive from traffic associated emissions, especially from the use of Ti in brake linings [244, 135] that may contain up to $200 \text{ g kg}^{-1} \text{ TiO}_2$ by weight.

Based on the enrichment factors obtained, only antimony shows an exclusively traffic-related accumulation character with EFs exceeding a value of 1000 (Fig. 12). The other 5 elements associated with the traffic related factor remain at values less than 10. Several authors do regard EFs smaller than 10 as not significant [86].

The second factor obtained by statistical analyses explains 17.3% of the total variance and shows high loadings of Ba and Ca and a minor contribution by Ti (Table 6). Calcium shows concentrations of 2 to 12 g kg^{-1} which is within the range reported for biogenic Ca-concentrations in pine needles [11, 154]. The enrichment factors for Ca are exceptionally high with values of 80 to 380 (Fig. 13, 12), which supports a preferential origin from biogenic sources. This is despite the fact, that a considerable proportion of average dust is composed of carbonate minerals [150]. Calcium accumulation over time in pine needles preferentially occurs in the form of Ca-oxalate crystals. Uptake of calcium by plants occurs via the root system and by wet atmospheric deposition onto needles or leaves. Self-detoxification for calcium as well as oxalate by conifers operates via isolation and accumulation of Ca-oxalate in crystal idioblasts rather than excretion. Ca-oxalate in conifers may thus comprise up to 800 g kg^{-1} by weight of the total inorganic element concentration [59].

Barium has been suggested to serve as traffic indicator element especially after the phase out of lead as gasoline additive [155]. It is known that barium concentrations of up to 100 g kg^{-1} by weight may occur in brake linings and a similar curve shape is

noted for Ba and Sb accumulation (Fig. 11). A major difference in the distribution is evident for the Cologne and Bonn locations, the former yielding by far the highest concentration for Sb the latter yielding the highest concentrations for Ba (Fig. 11). Barium partly originates from wind-blown dust due to lignite mining operations as seen in the accumulation curves similar to those of the REE. Normalization of barium concentrations to UCC indicates that enrichment is similar at all location except for Bonn (Fig. 13). The much higher EF for barium in Bonn does not correspond to a much higher EF in Cologne. In Cologne a strong traffic related emission was noted by several parameters and thus it is surprising that EFs for barium are twice as high in Bonn when compared to Cologne, whereas EFs for antimony are twice as high in Cologne when compared to Bonn (Fig. 13). As both elements preferentially originate from brake wear this contradictive distribution patterns point to additional factors influencing the barium concentration in pine needles and argues for a cautionary application of Ba as traffic indicator element. The very high abundance of calcium in needles may affect barium concentrations as similar geochemical behaviour allows Ba to substitute for Ca. Given the large concentration differences by a factor of about 2500 between Ca and Ba, a part of the Ba concentrations may arise from Ba substituting in dust-derived carbonate minerals or biogenic calcium oxalates. Similarities between average dust or UCC and barium accumulation (Fig. 11) may relate to the fact that abrasion of road pavement releases substantial proportions of barium into the atmosphere.

Factor 3 derived from the statistical treatment explains 15.8% of the total variance and combines the two elements molybdenum and lead, which after the phase out of lead as fuel additive relate to industrial processes. The high concentrations of Mo and Pb at the Dormagen site point to an input from the nearby petrochemical plant. Molybdenum concentrations at the Dormagen site are 8 times higher compared to the rural Fuessenich location. Mo is in use as catalyst in fluidized catalytic cracker units (FCCU, [273]). Petrochemical processing usually also emits higher quantities of V and Fe but this source-specific signature is obscured by traffic emissions. The EFs for Mo and Pb reach several hundreds at the Dormagen site whereas they comprise less than 50 at the rural locations (Fig. 13). This high range in EFs indicates that molybdenum at the Dormagen site is specifically emitted by point sourcing from the petrochemical site. Moderately elevated EFs are also noted for the sites Bonn and Cologne, where most of the emissions may relate to traffic, known to contribute Pb and Mo [86, 210]. The EFs for Pb maximize around 60 for the Dormagen location but still vary around minimum values of 10 for the least polluted site. This may indicate that traffic-sourced lead though banned as anti-knocking agent for decades is still recycled in the atmospheric deposition, as noted in other regions [155]. In addition, lead is one of the elements most prone to long distance atmospheric transport [241] and a notable proportion of the lead enrichment on pine needles in traffic and industry lean areas may have to be attributed to atmospheric import.

The last factor obtained by statistical analyses explains 12.1% of the total variance and is exclusively controlled by cadmium abundance. This element commonly derives from industrial processes and from combustion of fossil fuels, including coal and heavy oil [179, 86]. Cadmium concentrations are particularly high at Bedburg and Bergisch-Gladbach locations with values between 100 and 250 $\mu\text{g kg}^{-1}$, whereas the other stations range between 1 and 50 $\mu\text{g kg}^{-1}$ (Fig. 11). It is of particular im-

portance to note the strong seasonal pattern in cadmium concentrations. Cadmium is an element often associated with long residence time in atmosphere and long-distance transportation [241]. In temperate Europe cadmium is commonly precipitated by wet deposition and shows elevated concentrations in the summer period [158]. This is observed for all stations except for Bedburg, where a strong concentration increase in winter is related to shorter transportation distance of particle bound cadmium in cold air. Main emittents are the nearby lignite-fueled power plants. The inverse deposition scheme has been noted in environmental magnetic investigations [126]. Considerably elevated concentrations of cadmium occur in Bergisch-Gladbach, located in the eastern part of the Rhenic Massif, which is known for its lead/zinc-ore mining history. Natural background of cadmium in soils and bedrock is enriched and numerous old mine tailings favour wind-blown dispersal of Cd-enriched particles. The EFs for Cd are extremely high in the strongly affected location exceeding values of 100 in the first year needles. In a similar environment, the Stolberg mining district of the Eifel Mountains, concentrations of 7.6 mg kg^{-1} Cd have been found on 1-year needles [250]. A strong decline in the EFs over time may be associated with a pronounced self-detoxification capability of pines [11, 59].

Feasibility of *Pinus nigra* needles for biomonitoring Previous investigations have demonstrated that unwashed [200, 71, 212, 254] and washed [154, 63] needles of various pine species record air quality. Both washed and unwashed pine needles reveal a systematic increase in element loads with time, whereby the first year's needle often exhibit aberrantly low concentrations. It is thus recommended to omit the first year needles from biomonitoring studies. In this study samples were separately collected in summer and winter, thus enabling an assessment of seasonal influence on pollution loads. Individual elements showed enhanced or depleted seasonal concentrations and also opposite trends for individual locations. In order to account for such variations sampling should either be carried out seasonally or if reduction in sample number is required, seasonal composites should be prepared. The noted seasonal variability is attributed to needle surface abrasion and self-detoxification processes, whereby a notable decline in element concentration with needle age was observed exclusively for cadmium. For spatially resolved sampling programmes composites of one to three year old needles will provide a sufficiently time-integrated signal best representing local air quality. Normalization to UCC eliminates the accumulation effect over time, as anthropogenic pollutants will be deposited on needles at rates equal to lithogenic dust, but notable differences in enrichment factors allow improved recognition of site-specific emission scenarios.

2.2.5 Conclusions

Accumulation of major and trace elements in *Pinus nigra* needles studied over a period of 50 months occurred in a systematic manner, confirming the established utilization in passive biomonitoring of atmospheric pollution.

Identical results for major and trace element patterns when compared to environmental magnetic studies are observed for accumulation of atmospheric particulates on pine needles.

Sampling strategies in *Pinus nigra* biomonitoring studies should account for seasonal variability and aberrant element loads in young needles by preparation of needle age composites. Composite samples provide a time-integrated and site specific reflection of air quality, suitable for generating maps at high spatial resolution, which allow recognition of pollution hot-spots and pollution pathways.

Trace elements most reliable as source indicators for six sites in the Cologne Conurbation area were REE for lithogenic dust, Sb, Fe, V for traffic (including combustion and abrasion), Mo and Pb for petrochemical emissions, and Cd preferentially from mining activity. Barium, frequently applied as traffic indicator element was not recognized to be preferentially traffic controlled in the Greater Cologne Conurbation.

2.3 Accumulation history of airborne phenanthrene derivatives

Polycyclic aromatic hydrocarbons (PAH) comprise an important group of atmospheric pollutants that originates from a multitude of emission sources. Despite their known adverse health effects, long persistence and high atmospheric concentrations PAH are still unregulated. Numerous studies have investigated the sources, distribution and accumulation of PAH in soils, sediments and the atmosphere, many of those employing biomonitoring techniques. Commonly, out of the wide suite of PAH present the sixteen parent PAH specified in the EPA priority list are measured. Large differences in physicochemical properties of PAH do regulate their preferred mode of transportation and (re)deposition. For source recognition of PAH several diagnostic ratios of individual PAH are employed that are significantly controlled by differences in physicochemical properties. It is thus recommended to use individual PAH of similar properties in such ratios only [287], to minimize bias by transport fractionation. Three ring PAH and alkylated analogues comprise a very significant proportion of fossil fuel based combustion stock. Diesel fractions obtained upon petroleum distillation may contain up to 30% alkylated phenanthrenes and the proportion of unburned diesel fuel that is emitted from diesel engines may be up to 1.2%, consisting preferentially of three-ring PAH [272, 144, 214, 203].

In combination with emission of three-ring PAH during transportation and handling this contributes a substantial amount of PAH to the atmospheric pollution load. Biomonitoring studies generally have identified three-ring PAH as the most abundant atmospheric PAH [249, 61, 127, 96, 123, 37, 164]. Most studies on atmospheric PAH concentration and distribution do not or only partially consider alkylated PAH. Based on the large amounts of alkylated three-ring PAH emitted by anthropogenic processes, however, a study of these compounds seems warranted.

Source identification and allocation based on parent PAH is limited due to the low number of components used for differentiation. Utilization of alkylated analogues may improve the potential for source discrimination. The degree of alkylation has been proposed to serve as indicator for discriminating combustion from petrogenic emissions [226, 287, 129, 139], whereby combustion is characterized by a low degree of alkylation. Source allocation based on individual three-ring PAH compounds preferentially utilizes monomethyl-, dimethyl/ethyl-phenanthrenes (MP, DMP), 1-methyl-7-isopropyl-phenanthrene (retene) and cyclopenta[def]phenanthrene (CPP) also referred

to as 4,5-methylenepheneanthrene. Alkylated anthracenes are restricted to 2-,1-, and 9-methylanthracene, which in general have a low source-diagnostic potential. Thus, in the following the focus is set on the discussion on phenanthrene derivatives.

The ratio of 2/(2+1)-MP or (3+2)/(9+1)-MP is employed as traffic indicator [65, 40] and may possess some potential for discrimination of gasoline and diesel fuels [193]. Ratios of especially 1,7/(1,7+2,6)-DMP have been employed to differentiate wood combustion from traffic emission [15, 215, 119]. This is based on the assumption that the 1,7-isomer is a degradation product of retene, which preferentially originates from plant resins. Retene-based ratios for identification of wood combustion were established by Ramdahl [198] and applied in various studies [15, 225, 228, 86]. The origin of CPP is thought to be mainly traffic related [201, 225, 84, 72] though other combustion processes may not be excluded.

Whereas studies including the suite of alkylated phenanthrene isomers in air are rare, their concentration and distribution on plant biomonitors are even scarcer [96]. In this study the suitability of alkyl-substituted phenanthrenes to serve as biomonitoring indicators for atmospheric pollution and source discrimination is investigated.

The amount and fingerprint of alkylphenanthrenes primarily sorbed to pine needles and the processes leading to their accumulation over time will to a large extent be controlled by their physicochemical properties and transport behaviour. Based on the wide range of octanol/air partitioning coefficients for PAH these components occur preferentially in the gas phase, if the number of rings is three or less and almost exclusively particle bound, if the number of aromatic rings exceeds four [227]. The water solubility of PAH is low and in concert with their bioavailability decreases with mass and degree of alkylation.

The three-ring PAH and their substituted derivatives preferentially occur in the gas phase though sorption to ultrafine particles is noted especially for combustion sources. The water solubility and octanol/water partitioning coefficient (Table 8) are used to describe the bioavailability and uptake pathway. A numerical model developed by Riederer [204] identifies various compartments in plant leaves that may harbour persistent organic pollutants. Perylene was the only PAH encountered in this study and due to its lipophilic character preferentially sorbed to the cuticle.

Wild et al. [277, 279] demonstrated that transport of three-ring PAH into the cytoplasm occurs for anthracene but to a lesser degree for phenanthrene. Concentration of PAH sorbed to the cuticle or cuticular waxes, however, exceeded those in the cytoplasm by far.

Gaseous three-ring PAH may accumulate in foliage via stomatal uptake or by adsorption to and diffusion into the cuticle and its wax coating. Particle associated three-ring PAH will be deposited on foliage by wet and dry deposition and due to the highly lipophilic nature of the PAH these will partition into the plant wax or cuticle.

Once accumulated in or on foliage the PAH may undergo a variety of degradation reactions or removal processes. These involve photodegradation, which however, is hampered by embedding of PAH in cuticular waxes [263]. Wash-off and mechanical abrasion may remove previously accumulated PAH from plant surfaces [93]. For phenanthrene and alkylated analogues little is known about detoxification mechanisms utilized by plants to remove accumulated PAH. Revolatilisation of three-ring PAH from foliage may occur due to the comparatively low k_{oa} values of alkylated phenanthrenes (Ta-

compounds	mol. mass	water sol. [mg l ⁻¹]	log k _{ow}	vapour press. [mPa]	log k _{oa}	Henry's constant [10 ⁻¹ atm m ³ mole ⁻¹]
phenanthrene (P)	178	1.15	4.46	16.13	7.22	4.23
anthracene (A)	178	0.04	4.45	0.87	7.09	5.56
dibenzothiophene (DBT)	184	1.47	4.38	27.33	7.24	3.38
cyclopenta[def]phenanthrene (CPP)	190	1.10	4.60	4.16	7.67	2.08
3-methylphenanthrene (3-MP)	192	0.24	5.15	6.68	7.49	5.67
2-methylphenanthrene (2-MP)	192	0.28	4.86	6.68	7.49	5.67
9-methylphenanthrene (9-MP)	192	0.31	4.89	6.68	7.53	5.67
1-methylphenanthrene (1-MP)	192	0.27	5.08	2.00	7.78	4.93
2,6-dimethylphenanthrene (2,6-DMP)	206	0.10	5.44	1.01	8.03	6.25
2,7-dimethylphenanthrene (2,7- DMP)	206	0.10	5.44	1.01	8.03	6.25
Σ 1,3-, 2,10-, 3,9-, 3,10- dimethylphenanthrene (x4-DMP)	206	0.10	5.44	2.43	8.03	6.25
Σ 2,9-, 1,6-dimethylphenanthrene (2,9-, 1,6-DMP)	206	0.10	5.44	2.43	8.03	6.25
1,7-dimethylphenanthrene (1,7-DMP)	206	0.10	5.44	2.43	8.03	6.25
1,8-dimethylphenanthrene (1,8-DMP)	206	0.10	5.44	2.43	8.03	6.25
retene (Re)	234	0.03	6.35	0.35	8.70	11

Table 8: Physico-chemical properties of alkylated and parent three-ring PAH.

ble 8). The k_{oa} of the parent PAH phenanthrene (P) at 25°C is 7.22, those of the MP vary between 7.49 and 7.78, and those for DMP are estimated to 8.03. With time the ratios of $P/(P+MP)$ and $P/(P+DMP)$ of PAH accumulated in foliage are expected to change to the expense of phenanthrene.

For perennial plants the investigation of consecutive needle cohorts will reflect processes of ongoing PAH uptake, degradation and revolatilisation and for older cohorts a protective shielding effect of younger needles may diminish the rate of continuous PAH uptake. The variable processes that may affect three-ring PAH accumulating in/on foliage requires the investigation of consecutive needle cohorts for testing their suitability for biomonitoring atmospheric air pollution.

The use of *Pinus nigra* needles as passive samplers in atmospheric pollution studies has been proven for magnetic particles serving as proxy for fine dust loads and for major and trace elements by Lehndorff et al. [126] and Lehndorff and Schwark [125].

In this contribution the focus is set on the time dependent accumulation of the three-ring PAHs phenanthrene, its alkylated analogues, cyclopenta[def]phenanthrene, anthracene and the thio-aromatic dibenzothiophene measured on 3 to 50 months old needles collected at 6 locations with different emission background. The PAH concentrations are reported for single needle cohorts and different sampling locations and discussed with respect to accumulation behaviour, transportation processes and source specific relations between the compounds (ratios). In order to account for temperature-

induced revolatilisation processes and changes in seasonal PAH-emission, needles were collected separately in summer and winter to reflect the most contrasting environmental conditions. A systematic behaviour of alkylated phenanthrene accumulation in pine needles will facilitate improved source recognition and allow utilizing these atmospherically abundant components or ratios thereof in spatial mapping of air quality.

2.3.1 Sampling

The study area is located in the highly urbanized and industrialized greater Cologne Conurbation and comprises several different emission scenarios. The six sampling locations discussed here, are chosen to reflect the main emission types, by excluding very close point sources (i.e. traffic, Table 1). At each location three trees were sampled and each tree was subsampled at four compass directions to take care of intra-site variations. Each needle age class was collected separately (3 to 5 needle cohorts could be gained) in winter and summer 2004. PAH analysis was done on a composite sample for every needle cohort (n=50). Samples were stored deep frozen prior to analysis. Detailed aspects of sampling are described by Lehndorff et al. [126].

2.3.2 Analytical Methods

Sample extraction and clean-up PAH containing organic material of the needle surfaces was gained by accelerated solvent extraction (ASE 200, DIONEX, Idstein) with hexane:dichloromethane 99:1 (v/v) at 120°C and 75 bar. The aromatic fraction was separated from the total extract via centrifugation and medium pressure liquid chromatography (MPLC, Margot Köhnen-Willsch, Jülich) as described by Lehndorff and Schwark [123]. The error upon triplicate analysis yielded 15% for the three-ring PAH.

Instrumental analysis and compound identification Quantitative analysis of several PAH was done by GC-MS (HP5971) using d₁₀ pyrene as internal standard. Mass-spectrometry was carried out in SIM-mode to yield best peak separation and intensity for the low concentrated PAHs in a predominantly organic matrix. Here the results for masses m/z 178, 184, 190, 192, 206 and 219 plus 234 are reported. A detailed list of the PAH discussed is given in Table 8. Identification of alkylated phenanthrenes was done according to Radke [197], Benner et al. [15] and Poster et al. [193] as shown in Fig. 14a,b. For brevity the sum of 4 co-eluting compounds 1,3-DMP, 2,10-DMP, 3,9-DMP and 3,10-DMP is referred to x4-DMP.

Statistics and calculation of physico-chemical properties Physico-chemical properties were obtained from the Syracuse Research Corporation Physprop database (www.syrres.com/esc/databases.htm) or calculated using the US EPA EPI Suite ([152]; Table 8). Linear relations between PAH concentration and exposure time (slope, coefficient of determination and standard deviation) were analysed with MS Excel (Table 10) and graphically displayed for selected PAH (Fig. 16). The significance of inter-versus intra-site variations was determined using the non-parametric Kruskal-Wallis-*H*

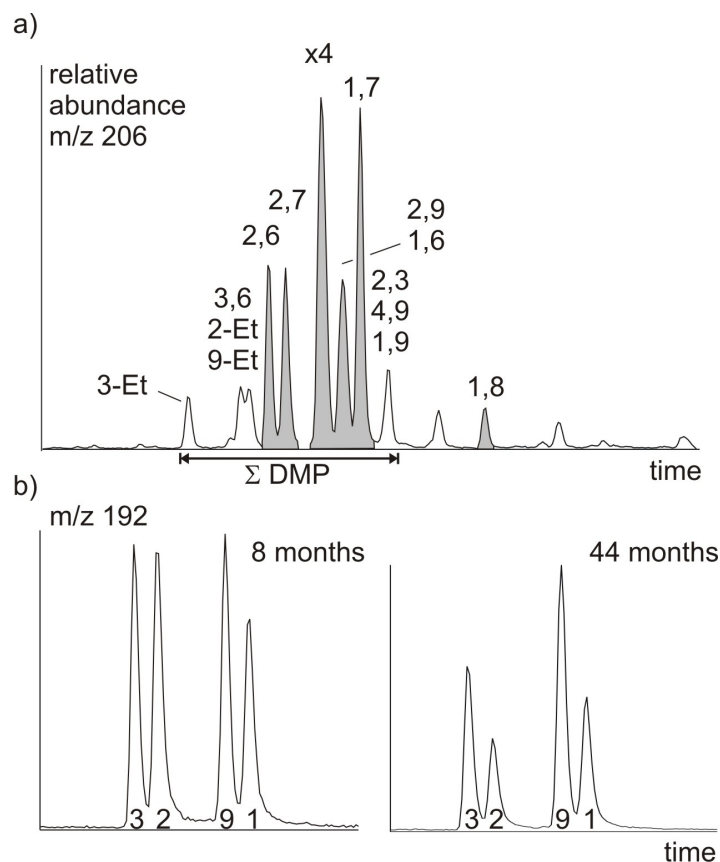


Figure 14: a) MS-trace m/z 206: identification of dimethylphenanthrenes (grey = separately quantified DMP, Σ DMP is integrated including ethylphenanthrenes and 2 more DMP). Predominance of x4- and 1,7-DMP is typical for urban emission scenarios. b) MS-trace m/z 192: identification and relative distribution pattern of 3-MP, 2-MP, 9-MP and 1-MP in 8 months and 44 months old needles of the winter sampling campaign collected at the Cologne site (peak identification is done as indicated by methylation numbers in the trace; Σ MP is calculated by addition of 4 MP). Relative increase of the biological 9-MP and 1-MP pair with rising needle age is recorded for all sample sets.

test (SPSS14.0, Table 9b), which is especially designed for not normally distributed data sets.

2.3.3 Results

Concentrations of the three-ring PAH phenanthrene, 10 of its alkylated isomers, anthracene, dibenzothiophene, cyclopenta[def]phenanthrene and retene were analyzed on pine needles of consecutive needle age classes from 6 locations with different air pollution characteristics. The aromatic fraction of the pine needle surface extracts revealed PAH concentrations that reached from $< 3 \mu\text{g g}^{-1}$ [dry weight (d.w.)] for 1,8-DMP to $< 40 \mu\text{g g}^{-1}$ for anthracene, 2,6-DMP, 2,7-DMP, x4-DMP, Σ 2,9-, 1,6-DMP, 1,7-DMP and retene (1-methyl-7-isopropyl phenanthrene). Concentrations up to $150 \mu\text{g g}^{-1}$ were found for DBT, CPP and monomethylated phenanthrenes, whereas the unalkylated parent PAH phenanthrene accounted for 300 to $2100 \mu\text{g g}^{-1}$ of needle dry

weight (Table 34 in appendix).

Intra-site versus inter-site variability The median concentrations (weighted average of consecutive needle age concentrations as calculated by Lehndorff et al. [126]) of individual compounds determined for each sampling site showed a high variability of pollutant loads between the six locations (Table 9a,c), which proved to be significant by the Kruskal-Wallis- H test (Table 9b). Highest "on-average" PAH concentrations were measured on needles taken at the industrial site Dormagen, except A, DBT and CPP that were highest in Bedburg, an area affected by lignite mining and combustion. The metropolitan Cologne site showed second highest concentration for all DMP, 9-MP, A and CPP. The rural areas Bergisch-Gladbach and Fuessenich exhibited the lowest PAH concentrations.

PAH accumulation trends The accumulation history was investigated based on the relation of PAH concentration versus needle exposure. A mathematical description of this relationship is given in Table 10 employing the slope of a linear regression line and the coefficient of determination " r^2 ". The latter indicates how much of the variance in PAH concentrations can be described by the exposure time of needles towards atmospheric pollutants. In general the parent PAH phenanthrene shows the steepest regression curve slope (m) beginning with $m=4$ and $m=8$ at rural Bergisch-Gladbach and Fuessenich, rising to a value of 10 in the city of Bonn. Maximum slope values of $m=20$ and $m=50$ were noted for the Cologne city, Dormagen and Bedburg sampling site, respectively (Table 10, Fig. 15). The slope of regression for the alkylated three-ring PAH versus exposure time was positive ($m=0.1$ to 7) except for selected DMP and retene that show constant concentrations with increasing exposure time in the city of Bonn and in rural Fuessenich. This can be related to these compounds being close to the detection limit, especially for older needle cohorts.

The coefficient of determination indicates that at the Dormagen site all PAH concentrations can be explained by exposure time with r^2 reaching from 0.6 to 0.9 (significance $p=0.01$). Pine needle concentrations in Bedburg also show a dependence on exposure, with relative variance being smaller than 70% for 1,7-DMP, 1,8-DMP and retene. In Bergisch-Gladbach r^2 is below 0.7 for anthracene, 2,7-DMP, 1,7-DMP, 1,8-DMP and retene. Needles sampled in Bonn, Cologne, and Fuessenich exhibit a linear correlation of $r^2 > 0.7$ only for the 1-MP, phenanthrene and anthracene.

a) season	P	A	DBT	CPP	3-MP	2-MP	9-MP	1-MP	Σ MP	2,6-DMP	2,7-DMP	x4-DMP	2,9-; 1,6-DMP	1,7-DMP	1,8-DMP	Σ DMP + EP	Re
L1 w	810	1.2	30	14	32	56	25	35	156	6.2	5.5	18	7.9	12	1.25	71	7.1
L2 w	153	2.3	6.2	5.2	5.7	4.5	5.3	5.3	23	0.5	0.4	2.5	1.0	0.9	0.13	9.1	1.3
L3 w	439	9.5	35	16	17	17	12	13	64	1.7	0.8	5.9	2.8	3.2	0.54	23	3.2
L4 w	429	12	13	16	14	12	18	12	62	2.0	1.4	7.8	3.5	4.4	0.73	29	4.2
L5 w	277	12	14	9.0	8.7	7.9	11	8.4	32	1.2	0.9	5.5	2.1	2.2	0.42	18	2.9
L6 w	167	5.6	8.4	5.7	4.7	5.1	3.9	4.6	19	0.5	0.4	1.9	1.1	1.7	0.28	7.7	2.5
L1 s	377	7.8	18	9.0	19	30	14	18	87	3.0	3.0	11	4.9	6.8	0.77	42	5.3
L2 s	144	1.3	5.0	3.7	5.6	4.0	4.5	20	20	0.2	0.1	2.1	0.6	0.4	0.05	9.9	1.2
L3 s	496	12	35	17	15	12	11	11	51	1.2	0.4	4.1	1.4	0.9	0.12	13	0.8
L4 s	405	1.9	11	13	12	9.7	14	8.4	48	1.0	0.8	5.1	1.5	1.2	0.17	15	1.6
L5 s	235	2.6	9.6	5.3	6.7	4.9	8.1	5.5	26	0.5	0.2	3.1	0.9	0.7	0.12	1.6	0.7
L6 s	152	1.2	4.5	3.1	3.6	3.6	2.8	3.0	13	0.04	0.02	0.9	0.2	0.4	0.01	3.9	0.9

b) P	A	DBT	CPP	3-MP	2-MP	9-MP	1-MP	Σ MP	2,6-DMP	2,7-DMP	x4-DMP	2,9-; 1,6-DMP	1,7-DMP	1,8-DMP	Σ DMP + EP	Re
H	9.62	5.23	10.15	9.15	10.77	9.85	10.54	10.31	8.54	8.38	9.85	8.54	6.85	6.69	56	5.92
p	0.087	0.388	0.071	0.103	0.056	0.080	0.061	0.067	0.129	0.136	0.080	0.129	0.232	0.245	0.314	0.314
Herit	9.24	4.35	9.24	7.29	9.24	9.24	9.24	9.24	7.29	7.29	9.24	7.29	6.06	6.06	4.35	4.35

c) P	A	DBT	CPP	3-MP	2-MP	9-MP	1-MP	Σ MP	2,6-DMP	2,7-DMP	x4-DMP	2,9-; 1,6-DMP	1,7-DMP	1,8-DMP	Σ DMP + EP	Re
L1	594	4.5	24	12	25	43	20	27	122	4.6	4.3	15	6.4	9.4	1.0	6.2
L2	148	1.8	5.6	4.5	5.6	4.2	4.9	4.9	21	0.3	0.2	2.3	0.8	0.7	0.1	1.2
L3	467	11.0	35	16	14	12	12	12	57	1.4	0.6	5.0	2.1	2.0	0.3	2.0
L4	417	7.1	12	14	13	11	16	10	55	1.5	1.1	6.4	2.5	2.8	0.5	2.9
L5	256	7.4	12	7.1	7.7	6.4	9.4	6.9	29	0.5	0.5	4.3	1.5	1.4	0.3	1.8
L6	159	3.4	6.5	4.4	4.1	4.3	3.3	3.8	16	0.3	0.2	1.4	0.7	1.1	0.1	1.7

Table 9: a) weighted means [ng g⁻¹ dry weight] for each location per sampling campaign, calculated from consecutive needle cohorts as described by Lehdorff et al. (2006), b) Kruskal-Wallis-*H* test, c) averaged mean for each location, bold and italic letters highlight highest and second highest pollutant load.

Location	P	A	DBT	CPP	3-MP	2-MP	9-MP	1-MP	Σ MP	2,6-DMP	2,7-DMP	x4-DMP	2,9-; 1,6-DMP	1,7-DMP	1,8-DMP	Σ DMP + EP	Re	
L1 Do	slope	20.93	0.41	0.67	0.48	1.17	2.19	0.81	1.27	7.11	0.26	0.25	0.64	0.30	0.50	0.06	2.67	0.23
L2 B-Gl	r ²	0.61	0.93	0.69	0.83	0.81	0.74	0.79	0.77	0.73	0.71	0.69	0.79	0.76	0.72	0.77	0.77	0.84
L2 B-Gl	r ²	4.30	0.08	0.11	0.14	0.20	0.13	0.20	0.16	0.98	0.01	0.01	0.07	0.02	0.02	0.002	0.22	0.01
L3 Bb	slope	51.14	0.97	3.36	1.63	1.54	1.27	1.17	1.17	6.40	0.86	0.32	0.82	0.69	0.44	0.13	0.60	0.10
L3 Bb	r ²	0.86	0.98	0.91	0.87	0.83	0.83	0.82	0.82	0.82	0.76	0.68	0.82	0.72	0.50	0.19	0.80	0.20
L4 C	slope	21.06	1.16	0.14	0.55	0.44	0.17	0.88	0.31	2.45	0.07	0.01	0.26	0.08	0.10	0.01	0.88	0.10
L4 C	r ²	0.93	0.94	0.11	0.74	0.59	0.20	0.88	0.45	0.92	0.59	0.03	0.67	0.28	0.23	0.13	0.55	0.33
L5 Bn	slope	10.05	0.33	0.17	0.22	0.11	0.02	0.30	0.10	0.76	0.001	-0.001	0.07	0.002	0.005	-0.001	0.19	-0.01
L5 Bn	r ²	0.90	0.55	0.39	0.70	0.35	0.02	0.86	0.29	0.65	0.003	0.001	0.34	0.002	0.01	0.003	0.11	0.02
L6 Fu	slope	8.58	0.16	0.24	0.15	0.20	0.19	0.16	0.18	0.95	0.01	0.01	0.04	0.01	0.03	0.003	0.19	0.06
L6 Fu	r ²	0.91	0.49	0.70	0.67	0.89	0.82	0.77	0.82	0.89	0.14	0.11	0.53	0.16	0.27	0.06	0.56	0.40

Table 10: Linear regression parameters for 6 to nine needle cohorts per location against exposure time (needle class with 44 months of exposure at the Cologne site is excluded from the calculations).

In figure 15 the relationship of phenanthrene, CPP, Σ MP, Σ DMP, retene and DBT to exposure time is visualized in binary plots. Despite a trend of systematic increase in PAH concentration with exposure time, non-linear behaviour of single compounds with time, differences in inter-site variability, and variations related to sampling in summer and winter can be recognized. PAH concentrations shown in figure 15 in general show a steady increase at locations Bedburg, Bonn, Fuessenich and Bergisch-Gladbach. PAH loads in Dormagen are notably higher for needles sampled in winter whereas at the Cologne site this was observed for Σ DMP and retene but not for other PAH. For retene variations related to the different sampling times can be observed for all locations except Bonn. The intersite variability is most obvious for Bedburg with highest P, CPP, and DBT loads and Dormagen showing maximum concentrations for Σ MP, Σ DMP and retene. Notable "above average" concentrations at the Cologne site were noted for P, CPP, Σ MP, Σ DMP and retene.

PAH ratios Absolute concentrations of PAH reflect accumulation whereas relative proportions between PAH isomers are more suitable to detect emission sources, relative changes due to sampling in summer or winter and eventually preferred uptake or selective degradation of individual components. We applied a variety of canonical variables based on ratios of i) parent phenanthrene to alkylated analogues, ii) parent phenanthrene versus DBT, iii) relative distributions of MP or DMP isomers, and iv) alkylated PAH versus CPP (Fig. 16).

The proportion of parent vs. alkyl-PAHs, reflected by e.g. the P/(P+MP)-ratio, is lowest for the industrial Dormagen location due to high amounts of alkyl-PAH (Fig. 16a). The rural locations Fuessenich and Bergisch-Gladbach show a notably lower proportion of alkyl-PAH. A trend to decreasing relative concentrations of alkyl-PAH with time was noted for the highly trafficked regions of Cologne and Bonn. The ratio of retene, an alkylated PAH of biological inheritance, versus the parent phenanthrene depicts strong dependence on season, with depletion in retene occurring for needles sampled in summer. This pattern is most prevalent for the urban sites Cologne and Bonn or the Bedburg and Fuessenich locations (Fig. 16b). The relationship between aromatic and thioaromatic hydrocarbons was investigated by the P/(P+DBT) ratio. The lowest P/(P+DBT) ratios and relative proportions of P are observed at the Bedburg site due to release of DBT upon lignite combustion. Metropolitan Cologne revealed the lowest relative DBT concentrations that notably decreased with time (Fig. 16c). The distribution of alkylated phenanthrene isomers is highly variable, depending on site-specific source characteristics and sampling time. The highest level of inter site variability derives from the relative distribution of MP. In figure 16d the ratio of (3+2)/(9+1)-MP is depicted that shows high values that are constant over time for the Dormagen site. Intermediate values with no variation related to residence time were observed for the rural Bedburg, Fuessenich and Bergisch-Gladbach sites. Lowest values for the (3+2)/(9+1)-MP ratio that notably decline with exposure time occur for the urban Cologne and Bonn sites. The ratio of 1,7/(1,7+2,6)-DMP has been applied as source recognition indicator differentiating wood combustion from other combustion fuels (Benner et al., 1995; Poster et al., 2003; Mandalakis et al., 2005). In this study the source indicator primarily differentiates the rural Fuessenich location from the remaining sites (Fig. 16e). These show a pattern of relative 1,7-DMP enrichment

for samples taken in winter, except for the Dormagen site that exhibits an opposite trend. The ratio of x4-DMP versus CPP reveals a clear inter-site differentiation, similar to the pattern observed for the (3+2)/(9+1)-MP ratio (Fig. 16d,f). This ratio shows only modest variability and no trend with exposure time. Three groups can be separated; the first represented by Dormagen exhibits an exceptionally high x4-DMP/(x4-DMP+CPP) ratio, the second including the urbanized sites Cologne, Bonn and in part Bergisch-Gladbach reveal intermediate values, and the last group made up by rural Bedburg and Fuessenich locations shows the lowest and most invariable ratios.

2.3.4 Discussion

In this study the potential of atmospherically abundant three-ring PAH of similar physicochemical properties for biomonitoring, thus avoiding influences due to emission, transport and uptake fractionation based preferentially on molecular size, is investigated. Improved source reconciliation and understanding of accumulation processes was achieved by investigating an extended number of phenanthrene derivatives. Results show that three-ring PAH on pine needles exhibit systematic accumulation trends and statistically significant variation between six study sites of differing emission background.

Following a short summary of physico-chemical properties of three-ring PAH, the discussion starts with accumulation trends based on absolute concentrations of individual three-ring PAH grouped into unsubstituted and alkylated PAH. Variation in accumulation characteristics for locations or individual PAH are then discussed based on PAH ratios and differences noted for summer vs. winter collected samples. Finally processes related to degradation or evaporative loss of semivolatile three-ring PAH from pine needles are addressed.

Differences in physico-chemical properties Physico-chemical properties of the 3-ring PAH regulate accumulation in/on plants (uptake), source dependence and preferential degradation processes over time (Table 8). In general the water solubility of PAH is very low and decreases with rising molecular weight (mw), for example phenanthrene (mw 178, water solubility 1.15 mg l^{-1}) shows a water solubility 10 to 40 times higher than estimated for DMPs (mw 206) and retene (mw 234), respectively. The configuration of the benzenoid rings forming an aromatic compound is important for the compound stability making the linearly annelated anthracene thermodynamically less stable than the angular phenanthrene of the same mass [236]. This results in lower water solubility for anthracene but much higher photodegradation and thermal destruction rates [146, 263, 278]. The octanol-water partitioning coefficient ($\log k_{ow}$) is a measure often used to describe the bioavailability of a compound. The constant increase of $\log k_{ow}$ with molecular weight of PAH signals a decline in bioavailability from phenanthrene to retene [45, 240]. The vapor pressure is highest for phenanthrene (16.13) and DBT (27.33), indicating a preference of these compounds to partition into the gas phase. Anthracene and retene have the lowest vapor pressures and, therefore, prefer particle phase sorption. With increasing molecular weight alkylated three-ring PAH tend to be bound to the particle phase. This is also indicated by the Henry's law constant, a measure of fugacity and the octanol/air coefficient ($\log k_{oa}$) that describes

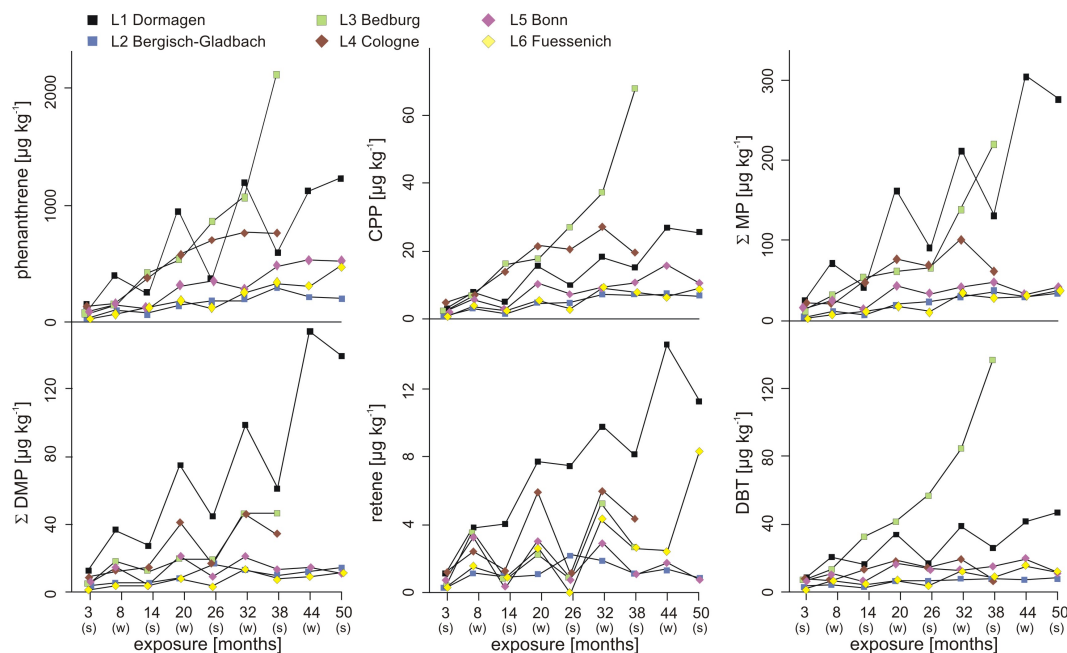


Figure 15: Concentrations of phenanthrene, cyclopenta[def]phenanthrene, sum of methylated phenanthrenes, 3-, 2-, 9-, and 1-methylphenanthrene, sum of dimethylated and ethylated phenanthrenes, retene and sulfur-PAH dibenzothiophene versus time of exposure to ambient air of the single pine needle generations (winter 2004 samples = filled symbols, summer 2004 samples = open symbols).

the relative partitioning of the compound between the air or plant surface expressed as octanol phase [204, 266].

Trends of PAH accumulation The absolute concentrations of individual PAH increased with exposure time of pine needles, whereby a rough categorisation into four location groups can be made. A very steady and strong increase is observed for P, CPP, Σ MP and DBT at the Bedburg site (Fig. 15), which is attributed to a nearby emission source of three large lignite fuelled power plants. The industrial site Dormagen exhibits a pronounced increase in concentration of phenanthrene but in particular of its alkylated derivatives, i.e. Σ MP, Σ DMP and retene (Fig. 15), these components resulting from petrochemical industry emissions. The Cologne site shows concentrations comparable to the former sites, except for diminished DBT loads (Fig. 15). This urban pattern is related to mixed traffic, industrial and domestic heating emissions. The last group involves the rural sites Fuessenich and Bergisch-Gladbach and a residential site in the city of Bonn. These locations are characterized by low emission (Fig. 15) and high atmospheric mixing rates. Phenanthrene has been reported to be the most abundant atmospheric PAH in biomonitoring studies [249, 127, 96, 123] and in this investigation also shows concentrations 100 to 1000 fold higher than its derivatives (Table 34 in appendix, Fig. 15). Accumulation rates as determined by slope of regression lines are app. 3 to 45 times higher than for phenanthrene derivatives. As the parent PAH has the highest water solubility and vapor pressure (Table 8) and consequently is most susceptible to secondary removal from pine needles, the high

concentration and accumulation rates are due to high primary atmospheric emission rates for phenanthrene.

Dormagen comprises the only site that shows a notable and systematic change in concentration between needles sampled in summer and in winter. The higher phenanthrene concentration in winter is attributed to a preferential uptake of gaseous phenanthrene originating from the neighboring petrochemical plant, emitting non-combusted phenanthrene. At the remaining sites phenanthrene is assumed to be preferentially particle bound and to originate from various kinds of combustion processes. A multi-sourced and balanced origin is assumed for the rural sites, whereas traffic dominated combustion prevails in Cologne but lignite combustion dominates in the Bedburg area.

The season-dependent concentrations of phenanthrene at the Dormagen location imply a significant proportion of evaporative losses during the summer months, favoured by the preferential gas-phase occurrence of phenanthrene exclusively at this site [266, 247]. The steady increase of phenanthrene in summer needles of longer exposure time indicates that not the entire phenanthrene load sorbed to the needle surface in winter is revolatilized during summer. A portion of the winter accumulated phenanthrene is translocated from needle surfaces to the interior and thus immobilized. This is in agreement with observations made by Kylin and Sjödin [115] for volatile components that exhibit steady accumulation in needle interiors but seasonally variable accumulation on needle cuticles. Wild et al. [277] have demonstrated that anthracene and other PAH can be translocated from needle surfaces into needle pegs and even into the cytoplasm of the epidermal cells.

DBT shows the highest concentrations and accumulation rate at the Bedburg site. This is related to emissions of thioaromatics from nearby lignite fuelled power plants. Regulations for power plant emissions in Germany require the removal of SO_x from exhaust fumes by precipitation as CaSO_4 . Therefore, lignite combustion is no longer detectable by monitoring SO_x in air [243] or in plant receptors. However, even modern filtering techniques are unable to capture thioaromatic sulphur species, which will serve as adequate indicators of lignite fuelled power plants. Thioaromatic concentrations in the urban areas are low due to the stepwise introduction of sulphur-lean diesel in Germany since 1996 [243]. The preferred phase of occurrence is suggested to be particle bound at all locations except for Dormagen, where the gaseous petrochemical emissions lead to differential accumulation during summer and winter as previously observed for phenanthrene.

The accumulation of CPP is very similar to the one observed for phenanthrene (Fig. 15). Physico-chemical properties of CPP indicate a vapour pressure lower than for MP and a thermal stability in between phenanthrene and its alkylated analogues (Tab.8 [236, 287]). A difference can be seen in the ranking of the locations: Bedburg and Cologne needles show the highest concentrations whereas in contrast to the phenanthrene concentration, Dormagen samples show notably lower CPP loads. This indicates CPP to preferentially originate from combustion and not from refinery emission.

The relative concentration of methylated vs. parent phenanthrene is often applied to separate between petrogenic and combustion sources [14, 228, 84, 86]. Petrogenic generation of alkylated phenanthrenes from biological precursor molecules in sediments occurs over geological time scales of millions of years at temperatures generally between 60° and 150°C . Hereby, the relative distribution of monomethyl phenanthrenes is con-

trolled by their respective thermodynamical stabilities [197, 65]. Upon combustion processes reaching 600 to 1500°C, phenanthrene is dominantly produced from small precursor molecules via pyrosynthesis [230] without formation of alkylated analogues. Presence of methylated phenanthrenes thus indicates direct emission of fossil fuel related sources or inefficient combustion thereof, thus preserving the petrogenic alkylation pattern. The high degree of alkylation noted for the Dormagen site implies a preferential release upon fossil fuel refining processes. The second highest concentration of MP were observed at the Bedburg site, however, in comparison to parent PAH concentrations determined at this location (P, DBT, CPP) a relative decrease in the degree of alkylation is noted (Fig. 15). The MP concentrations in urban Cologne are equivalent to those in Bedburg and thus similar to the accumulation trend of phenanthrene and CPP. For the alkylated phenanthrene derivatives, however, an increasing dependency on summer vs. winter collection is observed due to a higher proportion of gaseous petrogenic MP in Cologne. The remaining locations exhibited much lower accumulation rates for MP due to lower emission rates of non-combusted fossil fuel.

The higher alkylated DMP reveal an accumulation pattern comparable to that of MP, whereby the differences between summer and winter samples tend to increase for the Cologne and Bonn sites (Fig. 15). This indicates a preferentially gaseous origin of these components from petroleum products and only minimal influence of alkylated compounds bound to combustion particulates. The lowest degree of seasonal variation in DMP concentration is noted for the Bergisch-Gladbach location pointing to a secondary source of DMP at this site. This trend is even more obvious for retene accumulation, being monotonous exclusively at the Bergisch-Gladbach location but highly variable for the other sites (Fig. 15). For the Bergisch-Gladbach site a secondary source providing more constant accumulation of particle bound retene resulting from wood combustion [198, 15, 228] is inferred. An additional source for retene at the Bedburg and Fuessenich location in the west of the study area is the emission of retene from the lignite open pit mines.

Source recognition via PAH ratios Source discrimination ratios based on phenanthrene and its derivatives have been developed, generally applying the degree of alkylation and its dependence on combustion vs. non-combustion emissions. The best differentiation between the six locations is achieved by ratios based on non-alkylated phenanthrene or CPP vs. alkylated analogues or a ratio based on the relative distribution of MP (Fig. 16a, b, f). In contrast to the accumulation trends derived from absolute concentrations, the determination of individual PAH ratios in general leads to more constant values for needles of different exposure time. This indicates that for most ratios calculated the original PAH patterns prevail, demonstrating the source diagnostic potential of pine needle biomonitoring. Time-dependent changes in PAH ratios were observed for the P/(P+DBT) and (3+2)/(9+1)-MP ratio at selected locations (Fig. 16c, d). This is attributed to secondary alteration of PAH on the pine needles but not to preferential uptake over time. Another feature was observed for the phenanthrene/retene and 1,7-/(1,7+2,6)-DMP ratios that show strong differences for summer vs. winter collected needles except for the Dormagen and Fuessenich sites (Fig. 16b,e).

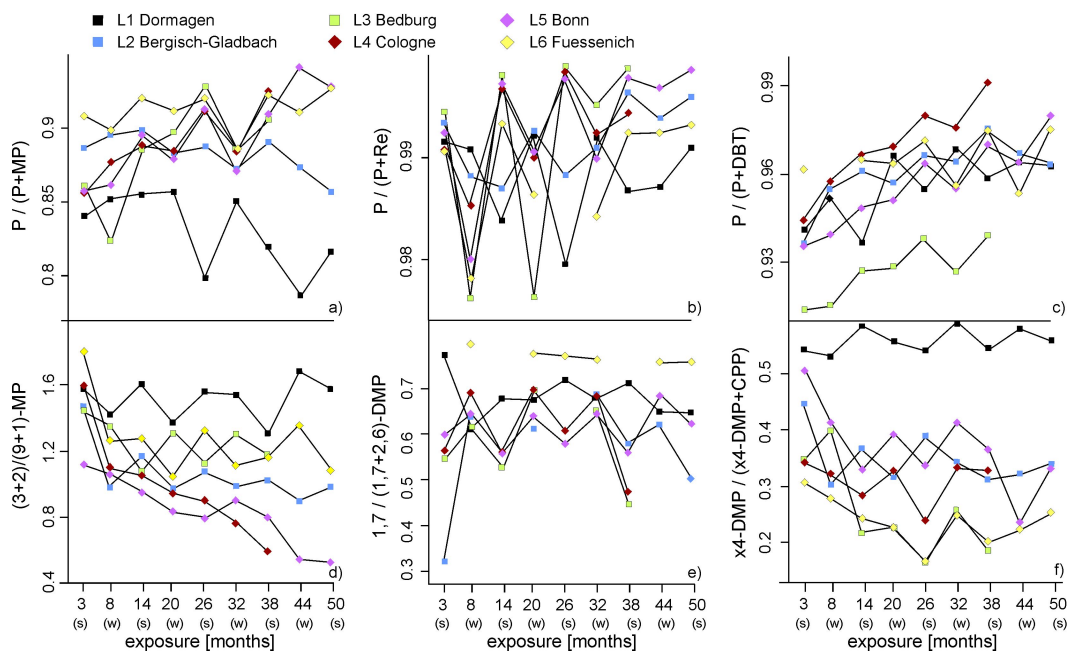


Figure 16: Several ratios of phenanthrenes used for source discrimination and here plotted versus time of needle exposure.

Petrochemical emissions The site Dormagen influenced by petrochemical emissions reveals characteristically low $P/(P+MP)$, and $P/(P+Re)$ ratios but exceptionally high $x4-DMP/(x4-DMP+CPP)$ ratios (Fig. 16a, b, f) all reflecting the degree of alkylation. For the Dormagen site these ratios evidently point towards dominance of direct emission of gaseous alkylated PAH from the petrochemical plant and a low contribution of particle-associated combustion PAH. Ratios depending on alkylation patterns are also suitable for petrochemical source recognition. The $(3+2)/(9+1)-MP$ ratio at the Dormagen site is notably higher than at all other sites, which may be inherited from the predominance of the 3- and 2-methyl isomers in petroleum [197, 65].

Wood and lignite combustion The ratio of $1,7/(1,7+2,6)-DMP$ has been used to differentiate wood combustion from traffic emission [15, 119, 139] with the 1,7-alkylation pattern originating from abietic acid being present especially in soft wood. This ratio indicates higher wood combustion derived particulates for the winter needles at the Cologne, Bedburg, Bergisch-Gladbach and Bonn stations. For a study site in Crete Mandalakis et al. [139] postulated a 37% contribution of wood combustion to the DMP inventory based on a $1,7/(1,7+2,6)-DMP$ ratio of 0.54. In summer similar $1,7/(1,7+2,6)-DMP$ ratios were noted but during winter an average value of 0.67 at these sites would correspond to 60% wood combustion derived DMP. These proportion seems implausible whereas a notable increase of 1,7-DMP at Cologne and Bedburg sites during winter may originate from short distance transportation of particles derived from lignite combustion. The dominance of particulates derived from lignite combustion during the winter months agrees with environmental magnetics data [126]. The rural Fuessenich location shows exceptionally high and nearly constant ratios over time, indicative of 1,7-DMP originating almost exclusively from wood combustion.

Lignite combustion markedly reduces the P/(P+DBT)-ratio (Fig. 16c) due to release of thioaromatics that are not scavenged by smoke stack filters. The relative proportion of the condensed CPP vs. alkylated PAH decreases notably at sites affected by lignite and/or wood combustion. The ratio of x4-DMP/(x4-DMP+CPP) consequently shows lowest values at the Bedburg and Fuessenich sites (Fig. 16f).

Traffic Relative concentration differences of substituted phenanthrenes have been employed to identify vehicular traffic emissions [14, 193, 139]. According to Mandalakis et al. [139] 1,7/(1,7+2,6)-DMP ratios of <0.43 are indicative for pure vehicle emissions. As stated above admixture of 1,7-DMP from wood and lignite combustion is omnipresent in the study area and therefore such low ratios are not encountered. At the Dormagen site direct emissions of non-combusted fuel led to 1,7/(1,7+2,6)-DMP ratio around 0.67, indicating that fuels and traffic emissions regionally may differ considerably.

In this study urban locations were found to show higher relative MP concentrations than rural sites (Fig. 16a) but also considerable variability within the MP distribution pattern (Fig. 16d). The (3+2)/(9+1)-MP ratio is lowest for the urban Cologne and Bonn sites revealing a fairly monotonous distribution over time. Values lower than 1.0 seem to be indicative for a predominance of traffic emissions when determined from methylphenanthrene concentrations analyzed in this study and re-calculated from literature data given [14, 234, 228]. Diesel usually contains a significant proportion of three-ring PAH [215, 193], whereas the gasoline fraction usually is free of these compounds. Incomplete combustion or direct volatilization may emit especially DMP from diesel and thus the ratio of x4-DMP/(x4-DMP+CPP) shows enhanced values, though not reaching the level of DMP release due to petrochemical processes (Fig. 16f).

Seasonal patterns, degradation and weathering Seasonal patterns affecting the relative distribution of phenanthrene derivatives were noted for the ratio of phenanthrene vs. retene and 1,7/(1,7+2,6)-DMP (Fig. 16b,e). A strong enhancement of phenanthrene over retene for winter collected needles occurred at the Bedburg, Bonn and Cologne sites due to high emissions of combustion particulates resulting from lignite combustion at the former and domestic heating in urbanized areas for the two latter locations. As mentioned above at these sites a preferentially particulate deposition of 1,7-DMP in winter was detected.

Long term trends in PAH ratios were observed for the P/(P+DBT), the P/(P+MP) and the (3+2)/(9+1)-MP ratio (Fig. 16a,c,d). The overall increase in the P/(P+DBT) ratio with residence time is attributed to the higher water solubility of DBT (Table 8) leading to preferential leaching from pine needles and enhanced evaporative losses due to a higher vapor pressure (Table 8). A notable decline in the (3+2)/(9+1)-MP and an increase in the P/(P+MP) ratio with residence time in pine needles is limited to the urban, traffic controlled sites of Cologne and Bonn. The β -substituted 3- and 2-MP are the thermodynamically most stable isomers [197] excluding isomerization reactions as driving forces. The log K_{oa} -values of 3- and 2-MP are slightly lower than those of the 9- and 1-isomers arguing for an increase with needle residence time. The fact that the decrease of the most stable isomers occurs in urbanized areas only, points towards

degradation mechanisms involving reactions with reactive hydroxyl radicals, ozone or NO_x components most abundant in urban atmosphere [226, 146, 42]. A decline of Σ MP with time (Fig. 16a) is restricted to urban locations and primarily due to the loss of the 3- and 2-MP isomers, attributable to degradation reactions involving reactive atmospheric species.

2.3.5 Conclusions

A study of pine needles collected at six locations of differing emission background in the greater Cologne area revealed the ubiquitous presence of phenanthrene, its alkylated derivatives, cyclopenta[def]phenanthrene and dibenzothiophene for 9 needle age classes 3 to 50 months old. The three-ring PAH on pine needles exhibit systematic accumulation trends and statistically significant variation between the six sites as controlled by local emission background. The concentration of phenanthrene and its derivatives generally increased with needle exposure time, though slopes of accumulation trends varied notably for individual PAH and between locations. The determination of individual source indicative PAH ratios in general lead to more constant values for needles of different exposure time. This indicates that for most ratios calculated the original PAH patterns persist, demonstrating the source diagnostic potential of pine needle biomonitoring. Substantial variation between PAH concentrations and in part ratios determined for winter and summer collected samples indicate notable losses of previously accumulated pollutants controlled by seasonally controlled partitioning processes. The continuous increase in PAH concentrations with exposure time even after substantial losses during summer indicates translocation of three-ring PAH into needle interiors and ongoing accumulation of particulates on needle surfaces. The systematic accumulation behaviour of phenanthrene and its derivatives on pine needles qualifies these component for biomonitoring studies of air quality. The high number of three-ring PAH isomers allows for improved source reconciliation and allocation needed in atmospheric pollution studies.

3 Cologne City - local-scale biomonitoring

This part of the study aims at the investigation of air quality at a local scale, covering the Cologne City area (300 km²). The sample set comprises locations with highly different emission input and varying distance to emitters, thus reflecting the heterogeneous urban emission mix, that is common for high population areas.

The Cologne City emission scenario is a composite of traffic and industrial emissions, further complemented by domestic heating, open fires, crematories, etc. A minor mixing of air masses in street canyons is supposed to lead to reduced dilution of emissions in the inner city [97, 98].

In chapter 2 the use of *Pinus nigra* needles as passive samplers for atmospheric pollution with particulate organic and inorganic matter was proven on a temporally resolved sample set. Here, time-integrated pollutant signals are investigated on a spatially resolved sample set.

3.1 Cologne City air quality - optical and magnetic properties

The spatial and temporal distribution of airborne pollutants within industrialised and urbanized areas is crucial to human health. When inhaled, fine particulate matter (PM) of grain sizes smaller than 10 μm or 2.5 μm (PM₁₀, PM_{2.5}) is associated with bronchitis, cardiopulmonary and lung cancer mortality [157, 192, 43, 191]. Ultrafine particles smaller than 0.1 μm may cause the most severe physiological effects [276, 172, 161]. Hitherto, three different methods have been used to measure the PM content of the air. All have various disadvantages. The use of high active volume air samplers equipped with filters is very common, yet expensive and time-consuming. Additionally, filters appear to be inefficient collectors for the smallest grains [161]. Collecting street dust or biomonitoring using passive samplers is less expensive. Street dust, however, will likely contain larger grains of additional PM, which never was airborne and poses little health risk [233, 200, 259, 242, 11, 281]. Volatile and semi-volatile organic compounds are also frequently analyzed using passive biomonitors [47, 231, 232, 39] but vegetation-atmosphere partitioning has to be considered in such approaches [29, 286, 102, 116, 60, 173, 271, 39].

The excellent potential of environmental magnetism as a proxy for atmospheric pollution levels has been reported based on analysis of soils and street or roof dust [88, 91, 223, 285], and vegetation samples including tree bark [109] and leaves or needles [147, 103, 156]. Generally, active and passive sampling will monitor accumulation intervals on different time-scales. Filters collect daily or even hourly-varying emissions. Therefore, temporal sources like building sites can be discriminated [223]. Biomonitoring in contrast reflects longer-term changes of environmental quality, because tree leaves or needles accumulate PM over several years (e.g. 1 to 3 for *Pinus nigra* used in this study). Any such monitoring of prolonged PM exposure is certainly relevant to human health. In this study microscopical analysis, various geochemical and environmental magnetic measurements of *Pinus nigra* needles were integrated to evaluate the degree and the spatial and temporal distribution of atmospheric contamination in Cologne City.

A major proportion of atmospheric pollutants is transported particle-bound. Our

approach towards the analysis of particle-bound pollutants is based on environmental magnetism in combination with microscopic observation. Here data on magnetic susceptibility and remanence properties, mainly saturation induced remanence magnetization (SIRM) and anhysteretic remanence magnetization (ARM) is presented to identify the carriers of magnetization. Magnetic analysis is complemented with Fe elemental analysis by atomic absorption spectrometry (AAS).

Magnetic properties of PM collected through active filters are thought to reflect the aerosol content of ambient air, the mineralogy of the magnetization carrier and the grain-size range of the particles [147, 160, 162, 285, 157]. Comparison of total particulate matter abundance with the concentration of magnetic minerals suggests an origin from similar sources [162]. The dominant sources of magnetic minerals and particulate matter in urban environments are traffic (motor vehicles, railway and trams), industry and building sites [147, 223]. Brown coal-fired power stations in proximity to the city may also influence its air quality [58]. The PM sources mainly emit combustion products and also particles released by friction. In 2002 there were 7 monitoring stations installed in Cologne to continuously measure the PM₁₀ fraction using filters. The current operation of five of these stations, maintained by the city of Cologne, is financially challenged. Therefore, a primary objective of this study was to test the most common evergreen tree species within Cologne City for its suitability as a biomonitor allowing for high spatial and temporal sampling density. The latter is a prerequisite for the generation of high-resolution distribution maps for various pollutants. Biomonitoring combined with magnetic measurements is discussed as a reasonably priced and reliable monitor of air quality over a wide area, because a financially comparable result cannot be generated by the use of active filters or costly geochemical analyses alone. The acquired data are easily stored in geographical information systems, thus enabling direct comparison with other environmental variables including local meteorology, topography, land use, traffic density, industrial emissions and allowing for merging and matching of different data sets. Parts of this chapter have been published in Urvat et al. [255].

3.1.1 Sampling

Cologne City covers an area of 300 km², which in this study is represented by a total of 69 samples of *Pinus nigra* (Fig. 17). The sampling campaigns were twofold, resulting in two data subsets, one spatial and the other temporal. The spatial subset contained data from 56 sampling locations spread over the entire city area. The temporal set contained data from 14 samples of a single pine tree (loc. 53, Fig. 17) taken at monthly sampling intervals from June to December 2002. The spatial sample set was collected in spring 2002, to avoid the growth period and collection of young needles with insufficiently accumulated PM. Additional 13 samples were taken in October 2004 and 2005 (Fig. 17). The locations were chosen to include presumably cleaner environments like parks and residential areas, as well as polluted areas near major roads, railways, airport and industrial complexes. The pine needles sampled cover the pollutant accumulation period 1999 to 2002. The temporal sample set was separated into fresh and older needles to study differences in the respective PM accumulations. All samples were obtained with pruning shears (total reach, 6 m height). To minimize climatic effects



Figure 17: Cologne City shows a typical urban, heterogeneous pattern in land use. Industrial zones are spread over the whole city, preferentially along the river Rhine. Street infrastructure occupies 61 km^2 of the total city area of 405 km^2 , with important ring roads at distances of 2, 3, 5, and 7 km to the city center and a freeway circle at app. 10 km to the city center. Radial roads serve as important commuter routes into the city. Radial patterns are noted for railway lines, with larger railway operations located in the SE-, SW and NW sectors adjacent to the city center. Green areas cover 37 km^2 , with parks mainly connected to an inner and an outer “greenbelt”. Sampling points are indicated by black circles with superimposed location number; locations 1-60 were sampled in 2002; locations 61-66 in 2004; locations 67-74 in 2005. Land use data was taken from CORINE [69].

on accumulation and abrasion, the needles were always taken after a rain-free period of at least two weeks. At each location a composite sample was collected to reduce the local effects of leaf canopy structure and resulting bias due to exposure direction. Composites contain needles of different height, direction and age and, in some cases, even were taken from closely spaced pines to maximise representativity [245]. The needles were cut directly from the branch, at about 1 cm from the base of the sprig. A

paper envelope was used for transport and storage. Sampling locations represent five specific environments: near the airport (n=2), exposed to railway operations (n=3), major roads including freeways (n=21), urban and suburban minor roads (n=16), urban parks (n=5) and suburban parks (n=9) in Cologne City (Fig. 22).

3.1.2 Analytical methods

Microscopical analysis PM on the surface of selected needles was investigated with a scanning electron microscope (CamScan 44 Editor with EDX microprobe) at maximum magnifications of 25,000. Each sample was sputtered with gold and arranged on the sampling table in such a way that both the abaxial and adaxial side of the needles could be observed. Several needles of different age and exposure were scanned to visually assess the extent of accumulation on the needles. The SEM-scans show the cuticle with epicuticular waxes. The cuticle as the most external plant layer serves as the interface to the surrounding atmosphere, allowing for gas exchange, water evapotranspiration and nutrient acquisition. The uptake of CO₂ and the emission of oxygen take place via the stomata (holes of about 20 μm in diameter embedded in the cuticle, see Fig. 18) [57]. Accumulation of atmospheric pollutants occurs on the cuticular surface and via the stomata. The EDX microprobe was employed to discriminate particles of different origins and especially to identify Fe-bearing spherulites.

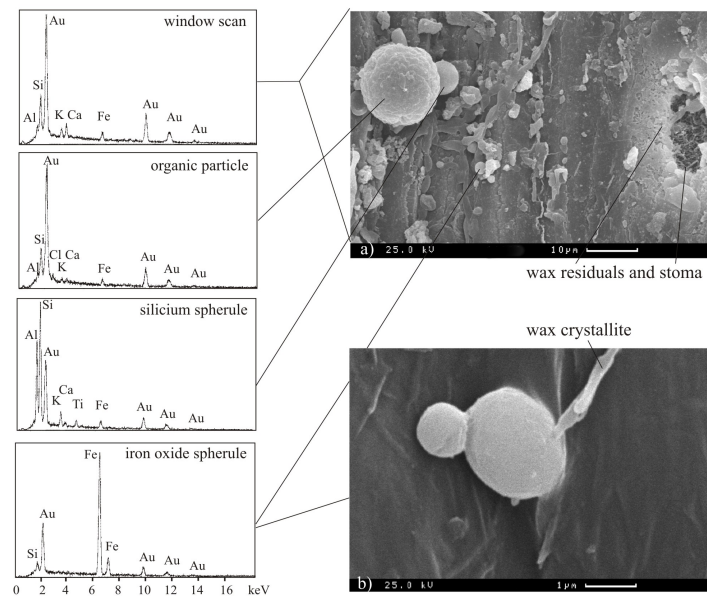


Figure 18: Identification of different air-transported particles accumulated on pine needle surface using SEM and microprobe: a) abaxial side of an older needle from the high traffic location 18 showing various airborne particles including organic particles (16 μm diameter, fungal spore), silicate glass spherule (6 μm diameter) and magnetite spherule (2 μm diameter), damaged epicuticular waxes due to wind and rainfall abrasion, and a stoma filled with wax and airborne particulate matter; b) two magnetite spherules (2.2 and 1.0 μm diameter) and a wax crystallite on a fresh needle (about 3 months in age, sample 44).

Elemental analysis Element analysis of Fe was carried out for all 69 samples in the Institute of Geography, University of Cologne by use of an Atom Absorbance Spectrometer with a flame oven (PERKIN ELMER PE 3100). For micro-wave assisted Fe-extraction finely ground sample (200 mg) was mixed with 5 ml HNO₃ and heated to 160° degrees for 6 hours.

Sample preparation for magnetic analysis For magnetic analysis ground needle material was placed in standard 8 cm³ plastic sample boxes. It was essential for measurements employing sample rotation that the needle material remained fixed within the boxes. The intensity of the magnetic signal is a function of the amount of sample and therefore as much material as possible was subjected to analysis in order to enhance the signal to noise ratio. Several tests were performed to optimize the analysis (see below). Microscopic observation confirmed that the grain size of the magnetic particles remained unaffected by the grinding process. The swing mill was equipped with an achat grinding vessel which was shown not to introduce any magnetic contamination into the samples.

Magnetic analysis All magnetic measurements were carried out in the Paleomagnetic Laboratory, Department of Geology, University of Cologne. The bulk magnetic susceptibility κ was measured at room temperature for the complete sample set on a KLY-2 susceptibility bridge (noise level 4×10^{-8} SI; AGICO, Czech Republic). Additional high-temperature susceptibility curves were determined for selected samples between room temperature and 600°C. The bulk magnetic susceptibility measures the magnetizability of a material (and hence is a concentration parameter), which is dominated, but not solely carried by ferromagnetic minerals like iron-oxides. The temperature dependence of magnetization clearly identifies the type of magnetic minerals due to their Curie-point (Dunlop and Özdemir, 1997). For 61 samples (no. 1-66, Fig. 17) a laboratory-induced anhysteretic remanent magnetization (ARM) was imparted using 100 mT peak alternating fields (AF) with a 40 μ T direct current (DC) bias field parallel to the AF. The ARM is a concentration-dependent parameter that is most sensitive to the smallest ferrimagnetic grains. The isothermal remanent magnetization (IRM) was acquired stepwise to 1.5 Tesla. Besides the mineral and grain-size-specific shapes of the acquisition curves, these measurements also provide a measure of the relative concentration of remanent magnetic particles (saturation IRM). The subsequent stepwise acquisition of the so-called backfield curve to 0.3 T allowed the calculation of additional grain size and mineral-specific parameters like the coercivity of remanence (B_{cr}) and the s-ratio [21]. Both the ARM and IRM measurements were carried out using the respective in-line solenoids and pulse-magnet of a three-axis 2G DC-SQUID superconducting rock magnetometer (model 755R, 2G Enterprises, CA, USA; noise level 5×10^{-12} A m²). Since the measurements are non-destructive, all parameters can be determined on a single sample.

3.1.3 Results

Preservation of original PM composition When attempting to use pine needles as proxies for atmospheric pollutants, it has to be firmly established that these

biomonitors are representative for airborne PM and that no fractionation or alteration occurred during work-up and analysis.

Hence, SEM microphotographs of intact and ground needles were compared, identifying ferromagnetic iron oxides with the microprobe (Fig. 18). All iron-bearing particles are present as spherules with a maximum grain size of 2 μm , none of which showed signs of fracturing. This could be confirmed by magnetic measurements of both ground and intact needles. The intensity of the IRM (contamination with additional magnetic particles) as well as the B_{cr} (grain size changes) remained unaltered within the analytical error indicating that there was no effect due to the treatment in the swing mill.

PM originally accumulated on leaf surfaces may later be partially removed by wash-off during rain or by wind abrasion thus reducing the strength of the magnetic signal. In contrast, some magnetic signal strength may be attributed to biological and not to pollutant PM sources. It was shown by Matzka and Maher (1999) that rigorous cleaning of leaf surfaces using detergents and ultrasonic agitation may remove 65 - 80 % of the magnetization, clearly indicating that the overwhelming proportion of the magnetic signal is due to PM accumulation. The non-removable fraction is either attributed to PM located in stomatal interiors and thus protected from cleaning or to biogenic magnetism. A two step cleaning procedure using distilled water and an organic solvent was employed to remove the wax coatings and to liberate PM that had been occluded by the latter. Figure 19 shows that the reduction in IRM for samples 38 and 24 due to water washing was 28% and 10%, respectively. Further clean-up of sample 24 with organic solvent removed another 35% of the magnetization. The magnetic particles were almost completely collected on a filter. This implies that although care was taken to collect samples after at least two weeks without rain, the magnetic signal is not severely affected by rain wash-off and stored reliably in pine needle biomonitors. Furthermore, magnetic PM is strongly bound to the needle, with a significant proportion incorporated into needle waxes and into stomatal cavities, thus minimizing the effect of wind abrasion of accumulated particles.

Identification of PM composition SEM identified varieties of PM on the pine needles (Fig. 18). The maximum particle size observed was up to 30 μm . Microprobe analysis indicates that the particles are dominantly silicates, iron oxides and organic. According to the visual SEM inspection Fe-bearing particles appear mainly as congealed spherules with a maximum diameter of 2 μm . Their spherical shape indicates combustion processes as the principal source [147]. IRM and ARM reflect the concentration of ferromagnetic minerals in a sample. Their excellent linear correlation ($r^2 = 0.9$) with the total iron content (Fig. 20) indicates that, in fact, Fe associated with the pine needles is almost exclusively bound to minerals that can carry a remanent magnetization. For zero magnetization the calculated regression line intercepts the y-axis at an iron content of 14 $\mu\text{g g}^{-1}$, which is ascribed to biogenic iron. It is suggested that this biogenic origin is diamagnetic (susceptibility <0).

Only a few iron oxides and sulphides are known to be carriers of remanent magnetization [46]. Indeed, the remanent magnetic signal of the pine needles is dominantly carried by the low-coercivity iron oxide magnetite (Fe_3O_4). This is confirmed by IRM acquisition and backfield measurements (B_{cr} , s-ratio), as well as high temperature sus-

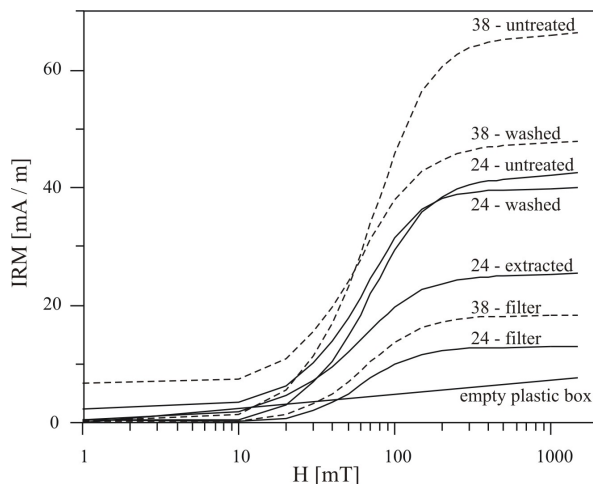


Figure 19: Effect of cleaning needle surfaces with water and organic solvent (hexane:dichloromethane, 99:1). Between 40 % and 60 % of total PM can be removed by gentle cleaning and collected on filters, the remainder is located in less accessible stomata and firmly incorporated in wax and cuticle. Results demonstrate that time-averaged PM accumulation is not significantly affected by wash-off during rainfall.

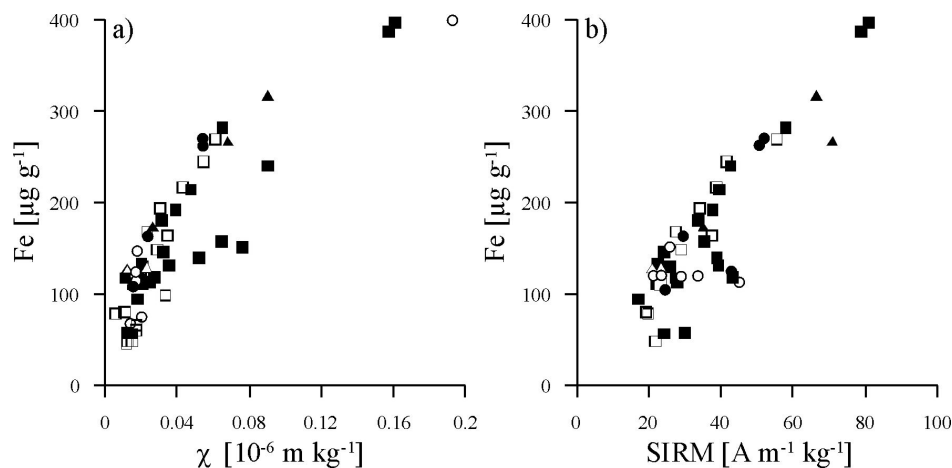


Figure 20: Correlation between iron content and magnetite concentration of pine needles (correlation coefficient $r^2 = 0.9$; $n = 40$, samples deviating from the general trend with relatively higher SIRM are excluded). Symbols refer to sample origin: open triangle = airport; filled triangle = railway; filled square = major street; open square = minor street; filled circle = urban park; open circle = suburban park (in a) $n = 56$ samples; b) $n = 48$ samples).

ceptibility curves. Over 95 % of the IRM saturation is typically reached at 350 mT which, however, is higher than would be expected for pure magnetite (< 200 mT). This is attributed to a minor contribution from the iron sulphide pyrrhotite, which is magnetically harder than magnetite of the same grain size. The presence of minor pyrrhotite in addition to the prevailing magnetite is confirmed by the high-temperature susceptibility measurements (see Fig. 21a). A distinct initial drop in magnetisation intensities occurs around 320°C (the Curie temperature of pyrrhotite), while the pres-

ence of sulphides in form of pyrite, which does not carry a remanence, is indicated by a rise in magnetisation at around 500°C. At this temperature pyrite is typically converted to magnetite, which subsequently becomes paramagnetic upon reaching the Curie temperature of magnetite at 580°C. The conversion of pyrite to magnetite leads to irreversible cooling curves in the high-temperature susceptibility runs (Fig. 21a). The presence of pyrrhotite is further suggested by relatively high IRM/ κ values plotting above the SD field (Fig. 21b) in the IRM/ κ vs. B_{cr} -diagram after Bradshaw and Thompson [25]. The additional sharp increase in magnetisation intensity around 500°C (Fig. 21a) might be a Hopkinson peak, typically caused by fine grained magnetite or a mixture of various mineralogies.

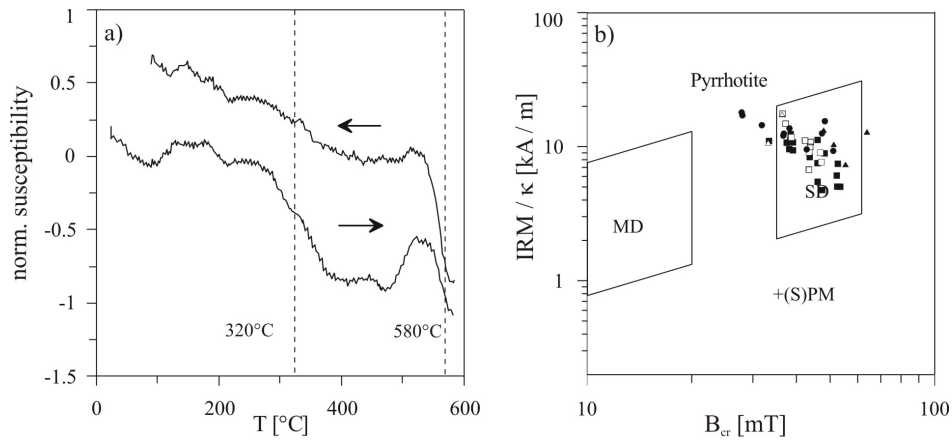


Figure 21: a) High temperature susceptibility curve for sample 23 showing significant breakdown of pyrrhotite and magnetite at their Curie temperatures (320°C, 580°C and the typical transformation of pyrite to magnetite at high temperatures; b) Bradshaw-Thompson diagram indicating that grain-size is dominated by single domain magnetite and a trend towards pyrrhotite as part of the mineral composition in a few samples from green areas (symbols as in Fig. 20).

The intensity of saturation IRM (SIRM) for the different sampling locations varies over one order of magnitude and ranges from 10.69 to 106.98 A m⁻¹/kg, while the susceptibility χ (kappa normalized by the sample weight) remains less variable between -0.7×10^{-9} and 0.13×10^{-9} m³ kg⁻¹. Susceptibility χ and SIRM are covariant (Fig. 22) and the almost linear trend between the two parameters in a binary diagram (Fig. 23) indicates that both are due to the ferromagnetic components of the PM. The constant ratio furthermore suggests that the most significant difference between the sampling locations is in the relative concentration of the ferromagnetic components. The deviation of one population of main street samples yielding elevated susceptibility from the linear trend may be due to an increasing contribution of ultrafine (superparamagnetic) particles from diesel emissions, which are known to possess exceptionally high susceptibility. Alternatively a higher contribution of paramagnetic particles to the total susceptibility might be envisaged, initiated by very high resuspension of street dust particles due to heavy traffic.

B_{cr} values (17.15 to 63.86 mT) and s-ratios (0.96 to 0.99) further confirm the low-coercivity mineral magnetite as the dominant remanent magnetic mineral in all samples. The B_{cr} value may indicate the mean grain-size [46], provided that one mag-

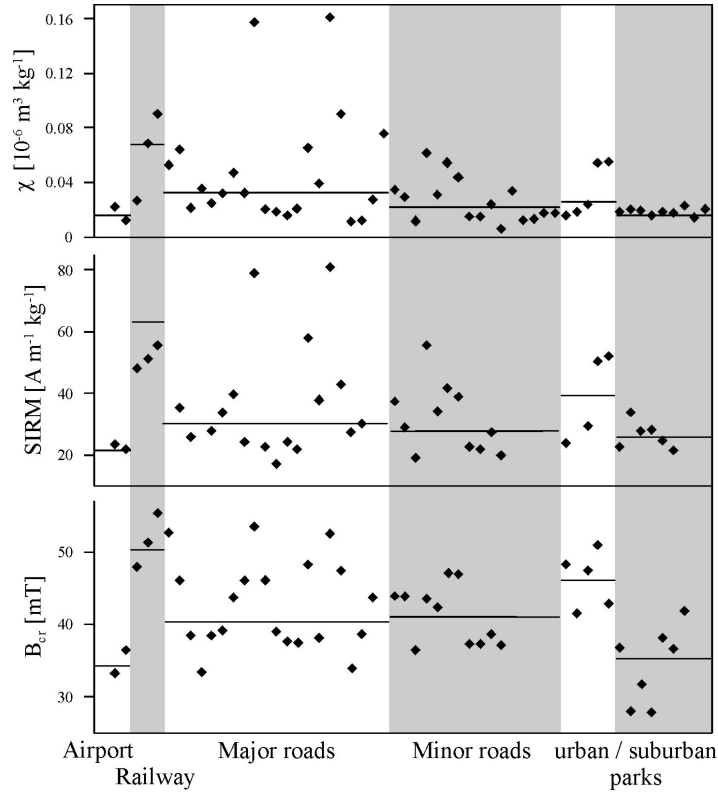


Figure 22: Selected magnetic properties (χ , SIRM and B_{cr}) of samples discriminated by traffic exposure. Lines show median value. Samples taken near the airport reveal low PM concentrations and large grain-size, those taken near railways exhibit higher PM load and small grain-size, major roads show a bimodal pattern with some sample showing high PM-load but variable grain size, minor roads reveal low PM-accumulation and larger grain-size and green areas/parks give lowest PM loads and bimodal grain-size distribution.

netic mineral dominates and that the grain-size distribution is narrow and gaussian. The samples almost exclusively contain single domain magnetite as determined by the discrimination diagram (Fig. 21b) after Bradshaw and Thompson [25]. The magnetite predominance is compatible with the SEM inspection and the ARM intensities. The latter range from 0.18 to 6.79 A m⁻¹/kg is well correlated with the IRM intensities (correlation coefficient $r^2 = 0.8$). The ARM is best developed in smaller, low-coercivity grains. These would cause a deviation from the constant SIRM/ARM ratio if there were contributions from larger grains in some samples. This is obvious for only one outlying sample in figure 23b that derives from a railroad operations site. Using Moessbauer analyses and high-temperature susceptibility measurements Muxworthy et al. [161] determined PM collected on filters in Munich to contain a mixture of magnetic particles with about 40% metallic iron and 60% maghemite. This cannot be deduced from the analysis performed in this work. In a subsequent paper Muxworthy et al. [162] demonstrated that PM in heavy traffic streets of Munich is strongly correlated with SIRM, which is due to ultrafine (<0.1 μm) magnetite-like particles carrying a maghemite oxidation rim.

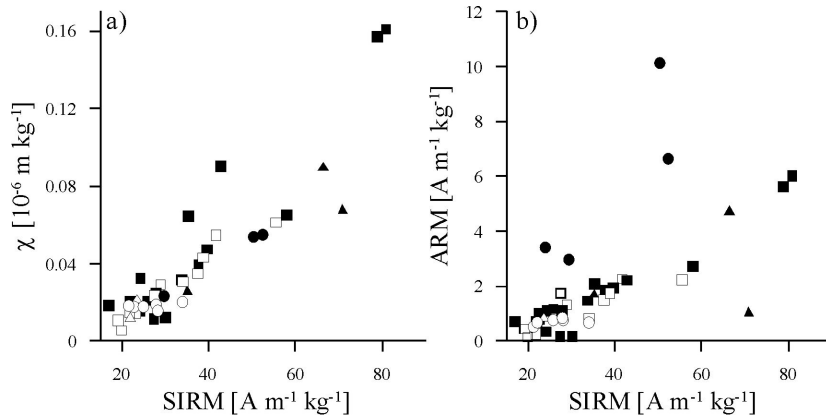


Figure 23: Grain-size effects on a) susceptibility and b) ARM analysis. Higher values indicate smaller grain-sizes. Deviations from linear trend (correlation coefficient $\chi/\text{SIRM } r^2 = 0.8$, $\text{ARM}/\text{SIRM } r^2 = 0.7$, $n=48$) for samples exclusively from major streets in a) may be due to street dust resuspension rather than contribution of ultrafine diesel soot particles (symbols as in Fig. 20).

3.1.4 Discussion

Quality and reliability of magnetic biomonitoring The key question in any biomonitoring study is whether the samples are compatible with the true $\text{PM}_{2.5}$ or PM_{10} content of ambient air. Morris et al. [157] suggested a good correlation between the susceptibility and the total PM_{10} fraction captured daily in filters, whereas Muxworthy et al. [160] assume that climatic effects may bias the grain-size composition in filters collected weekly. Our study was designed to collect PM accumulated over a longer time-period of 1 - 3 years, on the assumption that the average atmospheric pollutant load in a specific region over such an interval is more relevant to human health risks. Importantly, short-term climatic effects will be averaged out by the particle load accumulated on a pine needle [147]. Figure 24 displays three curves from the monthly sampled site (location 53, Fig. 17). The epicuticular wax content was separated from the needles by chemical means, i.e. precipitation of the wax out of an extract acquired by accelerated solvent extraction [123]. The amount of epicuticular wax recovered is strongly temperature-dependent [233] and no correlation with the respective magnetite concentration on fresh or older needles is observed (Fig. 24). This suggests that there is no significant temperature dependence on magnetic susceptibility and, hence, on the magnetic components of the PM in long-term biomonitoring studies. The drop in magnetite concentration during the summer months may result from dilution of PM_{10} [85]. The concomitant increase of susceptibility values of older and younger needles indicates that there is no uptake of fine particulate matter to the inner needle and the wax layer, as would be expected in a stagnating uptake process like that observed for PAH on young needles ([233, 123]).

Distribution patterns According to statistical data acquired by the local authorities (Landesumweltamt NRW) traffic contributes about 50% to the dust load (PM_{10}) in Cologne City, 35% is emitted by industry and 15% is related to domestic heating. Pollution due to railways is assumed to account for only 3% of the total traffic emis-

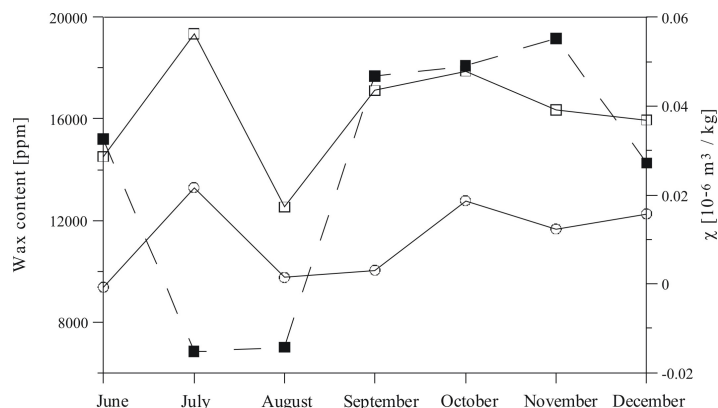


Figure 24: Concentration variation over 6 month (June to December 2002) of wax content and magnetic minerals accumulating on *Pinus nigra* needles. Broken line and filled squares = wax content of older needles; circles = susceptibility of young needles; open squares = susceptibility of older needles.

sion [117]. Moreno et al. [156] suggested that highest susceptibilities measured in the city of Rome (Italy) were caused by railway pollution. The average values of SIRM and susceptibility measured on *Platanus sp.* and *Quercus ilex* biomonitors in Rome were comparable to those determined for Cologne City, while maximum intensities in Rome were about 40% higher. The main sources of PM in urban areas are traffic emissions, especially those produced by combustion of fossil fuel. This is illustrated by the magnetite spherulites identified by SEM (Fig. 18). Unfortunately, industrial contributions or building sites cannot be discriminated by pine needle biomonitoring. Using glass fibre samplers for daily monitoring in Hong Kong Shu et al. [223] were able to differentiate these sources. The higher resolution efficiency of glass fibre filters gave 100 times higher SIRM and susceptibility values when compared to biomonitors. Certainly, daily measurements will reveal variations in specific sources more clearly than needles which time-average signals over periods of 1 to 3 years. Flanders [58] discussed the possibility of following pollution clouds from power stations by magnetic measurements over large distances in the USA (10 to 100 km). Sampling height exerts a major control on the contribution of PM with lower sampling height overemphasizing traffic and higher sampling height pronouncing long-distance atmospheric PM fall-out from power plants [251]. Samples taken in this study were collected at 1.5 to 6 m above ground level and may thus underestimate the contribution from domestic heating (chimney heights >6 m) and PM from ubiquitous coal-fired power plant emissions. Figure 22 shows the highest values and thus also the finest grain-sizes related to railway operations. The grain-sizes of all other locations vary more strongly than the aforementioned concentration parameters. This may partly result from difficulties in assigning the primary contamination source(s) to the respective localities. Some of the main street samples, for example, are also influenced by trams and therefore may have much higher values than other street samples. The distribution patterns of the PM concentration-dependent parameters SIRM and χ are illustrated in figure 25. The background concentration is relatively low with SIRM values of $\approx 30 \text{ Am}^{-1}/\text{kg}$. Only few samples at main roads (locations 18, 30, 38, 36, 50) and/or near tram lines (11, 29, 21, 47 - 49) in the inner city reach twice this concentration level. Location 11 in

the south of Cologne registered more than three times the regional pollution level (Fig. 17, Fig. 25a). The railway 5 m from this sample site is assumed to be the main source for this magnetic PM contamination. The magnetic susceptibility shows comparable isopleths (Fig. 25b), thus indicating an urban PM background concentration at $0.023 \times 10^{-6} \text{ m}^3 \text{ kg}^{-1}$. Samples taken at inner city locations reach six times higher SIRM-values. The denser sampling net for χ in the east of Cologne (Fig. 17, 25a,b) depicts a rural-urban gradient from suburban to inner city areas that is related to traffic volume and differences in air mixing and building development, respectively.

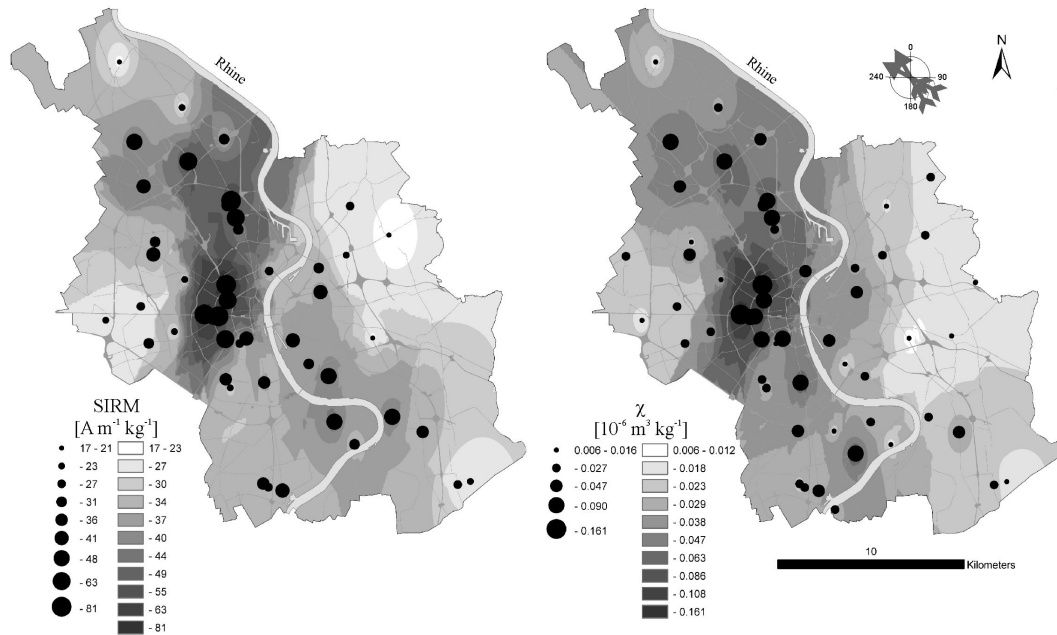


Figure 25: Contour maps showing the distribution patterns of magnetite concentration in Cologne determined by a) SIRM ($n=48$) and b) χ values ($n=56$). Major roads and freeways are shown in grey and prevailing north-westerly wind directions are indicated by the compass card. Highest PM accumulations occur along a NW trend predefined by the topography of the Rhine Valley. Hot spots occur in the western part of the city centre due to high traffic density and in the SE sector probably due to an industrial point source.

Spatial variation of magnetic particle grain-size for Cologne City is shown in figure 26. Relatively coarse magnetite grains ($B_{cr} < 40 \text{ mT}$) appear to be the background load, which is augmented by finer grains ($B_{cr} < 48 \text{ mT}$) at main streets and finest particles ($B_{cr} > 48 \text{ mT}$) near railways or tram lines. Sampling point 38 in a calm side street about 300 m from the highway represents a location characterized by small grain-size at high concentration. This indicates that, depending on local wind regime, PM may be transported over significant distances from its source. The same may be true for several locations in inner city parks, where exceptionally high SIRM values were recorded (see two SIRM maxima in Fig. 22: sample 36 and 53). The main source for the air pollution in Cologne seems to be motor vehicle traffic. The well-developed tram and railway system produces the highest PM concentrations of the most dangerous, ultrafine grain-sizes. Being almost completely electrified, trams and trains generate magnetic PM preferentially through wear and tear and not via combustion processes.

Additionally, in the inner city there seems to be a background signal originating from one or more downwind sources, suggesting the possibility of identifying pollution clouds from greater distances using biomonitors. The identification of such pollution clouds in the background of point sources is further illustrated in figures 25 and 26 where the dominant wind direction in Cologne is given. Both patterns exhibit the lowest concentrations towards the east and the west side of the city, suggesting a wind-driven accumulation of the pollution along the Rhine River valley. Atmospheric pollutants produced in the south of Cologne and in a major lignite-fired power station to the southwest appear to cause a SE-NW trending pollution corridor.

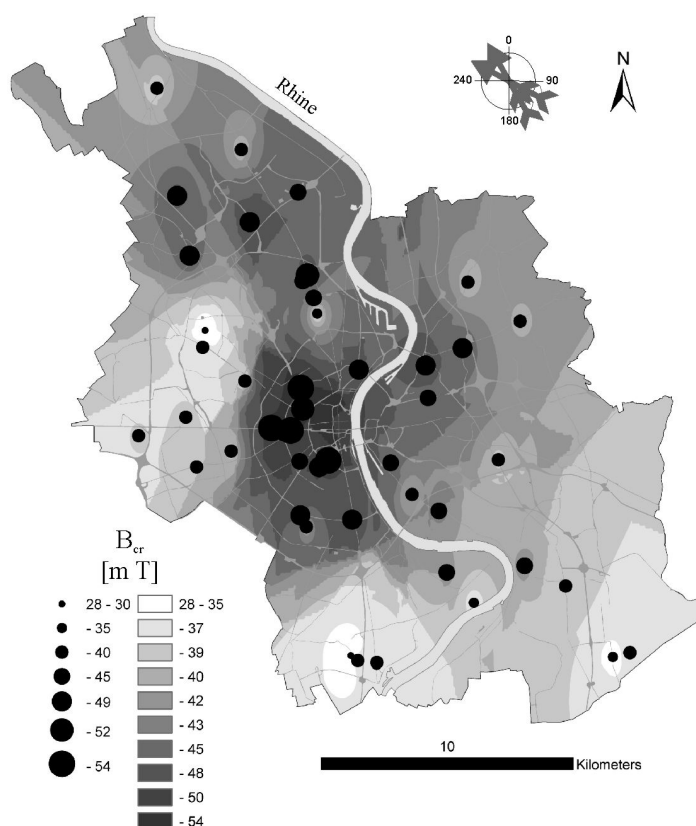


Figure 26: Contour map showing the distribution pattern of magnetite grain-size in Cologne determined by B_{cr} values (mT), with higher B_{cr} values indicating smaller grain-size. Major roads and freeways are shown in white and prevailing north-westerly wind directions are indicated by the wind rose. Smaller grain-sizes preferentially occur in a NW-trending corridor, parallel to the Rhine Valley. Areas with small grain-size predominating occur around the western part of the city centre and in the SE sector, coinciding with higher magnetic PM loads.

3.1.5 Conclusions

Microscopic investigations of pine needle surfaces revealed significant amounts of organic particles, siliciclastic fragments, glass spherules, and most importantly, iron-bearing spherules accumulation in the $PM_{2.5}$ range.

Iron bearing spherulites were identified as the main carriers of the magnetic properties and are almost exclusively composed of magnetite with minor pyrrhotite. Magnetite is assumed to derive preferentially from the combustion of fossil fuels, whereby in Cologne City traffic emissions predominate over power plant-derived fly ashes.

A second important source of magnetite is provided by the railway and tram system, which yields PM upon wear and tear. Samples influenced by these sources show characteristically high χ and SIRM values.

The magnetic properties, especially the B_{cr} -values, suggest that the grain-size of magnetic PM varies between 0.03 and 2.5 μm . An excellent correlation between the total iron content of pine needles and the SIRM-values confirms that environmental magnetic analysis serves as reliable proxy for PM-pollution. On average 14 $\mu\text{g g}^{-1}$ of the total iron content, which ranged between 40 to 400 $\mu\text{g g}^{-1}$ may be attributed to biogenic iron.

Spatial distribution patterns reveal that the highest PM-load is associated with areas of high traffic density. Contouring reveals pollutant maxima governed by the topography and associated wind regime of the study area. A corridor defined by the SE-NW-trending Rhine Valley acts as a sink for PM-accumulation.

Biomonitoring using pine needles is well suited for long term monitoring of air quality, whereby wash-off by rain and wind abrasion was found to be negligible in altering the accumulation state. Environmental magnetics offers a powerful tool to generate data sets at high spatial and temporal resolution in short times and at very affordable costs. This may allow for the continuation and extension of environmental monitoring as required under EU-regulation EU96-61-EC [3] even under constrained budgets.

3.2 Cologne City air quality - major and trace elements

Plants have been used intensively as biomonitors and bioindicators of atmospheric pollutants in urban, rural and in remote areas [142, 186, 11, 195, 143]. Plants can be used for sensitive biomonitoring, i.e. reactions of plants (injuries, physiological stress symptoms, changes in plant community structure) against environmental factors are assessed. Alternatively, accumulative biomonitoring is applied. Thereby, the capability of vegetation to bind gaseous, liquid and particulate atmospheric pollutants is employed [11]. In previous studies accumulative biomonitoring was used in Cologne City to assess abundance, spatial and temporal distribution and potential sources of selected atmospheric pollutants, namely magnetic particles and polycyclic aromatic hydrocarbons [255, 123]. In this chapter trace metals in pine needles as a third important class of atmospheric pollutants are addressed.

The detrimental effects of heavy metal uptake onto human health are undisputed [101]. Evaluation and monitoring of air quality as required by EU regulations [49, 50] includes determination of lead concentrations in air. This mandate necessitates monitoring air quality continuously and at high spatial resolution, which will be costly if achieved by active air sampling. Biomonitoring of trace metals as with other pollutants, e.g. PAH, PCB, sulfur, NO_x , offers low-cost and time-integrative alternatives.

Concentrations of trace metals in plants depend on root uptake or accumulation of dry and wet deposition on outer plant organs like foliage or bark. Several trace elements

may occur at toxic levels in soils and atmosphere, even if they are essential macro- and micronutrients (e.g. sulfur, iron, copper, zinc). Cadmium and lead are regarded as non-essential elements [142, 11]. The mobility of trace elements in soil and plant tissues is important for the understanding of accumulation and translocation processes [11]. Iron and organic sulfur are known as immobile elements, whereas copper, chromium and lead have intermediate mobilities [70]. Zinc, nickel and cadmium are easy to mobilise, highly bioavailable and therefore show rapid uptake rates in vegetation. The mobility of metals strongly depends on pH-values with higher solubility occurring in acidic environments [11, 195]. This leads to two opposing processes, wash-off of trace elements after corrosion of epicuticular waxes through acid rain and root uptake of soluble trace elements from acidic soils.

The most important sources of anthropogenic trace element emissions are mining and smelting of metallic ores, industrial production and application of iron and non-ferrous metals, combustion of fossil fuels in vehicular traffic and energy production, waste incineration, sewage sludge dispersal and cement production [171, 178, 180, 31]. In urban areas traffic pollution is supposed to be the main source for toxic trace elements like cadmium and lead [11, 33]. Some of the emitted trace elements are associated with solid particulates or occur in the gas phase, according to the prevailing combustion or manufacturing process. Lead concentration is still very high in urban dusts, even after abatement of leaded fuels in Germany [81]. Metals like iron, zinc, lead, copper and nickel often show a co-occurrence due to a common origin from sulfidic ores. During metal processing commercial cadmium is obtained as a byproduct of zinc, further explaining the covariance between both elements. Limited information exists about composition of emission from municipal refuse and sewage sludge because of their heterogeneity [11, 6]. Municipal waste incinerators often emit large amounts of zinc, cadmium and lead [33, 262, 6] and zinc is particularly enriched in tire wear [64, 35]. Anthropogenic emissions of cadmium, nickel and zinc exceed natural sources [169, 171, 170, 142, 178, 180, 11, 188] and have been proposed to lead to a “silent epidemic” by Nriagu [169].

The use of vegetation as passive sampler in biomonitoring bears the advantage of high spatial and temporal resolution, due to the excellent availability of plants and low sampling costs. Higher plants are regarded less effective as accumulative biomonitors for atmospheric pollutants when compared to mosses and lichens [11, 32]. The latter almost exclusively accumulate pollutants from atmospheric deposition but not via soil uptake [5, 32]. However, higher plants are more resistant and do occur in heavily polluted environments where lichens and mosses are very rare [11]. The reliability of plant tissues/surfaces as accumulators of airborne trace elements has been summarized in several publications [142, 11, 186, 195, 202, 143]. For biomonitoring trace element pollution lichens [142], fungi [38], mosses [79, 16, 32, 184, 154, 36, 140] and leaves/needles of higher plants [141, 4, 32, 216, 134, 138, 132, 110, 221, 140, 143] or tree bark [189, 104, 154, 181] have been used. In northern as well as in southern Europe pine trees are abundant in urban and rural areas due to their modesty and adaptability.

Trace element concentrations of pine needles have been measured frequently [166, 94, 70, 71, 200, 199, 259, 167, 242, 5, 104, 111, 154, 196, 44, 177, 250, 2, 17, 175, 52]. A summary is compiled in Tab. 11. Analysis of pine needles has been identified as a

reliable means of assessing air pollution for selected persistent inorganic and organic pollutants.

This contribution applies accumulative biomonitoring of trace metals in pine needles for detection of spatial and temporal variation in urban atmospheric pollution and for source identification. Improvement in the interpretation of foliar trace metal data is achieved through comparison with concomitantly determined magnetic properties and PAH burdens of pine needles in Cologne City.

3.2.1 Sampling

A description of Cologne City is given by Urvat et al. [255]. Over the study area 43 *Pinus nigra* samples were taken in representative locations. A time series of 14 individual samples was monthly collected from June to December 2002 at location 53 (Fig. 17). Samples were separated into fresh (current year) and old needles (previous two years). Locations were chosen to represent different urban and suburban environments and to fully reflect the heterogeneous pollutant load of the highly developed and diversified Cologne Conurbation. Based on land use the samples were divided into three groups representing residential, green and industrial areas. As a reference an additional pine needle sample was obtained from a semiurban site in Siegburg, a small town some 30 km southeast of Cologne City. For comparison three pine needle samples were collected from Poland (taken in summer 2002) comprising an urban, a semiurban and a rural area. Immediately after collection the samples were placed in paper envelopes and stored frozen to avoid changes of the pollutant concentrations in the needle before analysis.

3.2.2 Analytical methods

Sample preparation For elemental analysis the frozen needles were dried 3 to 7 days in an oven at 50°C. After that the needles were ground with a swing mill (3 min, 710 rpm). The mill was equipped with an agate grinding vessel which was shown not to introduce any contamination [255].

Elemental analysis Elemental analysis of iron, cadmium, lead, zinc, copper, nickel and chromium was carried out in the Institute of Geography, University of Cologne by use of an Atom Absorbance Spectrometer (AAS) using flame and graphite-furnace techniques (PERKIN ELMER PE 3100, PE-SIMAA 6000 Simultan-graphite-furnace-AAS). Method validation and accuracy was checked using four vegetation standard reference materials (*Olea europaea* BCR62, *Fagus sylvatica* CRM100, *Secale cereale* CRM281, pine needles NIST SRM 1575a). Iron and zinc were measured by flame-AAS, whereas cadmium, lead, copper, chromium and nickel were identified with ET-AAS (electrothermal graphite-furnace-AAS). For micro-wave assisted extraction of the target components the ground sample (200 mg) was mixed with 5 ml HNO₃ and heated to 160°C degrees for 6 hours. All analyses were done in duplicate, revealing that copper, chromium and nickel could not be determined with sufficient precision (maximum variance: $V_{Ni} = 100$, $V_{Cu} = 60$, $V_{Cr} = 9$). These trace elements were therefore not included in further discussion of temporal and spatial dispersion of pollutants. Con-

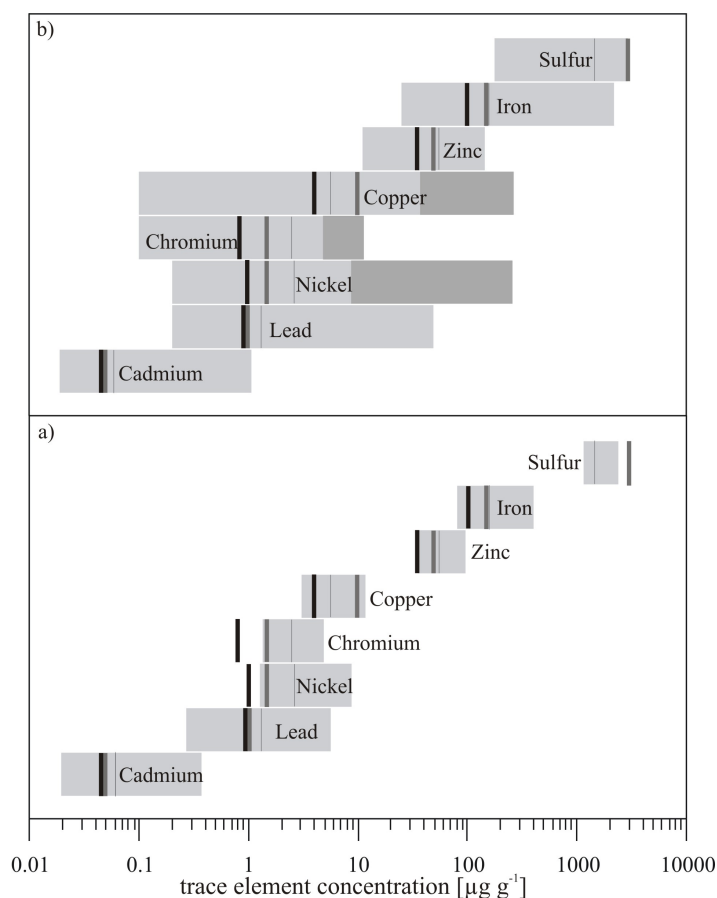


Figure 27: a: Trace element concentration ranges of pine needles in Cologne City (grey bars). b: Trace element and sulfur concentration ranges of pine needles all over Europe (grey bars). Darker grey bars indicate concentrations measured near a copper-nickel-smelter on the Kola-Peninsula, Finland. Thin vertical lines show median values, solid black lines refer to averages of unpolluted pine needles [11] and solid grey lines represent concentrations for a ‘reference plant’ after Markert [141].

concentration ranges determined for chromium, nickel and copper in Cologne pine needles agree with ranges reported for other vegetation samples (Fig. 27a, b).

3.2.3 Results and discussion

Foliar trace element and sulfur concentrations Cumulative absolute concentration of trace elements (Cd, Pb, Ni, Cr, Cu, Zn, Fe) from dried and ground needles from Cologne City vary between 124 and 489 $\mu\text{g g}^{-1}$ (n=52). The highest trace element content is reached in a Cologne pine standing 2 m beneath a high traffic road in the inner city (sample 47, Fig. 17). Sulfur contents of pines in Cologne range between 1167 and 2379 $\mu\text{g g}^{-1}$. The small city of Siegburg selected for comparison with the Cologne Conurbation gave low to intermediate trace element and sulfur concentrations (cumulative trace element concentration 199.5 $\mu\text{g g}^{-1}$, S-content 1373 $\mu\text{g g}^{-1}$) in pine needles.

Plant species	location	sampling time	needle age	Cd	Pb	Fe	Zn	S	Methods	Reference
<i>P. nigra</i>	phosphate fertiliser factory; Poland	1994 w	2			70	32		ICP *	Giertych et al. (1999)
	background site		2			45	25			
<i>P. nigra</i>	Cologne, residential area; Germany	2002 w	mix	0.045	1.5	194	62	1460	FAAS; S by EA	this study
	green area			0.071	1.48	156	54	1457		
	industrial area			0.106	1.32	130	54	1429		
	Siegburg, residential area; Germany			0.071	0.82	149	41	1373		
	rural area; Poland	2002 s		0.098	0.59	81	60	1680		
	Gdansk; Poland			0.052	1.32	145	77	1553		
<i>P. sylvestris</i>	10 - 30 km to power plants; Estonia	2000 s	2				40	700	unspecified	Ots (2003)
<i>P. sylvestris</i>	40 km to Cu/Ni-smelter; Kola Peninsula	1991	2	0.06	0.3	216	40	1130	ICP-MS *	Steinnes et al. (2000)
	10 km to Cu/Ni-smelter		2	0.11	5.8	702	31	1520		
<i>P. sylvestris</i>	400 km to Cu/Ni-smelter; Kola Peninsula	1990 / 91 w	2			35	13	678	XRF	Rautio et al. (1998b)
	10 km to Cu/Ni-smelter		2			337	79	1941		
<i>P. sylvestris</i>	30 km to Cu/Ni-smelter; Kola Peninsula	app. 2000	2			50	39	1212	ICP/AES+XRF *	Kopitsik et al. (2001)
	10 km to Cu/Ni-smelter					84	41	1552		
<i>P. sylvestris</i>	Holy Cross Mountains; Poland	1998 / 99	2	0.40	3.5	95	52	550	ICP/AES § FAAS, S%	Migaszewski et al. (2001)
<i>P. sylvestris</i>	Leipzig; special waste dump; Germany	1995 / 96 s	2	0.40	3.0	113	26		ICP-AES	Weissflog and Wenzel (1997)
	vehicle traffic			0.20	2.6	73	39			
	railway			0.30	0.3	132	38			
	firing plant for pit coal			0.10	3.0	40	26			
	production plant for charcoal			0.10	3.5	90	83			
	urban			0.80	2.3	105	100			
	rural			0.10	1.0	151	21			
	Island Rügen, coast			0.30	2.3	48	24			
<i>P. sylvestris</i>	Plantation, W- Rhodopes; Bulgaria	app. 1997	n.s.			172	38		unspecified *	Malinova et al. (1995)
<i>P. pinca</i>	Palermo, min.; Italy	1998 s	mix			4.0	120	11	INAA+ICP/MS	Alaimo et al. (2000)
	max.					50.0	2200	60		
<i>Pinus L.</i>	Berlin, rural; Germany	1991	n.s.			6.2		1621		Berlin Senate Department of Urban Development (1991)
	Berlin, suburban					6.9		1744		
	Berlin, urban					8.3		1905		
<i>Pinus L.</i>	urban-industrial (medians); Korea	app. 2000	mix	0.22		77	50		NAAS	Kang and Lee (2001)
	Dubna; Tver Region			0.06		240	39			
<i>Pinus L.</i>	Baltic	2001	2	0.20	3.7	67	46	1300	ICP-AES	Organization of Forest Monitoring System, Poland (2002)
	Carpathians			0.40	2.4	118	63	1400		
	N-Poland			0.20	3.6	74	46	1300		
	C-Poland			0.20	1.6	92	52	1300		
	S-Poland			0.50	3.2	140	76	1400		
<i>Pinus L.</i>	Dübener Heide; Germany	2002	1	0.19	0.6	57	41	1080	ICP-MS *	UBA, Germany (2004)
<i>Pinus spp.</i>	unpolluted areas; Italy		2	0.06	1.0	100	35		unspecified*	Bargagli (1998)

Table 11: Compilation of trace element data for pine needles in $\mu\text{g g}^{-1}$.
 * mean values, # median values, § mean of range, % sulfur determined by coulometry, w/s winter/summer samples, n.s. not specified.

Reference samples from Poland ($n=3$) show intermediate trace element concentrations with a range from 137 to 234 $\mu\text{g g}^{-1}$, whereby the pine located in the city of Gdansk presents the maximum trace element pollution for Polish samples (Tab. 11). Foliar sulfur loads in Polish samples vary between 1553 and 1786 $\mu\text{g g}^{-1}$, with the maximum yield occurring in a small town in central Poland.

Concentration ranges and median values of individual trace elements (Cd, Pb, Ni, Cr, Cu, Zn, Fe) and sulfur are shown in Fig. 27a and Tab. 11. Cadmium revealed the lowest ($0.06 \mu\text{g g}^{-1}$), iron and sulfur (165 and $1451 \mu\text{g g}^{-1}$) the highest median concentration. Median values determined for copper, chromium and nickel, although giving high variability upon duplicate-analysis, do fit levels characteristic for European pine needles (Fig. 27a,b).

Pollution of needles in Cologne City was previously shown by microscopical investigation to occur preferentially particle-bound [255]. Microscopically identified metallic particles revealed high correlation between enviromagnetic properties, total iron and PAH-concentration [123] and were interpreted to be preferentially combustion-derived. The rationale for source allocation of trace elements thus is based on iron abundance as discussed below.

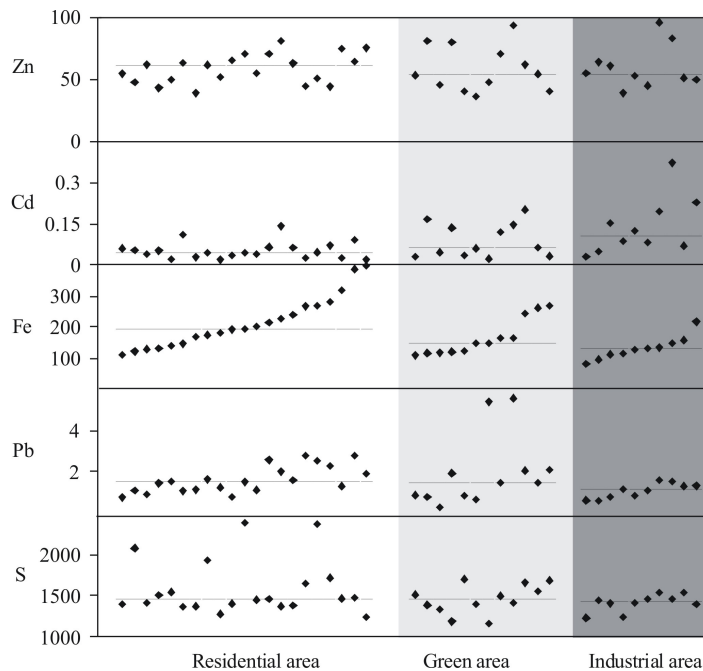


Figure 28: Trace element and sulfur concentrations of samples discriminated by land use. Horizontal lines show median values. Samples taken near industrial areas show high cadmium contents.

The differentiation based on land use shows that due to heavy traffic the median of foliar iron abundance (Fig. 28) is highest in residential areas ($194 \mu\text{g g}^{-1}$) and low in park and industrial areas ($130 \mu\text{g g}^{-1}$ and $148 \mu\text{g g}^{-1}$, respectively). Three samples from parks close to heavy traffic roads gave particularly high iron concentrations between $245 \mu\text{g g}^{-1}$ and $270 \mu\text{g g}^{-1}$ (Fig. 28). Low correlation between Fe and Pb, Cd, Zn and sulfur concentrations (Fig. 28) argues against a major control of trace element and sulfur due to traffic emissions. In residential areas lead shows a correlation with iron (Fig.

28) and may be preferentially related to vehicle emissions. Two park samples reveal significantly enhanced lead concentrations of $5.38 \mu\text{g g}^{-1}$ and $5.55 \mu\text{g g}^{-1}$ (Fig. 28), whereas the three iron-enriched park samples give only average lead values. No land use differentiation is observed for zinc, lead and sulfur arguing for multiple sources and intensive mixing of air masses in the Cologne Conurbations as reported by Lehndorff and Schwark [123]. Cadmium is the only trace element being enriched in industrial areas (Fig. 28).

Local environmental factors may exert a major control on foliar trace element abundance [142, 11]. Thus, prior to the detailed discussion of sources and spatial variability of trace metal pollutants, the influence of environmental conditions will be addressed.

Seasonal variations in trace element concentrations Time series samples taken from June to December 2002 at location 53 (Fig. 17) reveal systematic changes in element yields associated with needle growth and meteorological conditions (Fig. 29). Variability in iron, lead and cadmium concentrations reaches 30-60 %, with minima in August and November/December. Sulfur and wax show a profound low in the summer months July and August but relative constant concentrations in winter, whereas zinc contents are continuously rising till December. The coincidence in wax and sulfur decline is interpreted as wax erosion due to enhanced formation of sulfuric acid from sulfate aerosols in combination with warmer temperatures [199, 111]. Wax erosion affects the current year as well as the older needle generations. Amongst the trace elements cadmium concentration closely follows the wax erosion trend for the current year needles, whereas previous years needles are not affected (Fig. 29) due to a fixation of cadmium in deeper wax layers or in needle tissue. Previous years needles show parallel trends in Cd, Fe, and Pb concentrations indicating particulate accumulation of these elements as airborne pollutants on the needles surface. The constantly rising zinc contents lacking any connection to precipitation are characteristic for an essential bio-element [11]. The zinc decline in second year needles can be explained by the high mobility of this element and plant internal translocation [79].

In terms of seasonal variability it should be considered that physiological changes during the winter period may affect foliar trace element concentration. When normalized to needle dry weight the loss of starch or other storage compounds [11] may lead to relative enhancement of essential and pollutant trace elements. The substantial increase in iron and lead concentrations from current to previous year needles is explained by pollutant accumulation. Quasi-constant concentrations for diverse needle generations as observed in the case of sulfur and zinc indicates their role as essential bio-elements. This is in accordance with their median concentrations being close to or even lower than reported for unpolluted reference plants as shown in Fig. 27a.

Historical trends in trace element pollution Implementation of stricter environmental regulations during the past two decades lead to a strong decrease in atmospheric emissions [81, 30, 31, 143]. Especially for selected trace elements the installation of filters in coal fired power plants or the ban of lead-based fuel additives marked a significant decline. The Environmental Specimen Bank of the German Federal Environmental Agency from 1991 to 2003 annually collected and analysed the variation in trace elements of pine needles from the Dübener Heath, near Leipzig, Saxony [52].

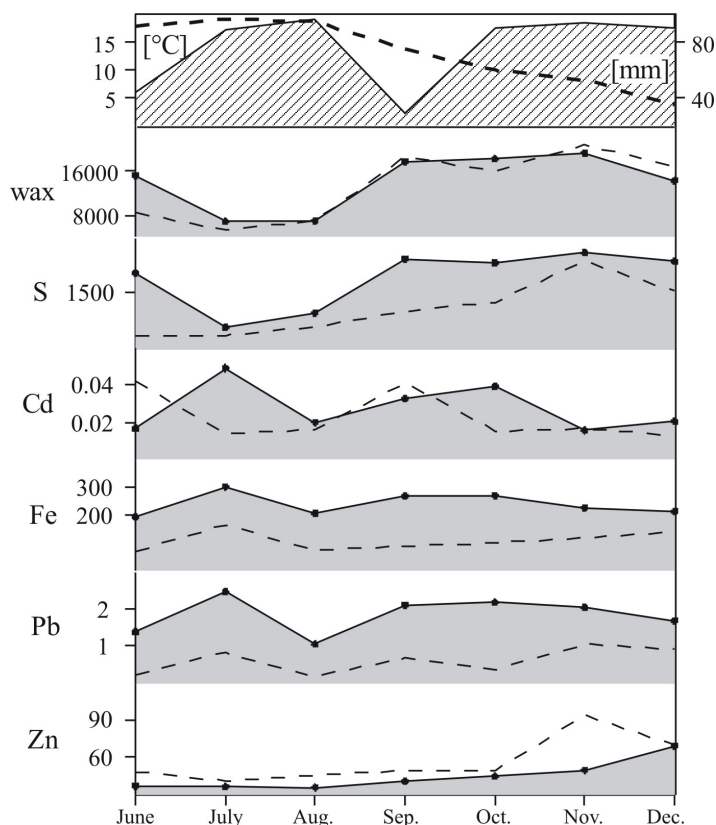


Figure 29: Seasonal variations in element contents of current year (dashed line) and 1 to 2 year old needles (solid line) of one selected pine tree in an urban park area in Cologne ($\mu\text{g g}^{-1}\text{d.w.}$). Temperature (dashed line) and precipitation curve for the year 2002 are given for comparison.

The data shown in Fig. 30 document that lead and iron are primarily traffic pollution derived elements, because there is a significant decline in the concentrations parallel to evolving environmental legislation. Fig. 30 also explains the constant sulfur level measured in Cologne pine needles in 2002. Reduction of sulfur emissions has come to an end since about the year 2000 and sulfur emissions have reached a constant level. The parallel decline in Fe-concentrations for this region (Fig. 30) is associated with the installation of effective filters in lignite-fired power plants following the German reunification in 1989. Relatively stable cadmium concentrations of the past decade testify to an origin from industrial processes, whereby the emissions have not changed. The small variability in zinc concentrations can be interpreted as environmentally induced change in nutrient availability.

Emission-dependent variation in trace element yield and composition In urban areas traffic comprises the dominant source of atmospheric emissions [225]. Therefore Cologne City samples were assigned to the following traffic exposure and land use characteristics: major roads, minor roads, railway, airport and parks. A clear differentiation of trace element loads in pine needles according to variable traffic exposure could not be observed. Therefore, a more simple and traffic-independent classification was applied. Samples were separated after location in residential areas, green areas

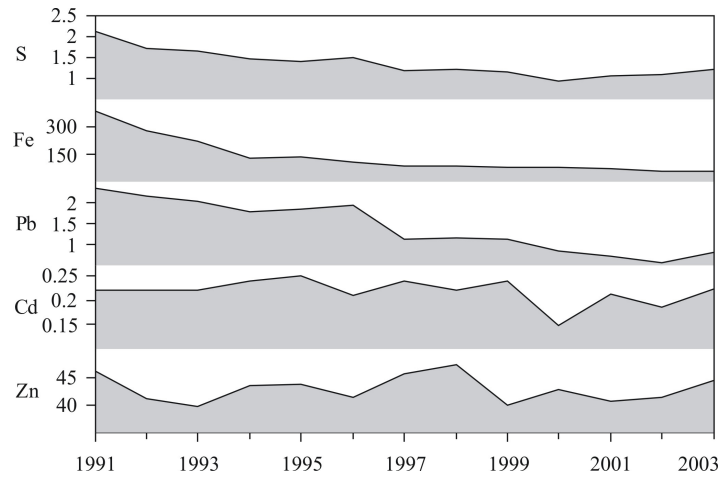


Figure 30: Annual variations in element contents of one year old pine needles in the Dübener Heath in northeast Germany (data from the Federal Environmental Agency, 2004). Cd, Pb, Fe, Zn in $\mu\text{g g}^{-1}$, S in mg g^{-1} . Lead, iron and sulfur show a decline over the years, with sulfur and iron approaching constant concentrations since about 2000.

and those taken near industrial areas (Fig. 28, Tab. 11). Details of land use characteristics are depicted in figure 17. The median values for cadmium concentrations in pine needles taken near industrial areas are higher ($0.106 \mu\text{g g}^{-1}$) than in residential areas ($0.045 \mu\text{g g}^{-1}$), pointing out industrial combustion processes as main source for the cadmium concentrations in the Cologne Conurbation. Alternatively, agricultural fertilizer application has been identified as a major source of cadmium emission [11]. Within Cologne City this interpretation is not appropriate because the spatial distribution of foliar cadmium load shows no correlation with agricultural land use.

Iron and lead show similar seasonal accumulation trends (Fig. 29) and a good coefficient of correlation ($r^2=0.54$, Fig. 31a). As iron was previously identified as a proxy for predominantly traffic-derived emissions [255, 123], an origin of lead from the same source is supposed. The correlation of iron with cadmium (Fig. 31b) separates two distinctive sample groups. The first while having highly variable cadmium contents but constant iron values is attributed to industrial emissions, in agreement with land use classification. The other group is composed of samples having highly variable iron contents but constant cadmium levels and reflects variation of traffic emissions in residential areas. Samples taken from parks and green areas show variable iron and cadmium concentrations depending on predominance of either traffic or industrial influence. The trace elements zinc and cadmium are geochemically closely related and usually show co-evolutionary trends and behaviour [142]. Foliar concentrations within Cologne City reveal a distinctively different correlation of both elements against iron (Fig. 31c) and thus confirm their different sources. The pollution origin of elevated trace metal concentrations in Fig. 31 is recognized by the deviation from indicated essential micronutrient concentrations. It is assumed that the enhanced zinc concentrations in residential areas are traffic-associated due to the known input from tire wear [35]. Multiple sources for iron and cadmium are also shown by a comparison of the source-significant ratios of Cd/Fe and fluoranthene/pyrene (chapter 3.3) as shown in Fig. 31d. Again three different groups are recognized. Residential areas are charac-

terized by traffic related variability in fluoranthene/pyrene and constant Cd/Fe-ratios. Industrial zones exhibit a high variability in Cd/Fe-ratios accompanied by invariant fluoranthene/pyrene-ratios. Parks being influenced by both emission sources show a constant trend between the two proxy parameters.

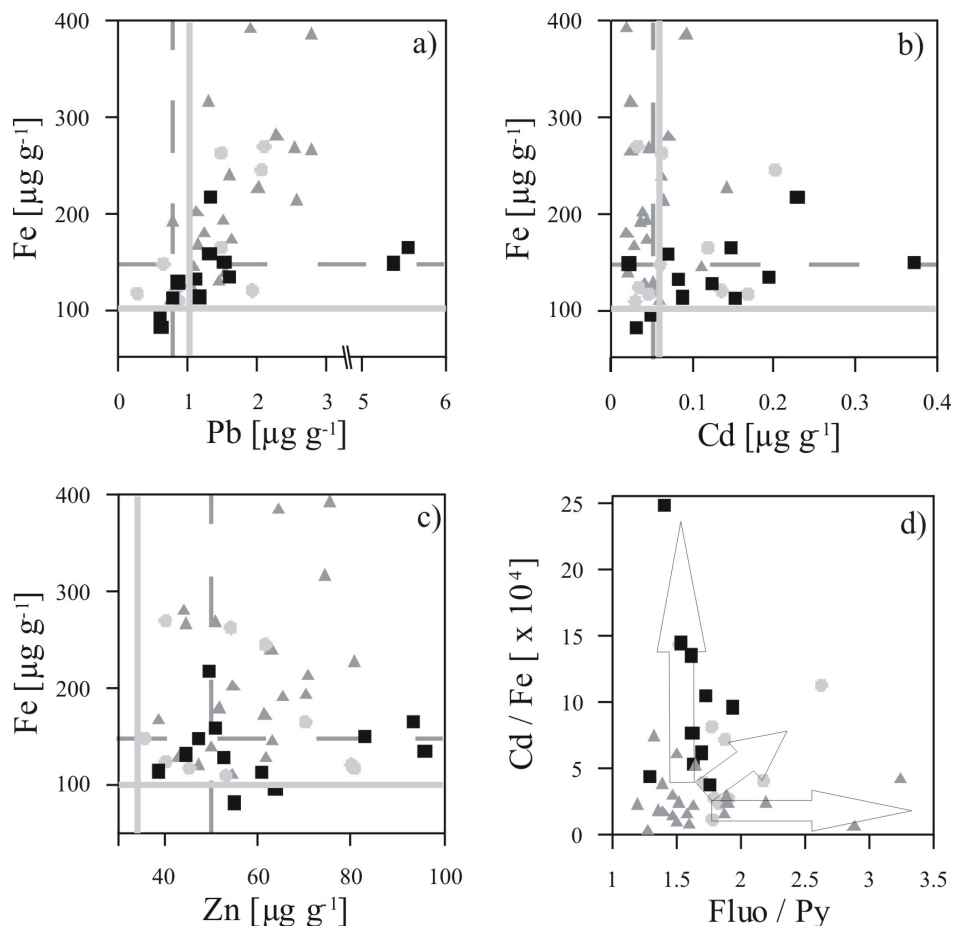


Figure 31: Bivariate plots a) to c) of traffic pollution proxy iron against lead, cadmium and zinc. Symbols are: grey triangles = residential areas, grey circles = green areas, black squares = industrial areas, grey line = ‘reference pine’ [11], dashed line = ‘reference plant’ [141]. The correlation coefficient of Fe/Pb is $r^2=0.54$, except for two samples taken near industrial areas with exceptional Pb contents, pointing towards Pb as being traffic derived. d) Plot of the PAH-ratio fluoranthene/pyrene (Fluo/Py) against Cd/Fe. Fluo/Py-ratio differentiates locations according to traffic combustion processes. Cd/Fe highlights samples taken near industrial areas.

Spatial variation The spatial variation of foliar trace metals in Cologne City shown in Fig. 32 reveals a pattern similar to those found for foliar magnetic properties [255] and PAH loadings [123]. Maximum foliar cadmium loadings occur in the NW-sector at sampling points 22, 31, 32 (for locations see figure 17) and are related to large industrial complexes. Similarly, in the NE-sector industrial activity leads to enhanced foliar Cd-concentrations around points 16, 19 and 21. The western outskirts of Cologne also show minor enrichment in industrial-derived foliar Cd-abundance around locations

35 and 46. In the southernmost part along the river Rhine minor industrial emission is indicated by slightly elevated Cd-concentrations around locations 8 and 9. The industrial emission character is confirmed for locations 8, 9, 16, 19, 21 and 22 by PAH profiles revealing enhanced ratios of benz[a]anthracene over benzo[a]pyrene (Fig. 40d). Locations 31 and 32 differ by low benz[a]anthracene over benzo[a]pyrene-ratios thus pointing to a different source or emission mode for industrial cadmium. The fluoranthene versus pyrene ratio also spatially resolves industrial pollution (Fig. 40e). Industrial areas with a low PAH-ratio coincide with high Cd-levels and vice versa. Low fluoranthene/pyrene-ratios in locations 8 and 9 are masked by elevated values of adjacent locations 6 and 7. The inverse relationship between Cd-concentrations and fluoranthene/pyrene-ratios observed in the spatial data set agrees well with the correlation observed in the land use classified data set discussed in Fig. 30d.

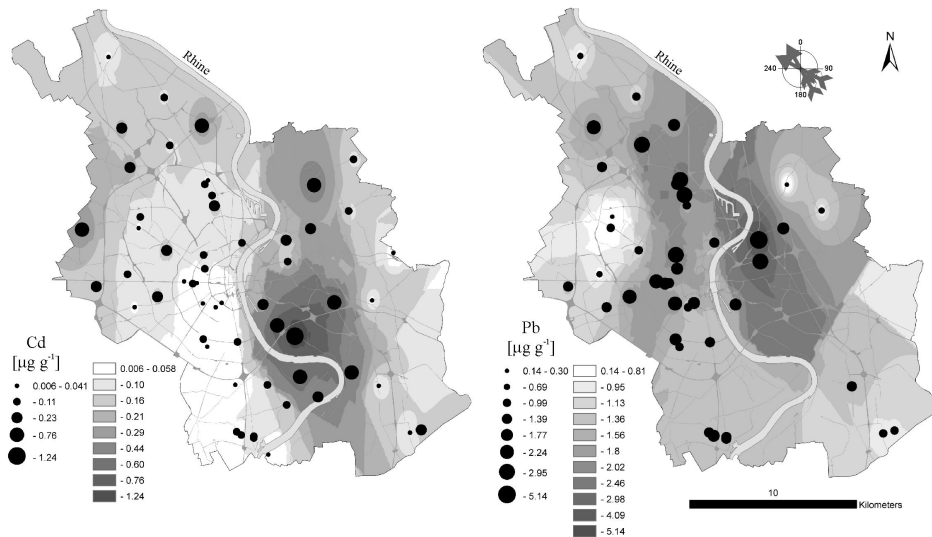


Figure 32: Isopleths maps of Cd ($n=56$) and Pb ($n=42$) concentrations ($\mu\text{g g}^{-1}\text{d.w.}$) within Cologne City. White lines indicate major roads, black lines represent freeways, for details of land use see Fig. 17. Open circles represent sample locations with different sizes indicating trace element concentration classes. Contouring was achieved using ArcGIS Spatial AnalystTM, discriminating 16 contour intervals. For prevalent wind directions see compass card taken from Brücher and Kerschgens [26]. Pb serves as tracer of traffic, Cd as proxy for industrial foliar pollutant loads.

Spatial distribution of foliar lead concentrations (Fig. 32) reveal higher values east of the Rhine river and in the high traffic area of the inner city. The western region of Cologne City is characterized by lower Pb-concentrations with minima observed around locations 33, 34, 35 and 37 (Fig. 17). This minimum is also evident from the spatial distribution of magnetic properties SIRM and B_{cr} (Fig. 25, 26). Accordingly, maximum values observed for Pb-concentration around locations 11 and 21 match maxima in magnetic properties. Traffic related PAH-concentrations and compound ratios also correlate with Pb-concentrations. The sum of 3- to 6-ring PAH provides a good measure of traffic density (Fig. 40b) and coincides with high foliar Pb-loads. The traffic-influenced indeno[1,2,3-c,d]pyrene vs. benzo[g,h,i]perylene ratio (Fig. 40c) is negatively correlated with Pb-concentrations and especially confirms the low input

of vehicular emissions around locations 13,14, 24, 31 and 32 [287]. In general a good correlation between foliar proxy parameters for traffic emission is observed for magnetic properties, PAH composition and trace element distribution.

3.2.4 Summary and Conclusions

Trace elements in pine needles growing in Cologne City preferentially reflect atmospheric pollutant loads. Seasonal variability of foliar trace element concentrations affects sulfur and cadmium concentrations due to their susceptibility to wax erosion during high precipitation periods. Fe and Pb are less affected and Zn reacts as an essential bio-element independent of precipitation events. Foliar lead and iron contents systematically increase with needle age, whereas sulfur and zinc remain on constantly low bio-element levels. Cadmium concentration of the current year needle generation is affected by wax erosion but cumulative concentration over 2-3 needle generations agrees with foliar Fe and Pb profiles. Pine needle trace element concentrations are suitable for biomonitoring purposes although other vegetation samplers like mosses and lichens may be preferred. Foliar trace element loadings significantly decreased in Germany over the past two decades and several elements including sulfur and zinc now approach background levels or micro-nutrient levels. High variability in Ni, Cu and Cr analysis and low foliar abundance of these elements argue against biomonitoring applications in Cologne City. Pollutant source differentiation is feasible based on foliar trace element ratios discriminating preferentially traffic-related versus industrial emissions. The spatial distribution of trace elements identifies areas receiving higher industrial immission by their elevated Cd contents and regions affected preferentially by traffic-derived immission based on elevated Pb and Fe contents. Iron concentrations can be predicted by highly sensitive and high-resolution but low-cost enviromagnetic techniques [255]. Therefore, foliar trace element analysis may preferentially serve as a complementary method to enviromagnetics in areas where industrial immission is suspected or has to be evaluated.

3.3 Cologne City air quality - polycyclic aromatic hydrocarbons (PAH)

Polycyclic aromatic hydrocarbons are the products of thermal decomposition, formed during incomplete combustion of organic materials and geochemical formation of fossil fuels. Most of them are released into the environment from anthropogenic sources such as combustion of fossil fuels in power plants, domestic heating, waste incineration, industrial processes and, most importantly, motor vehicle exhaust [20, 8, 128, 144, 257]. Carcinogenic, mutagenic and immunotoxic effects of PAH detrimental to human health have been reported frequently [20, 163]. Regulation of PAH emission and reliable monitoring of PAH concentration in ambient air is thus of paramount importance for public health. Motor vehicle exhaust is considered the most significant source for PAH in urban areas [128, 225]. EU regulation EU96-61-EC, becoming effective in 2005 (<http://europa.eu.int/comm/environment/ippc>), has identified benzo[a]pyrene as a proxy for the whole suite of PAH [3] and requires its determination on a yet non-defined but high spatial and temporal resolution. This might impose serious im-

plementation problems due to high costs associated with conventional monitoring using high volume air samplers. Biomonitoring methods using passive vegetation samplers [47, 245, 249, 269, 9, 264] may offer a practicable low-cost alternative, especially in terms of high spatial resolution and time averaged data series.

A variety of passive vegetation samplers exposed to PAH emissions have been employed including moss bags [260, 176], grasses and crops [233, 261, 105], plantago and other herbs (Bakker et al., 2001), kale and other garden vegetables [61, 10, 9], aquatic macrophytes [240] and various tree species. In the latter case preferentially evergreen species were selected enabling to monitor during the winter period although some deciduous tree species have been tested [10]. Evergreens amongst others included *Quercus ilex* and *Olea europea* [127], *Laurus nobilis* [145, 132], *Melaleuca sp.* [159]. The specific leaf properties of these plants and their limited distribution, however, restrict their utility and application in regional or even global studies. Conifers comprise several ubiquitous species with similar needle properties. As passive samplers for PAH but also for halogenated and oxygenated persistent organic pollutants needles of Norway spruce *Picea abies* [100, 260, 268] and most frequently Scott's pine *Pinus nigra* [47, 114, 231, 232, 233, 249, 269, 271, 173, 153, 92, 264] have been employed. The analysis of pine needles has thereby been identified as a reliable means of assessing air pollution for selected persistent organic and inorganic pollutants.

The needles exposure to vapor-state and particle-bound PAH is reflected in the pollutant concentrations found in the epi- and intracuticular waxes. Substances in the vapor phase can penetrate directly into the interior of the needles via the stomata, or they may diffuse through the wax and the cuticular membrane (Fig. 33, [218, 183]). Simonich and Hites [233] experimentally determined that gaseous PAH uptake of the inner needle reaches equilibrium after a short time period and that back-diffusion and (photo)degradation do not significantly alter the PAH loads. Particle-bound PAH accumulate on the leaf/needle surface, whereby during primary deposition a portion of particles will be lost due to bounce-off [9] and some particles will be removed quickly by wind abrasion [93] and wash-off during heavy rainfall. The overwhelming portion of particle bound PAH will, however, be adsorbed to the needle surface and rapidly be incorporated into the needle wax layer (Fig. 33).

Studies of PAH accumulation using passive pine needle samplers in urban environments with higher spatial resolution are relatively scarce. This chapter will focus on PAH burden of pine needles taken at 43 locations in the City of Cologne. Here, the PAH to the loads of magnetic minerals, also resulting from fossil fuel combustion, which were determined on the same sample set [255] are to be compared. Further the feasibility of PAH source reconciliation based on PAH isomeric distribution patterns is inspected and discussed in relation to PAH accumulation conditions. The study is complemented by a time series analyses of PAH taken over a six-month period from June to December in order to evaluate seasonal changes in airborne PAH-concentrations. Results discussed in this chapter have been published by Lehndorff and Schwark [123].

3.3.1 Sampling

A description of Cologne City is given in chapter 3.1. Over the study area 43 *Pinus nigra* samples were taken in representative locations. A time series of 14 individual

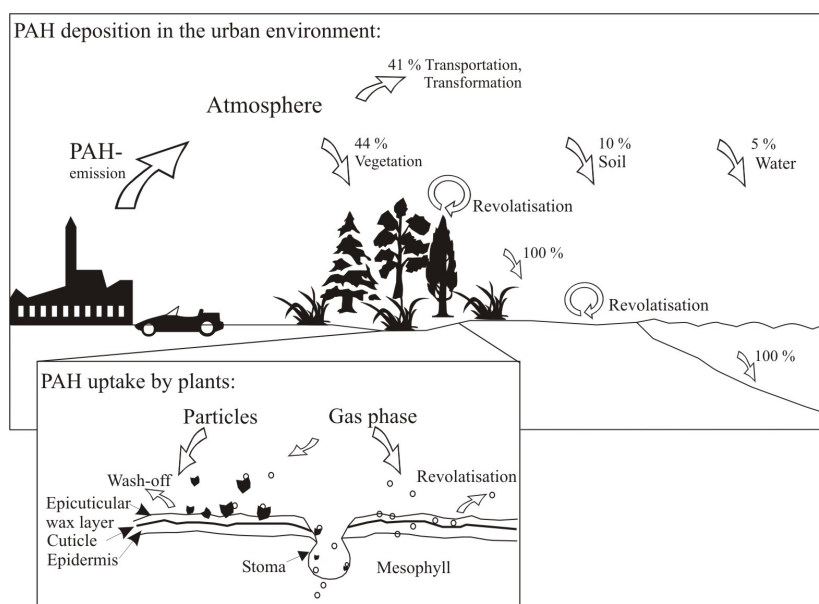


Figure 33: Generalized model of PAH transportation and deposition (modified from Simonich and Hites, 1994b). Vegetation acts as an important sink for lipophilic organic pollutants, scavenging about 44% of the total PAH emission in urban and 4% in rural environments [261]. The insert illustrates PAH accumulation modes on needles emphasizing differences in uptake of particle-bound and gaseous pollutants.

samples was monthly collected from June to December 2002 at location 53 (Fig. 17). Samples were separated into fresh (this year) and old needles (previous two years).

Locations were chosen to represent different urban and suburban environments (Fig. 17) and to fully reflect the heterogeneous pollutant load of the highly developed Cologne Conurbation. Based on land use and traffic exposure shown in detail in Fig. 17 the samples were divided into 5 groups according to the presumably dominating pollution source.

As a reference an additional pine sample was obtained from a semiurban site in Siegburg, a small town some 30 km southeast from Cologne City. For comparison three pine needle samples were collected from Poland (taken in summer 2002) comprising an urban, a semiurban and a rural area.

Immediately after collection in the field the samples were placed in paper envelopes and stored deep-frozen in the dark to avoid evaporation and photo-oxidation of volatile components before analysis.

3.3.2 Methods

Microscopic analysis Selected needle surfaces of *Pinus nigra* were scanned with a SEM (scanning electron microscope CamScan 44 Editor with EDX microprobe) at the University of Cologne as described by Urbat et al. [255]. The main purpose of the needle surface inspection by SEM was to assess the degree of epicuticular wax degradation in relation to pollutant exposure and to identify needle-bound particles that may serve as PAH carriers/adsorbents.

Sample extraction and clean up Extraction of the needle surface waxes was performed by placing intact needles into the extraction cells of an accelerated solvent extractor (DIONEX ASE 200) at $T = 120^{\circ}\text{C}$, $p = 75$ bar, using a binary solvent mixture of hexane:dichloromethane (99:1; v/v). This mixture has been shown to extract epi- and intracuticular waxes without release of polar interior needle constituents, e.g. chlorophylls [270]. All extractions were done in duplicate on app. 10 g of needles, which were not dried prior to analyses to avoid loss of particles only slightly bound to the needle surface. The dry weight of each sample was determined on a separate needle aliquot.

The raw extract, containing water and wax as different phases, was partitioned by centrifugation at 3500 rpm into a wax free extract (fraction A) and a wax fraction (fraction C). Fraction C was shown not to contain any occluded PAH compounds by re-dissolution in dichloromethane and re-precipitation of waxes in n-hexane.

Subsequently, fraction A was separated into 3 compound classes (aliphatic hydrocarbons, aromatic hydrocarbons, heterocompounds) by use of automated medium pressure liquid chromatography (MPLC) using a MKW-2 instrument (MKW, Juelich) as described in Radke et al. [197]. The resulting aromatic hydrocarbon fraction of the needles surface extract was then spiked with 1 μg D₁₀-Pyren (Promochem, Wesel) as internal quantitation standard.

Instrumental analysis GC-MS analysis was carried out using a Kodiak Triple Stage Quadropole MS/MS type 1200 (Chromtech, Idstein, Germany), coupled to a Hewlett Packard GC 6890 equipped with a PTV injector. Analyses of 15 EPA priority pollutant PAHs (excluding 6-methylchrysene) and in addition methylated phenanthrenes/anthracenes, benzo[e]pyrene and perylene (for abbreviations and molecular structure see Tab. 25 and 61 in appendix) was performed in SIM-mode recording m/z 128, 152, 154, 178, 192, 202, 212, 228, 252, 276 and 278. A HP 1 column, 25 m x 0.25 mm i.d., with 0.25 μm film thickness was used. Samples were injected via a PAL autosampler in split-mode at a ratio of 1:20. GC temperature program conditions were 60°C isothermal for 2 min, ramped at 10°C / min to 320°C and then isothermal for 10 min.

The mass spectrometer was operated in EI-mode at an electron energy of 70 eV and a cathode emission rate of 300 μA . The ion source temperature was 280°C. PAH were identified by matching each substance retention time with the retention times of an external standard mix (PAH-mix 9 and 36, Dr. Ehrensdorfer). Concentrations of the analytes were calculated based on the external and internal standard. All concentrations are given in [ng g^{-1} of dry weight]. For the three- to hexacyclic aromatic hydrocarbons the error upon triplicate-analysis was 15 %, with higher deviations up to 30 % noted for 2-ring PAH.

3.3.3 Results and discussion

Microscopic observations The SEM analysis shows variable states of epicuticular wax degradation on *Pinus nigra* needles. In Fig. 34a a fresh surface is shown (Location 53, park site: 3 to 4 months of needle age), where on the abaxial side of the needle epistomatal wax crystallites are still unaffected by environmental effects like wind or

rain abrasion. The beginning abrasion on the adaxial side of the same needle is pointed out in Fig. 34b. One to three year old needles taken at location 5, an intersection with high traffic density, preserve only minor wax residuals in their stomata, but reveal abundant aerosol particle adsorption on the cuticle and within stomata (Fig. 34c).

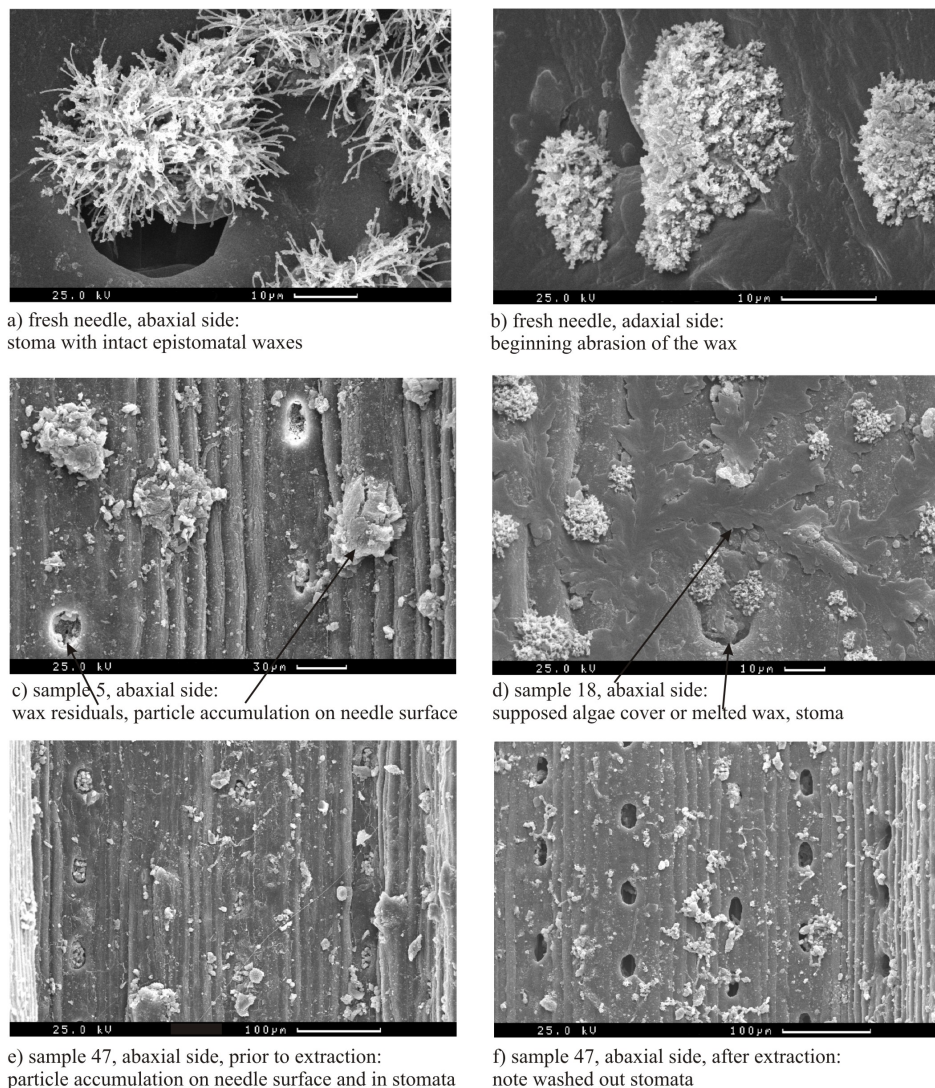


Figure 34: SEM scans of *Pinus nigra* needle surfaces. a)-c) different stages of wax degradation and particle accumulation; d) bionic, potentially algae cover or alternatively molten wax occluding stomata; e) and f) efficiency of the ASE extraction in cleaning needle surfaces and stomata.

Needles from location 18 as shown in Fig. 34d are of a similar age and were also exposed to high traffic density in the inner city district of Cologne. Residual epistomatal waxes can be recognized and an organic film that covers several stomata. After Kerstiens [106] and Bäck et al. [7] this could be attributed to epiphytic algae overgrowth probably resulting from increased atmospheric nitrogen deposition at this high traffic site. Alternatively, after Bytnerowicz and Turunen [28] this morphological feature may be explained by wax crystallite melting due to enhanced ozone exposure.

Fig. 34e and Fig. 34f show the effect of the needle surface extraction with ASE. To a large extent pollutant particles and wax crystallites are washed out of the stomata. Particles observed on the needle surface after solvent extraction were attributed to minerogenic and combustion magnetite aerosols.

Total extract yields Total extract yields (hexane:dichloromethane; 99/1; v/v) of intact pine needle epi- and intracuticular waxes in Cologne City vary between 15,000 and 38,000 $\mu\text{g g}^{-1}$ (n=56). The highest wax content is reached in pines from urban Poland (67,000 $\mu\text{g g}^{-1}$). In general a trend to higher extract yields is noted for needles recovered from low pollution areas. For Cologne samples fractions A (hexane soluble at room temperature) and C (hexane insoluble at room temperature) on average showed similar concentrations. Samples from Poland gave yields, which were twice as high for fractions A when compared to C. As these samples were taken in summer, this can be attributed to the loss of volatile components as observed by Kylin et al. [116], Lodovici et al. [133], Simonich and Hites [231, 232, 233].

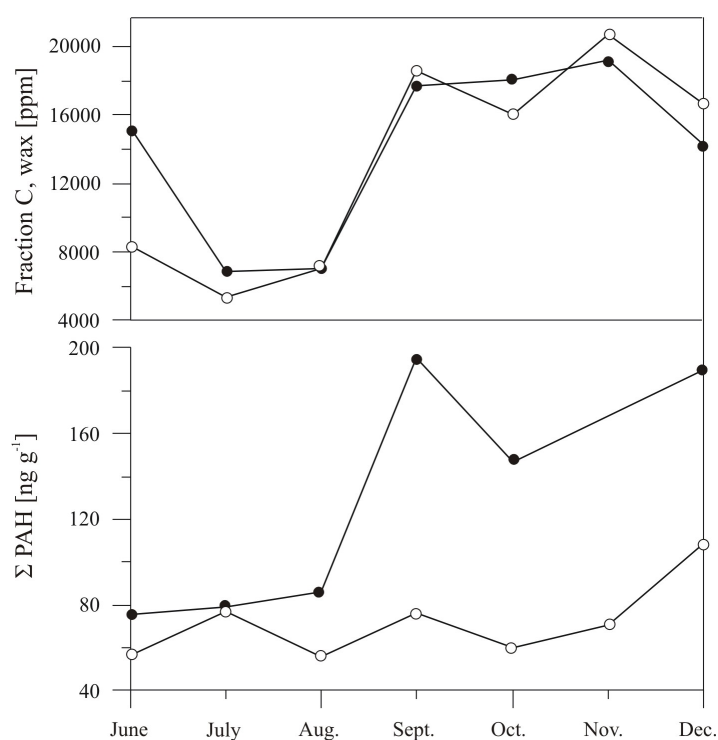


Figure 35: Seasonal variation in wax and PAH content of fresh (open circle) and older needles (filled circles). The wax concentration shows no significant difference between old and young needles, but “summer depletion”, due to volatilisation. PAH concentrations on older needles show a decline parallel to the wax content, due to establishment of equilibrium between inner and outer needle compartments. Lack of increase in PAH concentration on the younger needles surfaces before December, is attributed to disequilibria conditions.

The time series samples taken from June to December reveal drastic changes in total extract yields determined separately for this years and previous two years needles (Fig. 35). During bud bursting season, from June to August, the extract yields for young needles are generally low with less than 8,000 $\mu\text{g g}^{-1}$. This also accounts for old

needles during July and August, whereas in June the old needles show intermediate extract yields of $12,000 \mu\text{g g}^{-1}$ (Fig. 35). Any normalization of PAH on needle wax concentrations thus will be strongly affected by seasonal wax content variation.

Total PAH yields Concentrations of PAH in fraction C were negligible and for almost all samples analysed below detection limit. Concentrations of PAH in needle extract fraction A for Cologne City varied between 50 to 350 ng g^{-1} (d.w.) for total PAH (Tab. 12). The median value for PAH concentrations in needles determined for Cologne City is 120 ng g^{-1} (d.w.), the mean is 153 ng g^{-1} (d.w.). The reference site in Siegburg gave a value of 161 ng g^{-1} (d.w.) thus implying that the semiurban site carries a PAH load similar to Cologne City. The reference sites in Poland gave median and mean values of 358 and 381 ng g^{-1} (d.w.) respectively, indicating a significantly higher PAH load. The PAH burden in the City of Gdansk was lowest with 330 ng g^{-1} (d.w.), whereas the rural and semirural sites gave higher PAH loads of 455 and 358 ng g^{-1} (d.w.).

Seasonal variations in total PAH yields Seasonal variations on PAH content observed at location 53 in Cologne were significantly different for fresh and old needles (Fig. 35). During summer month June to August, corresponding to pine bud bursting season, the PAH concentrations for fresh needles are particularly low at on average 60 ng g^{-1} (d.w.). PAH loads of old needles are slightly higher averaging around 80 ng g^{-1} (d.w.) as shown in Fig. 35. A very strong increase in PAH loads for old needles is observed for the cold season, October till December, with values of 150 to 200 ng g^{-1} (d.w.), due to cold condensation caused by decreasing temperature [232, 233, 149, 61, 9]. The fresh needles exhibit only a very moderate increase to values of 100 ng g^{-1} (d.w.) for the month of December. The moderate increase in PAH over time for the fresh needles is attributed to diffusive displacement from the needle surface into the lower cuticle compartments [218, 233, 271] (“two-compartment model” discussed by Bakker et al. [9]). For older needles this process is less relevant because interior needle compartments have already reached PAH saturation levels in previous seasons and thus equilibrium between inner and outer cuticle is established. This temperature-dependent volatilisation process predominantly affects the 2- and 3-ring PAH which are preferentially transported in the gas phase [233, 93, 80, 149, 9].

Plant species	Location	Number of PAH	Total PAH range [ng g ⁻¹]	Total PAH avg. conc. [ng g ⁻¹]	Fluo / Py	P / MP	P / A	InP / BghiP	(2+3) / (4,5+6) -ring PAH	BaA / BaP	BeP / BaP	BaP / BghiP	Reference
<i>p. strobus</i>	urban (USA)	10 ^{a)}	800-1600	1200 ^{j)}	x	x	x	x	x	x	x	x	Simonich and Hites [232]
<i>p. sylvestris</i>	rural (U.K.)	16 ^{b)}	19-3091	323 ^{k)}	x	x	5.13	x	6.21	1.85	x	1.04	Tremolada et al. [249]
<i>p. sylvestris</i>	background (Czech Republic)	16 ^{c)}	0.3-18590	1345 ^{j)}	1.67	x	0.50	5.31	3.41	0.71	x	41.6	Holoubek et al. [92]
<i>p. sylvestris</i>	industry (Czech Republic)	16 ^{c)}	0.3-19251	7027 ^{k)}	3.01	x	2.32	0.17	3.06	2.04	x	1.85	
<i>p. strobus</i>	rural (USA)	18 ^{d)}		370 ^{j)}	x	x	x	x	x	x	x	x	Wagrowski and Hites [261]
<i>p. densiflora</i>	rural (Korea)	17 ^{e)}	31		1.55	2.85	26.8	1.02	2.91	0.71	0.93	0.86	Hwang et al. [96]
<i>p. densiflora</i>	urban (Korea)	17 ^{e)}	192		1.46	4.10	19.0	0.92	4.31	1.99	2.10	0.52	
<i>p. mazimartinezii</i>	urban (Mexico)	17 ^{e)}	102		0.62	30.19	39.6	0.89	1.86	1.74	2.43	0.38	
<i>p. mazimartinezii</i>	industry (Mexico)	17 ^{e)}	563		0.57	17.45	35.5	0.71	0.69	1.27	2.72	0.23	
<i>p. taeda</i>	rural (USA)	83			2.89	10.07	28.9	1.04	3.40	2.08	1.07	0.88	
<i>p. taeda</i>	semiurban (USA)	17 ^{e)}	111		2.51	5.89	17.1	0.89	2.43	2.85	1.66	0.41	
<i>p. taeda</i>	urban (USA)	17 ^{e)}	146		1.78	3.52	15.3	0.93	4.96	0.80	1.02	1.09	
<i>p. sylvestris</i>	rural (Poland)	14 ^{f)}	270		0.04	x	5.5	2.78	0.17	0.63	x	0.96	Migaszwski [153] Weißflog and Wenzel [269]
<i>p. sylvestris</i>	various locations (Germany): special waste dump	5 ^{g)}	198		1.18	x	13.9	x	7.78	x	x	x	
<i>p. sylvestris</i>	vehicle traffic	5 ^{g)}	86		1.67	x	9.55	x	4.76	x	x	x	
<i>p. sylvestris</i>	firing plant for pit coal	5 ^{g)}	254		1.62	x	62.3	x	6.46	x	x	x	
<i>p. sylvestris</i>	production plant for charcoal	5 ^{g)}	179		1.13	x	27.8	x	9.59	x	x	x	
<i>p. sylvestris</i>	industry	5 ^{g)}	492		1.76	x	291	x	8.51	x	x	x	
<i>p. sylvestris</i>	urban	5 ^{g)}	305		1.37	x	12.4	x	6.86	x	x	x	
<i>p. sylvestris</i>	rural	5 ^{g)}	123		3.00	x	25.3	x	10.18	x	x	x	
<i>p. nigra</i>	urban locations (Germany): airport	20 ^{h)}	51-71	61 ^{k)}	1.68	2.54	24.8	0.71	2.86	2.13	3.29	0.78	this study
<i>p. nigra</i>	railway	20 ^{h)}	120-195	185 ^{k)}	1.95	3.81	45.7	0.82	3.53	2.51	3.33	0.90	
<i>p. nigra</i>	major traffic	20 ^{h)}	80-355	122 ^{k)}	1.55	2.79	22.1	0.71	3.09	2.86	3.86	0.64	
<i>p. nigra</i>	residential area	20 ^{h)}	70-409	148 ^{k)}	1.70	3.54	37.7	0.61	4.41	2.53	3.54	0.54	
<i>p. nigra</i>	parks	20 ^{h)}	90-195	103 ^{k)}	1.65	3.39	33.2	0.80	4.01	3.77	3.62	0.75	
<i>p. nigra</i>	Siegburg (residential area)	20 ^{h)}	161		1.74	6.88	25.5	x	3.83	3.02	3.74	0.73	
<i>pinus L.</i>	Poland (rural+urban)	20 ^{h)}	330-455	358 ^{k)}	0.86	13.95	52.6	x	2.12	2.49	2.64	0.99	
<i>p. sylvestris</i>	various locations (Sweden): background site	25 ⁱ⁾	410-820	450 ^{j)}	1.91	0.17	0.14	0.14	0.76	4.00	5.63	0.37	Kylin [114]
<i>p. sylvestris</i>	traffic	25 ⁱ⁾	520-6100	2670 ^{j)}	0.86	0.02	0.29	0.20	0.70	15.96	6.15	0.20	
<i>p. sylvestris</i>	industry	25 ⁱ⁾	1000		1.00	0.06	1.35	x	0.64	x	x	x	
<i>p. sylvestris</i>	airport	25 ⁱ⁾	3000		1.43	4.16	7.73	x	5.01	2.83	2.50	x	
<i>p. sylvestris</i>	airport, air fuel tank	25 ⁱ⁾	1400		1.55	0.00	0.00	x	5.23	3.00	1.98	x	
<i>p. sylvestris</i>	oil shale plant	25 ⁱ⁾	1600		1.07	6.76	27.0	x	5.92	2.63	1.66	1.10	

Table 12: Compilation of PAH biomonitoring data for pine needles. For analyte abbreviations see above. ^{a)}-^{p)} = 15 EPA-PAH (excluding 6-methylchrysene) ^{a)}except Nap, Ace, Flu, BbF, BkF, DbA, plus triphenylene, BeP. ^{b)}except Nap, Flu, BkF, InP. ^{c)}plus Acy. ^{d)}except Nap, DbA, plus BeP, retene, triphenylene, coronene. ^{e)}except Nap, DbA, plus MP, BeP (concentrations given in ng g⁻¹ wet needles). ^{f)}except Nap, BbF, BkF combined. ^{g)}except Nap, Ace, Flu, BaA, Chry, BbF, BkF, InP, BghiP. ^{h)}except Nap, BbF, BkF combined, plus Acy, 4 MP (listed as sum MP), MA, BeP (all concentrations calculated as medians).

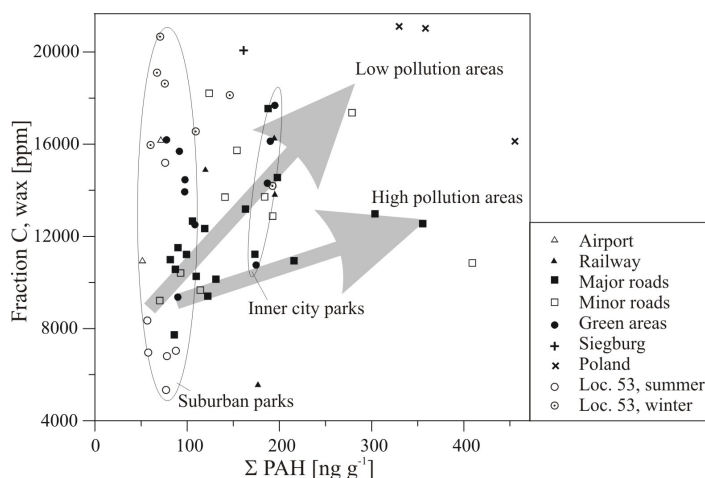


Figure 36: Relation between wax content (fraction C) and total PAH load [ng g^{-1}]. Two trends for i) higher pollution areas with low wax and enhanced PAH concentrations and ii) lower pollution areas with high wax and diminished PAH contents occur. Parks can be discriminated into suburban and inner city parks according to their respective PAH concentrations. Seasonal trends lead to high wax content during the winter and low wax content during the summer period, whereas PAH concentrations remain less variable.

Emission-dependent variation in PAH yield and composition In urban areas traffic emission comprise the dominant source of PAH [8, 128, 225]. Therefore, Cologne Conurbation samples were assigned to the following traffic exposure and land use characteristics: major roads, minor roads, railway, airport and parks. A clear differentiation of PAH loads in pine needles according to variable traffic exposure was not observed (Tab. 12). Surprisingly, the median values for PAH concentrations in pine needles taken along major roads (122 ng g^{-1} , d.w.) were lower than those for minor roads (147 ng g^{-1} , d.w.). Green areas gave lower median values of 103 ng g^{-1} (d.w.) but could be further differentiated into two groups (Fig. 36). Parks in the inner city of Cologne reach PAH concentrations of 180 ng g^{-1} (d.w.), whereas those in suburban areas average 90 ng g^{-1} (d.w.). The PAH burden only roughly correlates with the total wax lipid content of the leaves (Fig. 36) but trends towards more versus less polluted regions are discernible. Heavier pollution in combination with reduced wax content occurs predominantly along major roads.

Wax contents differ drastically for the park location sampled through summer and winter periods, though total PAH concentrations remain fairly constant. Samples taken near the airport were expected to show enhanced PAH loads but fell into the range of suburban park samples (Fig. 36). Proximity to railway operations, however, led to enhanced total PAH accumulation in pine needles with median values approaching 190 ng g^{-1} (d.w.). These enhanced values seem to be related to diesel-powered train engines not equipped with particulate filters.

In order to assign PAH burdens to specific emissions a variety of PAH profiles for various sources have been proposed [78, 77, 224, 286, 205, 206, 108, 280, 265, 214, 12, 144, 120, 287, 54]. These PAH ratios are certainly affected by primary sources, but strongly vary according to their preferred mode of transportation in the gaseous phase or adsorption to primary and secondary aerosols. Furthermore, during transportation

photolytic degradation of individual PAH may significantly alter the PAH distribution patterns [233, 80, 226, 146, 287]. With respect to accumulation in vegetation samplers variable air/plant partitioning has been reported [149, 9] to be of critical importance.

PAH distributions in pine needles analysed here will reflect a mixed transport and deposition mechanism. Low molecular weight PAH including the 2 and 3-ring components will be preferably transported in the gaseous phase, whereas 5 and 6-ring PAH are almost exclusively particle-bound. The 4-ring PAH detected in pine needles are preferentially particle-bound although a gaseous contribution has been observed [149, 287]. The ratio of fluoranthene versus pyrene (Fluo/Py-ratio) has thus been extensively applied for PAH source typing [78, 224, 287].

In needles collected in Cologne City, phenanthrene was always the dominating PAH with median concentrations of 47 ng g^{-1} (d.w.) followed by fluoranthene and pyrene at 22 and 13 ng g^{-1} (d.w.), respectively (Fig. 37). This is in agreement with previous observations [249, 100, 133, 127, 96] and points towards a predominantly traffic related source for the semivolatile PAH. Further discrimination of PAH sources can be achieved by using diagnostic isomer ratios. A crossplot of various PAH distribution ratios versus the Fluo/Py-ratio (Fig. 38) indicates a high variability, most likely due to intensive mixing of various PAH sources during airborne transport and deposition, again in agreement with previous studies [249, 96]. The Fluo/Py-ratio is selected for source discrimination because it covers the gaseous as well as the particle-transported PAH. The two compounds possess similar boiling points, vapor pressures, photo-oxidation properties and octanol/air- and plant/air- partitioning coefficients [93, 268]. Variations in the ratio will thus be primarily source associated. Unmodified transfer of source-inherited Fluo/Py-ratios into sediments and soils has previously been reported [287, 12].

Covariant trends of the Fluo/Py-ratio, amongst others, were observed with the P/A-ratio and the BaP/BghiP-ratio (Fig. 38e,f), both susceptible to traffic emissions [287]. The range of the Fluo/Py-ratio typical for traffic emission lies between app. 1.5 and 2.0 in this study and in several previous investigations (Tab. 12). For the three-ring PAH based P/A-ratio, samples from parks and selected minor roads in residential areas (Fig. 38e) gave significantly higher values, indicating enhanced contributions from unburned vehicle fuel, which had been transported in the gas phase. This deviation is not observed for the 5- and 6-ring PAH based BaP/BghiP-ratio, which separates the samples taken at major roads at less than 2 m distances from the street. These samples exhibit lower than average Fluo/Py- and BaP/BghiP-ratios (Fig. 38f), as previously observed in fossil fuels and diesel soot (see Yunker et al., [287] and references therein).

Samples taken close to railway operations are in general characterized by enhanced Fluo/Py-ratios. The ratio of 2- and 3-ring versus the 4- to 6-ring PAH also shows a covariance-trend with the Fluo/Py-ratio (Fig. 38b), whereby the railway affected samples are separated again by exceptionally high Fluo/Py-ratios. Samples from parks and minor roads in residential areas exhibit high values in the (2+3)/(4+5+6)-ring PAH ratio due to preferential transport in the gas phase. A combination of the Fluo/Py-ratio with the InP/BghiP-ratio exhibits a complex distribution (Fig. 38a). The railway-associated samples are discernible by their high Fluo/Py-ratio. A group of samples with exceptionally high InP/BghiP-ratios is attributed to vegetation burns [194]. The remaining samples originating from traffic exposure along roads and parks can be separated into three subgroups. One group is attributed to minor roads and distinguished

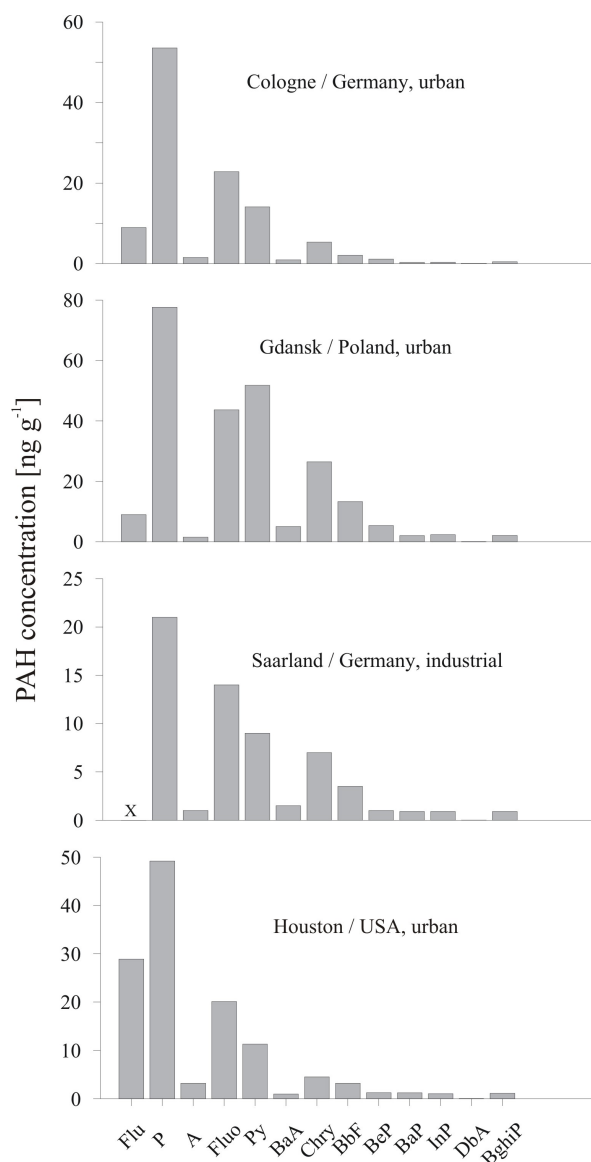


Figure 37: PAH distribution profiles of pine and spruce needles averaged for urbanized and industrialized areas in Cologne (Germany), Gdansk (Poland), Saarland (Germany) and Houston (USA). Phenanthrene is the dominating compound followed by fluoranthene and pyrene. In Gdansk the ratio of fluoranthene to pyrene is inverted due to elevated concentrations of pyrene. (X = not determined).

form the other by low InP/BghiP-ratios, which may be related to a dominance of gasoline fuel combustion [287]. Another group comprises samples taken along major roads at less than 2 m distance to the street (Fig. 38a). This group shows intermediate InP/BghiP-ratios and is thus separated from the parks and remaining major road group that shows increasing InP/BghiP-ratios associated with decreasing Fluo/Py-ratios. The variability in Fluo/Py-ratios is due to differences in vehicle emission, with low values preferentially reported for diesel [54] and higher ratios for gasoline combustion. Higher Fluo/Py-ratios are also indicative of emissions from coal-fired power plants [224, 27, 54]. The methylation pattern of parent PAH has also been utilized as

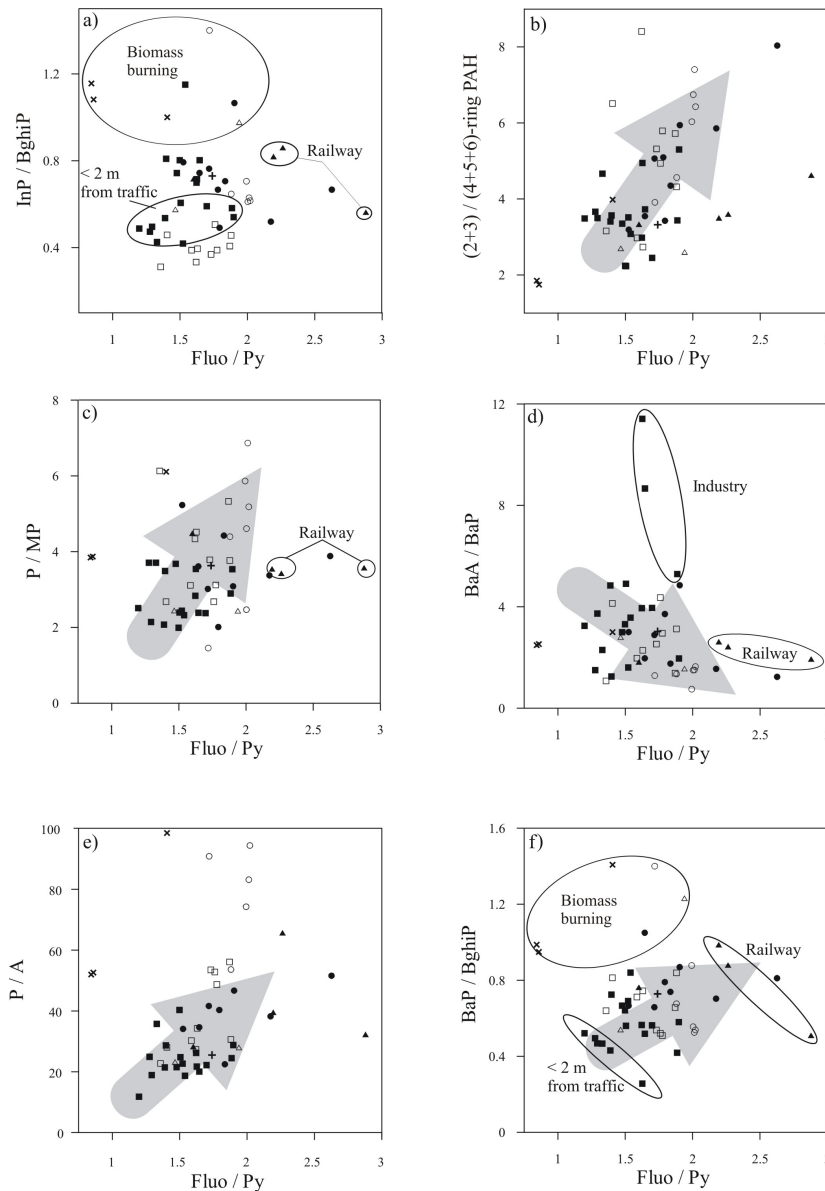


Figure 38: Bivariate plots of selected PAH ratios against the Fluo/Py-ratio for source discrimination. Fluoranthene and pyrene possess similar physicochemical properties, thus variability in the ratio will primarily reflect source character. Lower Fluo/Py-ratios indicate a dominant traffic source, especially diesel soot, higher values are attributed to domestic heating and power plant emissions. Samples taken near railway operations generally plot separately as well as reference samples origination from Poland. Higher BaA/BaP-ratios indicate industrial emissions and samples characterised by high InP/BghiP- or BaP/BghiP-ratios reflect biomass burning. In general a trend of co-variation is observed despite significant mixing of PAH during transportation. The origin of the grey arrows indicates a diesel soot end-member the tip of the arrow indicates significant admixture of diffuse coal combustion sources. Symbols are as in Fig. 36.

source indicator [287], with combustion sources showing a predominance of the parent compounds and petroleum or petrochemical products of their alkylated analogues. Samples from high traffic density sites in Cologne show higher abundance of methylated

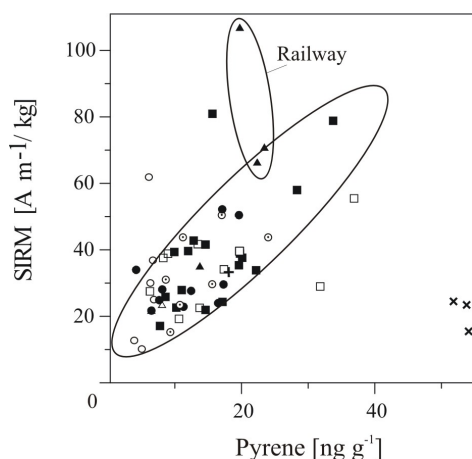


Figure 39: Correlation of a magnetic concentration parameter (SIRM) preferentially related to traffic emissions and pyrene serving as a proxy for urban PAH loads. A trend of covariance between the two parameters is noted although samples from Poland and railway associated locations in the Cologne Conurbation plot in separate groups. The high magnetic particle concentration near railways is attributed to mechanical and brake wear. Symbols are as in Fig. 36.

phenanthrenes (Fig. 38c) as observed especially for diesel emissions [128, 226, 205] and tire wear [206]. The ratio of BaA/BaP identifies enhanced contribution of industrial emissions (Fig. 38d) for selected samples. Application of this ratios is justified because both compounds are equally susceptible to photodegradation [226, 146]. Mixed origin of PAH in needles collected in Cologne City is evident from interpretation of the binary source plots, with traffic related sources predominating.

A correlation between the magnetic properties of pine needles, identified as pollution indicators by Urbat et al. [255] and the pyrene concentration is shown in Fig. 39. A trend of co-variation is observed for both parameters although the correlation coefficient $r^2=0.29$ for the data set excluding railway associated and Polish samples is low. Railway samples most likely emit higher abundances of metallic and magnetic wear particles not exclusively related to combustion processes. Magnetite spherulites and PAH both originate from combustion processes, although a clear-cut reconciliation of the various potential combustion sources is still difficult to achieve.

Spatial variation in Cologne City In chapter 3.1 the spatial distribution of magnetic dust in the $PM_{2.5}$ class was already linked to areas with high traffic densities and railway operations. Fig. 25 shows the spatial distribution of remanence saturation (SIRM), a magnetic particle concentration indicator, in comparison to PAH concentrations and isomer ratios.

The sum of total PAH is spatially distributed in a manner similar to the SIRM, with maxima along the topographic low of the SE-NW-running Rhine Valley. In the northern part of Cologne a significant additional PAH input (Fig. 40b), which is not complemented by a SIRM increase, is evident from large industrial complexes (for identification of major land use type see Fig. 17). This industrial input is also evident from elevated BaA/BaP-ratios (Fig. 40d). The high BaA/BaP-ratios identified in

location 20 in the eastern part of Cologne can also be attributed to industrial emissions. Slightly enhanced values of the BaA/BaP-ratio are also noted in the south-western part of Cologne City (locations 6 to 9 in Fig. 17) and can be assigned to petrochemical industrial complexes in this area. The western part of Cologne is preferentially occupied by residential areas, which show lower total PAH concentrations (Fig. 40b) and very low BaA/BaP-ratios (Fig. 40d).

The InP/BghiP-ratio is less variable throughout the study area (Fig. 40c) and high values of this ratio are associated with localized wood and biomass burning, as also observed by Yunker et al. [287]. Locations with elevated InP/BghiP-ratios are thus often associated with parks and cemeteries, where vegetation debris is combusted and where barbecues and bonfires are held. Locally, a high InP/BghiP-ratio may also be induced by industrial emission as proposed for location 24 (Fig. 17) in the northern edge of the study area.

Traffic is assumed to exert the major control on the Fluo/Py-ratio, which shows low values along all major roads (Fig. 40e; see also Fig. 17 for freeway system). Especially, frequented radial roads, which are subject to massive traffic congestions during commuters rush hours reveal particularly low Fluo/Py-ratios. In general lower Fluo/Py-ratios indicate preferential diesel soot sources, whereas slightly higher ratios point towards a predominance of gasoline-powered vehicle emissions. A preference for gasoline derived PAH can thus be identified in residential areas. The Fluo/Py-ratio also reflects input from diffuse sources, especially PAH originating from domestic heating and power plant emissions, which raise the Fluo/Py-ratio.

Two- and three-ring PAH although preferentially released through vehicle emissions will in contrast to the heavier isomers be transported further away from their point of origin and deposited in locations some kilometers away from major traffic centers. This is partially reflected in the (2+3)/(4+5+6)-ring PAH-ratio, which in general shows low values in the south-eastern part of Cologne City and enhanced levels in the north-western part (Fig. 40f). This distribution roughly reflects the prevailing wind directions within the Rhine Valley (see compass card in Fig. 40). Maxima in traffic related PAH along the inner city ring roads (Fig. 40a, b, e) are thus offset towards the west and northwest when compared with the (2+3)/(4+5+6)-ring PAH ratio (Fig. 40f), due to longer transportation distance of the higher volatile 2- and 3-ring PAH.

3.3.4 Summary and Conclusions

Pine needles serve as suitable passive samplers for persistent airborne PAH pollutants in urban and suburban areas of Cologne City in West Germany. Because of the high wax content of the pine needles, chemical work-up of PAH-fraction is non-trivial and time-consuming. However, the high wax content serves as excellent matrix to preserve accumulated PAH over time, thus allowing to sample different needle ages and also to obtain reliable time-integrated pollution records. Pine needles are ubiquitously available and allow for a high spatial resolution in the sampling grid.

The PAH concentrations found in needles of Cologne City are comparable with those determined for other urban environments. Their concentration agrees well with the independently determined amount of airborne magnetic particles in the PM_{2.5} class related to combustion sources. Total PAH accumulations on needles are highest along

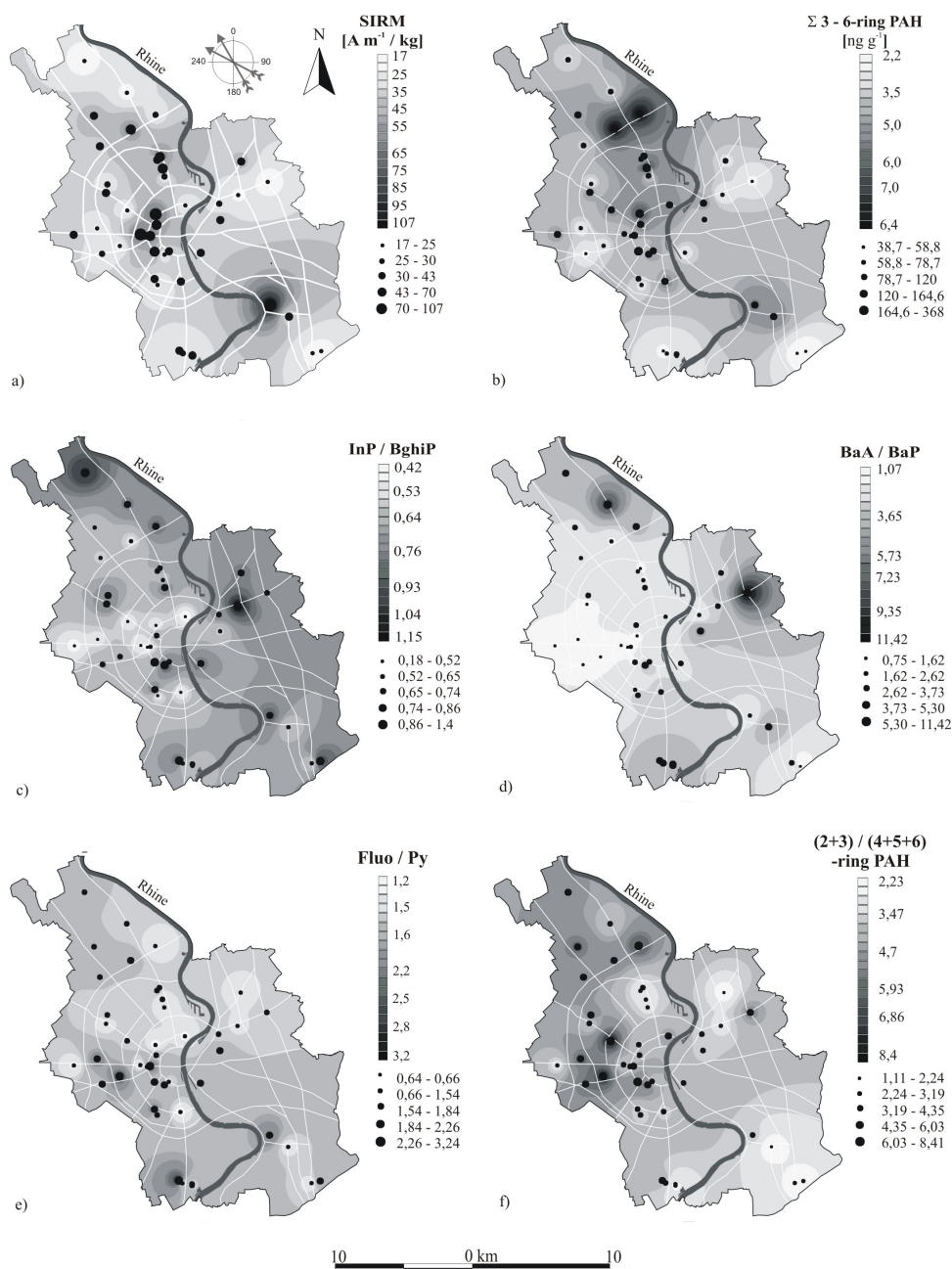


Figure 40: Spatial distribution patterns of selected magnetic particle and PAH concentrations and isomer ratios. White lines indicate major roads and freeways, for details of land use see Fig. 17. Black dots identify sampling locations with different sizes indicating concentration or ratio intervals. Contouring was performed using ArcView Spatial Analyst discriminating 20 contour intervals. Compass card in the upper left panel indicates prevailing wind directions. Panels a), b), e), and f) predominantly indicate traffic emissions, which are highest in the city center and along radial roads. Panel c) indicates areas with enhanced biomass burning, preferentially near parks and panel d) indicates areas with exceptional high industrial emissions. For details see text.

major roads, especially radial roads, and their concentration maximum follows the topography and preferred wind direction dictated by the river Rhine Valley. The lowest PAH concentrations were found in suburban parks, with inner city parks exhibiting intermediate values.

The PAH distribution is dominated by phenanthrene, fluoranthene and pyrene, as observed in several other studies. Selected PAH ratios that have previously been applied as specific source indicators showed general trends of co-variation but no high-rank correlations. This is attributed to the multiple sources of PAH, their mixing during transportation, and fractionation after accumulation on needles due to different physicochemical properties. PAH ratios allowed to separate samples taken in the vicinity of railroad operations from the vehicle traffic dominated sources.

Wood and biomass burning in parks locally contributes to the total PAH load, as indicated by elevated ratios of indeno[1,2,3-c,d]pyrene vs. benzo[g,h,i]perylene. Benzo[a]anthracene increases relatively to benzo[a]pyrene in areas receiving enhanced industrial PAH emissions.

The correlation between pyrene concentration and the SIRM (saturated remanence isothermal magnetization, a magnetic particle concentration indicator) points towards a common combustion source. This relationship bears potential for high-resolution studies using the affordable and non-destructive environmental magnetics technique to predict pyrene or total PAH concentrations in polluted areas.

4 Cologne Conurbation - regional-scale biomonitoring

This part of the study aims at the investigation of air quality at a regional scale, covering the Greater Cologne Conurbation (GCC) with approximately 3600 km². The samples were exclusively taken in low-polluted areas and thus represent the ambient average air quality. At this scale emission sources are spatially well separated and an interpretation of time-integrated pollutant loads on pine needles for their origin and atmospheric transport and dispersal is approached in this chapter.

4.1 Cologne Conurbation air quality - enviromagnetic proxies

The use of magnetic proxies in environmental studies is long established. Magnetic properties of recent subaqueous sediments were shown to correlate significantly with anthropogenic emissions [131]. Several studies revealed that magnetite is the dominating magnetic carrier of environmental pollution [58, 160, 161]. Especially coal combustion strongly affects magnetite concentration in sediments, soils, and on vegetation surfaces [74, 66, 82, 147, 137, 103]. Detailed magnetic studies on purified samples raise the opportunity to use magnetic parameters not only for mineral characterization and quantification, but also for interpretation in terms of grain size distribution [187]. Flanders [58] showed that coercitivity of magnetite is dependent on combustion educt and temperature, indicating for notable grain size differences of magnetite resulting from petroleum or coal combustion. It is also known that biologically derived iron being present in vegetation accounts to magnetic properties, but magnetite bearing atmospheric pollution loads clearly dominate magnetic signals [148]. Investigations of atmospheric pollution sources and particle transport distances have been done using active samplers [58, 209, 223, 284]. Spatial analyses of urban pollution utilizing plants as passive samplers of particulate matter (PM) was approached successfully for street transects or for sample sets comprising maximum 20 spatially distributed sites and were predominantly concentrated on magnetic concentration parameters [66, 82, 156, 147, 137, 148, 103]. In previous studies in the Cologne Conurbation the time dependent behaviour of magnetic proxies on pine needles of consecutive needle age classes was shown to reflect accumulation of PM [126]. In agreement with these data, samples from a spatial high-resolution study in Cologne City revealed magnetite as the dominant magnetic phase [255]. Significant and systematic variations in grain size were described for the Greater Cologne Conurbation (GCC), utilizing magnetic proxy ratios. In this study spatial analyses of magnetic properties on a highly resolved data set comprising 71 samples on 3600 km² is approached. Interpretation of several magnetic parameters with special interest on magnetic source diagnostic ratios shall reveal source details in the highly complex emission scenario of the Greater Cologne Conurbation.

4.1.1 Sampling

A spatially highly resolved sampling of pine needles was done in an area comprising 3600 km² in the Greater Cologne Conurbation, Germany. Composite samples of *Pinus*

nigra needles of up to 5 generations were sampled at 71 locations yielding an average pollutant signal of 4 years on the needle surface. Samples were taken every 5 km according to an equidistant sampling grid and display local air quality. Therefore, influence of dominant local sources like traffic were avoided. Selection of locations and sampling strategy is described in detail by Lehndorff et al. [126] and mainly focuses on a consistent sampling that is representative for the local air quality.

4.1.2 Analytical methods

Enviromagnetic analysis Magnetic properties of pine needles were detected on dried and ground needle material. Bulk susceptibility (κ) was analyzed with a KLY-2 susceptibility bridge (AGICO, Czech Republic) and normalized to needle dry weight (χ in $\text{m}^3 \text{kg}^{-1}$). Remanent magnetization of needles is described by analysis of isothermale remanence (IRM) and anhysteretic remanence (ARM) using a three-axis DC-SQUID magnetometer (model755R, 2G Enterprises, CA, USA). IRM acquisition and the back-field curve was achieved stepwise to or from 1.5 T, respectively. At 1.5 T the saturation IRM (SIRM) in all samples was reached. Resulting hysteresis curves enable identification of magnetic material and grain size. ARM values were aquired with a constant field of $0.4 \mu\text{T}$ parallel to an alternating field of 100 mT. In case of a pure magnetite contribution to the remanence signal of the sample material, ARM is most sensitive for identification of magnetite grain sizes below $0.4 \mu\text{m}$. χ , IRM and ARM measurements allow the determination of magnetic material, grain size classes, and degree of oxidation by the B_{cr} -value, the SIRM/κ , ARM/κ , IRM/ARM and s-ratio, respectively. Details about sample preparation, enviromagnetic analyses, and calculation of magnetic ratios are given in Urbat et al. [255] and Lehndorff et al. [126].

Statistical analysis The spatial distribution of enviromagnetic proxies was interpolated and visualized using the ArcGIS Spatial Analyst tool (ESRI). For interpolation of PAH distribution the "inverse distance weighted" method was chosen. Due to the high variability in environmental systems and insufficient data thereof, the interpolation between sampling sites is based on a linear relation (power = 1) and calculated with 6 nearest neighbours. Colour codings were extracted according to sample populations. A pre-classification of sampling sites according to emission data from the Environmental Agency NRW and land use data provided by the European Community [118, 69] was done to achieve a preliminary data description and is displayed in a box-whisker plot in figure 41.

4.1.3 Results

Enviromagnetic parameters Enviromagnetic parameters reflect quantitative and qualitative changes in magnetic material concentrations. Magnetic analyses are commonly applied to sediments and hard rocks in terms of geological questions, but were recently established for environmental analyses of soils and vegetation. Here, the susceptibility χ (normalized on dry weight) is a quantitative proxy indicating how much magnetisable material is apparent on the pine needle. Susceptibilities below zero are typical for diamagnetic materials like organic substances and water, whereas the ferro-

magnetic magnetite reaches approximately 10,000 times of signal intensity and would thus be dominant in vegetation samples. Pine needles sampled in the Greater Cologne Conurbation exhibit χ values between -0.02 and $4.4 \times 10^{-8} \text{ m}^3 \text{ kg}^{-1}$, thus indicating a high variation in atmospheric pollutants or magnetisable material load (Table 35). A classification of sampling locations according to estimated pollution background in locations near lignite fueled power plants (LFPP), sites attributed to lignite open pit mining areas, urban sites, forested and agricultural areas, and industrial zones allows a first data viewing (Fig. 41). Accordingly, highest susceptibilities are observed in urban areas and highest median susceptibility is apparent at locations in the vicinity of LFPP (Fig. 41). Lowest susceptibilities reaching negative values were measured for pine needles grown in forested areas. Highest variability was found in the "urban data set" (n=19). Lowest variations become obvious in pines attributed to industrial emission backgrounds (n=7). In previous studies IRM measurements showed to exclusively accumulate magnetite on pine needles sampled in Cologne City [255]. Thus, we here interpret SIRM values as a concentration proxy for magnetite, pointing at highest loads of magnetite in a sample with urban emission background and highest median loads at LFPP with $\text{SIRM} = 37 \text{ A m}^{-1} \text{ kg}^{-1}$ followed by a high median of $\text{SIRM} = 33 \text{ A m}^{-1} \text{ kg}^{-1}$ at industrial sites (Fig. 41). Data variability is highest in urban areas and forested sites with 15 to $57 \text{ A m}^{-1} \text{ kg}^{-1}$ and 3 to $47 \text{ A m}^{-1} \text{ kg}^{-1}$, respectively.

ARM methods are more sensitive for single-domain magnetites ($\text{SDM} < 0.4 \mu\text{m}$). Thus, ARM measurements on pine needles reflect the concentration of ultrafine PM accumulated on the passive sampler. In contrast to χ and SIRM, ARM values are exceptionally high at LFPP with a median of $0.5 \text{ A m}^{-1} \text{ kg}^{-1}$. Median values for remaining emission classes are very similar at $0.4 \text{ A m}^{-1} \text{ kg}^{-1}$. Again, highest scatter within a sample set is observed for urban locations (Fig. 41). Ratios of IRM over κ , ARM/κ , and IRM/ARM thus express differences in magnetite grain size as observed by Lehndorff et al. [126]. Ratios of IRM and ARM versus susceptibility are fairly constant (Table 35 in appendix) except for sites with negative susceptibility, where contributions of magnetite to the magnetic signal can be excluded and therefore an interpretation of these ratios in terms of magnetite grain size is needless. IRM versus ARM reveals higher "real" variability with values between 54 and 148 (Table 35 in appendix). B_{cr} , the remanent coercitivity of the pine needle samples gained from the IRM backfield curve varies significantly with 27 to 46 mT throughout the GCC, indicating for changes in grain size or magnetic mineral composition. The s-ratio calculated from the hysteresis curve of IRM analysis [21, 113] depicts a clear predominance of magnetite as remanent phase with values between 0.97 and 1. Sampling sites characterized by low s-ratios of about 0.95 are supposed to have minor contributions of a second mineral phase.

Spatial analysis of enviromagnetic PM proxies The spatial patterns of magnetic PM proxies were gained by interpolation between 71 pine needle sampling locations in the GCC. Resulting distribution maps display maximum values characterized by red to white colours and minimum values with green colours, respectively. Highest susceptibilities were analysed for pine needles taken in the central Cologne City, followed by pines in the vicinity to LFPP and the urban areas of Euskirchen, Dueren and Bonn (Fig. 42a). Susceptibilities smaller than $1 \times 10^{-8} \text{ m}^3 \text{ kg}^{-1}$ were observed in forested areas in the south-west, the central hills range, south of Bonn and in north-east. SIRM

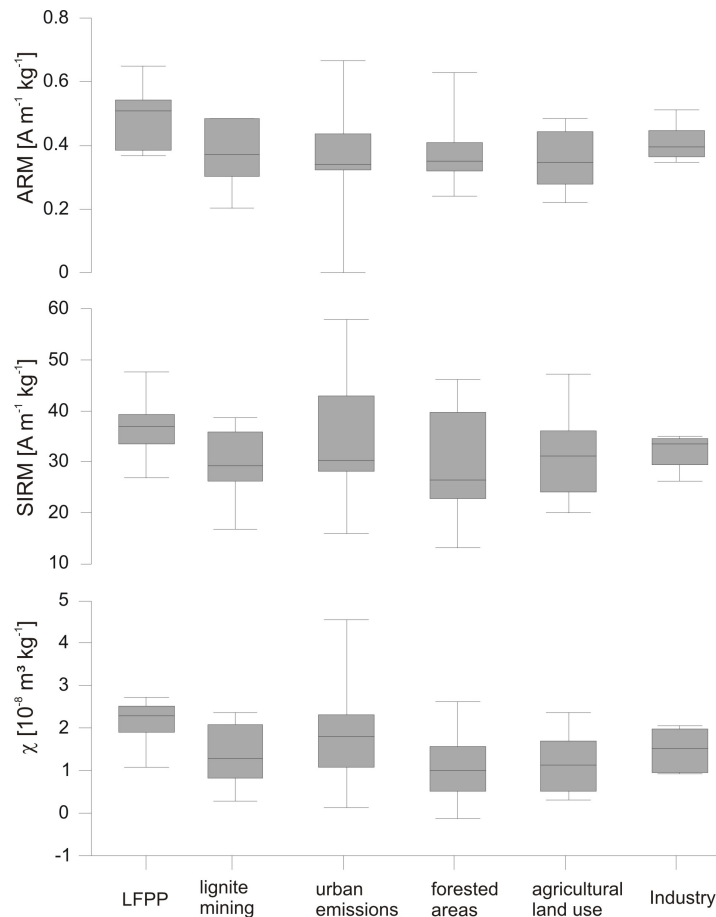


Figure 41: Enviromagnetic properties χ , IRM and ARM reflecting PM concentration and grain size on pine needles in the Greater Cologne Conurbation. Median values, quartiles, minimum and maximum values are displayed for six different emission scenarios.

values make up an almost identical distribution pattern with highest SIRM signals in urban areas and near LFPP, but an additional maximum is observed east of Bonn in the "Siebengebirge" (Fig. 42b). ARM values differ slightly from χ distribution, showing a predominance of higher ARM signals near LFPP over urban ARM values (Fig. 42c). The ARM maximum zone in Cologne City is found to be more to the west than observed for χ and SIRM. Sites located in the cities Bonn, Dueren and Euskirchen are not highlighted by ARM analysis. Lowest ARM signals resulting from pine needle analyses were found in forested areas to the east and south-west of the GCC (Fig. 42c).

4.1.4 Discussion

This study aims at the identification and differentiation of multiple pollutant sources and dispersal thereof employing a spatially high-resolved monitoring. Enviromagnetic biomonitoring provides a powerful tool, due to low costs, and undestructive and time-effective methods. The reliability of the results was shown in previous studies [255, 126] and here a detailed source reconciliation is approached on a regional scale. Sources of magnetic minerals are characterized by i) mineral phase, ii) concentration, and by iii) grain size. These factors contribute to the allocation and differentiation of four major

sources for remanence carrying magnetic mineral dust in the Cologne Conurbation.

Lignite fueled power plants Coal combustion is well known to emit magnetite spherules, that result from combustion of pyrite in lignite [58]. Several enviromagnetic studies showed coal combustion as dominant source of magnetite in the atmosphere, soils or sediments [131, 223, 74, 284]. In the Greater Cologne Conurbation the area of high lignite combustion, consuming approximately 80 mio t a⁻¹, is highlighted by elevated χ , SIRM, ARM and B_{cr} (Fig. 42a,b,c,e). Comparison with the traffic related magnetic maxima in Cologne City reveals relatively lower χ and SIRM, but higher ARM values near LFPP and thus indicates a dominance of ultrafine magnetite (SD) in emissions from lignite combustion. This is supported by high coercivities observed for needles taken near the large LFPP in the north-west and the low capacity plant in the south-west of Cologne (Fig. 42e).

Traffic emissions Traffic emissions comprise a mix of combustion products and abrasive PM [209, 223, 284], resulting in a wide grain size spectrum in high trafficked areas [126]. The maximum elevation of χ and SIRM in Cologne City thus is not only related to very high concentrations of magnetite emitted by traffic, but also to a higher contribution of pseudo single domain to multi domain magnetite (PSD-MD) to the total magnetic load when compared to LFPP emissions (Fig. 42a,b). This is equivalent to a dominance of coarser grain sizes to the PM load on pine needles. The contribution of PSD-MD magnetite is also pronounced by the interpolation pattern of the IRM/ARM ratio highlighting the cities of the study area (Fig. 42d). Extraordinary high B_{cr} values in Cologne City are contradictory, because they are related to fine grain sizes. This is interpreted as a result of high material mixing in an urban emission scenario. Additionally, comparison of signal intensities in B_{cr} and IRM/ARM distribution maps reflecting dispersal of "coarse" (app. 10 μm) and "fine" (app. 0.4 μm) magnetite, indicates that fine emissions from combustion of fuels are quantitatively higher than abrasion from traffic. Slightly higher B_{cr} values in urban samples compared to those taken near the LFPP are in agreement with a coercitivity ranking established by Flanders [58], showing that fossil fuel combustion yields highest coercivities in emitted PM directly followed by emissions from coal combustion. The ARM maxima in Cologne City shows a deviation from the inner city region to the west (Fig. 42c). This is related to a large ceramic production plant emitting ultrafine magnetite near location 29 (Fig. 42c). Low s-ratios in Cologne City can be related to an extraordinary weathering of magnetite in urban areas [162, 148] parallel to potentially higher amounts of highly reactive pollutants like O₃, NO_x and H₂SO₄ in the atmosphere.

Basaltic dust blow-out Enhanced SIRM in the south-east of the GCC is attributed to basalt deposits (Fig. 42b). Minerogenic dust from basalt outcrops is most likely the source for remanence carrying minerals in this area. Elevated IRM/ARM ratios indicate a blow-out of relatively coarse geogenically weathered particles (Fig. 42d). The exceptionally high s-ratio > 0.98 points to magnetite as dominant remanence carrier, which is not affected by oxidation as observed in urban areas in the Cologne Conurbation (Fig. 42e).

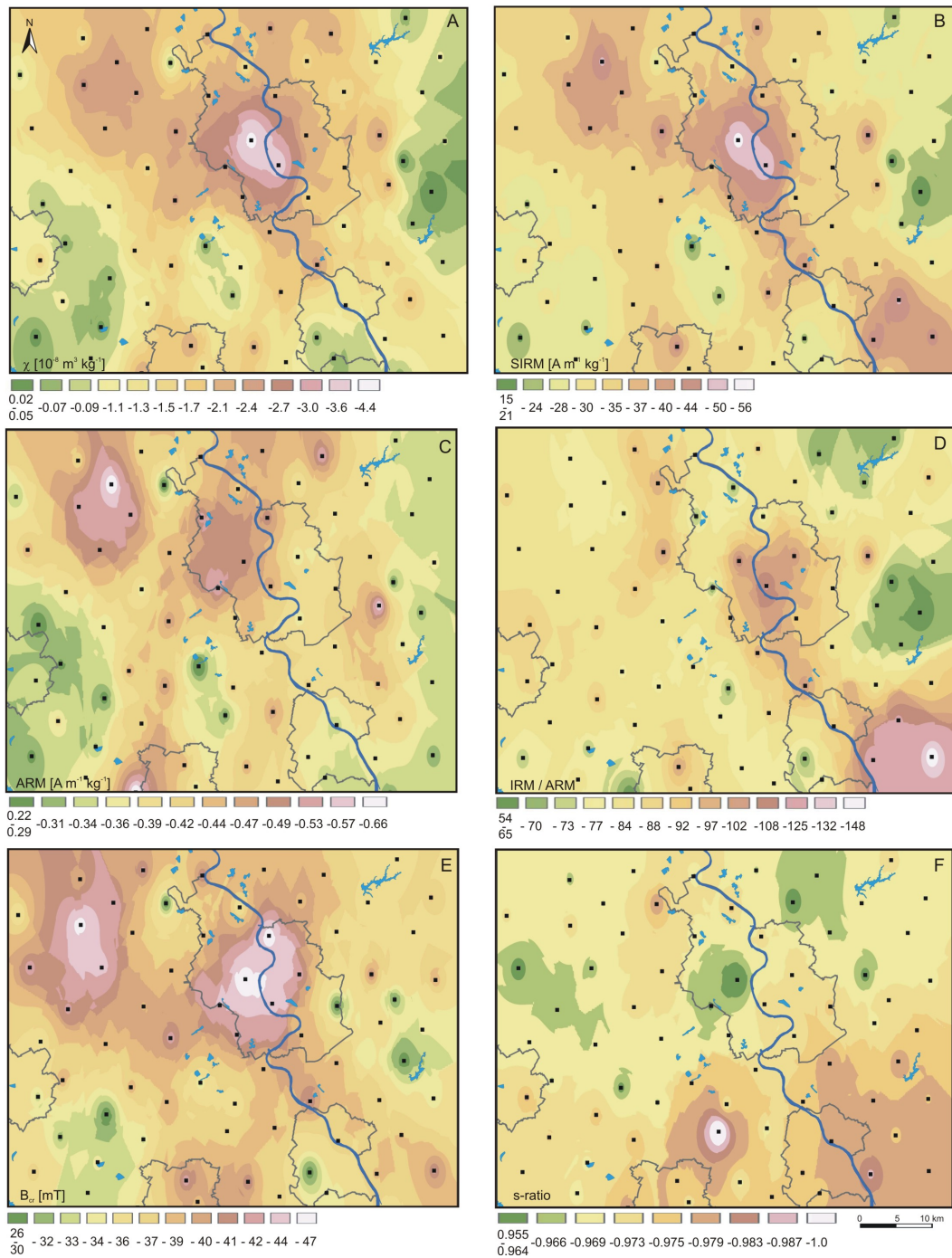


Figure 42: Isopleths maps of enviromagnetic proxies χ , IRM, ARM and IRM/ARM, s-ratio and B_{cr} as tools for source discrimination and recognition of atmospheric PM dispersal. For more information about land use see overlay transparency in the appendix (Fig. 62).

Lignite mining The area of active open pit lignite mining in the west of the Cologne Conurbation is highlighted by low s-ratios on pine needles (Fig. 42e), indicative of a strong weathering of magnetite or a contribution of hematite to the sample. The needles gained near lignite mining areas also reveal a high B_{cr} , that is in agreement with intermediate to low ARM and here preferentially interpreted as another indicator

source	LFPP	traffic	basalt dust	lignite dust
magnetite size class	SP-SD (0.03 - 0.4 μm)	SD-PSD-MD (0.03 - 10 μm)	PSD-MD (0.4 - 10 μm)	weathered magnetite
enviromagnetic proxy	ARM IRM	ARM, B_{cr} , SIRM IRM/ARM	SIRM, IRM/ARM s-ratio	B_{cr} , s-ratio

Table 13: Source diagnostic potential of enviromagnetic biomonitoring in the Cologne Conurbation.

for a change in magnetic material, than a change to smaller magnetite grain size.

Transport routes and distances A transport from source to sink covers a decrease in pollutant concentration and fractionation processes in e.g. a grain-size mixture. Thus, the spatial interpolation patterns of χ and SIRM show significantly elevated concentrations of pollution derived magnetite about 10 to 15 km from sources, i.e. Cologne City center and LFPP (Fig. 42a,b). Magnetic analyses further raises the possibility of monitoring grain size fractionation processes. By comparing ARM patterns to IRM/ARM distribution a "negative fractionation" appears with distance to the LFPP. This indicates that near LFPP high amounts of SD magnetite are deposited while in approximately 10 km distance to the east an increase in grain size to MD magnetite is observed (Fig. 42 d). These observations can be attributed to i) emissions from high LFPP stacks, coming to deposition in more than 3 km distance of the source and ii) to a spontaneous reaction of ultra-fine PM with atmospheric aerosols [276].

4.1.5 Conclusion

Magnetite is the main carrier of magnetic signals in the Cologne Conurbation. Biomonitoring employing spatial mapping allows identification of four emission sources by enviromagnetic means in the Greater Cologne Conurbation (Table 13). It was shown that magnetite emissions of traffic and lignite fueled power plants are highest at comparable amounts. Grain size effects reflected by magnetic parameters χ , SIRM and ARM show that emissions of power plants have considerably high contributions of ultrafine magnetic particles. Traffic emissions consist of a mixture of ultrafine to fine PM magnetite as indicated by high IRM/ARM and high B_{cr} values, respectively. Magnetic material changes are assumed for urban areas and characterize lignite mining areas by use of the s-ratio and coercitivity of remanence (B_{cr}). An approximation of PM transport distances based on atmospheric fractionation processes is potentially reflected by enviromagnetic parameters of samples taken nearby lignite fueled power plants. Detailed source diagnostic properties and the possibility of monitoring PM fractionation in high-resolution on a large spatial scale makes enviromagnetic biomonitoring a very powerful tool for air quality analyses.

4.2 Cologne Conurbation air quality - major and trace elements

Environmental monitoring of sources and distribution of major and trace elements with passive samplers allows for a high spatial resolution. Here, air quality is interpreted via major and trace element analyses of bulk pine needles. A high sampling resolution was achieved for the Greater Cologne Conurbation (GCC) comprising 3600 km². Recently, the use of vegetation as bioreceptor for major and trace elements has shown to be limited, due to active uptake and detoxification processes of plants. Some elements of high environmental concern like Fe, Cu, and Zn also are in need as essential plant nutrients. Thus, a biomonitoring of these elements has to account for biological concentrations of the vegetation sampler [142, 11]. Elements with a high uptake via leaf, bark or roots and high wash-off rates (e.g. Cd, Zn) might not be usable for interpretation of air quality.

A detailed study of accumulation behaviour of major and trace elements is provided by Lehndorff and Schwark [125]. There, effects accounting to non-systematic deposition patterns like seasonality and element translocation are discussed for Ba, Ca, Cd, Fe, Mo, Na, Pb, Sb, Ti, V, Zr and rare earth elements. Furthermore, a correction for geogenic dust is introduced, employing element enrichment factors (EF) calculated from upper continental crust concentrations (UCC) and rare earth element concentration (REE) for each compound [125]. Several authors proposed EF as base for environmental air quality analysis [283, 267]. Here, the discussion of spatial distribution and element source characterisation is approached utilizing spatial interpolation maps and factor analyses based on element concentration and element enrichment data for the Greater Cologne Conurbation.

4.2.1 Sampling methods

In the Greater Cologne Conurbation 71 pine needle samples were collected using an equidistant sampling grid. Each sample is considered to characterize overall air quality of its greater surrounding and yields a time-integrated signal of on average 4 years. Thus, a cautious sampling strategy was employed as described in detail by Lehndorff et al. [126].

4.2.2 Analytical methods

Elemental analyses were performed via ICP-MS on ground needle samples. Details of elemental analysis are given in Lehndorff and Schwark [125]. Of the 58 elements analysed, four compounds were near or below detection limits (As < 100 ppb, Sc < 10 ppb, Ta < 0.5 ppb, Te < 5 ppb, Table 36 in appendix). 38 elements were used for discussion of their source and dispersal, 15 rare earth elements (REE) were summed and used as reference elements for normalization on geogenic dust.

Calculation of element enrichment factors The enrichment of element concentrations on pine needles above geogenic dust level is calculated by normalization to average upper continental crust (UCC) concentrations and specific REE concentration on pine needles at each location. UCC data was gained from McLennan [150]. For Li

	min	max	reference		min	max	reference		min	max	reference
	[10 mg g ⁻¹]				[ng g ⁻¹]				[ng g ⁻¹]		
Mg	0.1	0.2	0.07	In	0.3	1.9	1	Tm	0.1	1.4	4
Ca	0.1	1.0	0.23	Hf	0.6	5	50	Lu	0.5	2	3
K	0.3	1.2	0.39	Re	0.1	7		Ho	0.3	3	8
	[μg g ⁻¹]			U	1.0	14	10	Tb	0.8	4	8
Pb	0.2	1.5	1.0	Nb	3.4	28	50	Eu	0.8	5	8
Ni	0.3	4	1	Ga	4.0	32	100	Yb	0.8	8	20
Ti	1.4	6	6.56	Tl	1.2	36	50	Er	0.8	9	20
Ba	0.5	7	1.5	Ag	2.4	52	0.1	Dy	1.6	15	30
Cu	1.5	8	4	Bi	6	61	10	Gd	2.2	16	40
Sr	0.9	14	6	Hg	6	73	0.06	Sm	2.2	20	40
Rb	0.4	19	50	W	9	89	200	Pr	4	23	50
B	6	43	18	Cs	5	104	200	Nd	14	95	
Zn	14	129	35	Zr	26	130	100	La	19	103	200
Fe	39	244	100	Au	1	173	1	Y	10	108	200
Na	6	623	379	Th	18	174	5	Ce	29	215	500
Mn	13	1370	40	Sn	44	235	200	Σ REE	99	673	
				V	60	544	0.7				
				Sb	28	599	0.02				
				Mo	58	697	0.5				
				Cd	17	712	0.06				
				Li	12	783	200				
				Cr	349	1520	0.8				
				Co	25	2350	0.1				

Table 14: Element minimum and maximum loads on pine needles in the GCC and associated reference values for non-polluted pines [11] and vegetation [141] given in bold letters.

and Tl UCC data was not available. Detailed performance and discussion of element normalization is provided by Lehndorff and Schwark [125].

Statistical analysis The spatial distribution pattern of selected elements was interpolated and visualized using the ArcGIS Spatial Analyst tool (ESRI). Details are provided in chapter 4.1. Factor analysis (FA) of element concentrations and element enrichment factors was done with SPSS 15.0. The FA was conducted with following parameters: extraction method: principal component, extraction analysis: correlation matrix, and rotation method: varimax.

4.2.3 Results

Element concentrations Element concentrations of pine needles of composite needle age taken at 71 spatially distributed locations were highest for Ca, K, and Mg contributing to the whole needle material with 0.1 to 1 %. The following elements were detected in μg g⁻¹ ranges in the order Mn > Na > Fe > Zn > B > Rb > Sr > Cu > Ba > Ti > Ni > Pb. All other elements including REE occur in ng g⁻¹ ranges (Table 14). Amongst the REE Ce, Y, La and Nd yield 77 % of the summed REE signal (99 - 673 ng g⁻¹).

Factor analysis was employed for a reduction of element concentration and enrich-

ment data to source characteristic informations (Table 15a,b). The FA for element concentrations in pine needles extracted five factors describing 23, 11, 10, 9 and 7 % of the data set, respectively (Table 15a). Elements bearing the most characteristic information are Zr, Hf, Th and Σ REE contributing to > 87 % to factor 1, and Ni and Ca with > 87 % on factors 3 and 4, respectively. Factor 2 is best reflected by Cu and W, factor 5 is represented with a maximum of 61 % by U, Cs, Li and Mg. All other elements show less dominant contributions to one factor. In case of Ga, Fe, In, Tl, Zn, Sr, Ba, Hg, U, Re and B element concentrations influence two or three factors. Chromium reveals no significant factor dependence.

Element distribution maps were created for a detailed interpretation of the spatial behaviour of single elements (Fig. 44a-f, 46c, 47a, 48a). These maps show maximum element concentration zones as a result of spatial interpolation between element data gained from 71 pine needle sampling locations. Most prominent is a zone with exceptionally high element concentrations in the north-west of the Greater Cologne Conurbation, as found for Σ REE, Th, Ti, Zr, U, Fe, and V (Fig. 44a,b,c,d,f; 46c; 47a). Additionally, Zr and U show high concentrations in the south of the study area, but differ notably in concentration for Cologne City sampling sites (Fig. 45d,f). Thus, high concentrations in Cologne City are observed for Zr, Fe and Pb (Fig. 46c, 48a). Chromium and titanium reveal maximum concentration levels west and east of Bonn City (Fig. 44c,e).

Element enrichment versus upper continental crust (UCC) For calculation of element enrichment factors versus average upper continental crust composition the summed REE concentration representing the geogenic dust fraction deposited on the needles surface was employed [125]. This is based on investigations made by Wyttenbach et al. [282, 283] and Tyler [253], showing that REE concentrations are almost unaffected by anthropogenic emissions. A factor analysis of the 15 REE determined extracted two factors, both describing 48 % of the data set. Factor 1 comprises 8 "heavy" HREE with Y and Tm yielding highest factor loadings. Factor 2 is best represented by Ce and contains 7 "light" LREE. All REE contribute with minimum 42 % to both factors except Lu and Ce with 27 % and 35 % on the second factor, respectively.

Element enrichment varies between < 1 and 1700 (Table 36 in appendix). Extremely high EF > 250 are observed for B, Cd, Re, Sb and Zn (Fig. 43). An enrichment of more than 50 times above geogenic derived dust level was calculated for Ag, Bi, Ca, Cu, Hg, K, Mg, Mn and Mo. Exceptionally low abundances (EF < 1) were observed for Au, Ga, Hf, Nb, Ti, U, Zr. All other elements are enriched between 1 and 30 times against UCC (Fig. 43). Factor analysis of EF yields 7 factors (Table 15b). Highest factor loadings are 87 % for indium on factor 1, 86 % on Hg for factor 2, 86 % for Cd on factor 3, 83 % for Cs on factor 4, 85 % on Nb for factor 5 and 75 % and 86 % for Ba and Re on factors 6 and 7, respectively. For Mo, Cr, Zr, Hf, V, Mg, Ti, Sr, and Ag significant contributions to two factors were noted (Table 15b). Spatial interpolation and mapping of element enrichment factors reveal local maxima that are used for source recognition. Cadmium is especially enriched at locations 21 and 32-34 near lead-zinc ore deposits in the Rhenish Massif, east of Cologne City and two single locations in the south and west of the GCC (Fig. 45a). Multiple ore bodies in the Rhenish Massif have been commercially mined until the first half of the 20th century

a)	f 1	f 2	f 3	f 4	f 5	b)	f 1	f 2	f 3	f 4	f 5	f 6	f 7
Zr	0.92	0.22	0.08	0.10	0.07	In	0.87	0.27	-0.03	0.05	0.09	0.07	-0.13
Hf	0.91	0.15	-0.04	0.08	0.01	Sn	0.84	0.32	-0.01	0.07	0.13	0.11	-0.11
Th	0.89	-0.04	-0.01	-0.10	0.22	Pb	0.80	0.03	-0.06	0.00	0.00	0.16	0.21
Σ REE	0.87	-0.08	0.20	0.01	0.08	Fe	0.76	0.17	-0.03	0.31	0.31	0.19	-0.06
Ga	0.82	0.09	-0.01	0.02	0.36	Sb	0.73	-0.07	0.28	0.06	0.33	0.20	-0.05
Fe	0.81	0.43	-0.03	-0.05	0.21	W	0.64	0.19	0.13	0.21	0.08	0.04	0.00
V	0.80	0.21	-0.06	0.13	0.12	Cu	0.61	0.31	0.38	0.37	0.10	-0.14	-0.12
Nb	0.79	0.08	0.11	0.06	-0.09	Na	0.53	-0.05	-0.13	0.16	-0.40	0.17	0.13
Ti	0.67	-0.07	0.22	0.02	-0.08	Hg	0.11	0.86	-0.14	0.11	0.16	0.12	0.11
In	0.65	0.53	-0.19	0.17	-0.28	Bi	0.29	0.82	-0.04	-0.13	0.06	0.10	0.10
Pb	0.62	0.47	-0.07	-0.01	-0.19	Ca	0.09	0.80	0.24	0.29	0.16	0.31	-0.01
Na	0.37	0.32	-0.02	0.12	0.03	Rb	-0.02	0.80	0.22	0.12	0.03	0.03	-0.07
Cu	-0.12	0.78	0.07	-0.05	0.16	Mo	0.55	0.64	-0.10	0.05	0.18	-0.15	-0.05
W	0.19	0.76	-0.01	-0.06	0.10	B	0.31	0.63	0.17	0.34	0.30	0.16	0.14
Sb	0.53	0.66	0.11	0.01	-0.03	Cr	0.44	0.54	0.31	0.13	0.13	-0.23	-0.05
Sn	0.56	0.60	-0.19	0.25	-0.25	K	0.34	0.54	0.36	0.31	0.29	-0.30	-0.08
Tl	0.16	0.56	0.12	0.34	0.33	Cd	-0.01	-0.01	0.86	-0.13	-0.15	0.09	0.00
Mo	0.15	0.51	-0.38	-0.06	0.01	Ni	0.18	0.17	0.81	-0.04	0.22	-0.23	0.18
Ag	-0.01	0.50	0.16	0.21	0.20	Mn	-0.22	0.06	0.75	-0.20	-0.02	0.05	0.14
Au	0.10	0.32	-0.10	0.16	-0.14	Zn	0.20	0.28	0.67	0.32	0.00	0.22	0.10
Ni	-0.01	-0.02	0.87	-0.13	-0.13	Cs	0.02	0.19	0.10	0.83	-0.08	-0.04	-0.07
Mn	0.09	-0.17	0.81	0.16	-0.14	U	0.11	0.10	-0.32	0.80	-0.07	0.05	0.18
Cd	0.12	0.00	0.77	0.25	-0.21	Ga	0.26	0.11	-0.25	0.71	0.03	0.19	0.07
Co	0.12	0.00	0.64	-0.17	0.16	Mg	0.24	0.46	0.30	0.66	0.22	0.01	-0.10
Zn	-0.02	0.34	0.64	0.31	0.07	Th	0.24	-0.28	-0.38	0.45	0.26	-0.06	0.03
Ca	0.07	0.05	0.11	0.89	0.16	Nb	0.16	0.16	-0.13	-0.10	0.85	0.16	0.11
Sr	0.26	0.17	-0.12	0.67	0.31	Ti	0.16	0.42	0.25	0.09	0.71	-0.05	0.02
Bi	0.18	0.12	0.10	0.58	-0.28	Zr	0.53	0.23	-0.12	0.10	0.60	0.31	0.16
Ba	0.42	0.18	0.18	0.58	0.11	Hf	0.51	0.19	-0.16	0.13	0.59	0.24	0.05
Rb	-0.29	-0.09	-0.06	0.55	-0.07	Ba	0.08	0.25	0.24	0.09	0.06	0.75	0.01
Hg	0.46	-0.13	-0.21	0.54	0.11	Sr	0.05	0.44	0.11	0.39	0.24	0.57	-0.13
K	0.16	-0.13	-0.13	-0.40	-0.10	V	0.40	0.10	-0.28	0.09	0.22	0.51	-0.09
U	0.49	0.00	-0.27	-0.06	0.61	Ag	0.29	-0.13	0.38	0.42	-0.03	0.44	-0.04
Cs	-0.17	0.18	-0.08	0.09	0.59	Au	0.23	-0.07	-0.08	-0.10	0.04	0.35	-0.03
Li	0.25	0.04	0.17	0.08	0.58	Re	-0.05	0.11	0.01	0.19	0.12	-0.04	0.86
Mg	-0.06	0.14	-0.21	0.29	0.56	Co	0.01	-0.06	0.27	-0.13	0.01	-0.06	0.85
Re	0.14	-0.13	0.43	-0.17	0.48	% var.	18	15	11	10	8	6	5
B	0.15	0.37	-0.09	0.34	0.40								
Cr	-0.08	0.04	0.21	0.01	-0.24								
% var.	23	11	10	9	7								

Table 15: Factor analyses of a) major and trace element concentrations on pine needles in the GCC, b) element enrichment (EF) on pine needles normalized for geogenic dust loads. For interpretation of factor loadings see text.

and mine tailings are still preserved. The EF of calcium is about 200 times higher in a morphologically elevated zone reaching south to north along the eastern Rhine Valley and at one location in the south-west also characterized by elevated height (Fig. 45b). A barium enrichment of about 6 times is recorded in the south-eastern part of Cologne City and the southern Rhine Valley (Fig. 45c). Sodium is 6 times higher than estimated for geogenic derived dust in areas of intensive agricultural land use in the

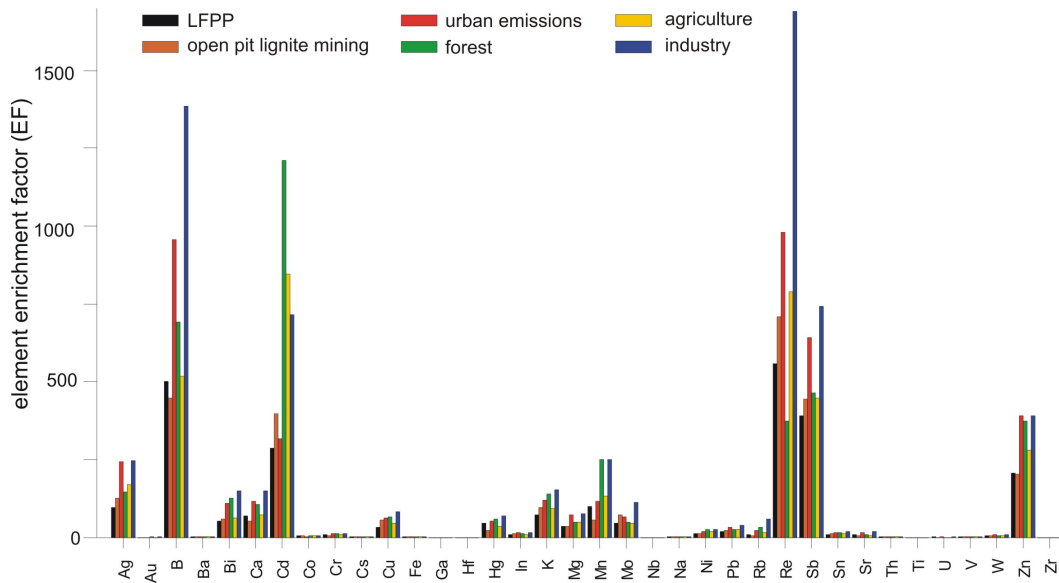


Figure 43: Variations in element enrichment factors (EF) observed on pine needles in the GCC. Samples are classified according to predominant emission scenario.

south-western Zuelpich Plain (Fig. 45d). For needles sampled in Cologne City sodium enrichment is observed, whereas in forested areas Na is at upper continental crust level. Antimony is enriched for a minimum of 90 times in the whole study area and reaches maximum values in Cologne City with over 1500 times higher loads than estimated for unpolluted areas (Fig. 46a). Similar observations are made for zirconium and iron showing maximum non-geogenic fractions on pine needles in Cologne City, the Rhine Valley and in cities of Dueren and Euskirchen (Fig. 46b,d).

In figure 47b-f enrichment of elements with maxima near highly industrialized zones are displayed. Vanadium and strontium are predominantly accumulated in the south of Cologne and the Sieg Valley, whereas Mo, Sn and In reach maximum enrichment in the industrial area Cologne-North. Besides, non-geogenic loads of Mo, Sn, In, and Sr on pine needles are relatively high near Dueren City. For all elements shown in figure 47 enrichment is observed in the high traffic zone of Cologne City.

Elements displayed in figure 48 are characterized by local elevated abundances that are spatially related to industrial emitters. Lead is about 60 times enriched in the industrial area Cologne-North, in the Sieg Valley, Dueren and in the Cologne City area. This was observed equivalently for Cu, W and B. Differences are noted for chromium that is especially enriched in Bonn City and less enriched at location 3 in the industrial zone Cologne-North (Fig. 48d). Boron also shows minor enrichment at the Cologne-North site, when related to Pb, Cu, and W (Fig. 48f). Tungsten shows strong parallels to lead enrichment but reveals notably lower occurrence in the Sieg Valley (Fig. 48e).

4.2.4 Discussion

The study aims toward identification of element origin detected in pine needles in the Greater Cologne Conurbation. Sources for elements are manifold and comprise ge-

ogenic, biological and anthropogenic input and combinations thereof. To account for the geogenic derived load on sampling devices normalization on typically geogenic elements is common [11, 55, 84]. Remaining element enrichment factors give the elements concentration increase in addition to the geogenic dust load. Thus, EF may still comprise biological element loads and anthropogenic input when working with bioreceptors. A discrimination of these two factors is approached by comparing absolute concentrations to concentrations of reference plants established by Markert [141], and Bargagli [11], where plants were considered to be free of pollutants (Table 14). Finally, local element enrichment above average UCC and common biological element concentration is discussed as derived from anthropogenic emission. The discussion of anthropogenic element sources is done for known emitters and emission scenarios utilizing spatially high-resolved data mapping.

Biological background concentrations Comparison of element loads detected on pine needles in the GCC with averaged element data for unpolluted pines by Bargagli [11] reveals a strong enrichment versus biogenic content for Mg, Ba, Mn, Ag, Hg, V, Sb, Mo, Cd, Cr and Co (Table 14). Other element concentrations are close to the "natural" biogenic concentration or even below. The latter is predominantly observed for comparison with data for an "average plant" given by Markert [141]. This "average plant" is mainly based on element concentrations determined on vegetables and obviously differs from pine needle element concentrations. Nevertheless, a high non-biological enrichment must not necessarily be related to anthropogenic emissions but can still be due to geogenic dust loads and, simultaneously, a low or moderate biological enrichment can appear as high enrichment versus UCC. The latter is the case for B, Ca, Cu, K and Zn, showing high EF versus UCC due to high biogenic concentrations (Fig. 43). An additional increase in concentrations above biological average is observed for all mentioned elements that can be related to anthropogenic input (Table 14). Besides, notable enrichment versus biological background and UCC is observed for Ag, Cd, Hg, Mg, Mn, Mo, Sb, and V indicating for additional sources (Fig. 43, Table 14). The differentiation of element data in six anticipated emission categories, points towards specific sources. For almost all elements the enrichment versus UCC is highest at urban and industrial sites supporting the assumption that maximum enrichment is dominated by anthropogenic processes. A detailed source discussion follows on spatially resolved element distribution maps.

Geogenic dust load A suite of elements is known to preferentially be of geogenic origin. Most common elements for normalization on geogenic material are Ti, Zr, Si and Al, the latter being out of discussion in biomonitoring studies due to their use in plant physiological processes [84]. Wyttenbach et al. [282, 283] and Tyler [253] introduced rare earth elements (REE) as most representative for geogenic dust loads while exhibiting lowest contributions from anthropogenic emissions. Here, spatial mapping of dust-related elements Σ REE, Th, Ti, and Zr is dominated by dust blow-out from the open pit lignite mining district in the north-west of the GCC and reveals minor dust loads in urban areas and areas of agricultural landuse (Fig. 44a-d). Titanium and zirconium show additional maxima in the south-east of the study area and the cities Cologne and Euskirchen, respectively, which is attributed to additional source input as

discussed below. Thus, REE and Th reveal lowest source diversity and therefore are the most reliable indicators for geogenic dust. Since the signal of summed rare earth elements is less sensitive to errors during sampling or analytics, Σ REE were preferred for normalization on geogenic dust in this study. Before normalization REE concentrations were subjected to a FA to evaluate the homogeneity of their origin. Extraction of two factors explaining 96 % of the data set indicates similar source characteristics and allows summing the suite of components. An additional factor analyses run for major and trace element concentration data comprises all elements associated to average geogenic dust in factor 1 (Table 15a). Nevertheless, the spatial patterns of Zr and Ti reveal additional source contributions (Fig. 44c,d), thus indicating that the FA does not allow for a detailed source differentiation.

Local geological characteristics Titanium and chromium bear maximum concentrations near Bonn in the Siebengebirge, where basaltic deposits are excavated (Fig. 44d,e). A dust blow-out enriched in Ti and Cr is assumed a likely consequence. Investigation of basaltic deposits west of Bonn gave enrichment factors for Cr of about 10; whereas V, Co and Ni revealed enrichment in between 7 and 13 and Ti yielded an EF of 4 [217]. Accordingly, spatial maps display enrichment of Cr and V on pine needles in this region (Fig. 47b, 6d). Enrichment of Co and Ni on needles due to basalt weathering is less obvious than for Ti and Cr. This can be related to a domination of element input by other sources. Factor analysis of element enrichment factors classifies most of the elements related to basaltic origin in factor 5 (Table 15b). Cadmium enrichment dominates in the east of the GCC (Fig. 45a). This region is today characterized by forest cultivation, but bears hydrothermal Pb-Zn-Ag deposits containing sphalerite species that is known to be rich in cadmium [68]. A root uptake for Cd is almost certain, supported by properties of Cd - it is easy to mobilize - and comparison with needle enrichment of major components of the ore: Pb, Zn and Ag show only slight enrichment on pine needles and are thus related to airborne input and a withgoing dilution of ore derived elements. High factor loadings on Cd, Zn, Ni and Mn enrichment in factor 3 (Table 15b) yield a satisfying source characterization for elements attributed to the former ore mining zone. Here, the better source dependence of the FA is related to the contribution of multiple elements that are almost exclusively released by a single source. In addition, investigations show that cadmium is not applicable as a tracer for biomonitoring atmospheric quality, but for soil contamination. This is supported by the following observations: i) cadmium enrichment on needles is higher than the enrichment of major Pb-Zn-ore derived elements, ii) known anthropogenic Cd emission point sources as provided by the Environmental Agency of NRW [118] do not appear in the spatial distribution map (Fig. 45a).

Carbonaceous deposits An enrichment of calcium occurs in conjunction with morphological elevation in the east and south-west of the study area (Fig. 45b). It is suspected that climatic changes lead to a local enhancement of Ca due to a decrease in temperature or an increase in precipitation, resulting in cold condensation or a plus in wet deposition, respectively. Sources for atmospheric Ca are sea spray and lubricating oils used in vehicles [67, 19]. The Ca EF distribution suggests that a calcium input into the atmosphere is most likely due to geological formations occurring in the south-

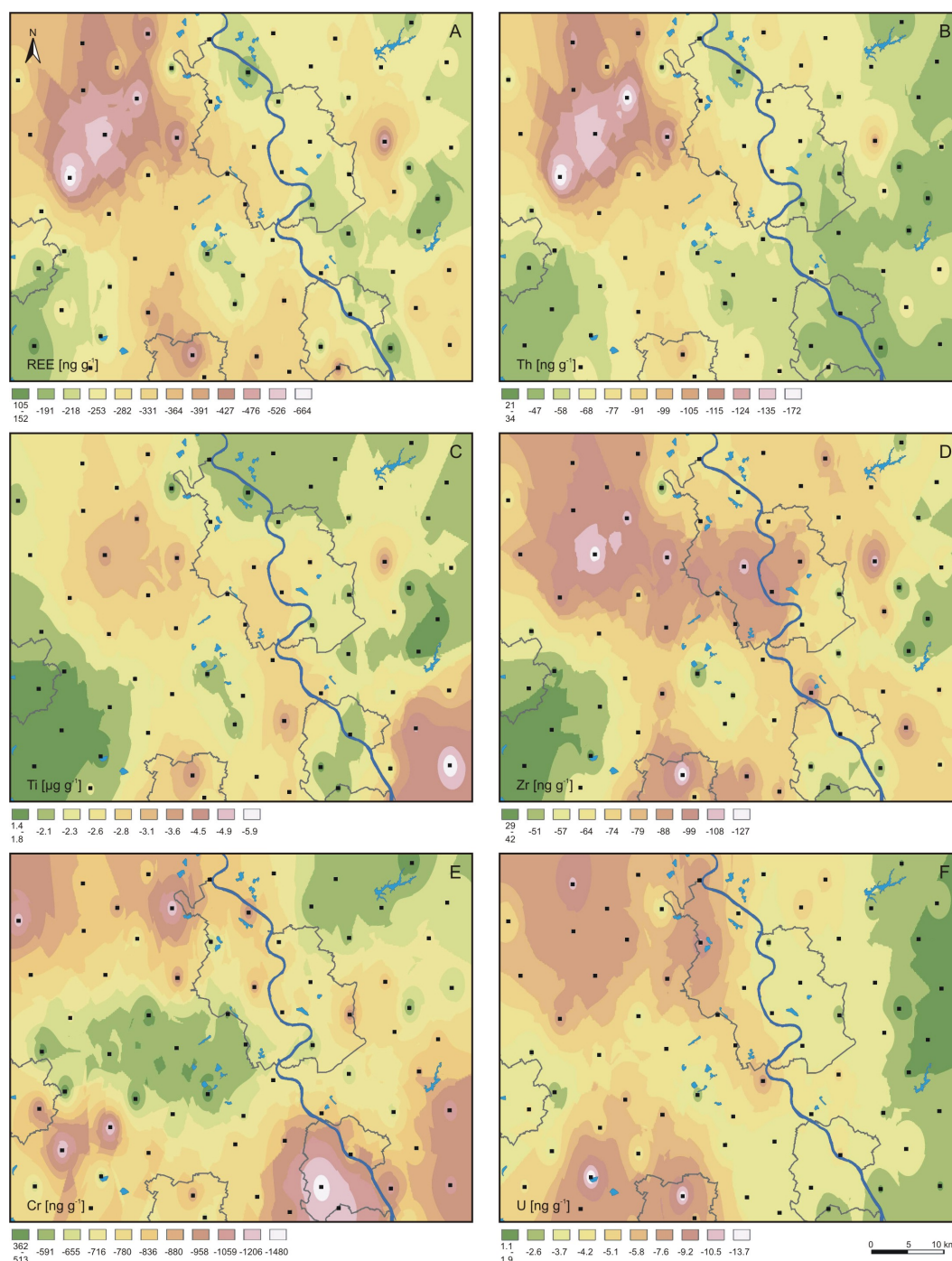


Figure 44: Isopleths maps of elements commonly attributed to geogenic sources. Maps are based on interpolation between pine needle sampling sites given in black squares ($n = 71$) and show outlines of cities in the GCC for orientation. Source characteristic patterns are discussed in the text. For details about land use see overlay transparency, provided in the appendix (Fig. 62).

east of the GCC (Fig. 45b). A study by Franceschi et al. [59] shows that excess Ca can be translocated as Ca-oxalate crystals into pine needles, thus a calcium uptake via roots from soil can not be excluded. The distribution pattern of barium and strontium

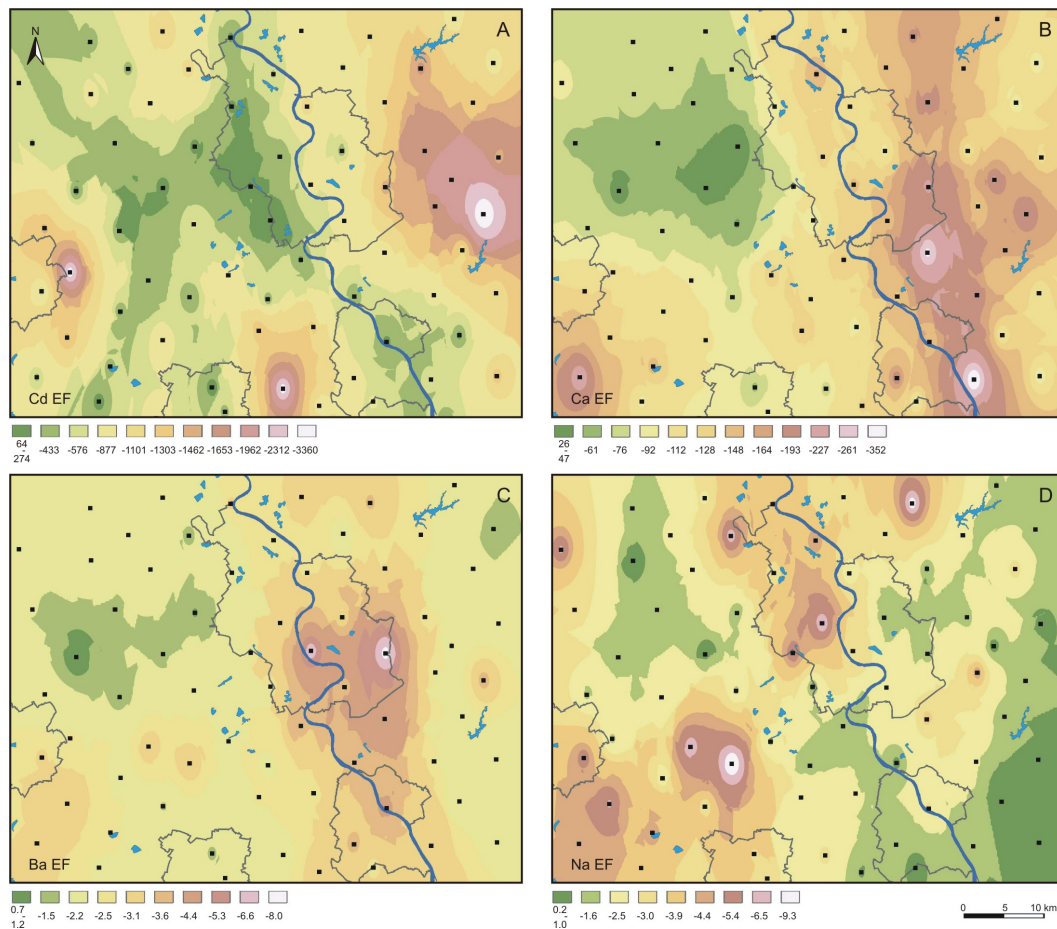


Figure 45: Isopleths maps of elements attributed to a) local geogenic sources and b-d) mineralic input of unknown origin. Maps are based on interpolation between pine needle sampling sites given in black squares ($n = 71$) and show outlines of cities in the GCC for orientation. Source characteristic patterns are discussed in the text. For details about land use see overlay transparency in the appendix (Fig. 62).

enrichment (Fig. 45c, 47f) is similar to calcium. A substitution of Ca by Ba and Sr in Ca-oxalate crystals on pine needles or in the emitted particles before deposition on the needle is possible, since the Sr EF is much lower with maximum enrichment of 23. Ba enrichment in the south of Cologne is discussed below as traffic and industry related.

Atmospheric input from fertilizers Sodium enrichment can be related to sea spray, geogenic sources or anthropogenic emissions. It is passively accumulated on needles and at the same time an essential plant nutrient. A reference value of 380 ppm is given for unpolluted pine needles indicating that needles sampled in the GCC are in a low pollution range. Anthropogenic sources are salt application for de-icing purposes in winter and consequent resuspension and use of Na-based fertilizers [125]. The latter is related to highest Na enrichment in the GCC that is observed in the south-west, where large agricultural crop lands dominate the landscape (Fig. 45d). Mercury enrichment on needles shows a very similar distribution pattern and is also attributed to the use of fertilizers. The FA was not able to discriminate fertilizer effects.

Urban dust The dust fraction in urban areas is characterized by multiple sources. Urban dust loads are mainly affected by road and building constructions, combustion products from fossil fuels, metallurgic processes and municipal waste incineration (MWI) being present in small grain size ($< 0.5 \mu\text{m}$). Abrasion products of higher grain size ($> 1.5 \mu\text{m}$) primarily derive from traffic (brakes, tires, chassis) [19]. Factor analyses was consulted for a discrimination of source input of single elements, but combines emissions of MWI, industry and traffic in factor 1. However, highly variable sources and a mix of element emissions in air demand a more detailed spatial analysis. The further discussion of element sources and dispersal is therefore based on spatial interpolation maps.

Urban dust - traffic fraction In this section traffic derived element emissions are discussed. Especially, high absolute concentration and enrichment versus upper continental crust in urban areas were observed for Sb, Zr and Fe (Fig. 46a-d). Antimony and its oxygenated compounds are potential carcinogenics and therefore listed as "priority pollutants" by the EC and US-EPA. Antimony was enriched up to 1600 times in the Cologne needles and its distribution in the city area almost perfectly reflects the high traffic zone. Antimony emissions are attributed to abrasion of brake pads as pointed out by Krachler et al. [112] and Birmili et al. [19]. Lowest Sb EF are obvious in areas of agricultural land use, but still show notable elevation with an EF of 90-400 (Fig. 46a), indicating for a transport of traffic derived Sb to remote areas. Bargagli [11] and Markert [141] provide reference values for pines and vegetation, respectively, yielding Sb concentrations of 20 - 100 ng g⁻¹ in unpolluted areas. In Cologne City Sb concentrations are 6 times higher, at remote sites concentrations are twice as high (Table 14, Table 36 in appendix). An admixture of Sb emissions from the Cologne municipal waste incinerator is likely at location 10 (Fig. 46a; [112]). A relative enrichment of zirconium is observed for the Rhine Valley, but at all locations EF are smaller than one, an effect related to analytical artefacts. Zirconium enrichment maxima are situated in the Cologne City district and are related to a traffic induced resuspension of street dust containing large fractions of geogenic material. The Zr distribution along the Rhine Valley indicates a preferential wind transport of compounds along this Valley, reflecting general pollutant transport mechanisms in similar grain size fractions. Iron concentrations in the study area are spatially related to emissions of the lignite open pit mining district and urban areas, whereas the calculation of EF solely depicts urban areas (Fig. 46c,d). Thus, the combination of spatial mapping of element concentration and element enrichment factor bears additional source discrimination potential: a differentiation of geogenic derived iron is achieved versus anthropogenic dust fraction. Correlation of the urban Fe EF maxima in Cologne City with Sb EF maxima indicates an additional contribution of MWI and refinery emissions upon traffic for iron (Fig. 46d, loc. 3, 10, 43 north and south of Cologne). A longer atmospheric transport for combustion derived iron may also lead to differences in Fe and Sb distribution patterns. Whether these differences are effects of source distribution or grain size could not be differentiated in this study. A good correlation of barium with high traffic zones as proposed by Monaci et al. [155] is not observed in the Greater Cologne Conurbation. Ba enrichment is mainly bound to calcium concentration in needles and maximum zones are found to be dependent on morphological elevation of the eastern Rhine Graben

shoulder to the east of Cologne. Nevertheless, an intermediate enrichment of Ba is obvious in Cologne, Bonn and Dueren city, indicating for partial contribution from traffic emission sources (Fig. 45c). Therefore, calculation and mapping of a Ca/Ba-ratio to elucidate traffic related Ba fractions was tested, but revealed no significant relation to high traffic zones. Another source contributing to pollution of urban atmosphere is the abrasion of asphalt especially emitting vanadium [130, 122]. This was supported by very steady and ubiquitous vanadium enrichment in the GCC, potentially resulting from omnipresent road wear in urban areas and at highways (Fig. 47b). In addition, an enrichment of copper is anticipated from road wear and brake linings [84] contributing to the urban dust load in the inner city of Cologne. The locally restricted maxima of Cu EF is related to short transport routes due to a preferential origin of copper from abrasion processes releasing coarse grain sizes (Fig. 48c). An enrichment of Pb on pine needles in the Cologne City area is in part attributed to traffic, since this element is still used for car batteries and balancing of wheels (Fig. 48b). Its persistence in the environment is also considered to lead to a continuing recycling of Pb, that was emitted by combustion of leaded gasoline during the last decades.

Urban dust - industrial emissions The Cologne Conurbation is home to many industrial branches. Dominating emitter in the north-west of the GCC is the lignite industry comprising two large open pit mines with enormous dust output and four power plants where about 80 mio t a⁻¹ lignite are combusted [208]. Along the Rhine Valley petrochemical industry and in the south-eastern Sieg Valley predominantly inorganic chemistry complexes are located. Especially metallurgic industry and organic reduction processes are known to release substantial amounts of major and trace elements into the atmosphere [101, 83]. Spatial analyses and calculation of element enrichment versus geogenic dust loads on pine needles revealed industrial emissions as major sources for V, Mo, Sn, In and Sr in the Cologne Conurbation (Fig. 47a-f). Vanadium concentrations are elevated near lignite fueled power plants (LFPP) in the north-west of the GCC and west of Cologne, in Cologne City and near ore deposits in the east (Fig. 47a). The normalization of V on geogenic background eliminates the ore signal, revealing a high V dispersal in the study area (Fig. 47b). In the river Rhine Valley, the Zuelpich plain and adjacent forested areas a wide-range transport of V becomes obvious, with main sources in industrialized regions south of Cologne, the Sieg Valley and the LFPP (Fig. 47b). Travel distance for notable V amounts was minimum 20 km to the west and north of the Rhine Valley. Evaluation of transport routes in the Rhine Valley is difficult, since various emitters are located therein. Another explanation for the ubiquitous dispersal of V in the study area is its origin from asphalt wear as discussed for traffic related urban dust above. In contrast, Mo enrichment is reduced to local hot spots around industrial complexes (Fig. 47c). Main Mo sources were found in the north of Cologne and in Bonn. A more precise source allocation would require analysis of source samples to be provided by the industry. An admixture of traffic related sources for Mo is not likely. Sn shows a similar source dependence being especially enriched near industrial complexes in the Cologne-North area (Fig. 47d). Transport distances seem slightly higher as observed for Mo, indicated by a slowly decreasing EF from sources to remote zones (Fig. 47d). Additionally, high Sn enrichment in Cologne City points towards notable contributions from traffic that were supposed to lead to the

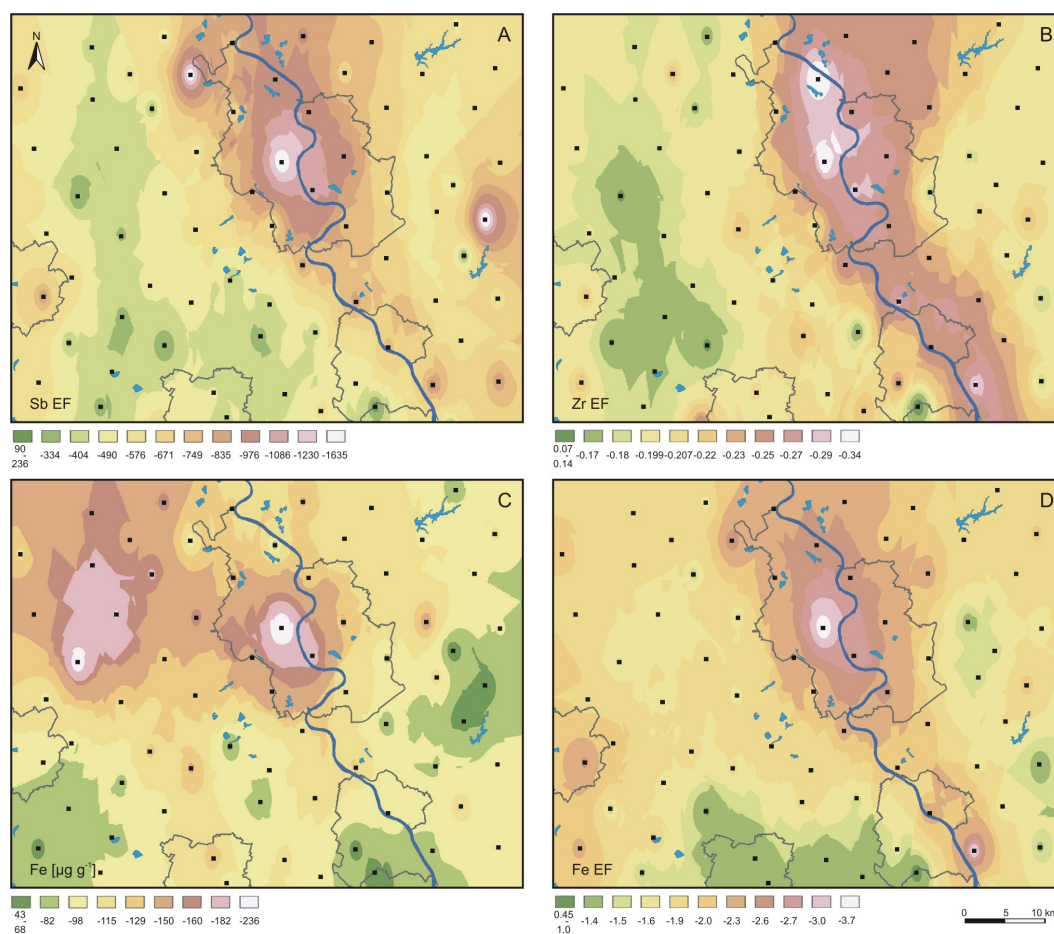


Figure 46: Isopleths maps of elements predominantly attributed to traffic emissions. Maps are based on interpolation between pine needle sampling sites given in black squares ($n = 71$) and show outlines of cities in the GCC for orientation. Source characteristic patterns are discussed in the text. For details about land use see overlay transparency in the appendix (Fig. 62).

high diversity in the spatial distribution of this element. Indium distribution is almost equal to the pattern shown for Sn (Fig. 47d,e). The dominance of emissions from the industrial area Cologne-North is even more pronounced, related to emissions from a large refinery complex, where In/Sn-oxide is used as a reducing agent for production of organics. Especially indium enrichment factors appear as perfect marker for this type of industrial emissions. Transport of indium was observed on a large scale in the northern Rhine Valley and was only limited to the east and west by morphological elevation (Fig. 47e). Highest approximated travel distance for In in the study area was noted from the refinery complex Cologne-North to the east with about 30 km. Strontium occurrence is concentrated at the refinery complex Cologne-South and in Bonn City (Fig. 47f). Sources for Sr in Bonn are not known. Enrichment of Sr in pine needles sampled at morphologically elevated sites in the east and south-west of the study area were attributed to a substitution of Ca primarily in the emission-product or secondarily on the needles as discussed above.

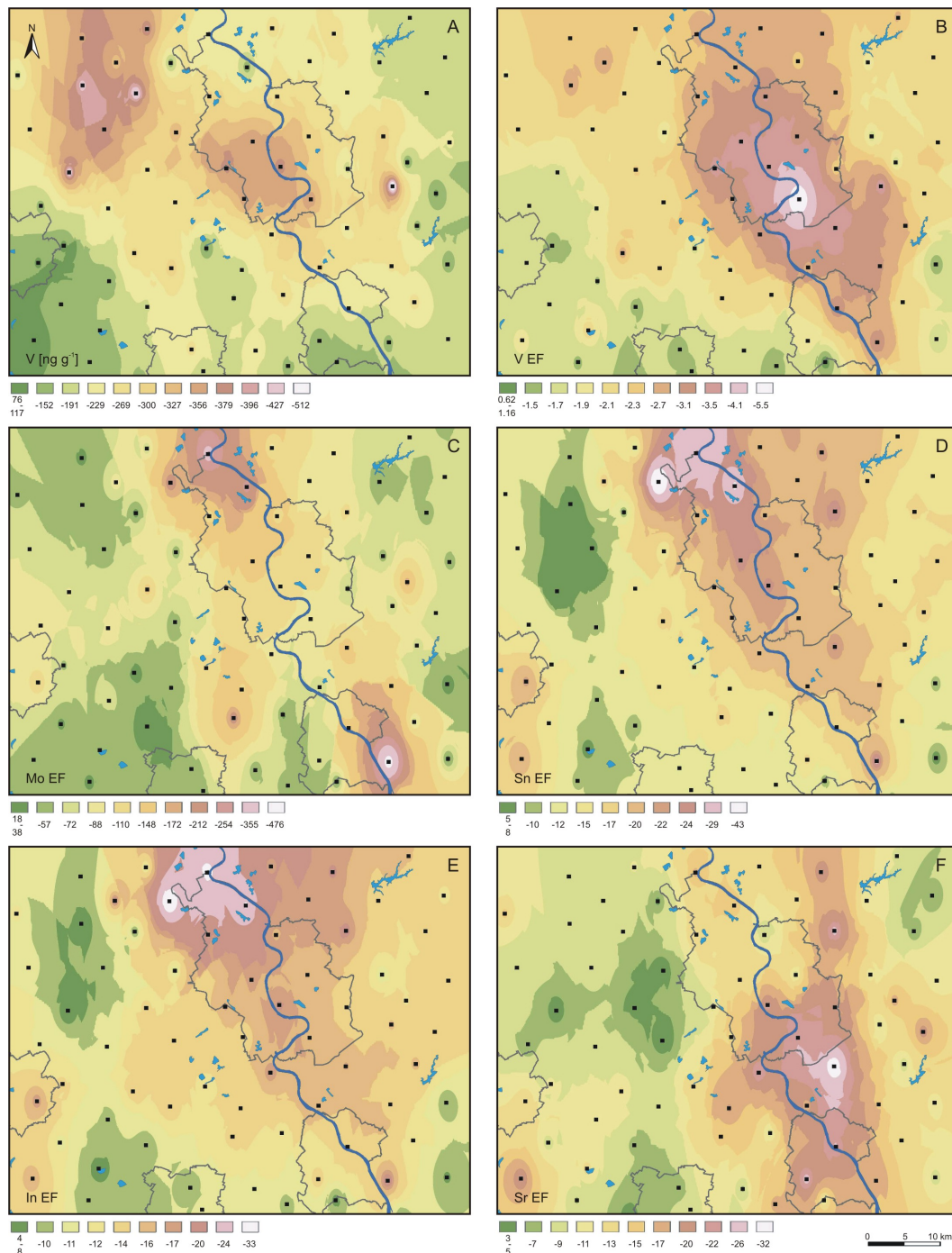


Figure 47: Isopleths maps of elements attributed to industrial emissions. Maps are based on interpolation between pine needle sampling sites given in black squares ($n = 71$) and show outlines of cities in the GCC for orientation. Source characteristic patterns are discussed in the text. For details about land use see overlay transparency in the appendix (Fig. 62).

Urban dust - municipal waste incineration Municipal waste incineration (MWI) may affect the emission of multiple elements, due to the combustion of various materials of variable composition. German law provides critical emission values for S Cd+Th, Hg, S As Cd, Co, Cr, BaP and S metals (Sb, As, Pb, Cr, Co, Cu, Mn, Ni, V, Sn), that have

to be met by MWI. In the GCC two major MWI are located combusting predominantly domestic waste. The Cologne MWI in the north of the city has capacities for 590,000 t a⁻¹ waste and the Bonn MWI is constructed for 245,000 t a⁻¹. More modern cleaning procedures in the Cologne plant lead to lower emissions, being below detection limits and emissions being close to critical values for the Bonn MWI, respectively [1, 22, 118]. The Environmental Agency records the MWI Bonn as one of the major emitters of metals in this area (4 kg a⁻¹ for all critical metals, except Cd with 1 kg a⁻¹ and Hg with 6 kg a⁻¹ in 2004 as notified by the plant operator for the official emission register [118]. The MWI Cologne only provides data for Hg emitting 7 kg a⁻¹ in 2004. MWI are also supposed to emit Sb from PET-plastic combustion [112].

The time-integrated pollution signal found on pine needles promises better results for a biomonitoring of MWI, than punctual measurements as applied for the public Emission Register. Additionally, accumulated pollutant loads on vegetation surfaces reflect the long-term exposition of the surrounding areas and their inhabitants to elements with severe health effects. Thus, enrichment of Pb, Cu, Cr, W and B on pine needles were discussed to reveal MWI emissions on pine needles in Cologne and Bonn. Cadmium and mercury show intermediate enhancement of the non-geogenic fraction at location 10 in the vicinity of the Cologne MWI. Because other sources dominate the distribution pattern of Hg and Cd (Fig. 45a), discussion of these elements as source indicator for MWI is not deepened. Comparison of lead concentration and enrichment in figure 48a and b shows that Pb was apparently bound to geogenic particles or originating from geogenic sources. The calculation of enrichment factors allowed an allocation of anthropogenic sources of Pb, pointing out emissions in highly industrialized areas in Cologne-North, the south-eastern Sieg Valley and Dueren (Fig. 48b). The distribution of lead in the north and the inner city of Cologne supported emission from multiple sources in industry and traffic. Most dominant enrichment appears in Dormagen next to an industrial complex producing organics. Enrichment of Pb at location 10 is related to MWI (Fig. 48b). Relatively low Pb EF near the Bonn MWI neither support nor deny the emission of lead into the atmosphere. For copper it has to be noted, that a huge fraction is essential for plants. Bargagli [11] gives unpolluted copper levels in pine needles with 4 $\mu\text{g g}^{-1}$. Copper load on needles in the Cologne Conurbation varies between 1.5 and 8 $\mu\text{g g}^{-1}$ with very small amounts being from geogenic sources. Thus, biological and anthropogenic Cu occurred in needles in nearly equal amounts. Copper is preferentially enriched in the Cologne-North industrial area, in the vicinity of Dueren and in Bonn City (Fig. 48c). The northern maximum was related to emissions from organic chemical industry and MWI (loc. 3, 10). Additional sources for Cu are abrasion from pavement [122] and from brake linings [84] as discussed for traffic derived urban dust above. Spatial analysis of Cr EF shows substantial elevation near MWI plants in Bonn and Cologne (Fig. 48d). In addition, it is notified by the Environmental Register NRW [118], that a print company emits significant amounts of Cr into the atmosphere in the Cologne-North industrial complex. Further industrial emissions are likely near Dueren and in the south-eastern Sieg Valley (Fig. 48d). Note, that Cr is not emitted by organic chemical industry and that no enrichment is observed at high traffic places. Therefore, chromium serves as a reliable tracer for industrial activity. For a concrete denotation of municipal waste incineration as emitter of chromium in situ combustion residues need to be investigated. Major contributions of pavement

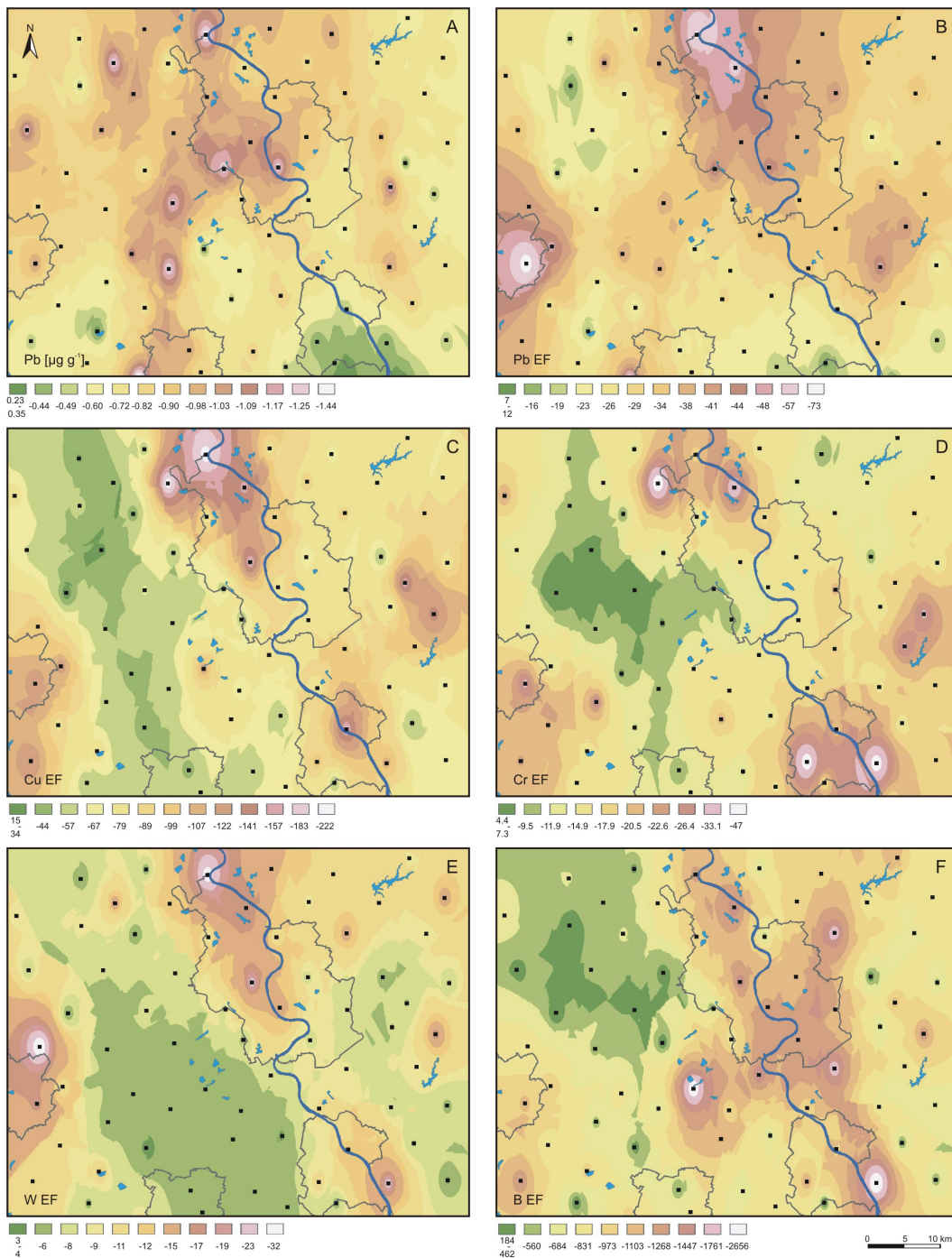


Figure 48: Isopleths maps of elements attributed to municipal waste incineration (MWI). Maps are based on interpolation between pine needle sampling sites given in black squares ($n = 71$) and show outlines of cities in the GCC for orientation. Source characteristic patterns are discussed in the text. For details about land use see overlay transparency in the appendix (Fig. 62).

wear to chromium and copper load [122] on pine needles can be neglected, because their EF differ dramatically in the high traffic area of Cologne (Fig. 48c,d). Tungsten loads in pine needles are close to the geogenic dust load in areas of agricultural land use

sources	lignite combustion	urban dust - traffic	industry I (refinery)	industry II (Cologne-N)	industry III (Cologne-S)	industry IV (MWI)
tracer elements	-	Sb, Fe	In, Sn, Mo, Cu	W	Sr	Cr
related elements	V, Pb	Zr, V, Pb, Ba, Na, Cu, W, B, In, Sn	V	Pb	V, B	B, Hg, Cd

sources	UCC	basalt	ore deposits	fertilizer	carbonaceous accumulation
tracer elements	REE, Th	Ti	Cd	-	Ca
related elements	Zr, Ti, Fe, U	Cr	Ca, Sb, V, Mo, Sr, Pb, Cu, Cr, W, B	U, Hg	Ba, Sr

Table 16: Sources for major and trace elements in the GCC, identified via spatial high-resolution biomonitoring.

and in forested regions (Fig. 48e). Enrichment is observed for highly trafficked urban areas, but especially in the industrial areas Cologne-North, Bonn and Dueren. The linkage between W and Pb occurrence is typical for refinery emissions, but emissions from MWI in Cologne and Bonn are also possible sources for W (Fig. 48e). Boron enrichment is obviously linked to emissions near location 10, which is situated in the closest vicinity to the Cologne MWI (Fig. 48f). Thus, boron might be a good indicator element for waste combustion in combination with chromium. Further investigations of MWI combustion residues are needed to assure this assumption. The enrichment of boron in the south of Cologne must be connected to other sources limiting its use as a MWI tracer element against chromium.

4.2.5 Conclusions

Spatially high-resolution biomonitoring of a suite of elements in the GCC allowed for a distinctive source allocation. Factor analyses provided a reliable tool for a first grouping of elements with similar emission background and facilitated further interpretation. Detailed investigation of source dependence was not achieved by FA. Spatial interpolation and mapping was shown to have a far better ability for source recognition, since the relation of elements to multiple and spatially heterogeneous distributed sources could be analysed.

A high source characterization potential was found for several elements leading to a differentiation of 11 sources in the Greater Cologne Conurbation (Table 16). Most indicative elements for environmental purposes are i) REE and Th concentrations characterizing the geogenic dust fraction; ii) the enrichment factors of antimony and iron perfectly reflecting high traffic volume in urban areas; iii) a detailed separation of industrial emissions is achieved by major and trace element biomonitoring in the Cologne Conurbation. Three types of industrial emission scenarios were described by tungsten,

strontium and chromium. Spatial mapping in the GCC revealed a high potential for high-resolution biomonitoring and in particular for source allocation of airborne pollutants. Nevertheless, a detailed denotation of emitters requires a comparison with other pollutant groups and analyses of emissions directly at the source.

4.3 Cologne Conurbation air quality - parent PAH

Detailed investigations concerning spatial appearance and distribution of polycyclic aromatic hydrocarbons are of world-wide importance. Most of the PAH are well correlated with human diseases [190], occur in large amounts in the environment, and are attributed to a long-range, transboundary transport [24]. Their ubiquitous prominence in air and input into food-chains, soils and oceans is of great environmental concern due to the persistence and high toxic potential at least of some compounds of this class. PAH with two to eight aromatic rings are primarily released by anthropogenic combustion, evaporation and distillation processes [24, 228]. Two-ring PAH, three-ring PAH and part of the four-ring PAH are predominantly abundant in gaseous form at atmospheric conditions. PAH of higher molecular weight are preferentially transported in particle-bound phase in the atmosphere. PAH like anthracene, benz[a]anthracene and benzo[a]pyrene are susceptible to photolytic degradation [73, 263]. Thus, variation in the preferred state of appearance, degradation, revolatization, solubility and withgoing uptake into environmental tissues lead to depositional differences. Especially the use of bioreceptors for PAH monitoring requires a detailed investigation of pollutant accumulation systematics. This is addressed by a time-resolved sample set of 2-ring to 6-ring PAH concentrations (PAH-2 to PAH-6) of *Pinus nigra* needles from six locations, reflecting dominant emission scenarios of the Greater Cologne Conurbation (GCC). Dispersal and source dependent patterns of low to high molecular weight PAH are discussed on pine needles sampled in spatial high-resolution on 3600 km². PAH dispersal is discussed with respect to the number of aromatic rings and molecular weight, whereas the discussion of PAH sources depends on distribution patterns of single PAH and PAH ratios. A detailed source characterization is achieved by the determination of source diagnostic PAH ratios that are primarily based on differences in emission process (e.g. combustion temperature) and transport fractionation [27, 73, 287, 139, 51]. Here, PAH ratios are tested first-time for their use as source diagnostic tools in air quality biomonitoring. The study area is characterized by multiple emission sources, including high trafficked regions, industrial complexes, refineries, as well as large-scale lignite mining and attributed power production. Source dependencies, transport mechanisms and atmospheric fractionation processes are investigated using factor analysis and spatial analysis of PAH loads on pine needles. Sources and dispersal of three-ring PAH are excluded here and discussed in chapter 4.4.

4.3.1 Sampling

Sampling of i) time-resolved pine needle samples (n=51) gained from six locations in the Cologne Conurbation with different emission background was done as described in chapter 2.1 by Lehndorff et al. [126]; ii) spatially high-resolved pine needle samples of composite needle age classes was conducted at 71 locations on 3600 km². Samples cover

aromatic rings	mw	compounds	abb.	% of PAH-X
PAH-2	166	Fluorene	Flu	100
PAH-3	178	Phenanthrene	P	94
	178	Anthracene	A	1
	184	Dibenzothiophene	DBT	3
	190	Cyclopenta[def]phenanthrene		2
PAH-4	202	Fluoranthene	Fla	50
	202	Pyrene	Py	28
	216	Benzo[a]fluorene	BaFlu	1
	216	Benzo[b+c]fluorene	Bb+cflu	1
	226	Benzo[ghi]fluoranthene	BghiFla	3
	226	Cyclopenta[cd]pyrene	CpcdPy	0.05
	228	Benzo[c]phenanthrene	BcP	1
	228	Benz[a]anthracene	BaA	1
	228	Chrysene + triphenylene	CT	11
	234	Retene	Re	1
	234	Benzonaphthothiophene	BNT	1
	PAH-5	252	Benzo[b+j]fluoranthene	Bb+jFla
252		Benzo[k]fluoranthene	BkFla	17
252		Benzo[e]pyrene	BeP	19
252		Benzo[a]pyrene	BaP	6
252		Perylene	Per	0.05
278		Dibenz[a,h]anthracene	DbahA	0.05
PAH-6	276	Indeno[1,2,3-cd]pyrene	Ip	35
	276	Benzo[ghi]perylene	BghiP	58
	300	Coronene	Cor	9

Table 17: Abbreviations and classification of PAH according to aromatic ring number and molecular weight; percentaged contribution to ring number classes as determined for the GCC.

a time span with an integrated pollution signal of approximately 4 years. Selection of locations, sampling strategies and methods follow methods established for the time-resolved sample set (chapter 2.1 and Lehndorff et al. [126]) and mainly focus on a consistent sampling that is representative for local air quality and free of emission point sources.

4.3.2 Analytical methods

PAH analysis Analytical work-up and analysis is done employing accelerated solvent extraction of needle surfaces with hexane:dichloromethane, 99:1 (v/v), $T = 120\text{ }^{\circ}\text{C}$, $p = 120\text{ bar}$ [123]. Prior to GC-MS analysis, wax elimination via centrifugation and PAH clean-up with liquid chromatography methods (MPLC, M. Köhnen-Willsch, Jülich) was applied as described by Lehndorff and Schwark [123] and in chapter 3.3. Quantification of 27 PAH (Table 17 and Table 61 in appendix) was achieved using d_{10} pyrene as internal standard.

Statistical analysis This study deals with two data sets, one comprising temporally resolved concentrations of PAH on pine needles at six sampling sites and one reveal-

ing spatial variations of integrated time-signals on pine needles at 71 locations in the Greater Cologne Conurbation. Statistical approaches for the temporal resolved data set yield linear correlations in bivariate plots and linear regression analysis of PAH loads versus time of needle exposure (Fig. 49, Table 18). A Kruskal-Wallis- H test to prove intra-site systematics versus inter-site variability as shown by Lehndorff et al. [126], and in chapter 2 was not applicable, due to high seasonal inter-site variability of the PAH data set. The spatial distribution pattern of absolute PAH concentrations and PAH ratios are visualized using the ArcGIS Spatial Analyst tool (ESRI). For interpolation of PAH distribution the "inverse distance weighted" method was chosen. Due to the high variability in environmental systems and insufficient data thereof, the interpolation between sampling sites is based on a linear relation (power = 1) and calculated with 6 nearest neighbours. Colour codings were extracted according to sample populations. Additionally, factor analysis (FA) was done with SPSS 14.0 with principal component extraction and varimax rotation to support source characterization. The linear correlation between single PAH was studied utilizing biplots with sample sites pre-classified according to emission data from the Environmental Agency North Rhine-Westphalia and land use data provided by the European Community [118, 69].

4.3.3 Results

Time-resolved analyses of PAH-2 to PAH-6 PAH concentrations on *Pinus nigra* needles were analysed for each needle cohort at six locations with different emission background. Emission scenarios are characteristic for the Greater Cologne Conurbation and comprise 1) emissions of organic industry and refinery in Dormagen, 2) a remote site on morphological elevated terrain in Bergisch-Gladbach, 3) emissions of lignite open pit mining and lignite fueled power plants (LFPP), 4) urban emission mix of traffic, industry, and domestic heating in Cologne City, 5) urban emission mix of Bonn City, 6) remote and morphological plain site in Fuessenich. A time resolved sampling of pine needles in summer and winter 2004 allows for a biannual resolution of PAH accumulation, thus, highlighting a time period of maximum 50 months (Fig. 49). The slope of the PAH accumulation curves versus time of needle exposure and standard deviations are given in Table 18. For the 2-ring PAH fluorene only a moderate increase from young to older needle cohorts is observed at locations Dormagen, Cologne, and Bonn. Urban sampling sites Cologne and Bonn show an intermediate pollutant load when compared to neighbouring locations in the Cologne Conurbation with slightly higher PAH-2 concentrations in winter samples. At the industrial site Dormagen PAH-2 concentrations reveal a strong dependence on sampling season. Although a continuous increase from 10 to 50 ng g⁻¹ over a time period of 50 months can be observed, summer samples are relatively depleted in PAH-2. Lowest concentration levels were analysed on needles from remote Bergisch-Gladbach and Fuessenich sites. Highest PAH load (400 ng g⁻¹) and a constant increase over time is observed at the Bedburg location with a curve slope of 10 ± 1.9 (Fig. 49, Table 18).

Three-ring PAH phenanthrene, anthracene, dibenzothiophene, and cyclopenta[def]-phenanthrene account for the highest part of the PAH analysed on pine needles with up to 2000 ng g⁻¹. Curve slopes are notably steeper than for PAH-2 and vary between 5 for remote Bergisch-Gladbach pines and 56 for Bedburg needles (Table 18). PAH-

location		PAH-2	PAH-3	PAH-4	PAH-5	PAH-6
Dormagen (refinery)	slope m	0.46	22	18	0.76	0.15
	std dev (m)	0.54	6.4	3.2	0.32	0.08
	r	0.10	0.6	0.8	0.45	0.32
Bergisch- Gladbach (remote)	slope m	0.28	4.5	4.5	0.10	0.01
	std dev (m)	0.11	1.0	0.7	0.08	0.02
	r	0.49	0.7	0.9	0.20	0.06
Bedburg (LFPP)	slope m	10	56	25	0.27	0.03
	std dev (m)	1.91	9.5	4.4	0.26	0.06
	r	0.84	0.9	0.9	0.19	0.04
Cologne (metropolitan)	slope m	0.94	22	19	0.64	0.19
	std dev (m)	0.62	3.0	4.3	0.37	0.11
	r	0.31	0.9	0.8	0.38	0.38
Bonn (urban)	slope m	0.41	10	11	0.14	0.03
	std dev (m)	0.16	1.4	2.0	0.23	0.02
	r	0.50	0.9	0.8	0.05	0.21
Fuessenich (remote)	slope m	0.52	8.9	4.8	0.06	0.01
	std dev (m)	0.12	1.1	1.3	0.08	0.01
	r	0.73	0.9	0.7	0.06	0.03

Table 18: Statistical parameters of PAH accumulation with time, simplified by linear regression analyses; bold = slopes (m) > 8, standard deviation of slope > m, and measure of determination (r) > 0.6.

3 concentration on needles is highest in the lignite combustion area Bedburg and at the refinery site in Dormagen. Emissions in Cologne City are slightly lower than in Dormagen with a median of 456 ng g⁻¹ calculated from consecutive needle generations (Table 46 in appendix). Seasonal dilution effects accounting for variations of over 500 ng g⁻¹ in PAH-3 loads on pine needles are observed at the refinery site (Fig. 49b). These variations were previously discussed by Lehndorff et al. [126], Lehndorff and Schwark [125], and Lehndorff and Schwark [124] for magnetic particulates, major and trace metals, and PAH-3, respectively. Four-ring PAH concentrations are dominated by fluoranthene and pyrene contributing with 80 % to the sum of 11 analysed PAH-4 (Table 17). Highest PAH-4 concentrations are reached at the refinery site and in Cologne City with 1070 and 900 ng g⁻¹, respectively. Second place take the samples from the lignite area Bedburg, followed by pine needles gained in Bonn City. Slopes of accumulation curves (4 - 25) show lower variation than observed for PAH-2 and PAH-3. A seasonal scatter is obvious for all locations except for the remote site Bergisch-Gladbach and the lignite area Bedburg. Concentration of 5-ring PAH is highest in Cologne and Dormagen and reach maximum with 60 ng g⁻¹ near the petrochemical plant at the latter location. Accumulation trends become less systematic, which is expressed by flat curve slopes, high relative standard deviations and a low correlation coefficient of PAH load versus needle age (Fig. 49 49, Table 18). Systematic variations due to sampling season are observed for remote Fuessenich and Bonn City. Summed concentrations of indeno[1,2,3-cd]pyrene, benzo[ghi]perylene and coronene (PAH-6) are below 20 ng g⁻¹ at each location. Dormagen needles reveal highest PAH-6 concentration, followed by Cologne City needles. Fuessenich and Bonn samples are depleted in PAH-6 in summer, whereas the Dormagen site shows a mirror image with decreasing concentrations in

emission characteristics	PAH-2	PAH-3	PAH-4	PAH-5	PAH-6
LFPP	76	701	673	17	4.0
open pit lignite mining	22	296	322	15	3.7
urban area	35	420	387	18	3.4
forest	23	211	191	10	2.3
agriculture	19	208	204	9	2.8
industry	36	266	259	11	3.4
total median	24	257	297	14	3.2

Table 19: PAH median concentrations on pine needles in the Greater Cologne Conurbation given in ng g^{-1} ; classification of samples according to known emission sources and land use; bold = highest median concentrations.

winter. Systematics of pollutant accumulation is not very distinct giving curve slopes below 0.19 with high standard deviations for the rural locations Bedburg, Bergisch-Gladbach and Fuessenich (Table 18).

Spatial distribution of PAH-2 to PAH-6 The spatial distribution of summed 2-,3-,4-,5-, and 6-ring PAH was interpolated on the base of pine needle samples of composite needle generations and thus reflects the pollutant deposition of a time-period of up to 4 years. High-resolution sampling was achieved by establishing a sample set with 71 equally distributed sampling locations on 3600 km^2 (Fig. 50a). For data interpretation in terms of emission sources and PAH dispersal two approaches were chosen. First, locations were differentiated according to characteristic emission scenarios on base of public emission data and dominant land use. Median values for sampling sites of characteristic emissions are shown in Table 19. Second, PAH-2 to PAH-6 distribution was visualized generating isopleths maps (Fig. 50).

The spatial distribution of the 2-ring PAH fluorene shows two maxima in the north-west and middle of the study area, which are related to high PAH-2 concentrations in average 76 ng g^{-1} obvious at several locations in the slipstream of the four lignite fueled power plants (LFPP) in the Cologne Conurbation (Fig. 50a,b: loc. 1, 2, 12, 15, 36). The north-western maximum is spatially connected to elevated PAH-2 loads on pine needles sampled to the south of the three larger LFPP (loc. 28, 38). High amounts of PAH-2 in the east result from a single sampling location (loc. 19). Needles grown in the cities of Cologne, Bonn and Euskirchen show intermediate fluorene concentrations, and needles sampled in remote forested and agricultural areas reveal minor loads with 23 and 19 ng g^{-1} , respectively (Fig. 50b, Table 19). Concentration differences for PAH-2 between the sampling sites are very high, leading to a highly variable spatial distribution pattern in Fig. 50b. In Table 19 median values of PAH concentrations of characteristic emission zones are compared to the total median calculated for the GCC. Thus, the PAH-2 median for locations close to LFPP is shown to be 3 times higher than the overall pollutant load of the study area. Lowest PAH-2 loads were measured at pine needles grown in the vicinity of open pit lignite mines and at agricultural sites. Sampling locations in urban and industrial areas have median values that are only 1.5 times higher than GCC average.

PAH-3 distribution is more homogeneous (Fig. 50c), although maxima occurrence is very similar to the spatial pattern observed for PAH-2. Concentrations at sampling locations 28 and 38 to the south of the three large LFPP are closer to the GCC median, than observed for PAH-2 (Fig. 50c, Table 19). The spatial concentration pattern of PAH-4 reveals a slight change towards higher amounts of pollutants in the cities Cologne and Euskirchen when compared to PAH loads in the north-western lignite area (Fig. 50a,d: loc. 22, 23, 30, 63, 68). The median of PAH-4 near LFPP is closer to the total GCC median than observed for lower molecular weight components (Fig. 50b,c,d, Table 19).

For PAH-5 two additional maxima occur south of the central study area (loc. 24, 37, 42, 55, 62) and in the east (loc. 6, 8, 19, 21, 34) in regions which are primarily characterized by forest cultivation. PAH-5 concentrations near the LFPP are high, but drop to intermediate values within app. 7 km from the power plants in the north-west of the Cologne Conurbation (Fig. 50e). PAH-5 emissions from the small LFPP in the central GCC are neglectable (Fig. 50e: loc. 38). Inflexible classification of sampling locations in emission specific medians results in differential information for urban areas and sampling sites attributed to LFPP emissions when compared to PAH-5 isopleths maps. Thus, a spatial analysis in high-resolution biomonitoring is strictly required.

Concentrations of 6-ring aromatics are highest at locations directly down-wind the LFPP and in the forested NE (Fig. 50f), but may decrease dramatically to neighbouring locations. The urban emissions of Cologne and Euskirchen contribute notably to the PAH-6 loads on pine needles.

Spatial distribution of individual PAH For a detailed detection of PAH sources it is important to study the origin and distribution of single PAH. Therefore, six components were selected for spatial discussion out of 27 PAH-4, PAH-5, and PAH-6. Spatial distribution of PAH-3 is shown in detail in chapter 4.4. Besides the selection of PAH that are commonly used for source description in environmental studies, factor analysis was employed to highlight PAH with best source discriminating potential. Factor analysis extracted 4 factors with f1 describing 35 % of the variance in the data set, f2 explains 25 %, f3 and f4 yielding 20 and 10 %, respectively (Table 20). PAH with emphasis on one factor (Ip) and PAH contributing to more than one factor (Py, CpdPY, BaA, B[b+j]Fla, BeP) were chosen for spatial analysis. The six-ring aromatic indeno[1,2,3-cd]pyrene (Ip) is described to 100 % by f1 of the factor analysis (Table 20). The isopleths map of Ip shows high concentrations on needles sampled in the forested north-east, in the LFPP region (Fig. 51a, loc. 2, 12), the cities Cologne and Euskirchen and adjacent forested areas. Distribution patterns of summed PAH-6 are comparable (Fig. 50f).

Benzo[e]pyrene (BeP) concentration is chosen for spatial discussion as representative of the environmentally highly significant benzo[a]pyrene, which itself is abundant in low to non-detectable amounts on pine needles in the GCC (Table 48 in appendix). It is also known to be very stable in the atmosphere and thus is commonly used as reference PAH [165, 53]. BeP contributes to 90 % to f1 and to 30 % to factor 3 (Table 20). BeP loads are highest at locations 2 and 12 near the LFPP forming a local distribution maxima that is followed in intensity by regional emissions in the forested region in the north-east of the Cologne Conurbation (Fig. 51b). An intermediate concentration of BeP

is observed in the cities Cologne and Euskirchen (Fig. 51b). Benzo[b+j]fluoranthene (BbjFla) is the most abundant PAH-5 in this study (Table 17). BbjFla makes up 80 % of factor 1 and contributes with 50 % to factor 3 of the factor analysis (Table 20). BbjFla maxima are almost equal to those observed for Ip and BeP, but BbjFla is apparently higher in the NW-SE trending former lignite mining zone, that is today a predominantly forested recultivation area (Fig. 50a, Fig. 51c).

Pyrene (Py) and fluoranthene (Fla) are the quantitatively dominant PAH-4 (Table 17), but their spatial distribution shows a strong correlation to sources and dispersal of PAH-3. This is obvious from factor loadings of the FA, showing a contribution of 80 % to factor 2 that is completely related to the 3-ring PAH phenanthrene (Table 20). Since pyrene and fluoranthene concentrations equal each other, only the isopleths map of pyrene is displayed in Fig. 51d. The absolute Py maxima is found near LFPP at locations 1, 2, 12 and 15. Needles gained from the cities Cologne, Euskirchen and Bonn contribute to the lower concentration class. Elevated pollutant loads at location 19 in the north-east of the GCC are related to an unknown point source. Lowest Py concentrations were recognized in forested and slightly elevated areas to the south-east and south-west (Fig. 51d).

Benz[a]anthracene (BaA) is a 4-ring aromatic compound with a distribution pattern that clearly differs from the Fla and Py pattern (Fig. 51d,e). BaA concentration yield maximum values in the LFPP region and near mining locations. Samples gained in the forested regions in the NW-SE trending recultivation area, in the forested east, and in the cities Cologne, Euskirchen and Bonn show high BaA loads. Factor analysis reveals a relation of BaA to multiple factors, yielding highest influence on factor 3 and minor contributions to factor 1 and 4 (Table 20).

Cyclopenta[c,d]pyrene (CpcdPy) is associated to f1, f3 and f4. A clear factor dependence is missing (Table 20). The spatial distribution of CpcdPy in Fig. 51f reveals a third pollution pattern within the PAH-4 group, with maximum concentrations in the city of Cologne, followed by intermediate concentrations in the forested but highly industrialized Sieg Valley in the south-east of the GCC and the active lignite mining area in the north-west. Lowest concentrations of CpcdPy were found in the forested region of the Ville Hills in the central study area, in the Eifel hillside, and Bergische hillside in the south-west and north-east, respectively.

Temporal variation of PAH ratios The behaviour of selected PAH ratios with time was analysed before the determination of spatial variations thereof. PAH ratios of compounds with i) same ring size and molecular weight and ii) aiming at differential stability of the ratio partners in the atmosphere, were chosen for discussion. Variation of ratios with needle exposure time was plotted in Fig. 52 for six sampling locations in the Greater Cologne Conurbation (Fig. 52). The Fla/(Fla+Py) ratio (Fig. 52a) reveals no preferential degradation of Fla or Py in 4 years of deposition. Higher ratios for summer samples are obvious at all sampling locations, but balanced at Fla/(Fla+Py) = 0.67 ± 0.05 during the whole accumulation time.

BaA/(BaA+CT) ratios show low variation with a value of 0.1 ± 0.05 over a time span of 50 months. At the residential site Bonn BaA was not detectable for some needle cohorts and in remote Fuessenich CT concentrations of needles are near detection limits in summer months leading to extraordinary ratios of 0.3 and more (Fig. 52b, Table 46

in appendix).

The ratio of Ip to BghiP reveals a larger scatter over time and between the six sampling locations (Fig. 52c). In juvenile needles the ratio drops from the maximum of 0.5 to 0.35 at the Cologne sampling site. Similar trends were observed for locations Bonn, Bedburg and Dormagen. Needles sampled at remote locations Fuessenich and Bergisch-Gladbach show more constant ratios over time. After two years ratios are almost stable at 0.45 to 0.35 at all locations (Fig. 52c).

BaA/(BaA+BaP) ratios reveal a high variability over time at and in between locations, reaching from 0.4 to 0.9 (Fig. 52d). The data base for this ratio is limited due to non-detectable amounts of BaA at most of the Bonn City needle cohorts and BaP being below the detection limit at 8 month old needles from Dormagen and Bergisch-Gladbach locations. Nevertheless, summer needles generally show lower ratios at all locations. Seasonal changes do not lead to a successive reduction in the BaA/(BaA+BaP) ratio. A differentiation of locations with remote sites showing highest ratios and urban sites showing lowest ratios is observed.

The time dependent behaviour of the BeP/(BeP+BaP) ratio shows constant values of 0.8 (Fig. 52e). The low concentration of BeP in Fuessenich summer needles lead to exceptionally low ratios between 0.3 and 0.4. Inter-site variability reveals no characteristic trends for the ratio of BeP/(BeP+BaP).

Spatial analysis of PAH ratios A spatial analysis of PAH ratios is achieved by correlation of PAH concentrations of pre-classified sampling sites in biplots (Fig. 53) and by interpolated PAH isopleths maps (Fig. 54a-d).

Fla and Py show parallel appearance on pine needles (Fig. 53, $r^2 = 0.98$). Correlating Fla with Py distinguishes sample sites by concentration and supports estimated site classification. Needles taken near LFPP show highest concentrations of Py and Fla followed by lower concentrations at sites located in urban areas. At this sites a trend to higher loads of pyrene is observed. Locations situated in mining, industrial, forested or agricultural areas reveal comprehensible concentrations of both PAH-3 (Fig. 53a).

Calculation of the Fla/(Fla+Py) ratio allows plotting their relationship in a spatially resolved map. In Fig. 54a urban and industrialized areas are marked by low ratios of 0.6, whereas forested and agricultural areas show highest Fla/(Fla+Py)-values (0.65 - 0.7). Areas characterized by lignite mining activities (Fig. 54a, loc. 13, 39) are especially highlighted by low ratios. The BaA versus CT biplot reveals a higher scatter between the sampling locations. BaA and CT loads on pine needles are highest at the larger LFPP in the NW followed by the cities of Cologne, Bonn and Euskirchen. A systematic trend to a predominance of one PAH cannot be observed (Fig. 53b). The spatial interpolation of the BaA/(BaA+CT) ratio highlights the Cologne City area with values of 0.2, forested zones and the west of the GCC which is dominated by open pit lignite mining. Lowest ratios occur at sites that are predominantly in agricultural use (Fig. 54b).

Correlation of Ip with BghiP gives a coefficient of determination of 0.94 (Fig. 53c). Locations with different emission background are predominantly separated by concentration changes, that are similar for both PAH. For urban locations and forested areas a trend to more BghiP or more Ip can be observed, respectively (Fig. 54c).

In Fig. 53d 4-ring BaA is related to 5-ring BaP. The biplot reveals an overall trend

of $BaA/(BaA+BaP) = 0.88$ with consistently higher amounts of BaA in urban areas (0.9) and areas in agricultural use tending to a low value of 0.8. Pine needles sampled at locations 2 and 12 situated in the LFPP region have highest loads of both PAH, followed by two forested sites (Fig. 53d, 6d, loc. 6, 7), where local PAH point sources are assumed. The isopleths map of the $BaA/(BaA+BaP)$ ratio shows maximum values in cities and agricultural areas (Fig. 54d). Forested areas in the north-east, south-west and central GCC are dominated by lower values of the $BaA/(BaA+BaP)$ ratio of 0.7 to 0.8. The LFPP area in the north-west shows comparable low ratio values.

4.3.4 Discussion

The sources and dispersal of PAH in the Greater Cologne Conurbation are here investigated by biomonitoring purposes. This requires a systematic accumulation behaviour of PAH on *Pinus nigra* needle surfaces, which is discussed on a temporal-resolved data set at first place. Thereafter, the overall dispersal of PAH categorised in ring size classes is shown by isopleths maps with a first approach of source allocation. The final differentiation of PAH sources and emission processes is entered by the spatial discussion of single PAH with a special source diagnostic potential. This is topped by the extraction of more detailed source discriminating informations out of pine needle surface loads utilizing PAH ratios. Prior to the use in spatial source allocation the time dependency of source diagnostic PAH ratios are tested for a conservative behaviour.

PAH accumulation histories Systematics of the time-dependent accumulation of polycyclic aromatic hydrocarbons on pine needles are displayed in sum for PAH-2, PAH-3, PAH-4, PAH-5, and PAH-6 in Fig. 49. PAH concentration changes are obviously highly variable depending on sampling site, sampling season, and PAH ring number. This is a result of the natural variability found in environmental systems, where the accumulation of POPs on vegetation surfaces is primarily influenced at three points that may interact: i) the physico-chemical properties of the pollutant, ii) atmospheric conditions (climate, temperature, photo-oxidation), iii) the ability of the bioreceptor for uptake or detoxification [11, 278, 279]. The analysis of needles of different age allows an interpretation in terms of these questions (Fig. 49, Table 18).

The factors driving PAH accumulation curves were addressed by correlating the accumulation behaviour of PAH of different ring number. Most important differences in physico-chemical properties between PAH of different ring number are molecular weight (Table 17) and preferred phase of appearance at prevalent atmospheric conditions. Furthermore, the local mode and amount of emission contributes to a major part to variations in accumulation patterns.

The overall concentrations of PAH classes vary substantially. PAH-2 are known to be preferentially abundant in the gas phase. A long-range distribution is therefore supposed [18], leading to low but relatively similar concentrations at all locations. Pine needles taken near the lignite fueled power plants (LFPP) make a notable exception, related to huge emissions as result of a coal combustion > 68 mio tons per year [208]. The continous increase at the LFPP related location Bedburg shows that limits of fluorene deposition on pine needles are not reached in the Greater Cologne Conurbation (Fig. 49a). PAH-3 and PAH-4 appear in very high amounts on the needle surfaces.

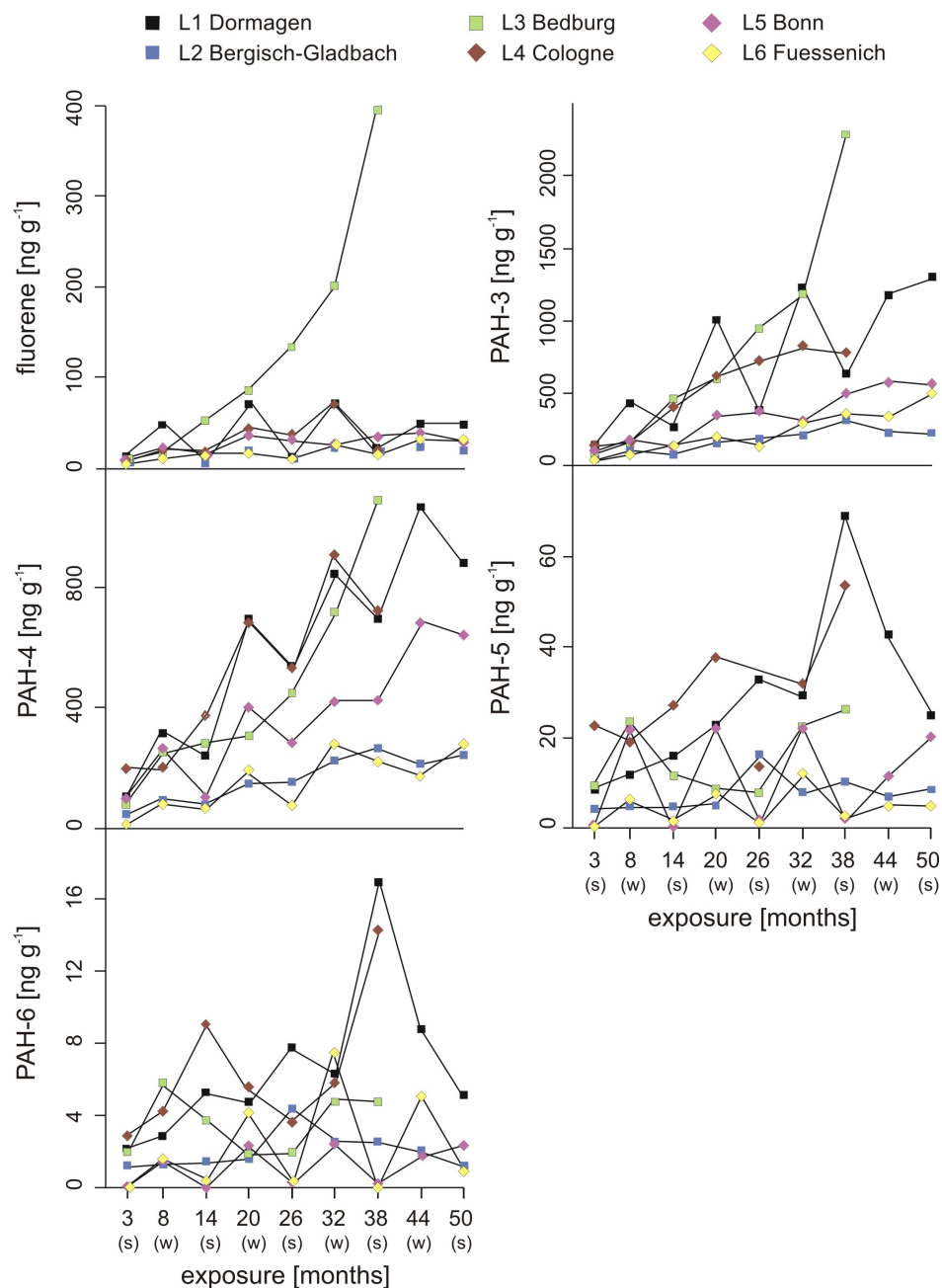


Figure 49: Accumulation trends of PAH on pine needles taken at six locations in the GCC. PAH were summed according to aromatic ring number and plotted versus increasing time of needle exposure. Needle cohorts were gained in winter (w) and summer (s) 2004.

PAH are predominantly derived from fossil fuel combustion in motor vehicles [272, 214]. Ubiquitous traffic emissions explain the more consistent concentrations between the six locations, although transport of predominantly particle-bound PAH-3 and PAH-4 is shortened when compared to PAH-2 (Fig. 49a-c). Seasonal dilution is related to their vapour pressure being around 25 °C, resulting in re-volatilization of deposited components into the atmosphere in summer as previously described for the suite of phenanthrenes and alkylated analogues by Lehndorff and Schwark [124]. Nevertheless,

the accumulation curves shown in Fig. 49b and Fig. 49c increase over time, because the overwhelming part of PAH-3 and PAH-4 are bound to epicuticular waxes or adsorbed by the cuticula after deposition [277, 278, 279, 263]. PAH-5 and PAH-6 were detected in very small amounts, so that natural impreciseness accounts higher to the data set (Fig. 49d,e). A revolatisation in summer can mostly be neglected, since PAH-5 and PAH-6 are characterized by low vapour pressures and therefore remain on the plant surface in summer. Especially loads of BeP and BghiP are known to be very stable in the atmosphere and thus are expected to behave conservative on seasonal temperature changes [165, 151, 235]. In contrast, BaP, BaA, and Ip are more susceptible to solar radiation [174, 73], expecting these PAH to contribute to losses observed for PAH-5 and PAH-6 in the summer months on Fuessenich and Bonn pines (Fig. 49c,e).

Source characteristics like type of emission (combustion or evaporation), PAH amount and content is also obvious from the "accumulation data set". High PAH-2 emissions can be related to LFPP activity and the refinery in Dormagen. For PAH-3 and PAH-4 traffic combustion processes in Cologne City become an important source besides LFPP and refinery. For PAH-5 and PAH-6 traffic is the dominant source. The increasing concentrations of higher molecular weight PAH in remote and forested areas Bergisch-Gladbach and Fuessenich is related to biomass burning [228]. A more precise source allocation requires a higher spatial data distribution and is given in the following section.

Spatial dispersal of PAH according to aromatic ring number The isopleths maps of PAH with two to six aromatic rings, are base for the analysis of their emission source and atmospheric dispersal. For data interpretation several supplementary factors have to be considered, that may influence PAH loadings on pine needles. To minimize those factors to source characteristic information a consistent sampling strategy, the knowledge of climatic variability (e.g. prevalent wind regime of the last 5 years), morphology and plant specific aspects (habitat conditions and healthiness) are of importance.

Due to a relatively flat morphology of the GCC and a careful sampling only wind direction is reflected by the data set. This is obvious at the most striking maxima in the north-west, that is related to lignite combustion in three large power plants. Wind transport of PAH at locations 1, 2, 12, 15 and 36, Fig. 50 is to the west and, additionally, an intensive air mixing into the southern Zuelpich Plain is suspected due to the flat morphology and low vegetation in large agricultural areas.

Beyer et al. [18] have shown that long-range atmospheric transport is notably different for PAH of different molecular weight. Fig. 50 reveals that the LFPP emit significant amounts of 2-, 3-, 4-, 5-, and 6-ring PAH and that atmospheric transport is shortened with increasing PAH ring number. This is obvious at locations 28, 38 in the central south, where PAH-4, PAH-5 and PAH-6 concentrations are lower than PAH-2 and PAH-3 loads. This is related to a change of low molecular size PAH being preferentially in the gas phase to PAH with four and more aromatic rings preferring the particle phase at atmospheric conditions [227].

Correlation in changes of PAH distribution also reveals differences in regions of maximum pollution, that are related to differing sources for PAH of differential ring number. For PAH-2 the LFPP is the dominant emitter of the region, whilst for PAH-3

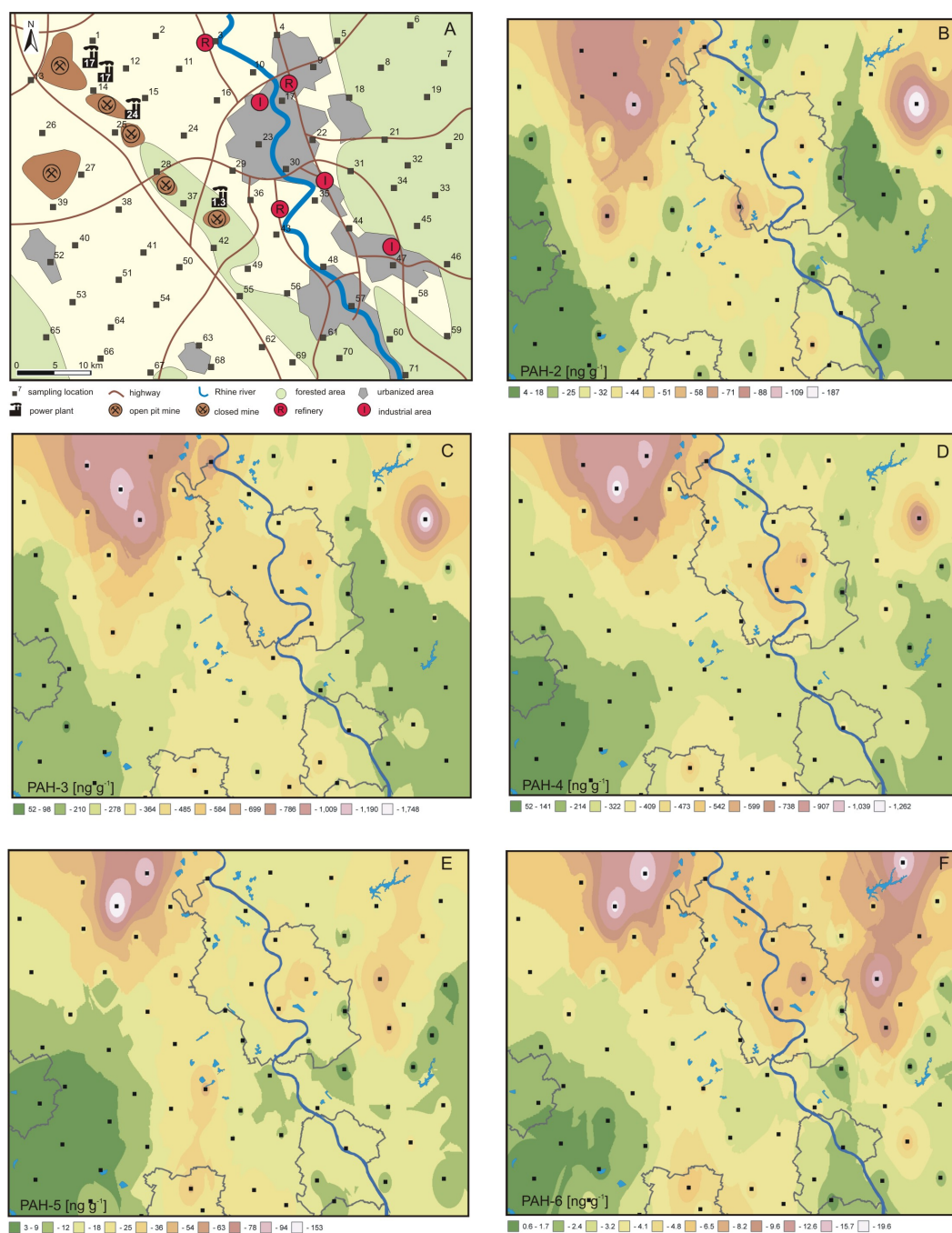


Figure 50: A = Land use and emitters characteristic for local emission scenarios; B-F = spatial distribution maps of summed PAH-2 to PAH-6 based on interpolation between 71 pine needle sampling sites in the GCC. Source diagnostic patterns are observed at LFPP (B-F), high traffic region Cologne (C-F), and forested areas to the east (E,F). For more information about land use see overlay transparency in the appendix (Fig. 62).

and PAH-4 emissions of urban areas become dominant (Fig. 50a-d). Note that urban emissions consist of a mixture of diverse sources including traffic, domestic heating, and industrial emissions as discussed previously in chapter 3.3. A discrimination of these sources can not be achieved here, but is approached by single PAH and ratios

thereof in the following. The 4-ring PAH retene with a biological origin is described as a marker for biomass combustion [198]. Since retene only accounts for 1 % to the sum of PAH-4, the distribution pattern allows no differentiation of biomass combustion processes (Fig. 50d). Simoneit and Elias [228] have shown that incomplete combustion of wood emits PAH with high ring numbers in condensates. Thus, PAH-5 and PAH-6 pollution zones occurring in forested regions of the GCC are related to a high input of biomass combustion residues to the atmosphere.

Limits of the spatial interpolation method are revealed by elevated PAH loads at location 19 in the north-east (Fig. 50). Here, a PAH emitter with a very low emission radius is supposed to artificially highlight a pollution zone that is not existing.

Source dependent distribution patterns of individual PAH Variation in the atmospheric PAH load is a question of feed stock and physico-chemical properties. The latter lead to PAH fractionation processes during atmospheric transport and deposition on sampling devices. Photooxidation, molecular phase and particle size influence especially the transport distances. Thus, in the discussion of spatial PAH distribution three factors have to be considered: i) emission type, ii) transport fractionation, iii) uptake or depositional effects. Since it is the overall aim of this study to show sources of atmospheric PAH pollution, the discussion is sorted according to results of the factor analysis, interpreting those factors as different emission scenarios.

Biomass burning, municipal waste incineration Indeno[1,2,3-cd]pyrene matches all properties described by factor 1 (Table 20). The isopleths map in Fig. 51a reveals hot spots of Ip pollution near the lignite fueled power plants (LFPP) and in the cities Cologne and Euskirchen, that have analogues in all PAH classes (Fig. 50). Urban pollution can be attributed to combustion of fossil fuels especially of gasoline in traffic [119, 51].

Exceptional pollution zones can be recognized in forested regions in the east and at the NW-SE tending Ville high (Fig. 51a). An elevated Ip concentration was previously related to biomass burning [287, 220]. Thus, Ip emissions in forested areas are here related to domestic heating utilizing wood. Even in city centers private firesides are more and more in use as a comfortable way of heating, explaining part of the Ip concentrations in Cologne and Euskirchen. This is supported by the German Environmental Agency stating that PM₁₀ emissions of wood combustion in domestic heating and small trades equal traffic combustion emissions [246]. Thus, biomass burning turns out to be a considerable pollutant factor in residential areas, that is often ignored when discussing roadside pollution. In addition, high concentration of indeno[1,2,3-cd]pyrene was observed only a few kilometers apart from the Cologne municipal waste incineration (Fig. 51a, loc. 10), indicating an additional source of this PAH as compiled by Fang et al. [51].

A high dependence of Ip appearance to coal combustion was noticed in Taiwan, supporting the observation that Ip is emitted by the local LFPP ([51], Fig. 51a). The dispersal of Ip near the LFPP in the north-west of the study area reflects transport conditions of PAH with high molecular weight (HMW > m/w 252) and a total attribution of Ip to particle phase. Highest amounts of indeno[1,2,3-cd]pyrene are measured

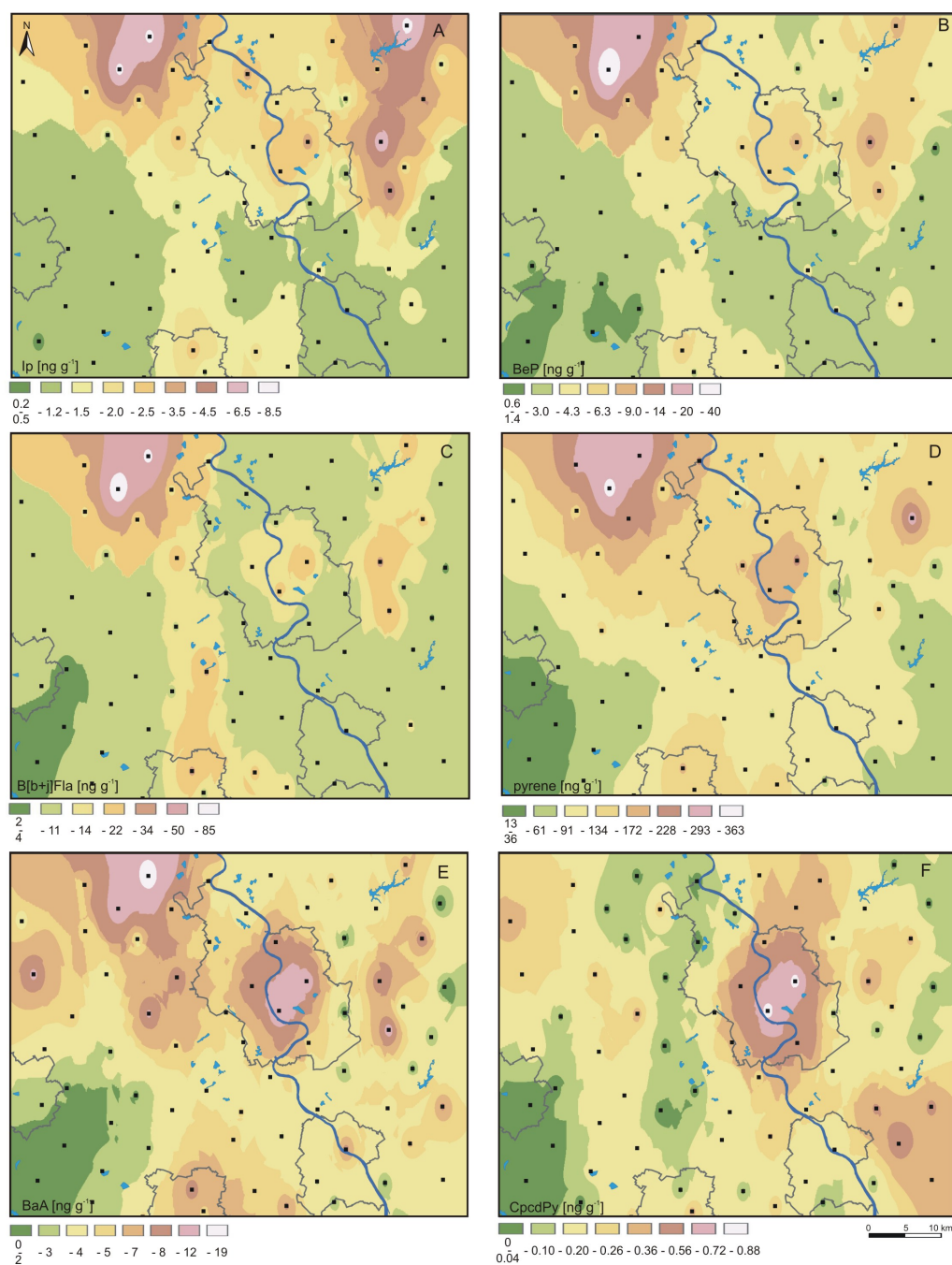


Figure 51: Spatial distribution of Ip, BeP, Bb]Fla, Py, BaA, and CpcdPy. Source characteristic patterns are discussed in the text. For more information about land use see overlay transparency in the appendix (Fig. 62).

at location 2 and 12 situated in the wind trail of three power plants in 3 and 7 km distance, respectively. Notably lower Ip concentrations are observed only 5 km apart (loc. 1 and 15) indicating a rapid deposition of PAH-6 in the environment beside the main transport route. This is due to very short transport distances of PAH-6, as previously described by Beyer et al. [18].

Benzo[e]pyrene is exclusively present in particle phase at atmospheric conditions

	f1	f2	f3	f4
Ip	1.0	0.0	0.1	0.0
BghiP	1.0	0.1	0.2	0.2
BaP	0.9	0.0	0.1	0.1
BeP	0.9	0.1	0.3	0.1
Coronen	0.9	0.1	0.1	0.2
Bb+jFla	0.8	0.1	0.5	0.1
phenanthrene	0.0	1.0	0.1	0.2
CPP	0.1	0.9	0.2	0.0
DBT	-0.1	0.9	0.0	-0.1
Fluoranthen	0.3	0.8	0.4	0.2
pyrene	0.3	0.8	0.4	0.3
TRI	0.2	0.3	0.9	0.0
BNT	0.2	0.3	0.8	-0.1
BaA	0.4	0.1	0.7	0.5
BghiFLA	0.5	0.2	0.6	0.5
Re	0.1	0.2	0.0	0.8
CPcdPY	0.5	0.1	0.4	0.5
variance [%]	35	35	20	10

Table 20: Factor analysis of PAH concentrations analysed on pine needles in the GCC ($n = 71$, bold = PAH chosen for spatial mapping). FA roughly discriminates the following emission scenarios: f1 = biomass burning, LFPP, f2 = combustion in traffic, LFPP, f3 = lignite mining, f4 = forested areas.

[237]. It is stable against degradation through solar radiation and therefore is expected to behave conservative on seasonal temperature changes [165, 151, 121]. Thus, it is assumed that BeP loads on pine needles are solely driven by source and distance to the emitter. In former studies BeP was related to combustion of diesel [119], coal [8] and steel industry [51] or was generally attributed to low temperature combustion processes [287]. In this study BeP is most likely emitted by lignite combustion in power plants (Fig. 51b) and biomass burning as indicated by high loadings on factor 1 of the FA (Table 20). In urban areas a mixed signal of biomass burning and traffic emissions is assumed as discussed for Ip. Transport distances for BeP are comparable to those observed for Ip.

Benzo[b+j]fluoranthene appearance was related to wood burning by Sergey et al. [220]. This is coherent with observations made in the Cologne Conurbation. Fig. 51c shows elevated BbjFla concentrations in the forested region to the east and in the central GCC, which is also indicated by high factor loadings on f1 and f3 (Table 20). Factor 3 comprises higher PAH loads at locations of the Ville Hills region in the center of the study area, which is characterized by large forested areas and former open pit lignite mines. Due to extensive recultivation activities of the local power producer it is neither likely that a lignite dust blow out appears nor that this dust could be enriched in BbjFla. According to Ip, urban BbjFla loads are related to biomass burning in firesides. The larger LFPP again contribute to atmospheric BbjFla concentrations, with short transportation ranges as seen for BeP and Ip (Fig. 51a-c).

Combustion of fossil fuels in traffic, LFPP and refineries Four-ring PAH pyrene is present in gaseous and particle phase in the atmosphere [237]. Gas-particle partitioning is strongly dependent on season [53]. Due to its high and ubiquitous appearance as atmospheric pollutant pyrene origin and fate was investigated several times and is now well understood [27, 287]. Main sources are incomplete combustion of diesel, industrial combustion of oil, coal and municipal waste as compiled by Fang et al. [51]. Accordingly, factor analysis reveals contributions of pyrene to all 4 extracted factors, with emphasis on factor 2. This factor is described to 100 % by phenanthrene concentrations, that is predominantly related to traffic and LFPP emissions (chapter 4.4). The isopleths map of pyrene in Fig. 51d clearly shows a dependency to highly trafficked areas in Cologne, Euskirchen and Bonn. Aerial occurrence of pyrene in the north-west is interpreted as LFPP emissions revealing a transport of about 20 km to the east and south. Longer atmospheric transport routes of pyrene compared to PAH-5 and PAH-6 lead to a more intensive mixture of pyrene emissions from different sources (Fig. 50, Fig. 51d). Thus, urban emissions of traffic combustion processes mix with the LFPP emissions in the north-west of Cologne City (Fig. 51d). Exceptionally high pyrene concentrations at location 10 near the municipal waste incinerator (MWI) were not found as observed for indeno[1,2,3-cd]pyrene. This can be related to a dilution of MWI emissions with many times higher traffic emissions in air. Contributions of industry to the pyrene load in urban air are likely at refineries situated in the north and south of Cologne (Fig. 51d, loc. 4, 30). Location 19, where samples are taken in the garden of a small private farm, shows high Py loads, that are related to unknown activities.

Lignite open pit mining BaA is a 4-ring PAH showing a relatively fast decay during atmospheric transport [73]. It is also partially present in the gas phase [151]. Yunker et al. [287] showed BaA concentrations to be of petrogenic origin. Factor analysis and isopleths map reveal a notably different source characteristic for BaA, than observed for pyrene (Table 20, Fig. 51e). Thus, investigations of summed PAH-4 as shown in Fig. 50 bears only superficial information and a study of single PAH is required for detailed source reconciliation or estimation of ambient concentrations of environmentally harmful compounds. As indicated by spatial and factor analyses greatest difference to the whole data set appears in areas where open pit lignite mining is or has been active (Fig. 51e, loc. 26, 27, 28, 38). Here BaA is supposed to derive from lignite dust. Furthermore, a relation to biomass combustion is assumable, as emissions of BaA are also higher in the eastern forested region. Nevertheless, most reasonable BaA sources are combustion of fossil fuels in traffic resulting in maxima in the cities Cologne, Bonn and Euskirchen and lignite combustion in the power plants in the north-west of the Cologne Conurbation. Transport distance of BaA from LFPP to the south and east is reduced, when compared to pyrene, suggesting that transport is mainly a matter of molecular weight and ring number [18, 249].

Gasoline combustion Cyclopenta[cd]pyrene occurs in gas and particle phase at atmospheric conditions [151]. Its origin was previously related to power plants, industrial oil combustion, and gasoline combustion [51]. In this study traffic emissions are clearly the dominant source for cyclopenta[cd]pyrene. Pine needles sampled in urban

areas of Cologne and Bonn yield high CpcdPy concentration, due to high traffic density. Elevated CpcdPy loads were also observed for sampling locations with less than 3 km distance to highways in remote areas (Fig. 51f, loc. 13, 21, 25, 28, 39, 38, 46, 47, 58, 59, 67, 69). This convincingly shows that cyclopenta[cd]pyrene is a perfect traffic marker even in regions with a high mixture of different emission types.

Source reconciliation based on PAH ratios For a more distinct source allocation and determination of PAH transport several diagnostic PAH ratios are in use [287, 286, 235, 174, 151, 73, 139, 119]. Here five ratios concerning i) different origin (Fla/(Fla+Py), ii) differential stability in the atmosphere (BaA/(BaA+BaP), BeP/(BeP+BaP), and iii) a mixture of both (BaA/(BaA+CT)), are discussed.

PAH ratios versus time of exposure It is of importance to assure that ratios used in a spatial monitoring study are not altered by pollutant residential time on the sampler surface. Therefore, ratios were compared to needles aging 3 to 40 months (Fig. 52). The Fla/(Fla+Py) ratio is used to discriminate petrogenic from pyrolytic sources [27]. In contrast, Fig. 52a shows no significant differentiation between the single locations and ratios are very similar with a median of 0.67. About 0.05 higher values of the Fla/(Fla+Py) ratio are observed for samples gained in summer. This is related to a loss or a reduced input of pyrene during summer months. The latter seems more reasonable, because fluoranthene shows a higher tendency to appear in the gas phase [237]. The overall stability of the Fla/(Fla+Py) ratio over time allows the further interpretation of samples composed of mixed needle ages in terms of source allocation.

Relation of BaA to CT was established for discrimination of pyrolytic from petrogenic sources [73]. It has to be considered that BaA shows rapid decay due to solar radiation [73]. Except for the rural Fuessenich location ratios remain constant at 0.1 for all needle generations (Fig. 52b). This indicates that a decay of BaA once deposited on the needle does not appear. This is supported by photoexperimental data by Wang et al. [263]. A potential decay of BaA due to solar radiation on its way from source to deposition makes the ratio as source indicator questionable. Low variability in between the six locations shown in Fig. 52b reveals only minor emission characteristic details.

The Ip/(Ip+BghiP) ratio is used to distinguish petroleum, emissions of vehicular traffic, and biomass combustion [119, 139]. The ratio has highest "real" variability between 0.3 and 0.5 (Fig. 52c), herewith supporting findings by Gogou et al. [73] and Mandalakis et al. [139]. A decline of the ratio of about 0.05 in the first year of pollutant accumulation can be observed. Nevertheless, interpretation of age-composite samples makes sense.

The correlation of BaA to BaP is critical, because both PAH are strongly affected by solar radiation [73, 174]. Since both PAH are related to traffic emissions, this ratio may dominantly reflect their sensibility to NO₂ [48]. The ratio of BaA to BaP is constant with time (Fig. 52d). Outlying and missing data points are due to very low or non-detectable concentrations of both PAH. All sampling locations do show a characteristic variation in the BaA/(BaA+BaP) ratio, allowing for emission scenario interpretation. A seasonal change to lower values of BaA/(BaA+BaP) in summer is observed, but does not influence the general interpretation of the ratio.

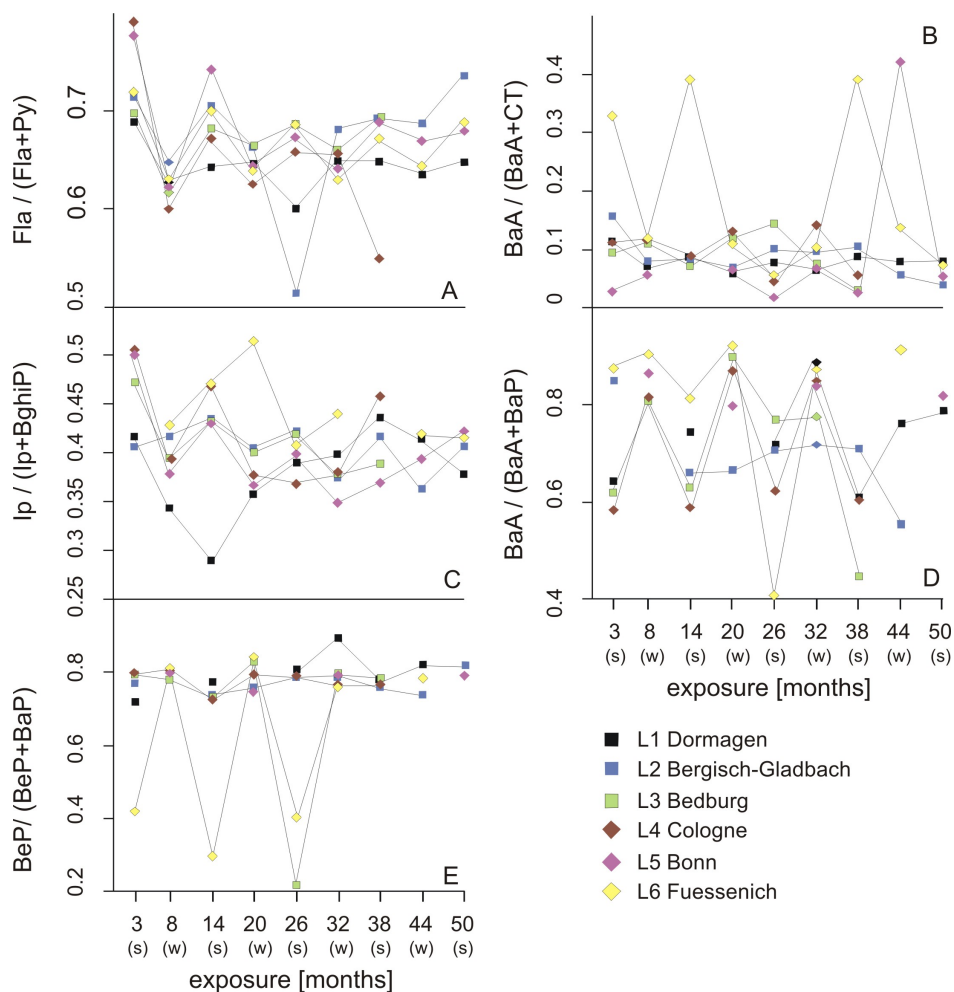


Figure 52: Variability of selected PAH-ratios with time of needle exposure. A = PAH-4 ratio Fla/(Fla+Py); B = PAH-4 ratio BaA/(BaA+CT), missing data at Bonn location is due to undetectable concentrations of BaA; C = PAH-6 ratio Ip/(Ip+BghiP), missing data at Fuessenich location due to non-detectable amounts of both PAH; D = PAH-4/PAH-5 ratio BaA/(BaA+BaP); E = PAH-5 ratio, missing data in D and E are due to non-detectable concentrations of BaP. Needle cohorts were gained in winter (w) and summer (s) 2004.

The BeP versus BaP ratio reflects transportation distances, since BeP is more stable in the atmosphere [182, 288]. A very constant value with time of 0.8 is observed for all sampling locations (Fig. 52e). Though, exceptional BeP/(BeP+BaP) values are related to very low concentrations. Interpretation in terms of source or transport distance is therefore allowed but difficult. The constancy of the BeP/(BeP+BaP) ratio throughout all needle generations indicates that the decay of BaP when arrived on the needle is stopped. Thus, a discussion of the spatial variability of this ratio is not useful on the raster sample set.

Source characterization The distribution pattern of pyrolytic pyrene versus petrogenic fluoranthene (Fig. 54a) in Cologne City shows a slowly increasing ratio from the inner city (0.6) to residential suburbs (0.63). This reflects elevated pyrene

emissions due to high traffic volume coinciding with low air mixing rates. Only slightly lower Fla/(Fla+Py) ratios of 0.4-0.45 were observed by Larsen and Baker [119] for gasoline fueled vehicles. Yunker et al. [287] relate values < 0.4 to petroleum sources, intermediate ratios of 0.4 to 0.5 to combustion of fossil fuel in traffic and values > 0.5 to combustion of grass, wood and coal. In the Cologne Conurbation Fla/(Fla+Py) ratios are slightly higher with 0.6 in the city and 0.67 near the LFPP. This is a result of mixed emissions, indicating that a Fla/(Fla+Py) value of 0.6 in the city reflects an urban emission scenario, that is dominated by traffic emissions but also influenced by biomass burning. Low Fla/(Fla+Py) values in the south-eastern Sieg Valley are due to high temperature combustion in local industry, where the thermodynamic more stable pyrene is preferentially build [27]. Locations 13 and 39 close to active lignite mining areas are characterized by low Fla/(Fla+Py) ratios. Here a relation to unburned coal dust can be supposed, but also combustion products from the nearby highways may influence the Fla/Py composition of the ambient air quality. Highest ratios of about 0.7 are observed at locations where lowest absolute Fla and Py concentrations were detected (Fig. 54a, 51d). Thus, analytical limits have to be considered leading to artificially enhanced ratios.

The ratio of benz[a]anthracene (BaA) to the sum of chrysene and triphenylene (CT) is discussed as a marker for petrogenic or pyrolytic emissions, respectively [224, 73, 287]. It has to be noted, that both PAH are much more abundant in asphalt, coal or bitumen than in refinery products [287]. Fernandez et al. [56] and Grimalt et al. [76] use the BaA/(BaA+CT) ratio as an indicator for transport and fractionation processes. Twofold use is due to the low stability of BaA to solar radiation and to the differences in emission source. BaA concentrations are higher in combusted materials than in the original fuel [287], whereby chrysene and triphenylene are found in light duty diesel and gasoline [77, 24, 213]. Larsen and Baker [119] found CT enriched due to coal combustion. The typical BaA/(BaA+CT) ratio value for aerosols in winter is 0.12 [54], which is in very good agreement with the here presented pine needle data. In Fig. 53b higher amounts of BaA are observed at locations in forested zones, at some urban sites and near lignite mining areas. This is attributed to emission scenarios, that are dominated by combustion products from biomass burning and/or fossil fuel combustion. BaA occurrence near active open pit mines can either be explained by lignite dust with a high BaA/(BaA+CT) ratio, or is due to traffic emissions from nearby highways (Fig. 54b). The latter would indicate a transport of up to 3 km for the BaA/CT mixture, which is unlikely due to the photoreactivity of BaA. The biplot of BaA versus CT shows a relative enrichment of CT at sampling locations near LFPP and at agricultural sites (Fig. 53b). These observations are related to coal combustion and a transport of the photostable CT over more than 10 km to agricultural sites (Fig. 54b). An interpretation of transport or residence time in atmosphere cannot be done, due to the input of multiple sources in the study area.

The interpretation of the Ip/(Ip+BghiP) ratio as suggested by Yunker et al. [287] is < 0.2 for petroleum, up to 0.3 for gasoline and 0.5 for diesel combustion residues, respectively. Values larger than 0.5 indicate biomass burning. This is in agreement with ratios of 0.5 observed in forested regions of the GCC (Fig. 53c, Fig. 54c). Ratios between 0.3 and 0.4 in urban areas reflect mixed sources, that are dominated by gasoline combustion and/or uncombusted petroleum. The latter is most likely in the

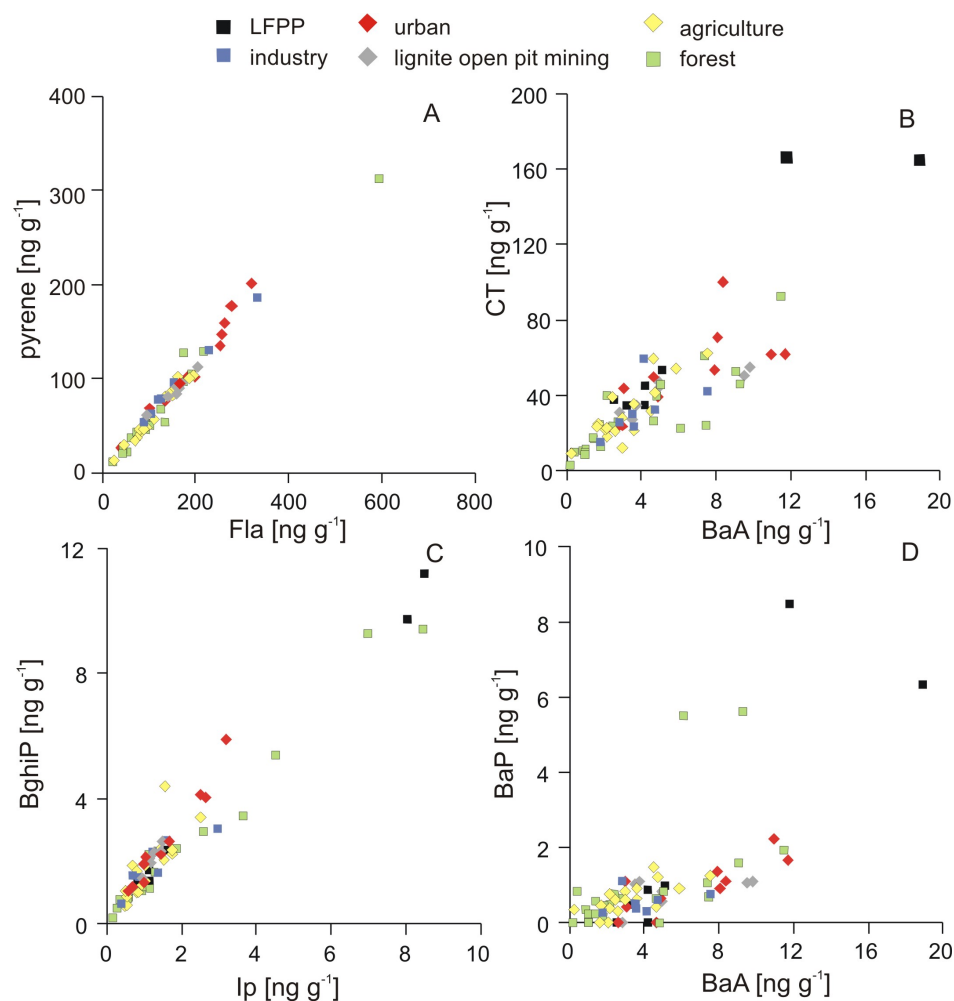


Figure 53: Bivariate plots of source indicative PAH. A = correlation of Fla to Py is good with $r^2 = 0.98$; B = BaA to CT separates sampling locations according to varying BaA loads; C = Ip and BghiP loads are highest at forested sites; D = correlation of BaP to BaA separates sampling locations according to variations in BaP and BaA input.

south of Cologne, at closest vicinity to a large refinery complex (Fig. 54c, loc. 35, 43). As already noted for absolute Ip concentrations, the Ip/(Ip+BghiP) ratio highlights needles sampled in the vicinity to the MWI of Cologne (Fig. 54c, loc. 10). Low ratios in the inner city of Cologne cannot verify the slower reactivity of Ip to NO_2 , which was described by Esteve et al. [48].

Benz[a]anthracene and benzo[a]pyrene are strongly related to each other. They are both affected by solar radiation [73] and are produced by biomass burning, lignite combustion in power plants and by vehicular traffic as shown above. Therefore, the isopleths of the BaA/(BaA+BaP) ratio are constant in urban and agricultural areas (0.9). Mapping of BaA/(BaA+BaP) reveals reduced values near LFPP and in the north-east (Fig. 54d) that are due to higher amounts of BaP on the pine needles (Fig. 53d). This can be a result from higher BaP emissions as supposed near the LFPP (Fig. 54d, loc. 2, 12) or a reduced decay of this PAH. A possible explanation is offered by Esteve et al. [48], showing that BaP is relatively stable to a degradation by NO_2 .

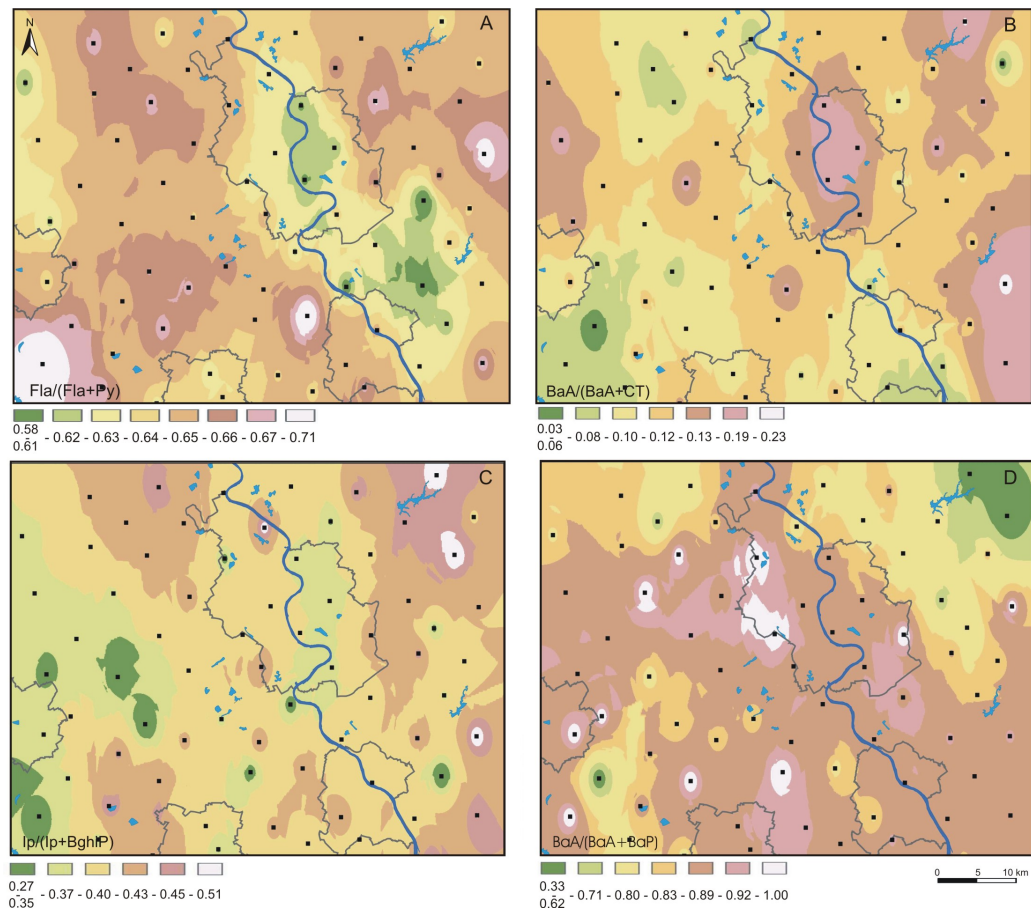


Figure 54: Isopleths maps of source indicative PAH ratios. A) traffic indicator $\text{Fla}/(\text{Fla}+\text{Py})$, B) $\text{BaA}/(\text{BaA}+\text{CT})$, C) $\text{Ip}/(\text{Ip}+\text{BghiP})$, D) $\text{BaA}/(\text{BaA}+\text{BaP})$. Source characteristic patterns are discussed in the text. For more information about land use see overlay transparency in the appendix (Fig. 62).

Accordingly, lowest ratios appear in the north-east and south-west of the GCC where highways are at greatest distance (Fig. 54d).

4.3.5 Conclusions

Accumulation of PAH with 2, 3, 4, and 5 aromatic rings on *Pinus nigra* needles is systematic and depends on local emission schemes. PAH ratios used for source discrimination were tested positive for their stability over 4 years of deposition on pine needle surfaces.

The spatial analyses of PAH summed according to aromatic ring number gives insights into differences in PAH sources and transport characteristics. A dependency of pollutant dispersal to wind direction is revealed by spatial mapping. The spatial interpolation of biomonitoring data allows for a detailed source recognition with PAH concentrations and ratios.

Seven sources are here identified for the Cologne Conurbation (Table 21). In general, PAH emissions of the lignite fueled power plants were shown to be dominant in the Cologne Conurbation. Thus, lignite combustion can be characterized by biomonitor-

source	LFPP	traffic	biomass burning	refinery	industry	MWI	lignite dust
PAH	Σ PAH, LMW PAH, Py, Bep, Ip, BbjFla	CpcdPy, Py, BaA	HMW PAH, BaA, BbjFla, BeP, Ip	PAH-3, PAH-4, Py	PAH-6, CpcdPy	Ip	BaA
PAH ratio		< 0.62 Fla/(Fla+Py), > 0.13 BaA/(BaA+CT)	> 0.13 BaA/(BaA+CT), > 0.43 Ip/(Ip+BghiP), < 0.8 BaA/(BaA+BaP)	< 0.08 BaA/(BaA+CT)	< 0.62 Fla/(Fla+Py)	> 0.43 Ip/(Ip+BghiP)	< 0.63 Fla/(Fla+Py), > 0.13 BaA/(BaA+CT), < 0.37 Ip/(Ip+BghiP)

Table 21: Source diagnostic potential of PAH biomonitoring in the Cologne Conurbation.

ing indeno[1,2,3-cd]pyrene, benzo[b+j]fluoranthene and pyrene emissions, traffic emissions are highlighted by isopleths maps of cyclopenta[cd]pyrene, which is highly recommended as a traffic indicator even in remote areas. Pyrene, indeno[1,2,3-cd]pyrene and benz[a]anthracene are linked to multiple sources like traffic, biomass burning, dust blow out of lignite open pit minings, and lignite fueled power plant emissions (Table 21).

The Fla/(Fla+Py) ratio is indicative for fossil fuel combustion by vehicular traffic in Cologne City with increasing values of 0.6 to 0.65 from urban to suburban zones. Vice versa low Fla/(Fla+Py) values of 0.6 are indicative for industrialized regions and lignite mining areas. Extraordinary low BaA to CT values are related to lignite combustion in power plants. The spatial pattern of Ip/(Ip+BghiP) is characterized by high ratios in areas dominated by emissions of wood combustion. Municipal waste incineration in Cologne City is attributed to high Ip/(Ip+BghiP) values, whereas low ratios are due to emissions of traffic and a large refinery complex. Thus, a spatially high-resolution biomonitoring of air quality utilizing PAH concentrations and ratios is suitable for source differentiation in areas characterized by emission mixtures of multiple sources.

4.4 Cologne Conurbation air quality - parent and alkylated three-ring PAH

Monitoring and spatial analyses of three-ring PAH is required for a recognition of quantitatively most dominant anthropogenic emission source - the combustion of fossil fuels. Phenanthrene and alkylated derivatives occur in high amounts in the atmosphere mainly due to substantial emissions from fossil fuel combustion and evaporation. Since analysis of feed stock directly at the emitter is often not realizable, as much information as possible has to be extracted from the environmental receptor. In a real-world scenario several factors influence quantity and composition of emitted PAH, i) combustion feed stock, ii) combustion conditions (including reduction techniques), iii) atmospheric transport processes including degradation and mixing, and iv) receptor specific discrimination. PAH-3 concentrations and diagnostic source ratios were previously established as pollution indicators by [15, 287, 193, 139]. In high purity source samples, laboratory experiments and active air sampling PAH-3 were used to identify wood combustion residues and fossil fuel derived emissions. Especially phenanthrenes and its derivatives are of major importance as source diagnostic tools, due to their high quantity in the atmosphere and diversity in sources and emission processes. Here, a source allocation based on diagnostic ratios of alkylated phenanthrenes with biomonitoring in a high

trafficked region is approached for the first time. Additionally, spatial monitoring of thioaromatic compounds, e.g. dibenzothiophene is applied to determine sulfur emitting sources. This is of special interest in the Cologne Conurbation, due to several lignite fueled power plant complexes, in which large amounts of sulfur bearing lignite are combusted.

A discrimination of local emission sources on regional scale is approached here with a spatially high-resolved sample set with sampling stations off point sources, thus reflecting average local air quality. Factor analyses and biplots supported by spatial variability are utilized for interpretation of pollutant source and dispersal.

4.4.1 Sampling

Collection of pine needles was done in an area comprising 3600 km² in the Greater Cologne Conurbation, Germany. Composite samples of *Pinus nigra* needles of up to 5 generations were sampled at 71 locations (Fig. 55a). Samples were taken every 5 km according to an equidistant sample grid and display the local air quality. Therefore, influence of point sources like traffic were avoided. Details of sampling have been described by Lehndorff et al. [126].

4.4.2 Analytical methods

Sample extraction and clean-up Surface extraction of intact pine needles was done with hexane:dichloromethane (v/v 99:1) employing an DIONEX, ASE 200 (p = 75 bar; T = 120°C). Separation of extracted compounds with higher polarity, particularly epicuticular waxes, was achieved by centrifugation. Medium pressure liquid chromatography (MPLC, Willsch, Juelich) was applied to gain the aromatic fraction of the needles surface extract. More details and standard deviations upon triplicate analysis see Lehndorff and Schwark [123, 124].

Instrumental analysis and compound identification The aromatic fraction of the pine needle surface extracts was analyzed for its PAH concentrations using a HP5971 GC-MS in SIM-mode and d₁₀ pyrene as an internal standard for quantification. Here, a focus on the concentrations of PAH-3 comprising phenanthrene (P), anthracene (A), dibenzothiophene (DBT), monomethyl-, dimethyl-/ethylphenanthrenes (MP, DMP), 1-methyl-7-isopropyl-phenanthrene or retene (Re) and cyclopenta[def]-phenanthrene (CPP) is set (Table 50, Fig. 61 in appendix). Identification of MP and DMP according to Benner et al. [15], Poster et al. [193], and Lehndorff and Schwark [124].

Statistics Locations were grouped according to known dominating emissions of the local environment as given by the Emission Register of the Environmental Agency NRW [118] and CORINE landcover data provided by DLR and the European Community [69]. Six characteristic types were established: locations < 8 km downwind of lignite fueled power plants (LFPP), samples taken close to industrial areas including petrochemical industry/refineries, needles from regions stressed by dust blow-out of open pit lignite mines, and locations characterized by forest or agricultural background

PAH	f1 evaporation refineries	f2 combustion LFPP, traffic	f3 distillation traffic	f4 distillation forests
1,8-DMP	.888	.111	.008	.392
2,6-DMP	.849	.262	.352	.195
x4-DMP	.841	.323	.397	.086
1,7-DMP	.823	.134	.300	.425
P	.182	.968	.048	.062
DBT	.042	.940	.253	.037
9-MP	.441	.749	.341	.090
2-MP	.463	.461	.691	.268
1-MP	.490	.527	.621	.280
retene	.454	.066	.198	.858
variance [%]	38	31	15	13

Table 22: Factor analysis of PAH-3 concentrations.

emissions (Fig. 55a). The spatial distribution of PAH-3 was interpolated and visualized using the ArcGIS Spatial Analyst tool (ESRI), for details see chapter 4.1. Factor analysis of phenanthrenes concentration was applied using SPSS14.0 to support source discrimination (Table 22). For extraction of factors the principal component method was chosen with varimax-rotation and Eigenvalues >0.4 . PAH-3 concentrations at locations 19 and 28 were excluded from statistical analyses.

4.4.3 Results and Discussion

Differences in distribution of pollutants in air are a result of several factors that are related to environmental conditions including e.g. temperature, precipitation, wind strength and direction, and of differing physico-chemical properties of investigated compounds. To minimize effects of physico-chemical properties, here the focus is set on the spatial analyses of 3-ring PAH (PAH-3), comprising parent PAH and alkylated derivatives thereof. The systematic accumulation of PAH-3 on *Pinus nigra* needles was tested and proven in a previous study by Lehndorff and Schwark [124].

Robustness and representativeness of the spatial data set is investigated by factor and spatial analysis. The spatial variability of PAH-3 accumulated on pine needles reveals systematic trends but also some local aberrations, that are typical for natural systems and their indigenous heterogeneity. Thus, point excursions may relate to point sources or physiological influences in receptor plants and have to be differentiated from regional air quality trends.

Concentration of 3-ring aromatics (PAH-3) Analysis of spatial variation of summed PAH-3 shows highest loads in an area affected primarily by emissions from lignite fueled power plants (LFPP), followed by urban areas with high traffic, industrial and household emissions. The lowest concentrations were determined for areas of agricultural use and forested regions (Fig. 55b). The spatial variability in PAH-3 concentrations is only partly resolved by factor analyses. Factor analyses including all

17 PAH-3 components reduced the number of variables to 10 of highest importance (Table 22). Two factors with Eigenvalues >1 , explaining 38 and 31 % of total variance and two factors with Eigenvalues of 0.4, explaining 15 and 13 % of total variance were extracted. The factors discriminate preferentially after component molecular weight or vapor pressure, i.e. parent PAH-3, mono-, di-, and polyalkylated PAH (Table 22).

Total PAH-3 concentration differences are most suitable to detect influence of LFPP emissions. Locations 1, 12, and 15 are immediately downwind of three LFPP with a cumulative production of 60×10^9 kWh. Sampling points 36 and 29 are downwind of a much smaller LFPP of only 1.3×10^9 kWh capacity and show only moderate enrichment compared to vicinal locations (Fig. 55a,b). The total load of PAH-3 is exceptionally high at location 19 due to an unknown point source, thus spatial interpolation leads to a misinterpretation of PAH distribution in the surrounding area. In natural systems such intrinsic heterogeneities occur, their detection requiring a sufficient number of neighboring data points. In a spatially high-resolved data set sampling locations with aberrant pollutant level may then be eliminated from statistical treatment or interpretation.

Source allocation according to PAH-3 with identical degree of alkylation

Source reconciliation based on PAH-3 accumulated on pine needles must consider effects of transportation and partitioning, which is most pronounced for components of different physico-chemical properties. First components with identical degree of alkylation: i) non-alkylated P to DBT, ii) mono-methylated 1-MP versus 9-MP, iii) di-methylated 1,7-DMP to 2,6-DMP, and vi) x4-DMP- to 1,8-DMP are compared.

i) P and DBT reveal a good correlation ($r^2 = 0.84$) whereby separation of locations and emission sources occurs primarily by concentration (Fig. 56a). Samples in the vicinity of LFPP show the highest DBT and P concentrations, whereby a subgrouping distinguished: a) highest concentration of P and DBT at downwind locations in <3 km distance to the three high capacity LFPP (Fig. 55a; locations 1, 12, 15), b) high concentrations determined in upwind direction or at a distance of up to 8 km (locations 2, 11, 14, 25), and c) samples taken downwind of the smaller power plant yielding the lowest concentrations (locations 36, 29). Locations chosen near industrial areas separate into two groups: one with enhanced P and DBT concentrations due to direct emissions from refineries/petrochemical plants (locations 3, 7, 35), and one with low P and DBT concentrations in regions of mixed industrial activities. Urban areas follow industry and power plant emissions by concentration. Lowest amounts of DBT and P were analyzed for locations near lignite mining, agricultural and forested areas.

ii) The correlation of 9/(9+1)-MP is less pronounced ($r^2 = 0.68$) due to a predominance of samples with a constant ratio of 9/(9+1)-MP (Fig. 56b). However, a separation into several subgroups with systematic deviations from the main trend is possible. The highest 9/(9+1)-MP ratio of 0.56 occurs in urban areas with heavy traffic, whereas less trafficked residential areas show slightly reduced ratios of around 0.5 (Fig. 56b). A 9/(9+1)-MP ratio of 0.53 is noted for the samples near the LFPP and high 9/(9+1)-MP ratios of 0.55 are characteristic for areas of agricultural use. Lower 9/(9+1)-MP ratios of 0.45 were found in locations exposed to petrochemical emissions due to a relative enrichment of 1-MP (Fig. 56b). Needles from forested areas and those affected by blow-out from open pit mines also exhibit very low 9/(9+1)-MP ra-

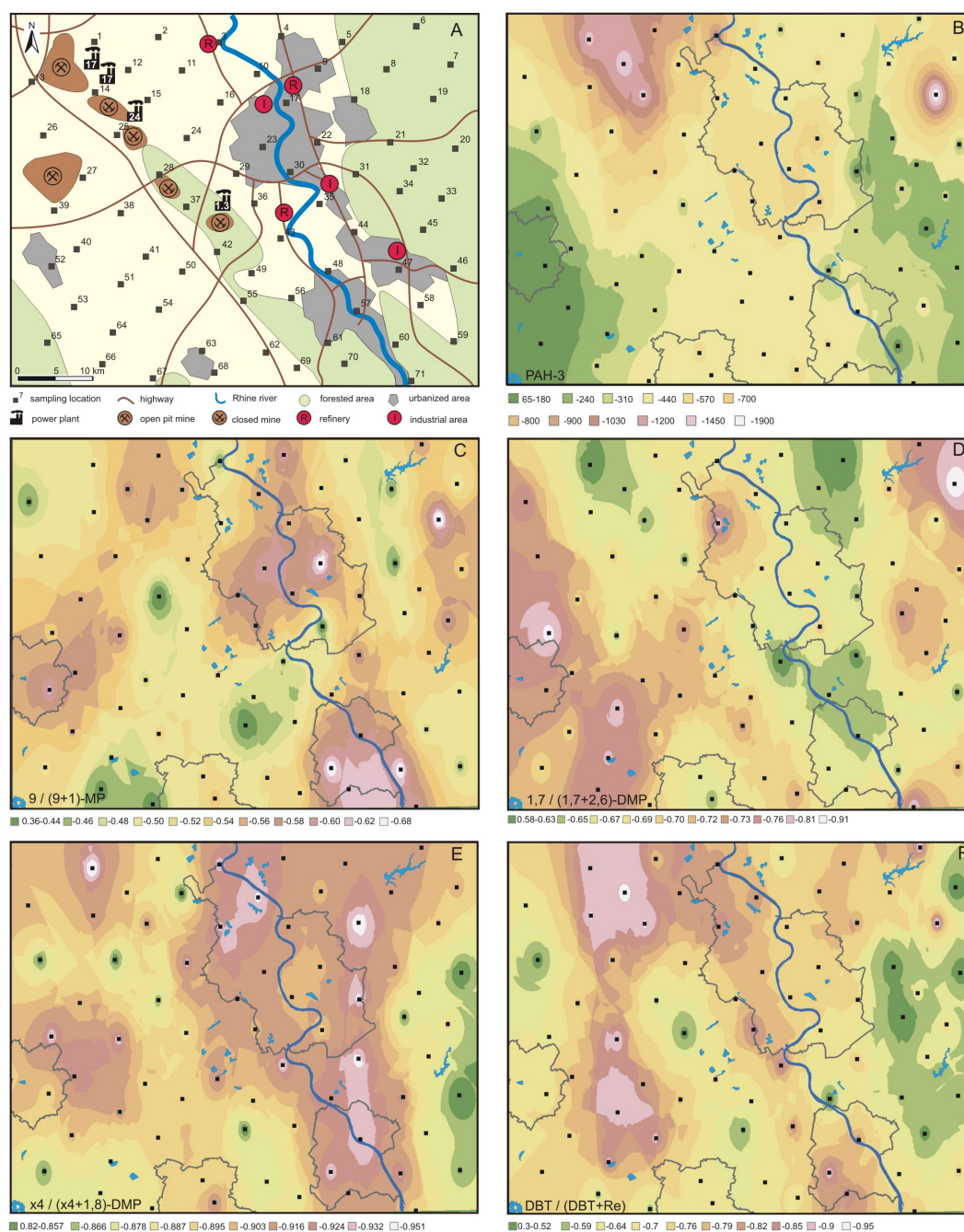


Figure 55: (A) Sampling locations, preferential land use and emission characteristics. Power generation for lignite fueled plants is given in 10^9 kWh, dominating land use in undefined (yellow area) is agriculture. (B-F) Spatial distribution indicating source dependence and transport mechanisms of summed 3-ring PAH in $\mu\text{g kg}^{-1}$ and selected PAH-3 ratios. River Rhine and cities Cologne (northern Rhine Valley), Bonn (southern Rhine Valley), Euskirchen (south) and Dueren (west) are highlighted for better orientation.

tios of around 0.4. The spatial distribution of the $9/(9+1)$ -MP ratio shows hot spots in urbanized areas associated with values >0.6 , and only moderately enhanced values around 0.56 downwind of the LFPP (Fig. 55c). Some aberrantly high $9/(9+1)$ -MP ratios may occur at point sources as observed for location 19 (Fig. 55c). Particularly

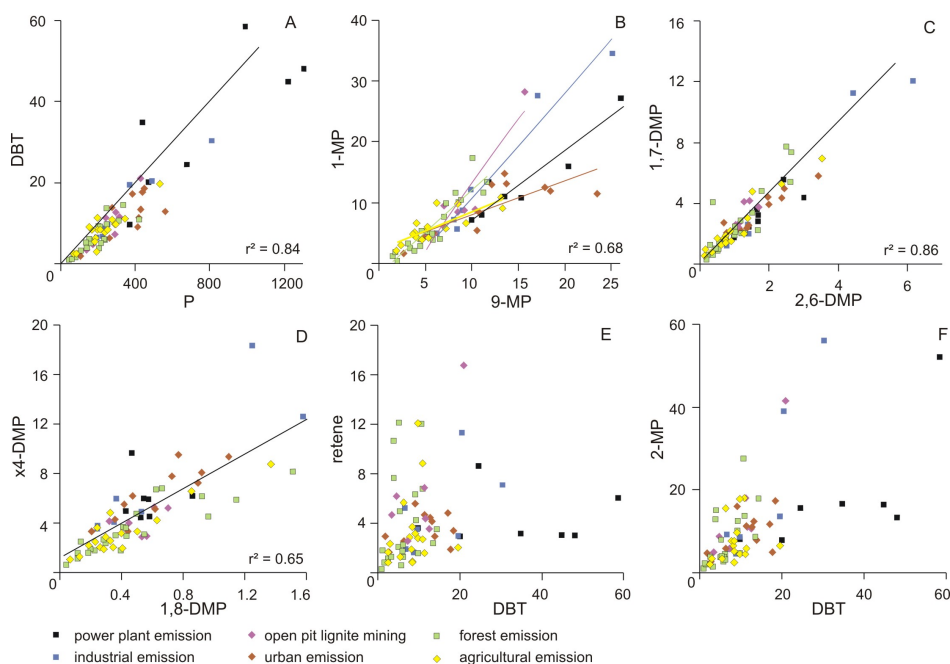


Figure 56: (A) Comparison of non-alkylated, (B) mono-alkylated, and (C), (D) di-alkylated PAH-3 given in $\mu\text{g kg}^{-1}$. (E), (F) Relationship of PAH-3 with different degrees of alkylation. Fits in B, see text. Plots A, B, E, F displayed without location 19; plots C, D displayed without location 28.

high relative amounts of 1-MP were noted in areas downwind of refineries (locations 3, 35, 43) or in forested regions (locations 8, 21, 49, 55, 56, 64, 66, 67).

The differential behaviour of methylphenanthrene isomers can be explained by their control through thermodynamic or kinetic driven processes. Alkylated phenanthrenes are not directly biosynthesized products but enter the anthroposphere as degradation products of e.g. functionalized plant resins or as components of fossil fuel. As such they have been formed over geological time (millions of years) via thermodynamically-controlled diagenetic processes occurring at about 60 to 130 °C that favour the more stable 2-MP and 3-MP isomers [197, 65]. If fossil fuel feedstock containing methylphenanthrenes is subjected to combustion at 500-1500 °C, e.g. in vehicle engine or power plants, generation of the 9-MP isomer is kinetically favored over 1-MP [236]. Regions where thermodynamically formed methylphenanthrenes predominate are thus characterized by emissions from non-combustion sources including refineries. Forests may emit enhanced amounts of 1-MP, due to diagenetic breakdown of abietane precursor products especially from conifer resins [229].

iii) The ratio of 1,7/(1,7+2,6)-DMP has been extensively used in source apportionment [15, 287, 139]. The coefficient of determination for this ratio is 0.86 with separation due to high concentrations for both isomers in petrochemical emissions and preferential enrichment of the 1,7-DMP in locations affected by lignite blow-out and forest emissions or wood combustion, respectively. The 1,7/(1,7+2,6)-DMP ratio has been determined as 0.4 for vehicular traffic and 0.45 for urban emissions, 0.66 for hardwood and 0.83 for softwood combustion [15, 287, 193, 139]. Most 1,7/(1,7+2,6)-DMP ratio values fall on a regression line around 2.0 (equals a ratio of 0.66) with a subset

of samples from areas affected by wood combustion and lignite dust blow-out following a trend at a 1,7/(1,7+2,6)-DMP ratio of 0.62 (Fig. 56c). Lignite combustion is not differentiated by this ratio with values <0.66 rather equivalent to those noted in cities (Fig. 55d). The westernmost town (locations 52, 40, 39) shows a deviating 1,7/(1,7+2,6)-DMP ratio >0.73 , which is due to blow-out of lignite dust from adjacent open pit mines (Fig. 55a,d). Unaccounted point sources may lead to aberrant values for this ratio as noted at locations 7 and 16 (Fig. 55a). Based on the 1,7/(1,7+2,6)-DMP ratio of 0.58 to 0.67 in urban regions it is calculated that $>75\%$ of the DMP emission results from vehicular traffic and 10 - 25 % from other sources, mainly from wood combustion (assumed 1,7/(1,7+2,6)-DMP ratio 0.8 for a mix of hard and soft wood).

iv) The correlation between x4-DMP and 1,8-DMP calculates to $r^2 = 0.65$ showing a trend for separation of samples from rural areas, enriched in 1,8-DMP versus urban areas and those affected by LFPP emissions, characterized by higher x4-DMP concentrations (Fig. 56d). The ratio of x4/(x4+1,8)-DMP in rural areas, including forests, agricultural croplands and regions affected by lignite blow-out, remains below 0.89 (Fig. 55e) and in general exceed 0.9 in urban areas. A north-south trending zone in the east of the study area shows enhanced x4/(x4+1,8)-DMP ratios caused by forests to the east characterized by very low x4/(x4+1,8)-DMP value areas, such that admixture of elevated x4-DMP concentrations from urbanized regions in the west leads to exceptionally high x4/(x4+1,8)-DMP ratios. The differentiation between these two DMP is preferentially due to the origin of x4-DMP from diesel evaporation and diesel combustion [193] whereas 1,8-DMP preferably derives from combustion of wood and vegetation residues. The emission of x4-DMP from fossil fuel is well expressed by the exceptionally high concentrations around petrochemical plants (Fig. 55e).

Source allocation according to PAH-3 with variable degree of alkylation
PAH-3 compounds of notably different physico-chemical properties are subject to diverse fractionation and partitioning processes and thus it is advisable to develop molecular source reconciliation parameters based on compounds of similar properties [287]. Selected PAH-3, however may be of high source diagnostic value, if compared with others differing in degree of alkylation. In this study three-ring aromatic hydrocarbons (PAH-3) are exclusively utilized assuming that physico-chemical differences between components of variable degree of alkylation are acceptable.

i) DBT versus retene shows a high variability indicating notably different sources (Fig. 55f). Areas affected by combustion of lignite or direct emission from petroleum show DBT concentrations $>20 \mu\text{g kg}^{-1}$ (Fig. 56e). Areas affected by lignite blow-out or by wood combustion show enhanced retene concentrations, generally $>6 \mu\text{g kg}^{-1}$ (Fig. 56e). In areas with conventional mix of urban traffic and industrial emissions or rural areas without strong wood combustion a covariance between DBT and retene is noted (Fig. 55f). The high abundance of DBT can be attributed to neof ormation of DBT in lignite combustion with inorganic species (e.g. pyrite or marcasite) as sulfur donors. Whereas SO_x components are retarded by filter equipment, organosulfur components like DBT are released to the atmosphere [124]. Due to effective regulation of sulfur contents in diesel fuel, enhanced DBT concentrations in urban air are no longer detectable [124].

Retene is a typical marker for either wood combustion [198] or for degradation products of conifer resins [229]. The comparison of DBT and retene allows for improved differentiation between wood combustion ($\text{DBT}/(\text{DBT}+\text{Re}) < 0.75$) and lignite combustion ($\text{DBT}/(\text{DBT}+\text{Re}) > 0.88$). The $\text{DBT}/(\text{DBT}+\text{Re})$ ratio thus allows to identify areas affected by lignite combustion including emissions from the low capacity LFPP and their downwind transport to locations 29 and 36 (Fig. 55f). The southward transportation of LFPP sourced DBT over a distance of up to 40 km is recognized in Fig. 55f (locations 51, 64, 66), because of the strong contrast between retene and DBT.

ii) The comparison of DBT versus 2-MP concentrations (Fig. 56f) allows extracting additional information supporting those observations made in the DBT/Retene analysis. The petrochemical influence is more clearly depicted by high 2-MP concentrations originating from direct vaporization of non-combusted petroleum or diesel. The high concentration of 2-MP points to an additional influx of petrochemical pollutants at location 1, which by using most other indicators exhibits a dominant lignite combustion signal (Fig. 56a,f). The admixture of petrochemical emissions at location 1 is corroborated by the exceptional enrichment of x4-DMP over 1,8-DMP (Fig. 56d). Among the rural agricultural sites three samples (locations 58, 66, 67) show deviations due to admixture of forest derived components to agricultural PAH distribution patterns. The agricultural locations with elevated concentrations of 2-MP ($> 10 \mu\text{g kg}^{-1}$) are identical to those giving retene concentrations $> 5 \mu\text{g kg}^{-1}$ (Fig. 56e,f) and to those yielding 1,7-DMP concentrations $> 4 \mu\text{g kg}^{-1}$ (Fig. 56c). The observed trend of covariation for retene, 2-MP and 1,7-DMP confirms that locations 58, 66, 67 with agricultural land use do receive considerable atmospheric input of PAH-3 from nearby forests. Furthermore, the agreement of the enhanced $\text{DBT}/(\text{DBT}+\text{Re})$ and $\text{DBT}/(\text{DBT}+2\text{MP})$ ratios for locations 38, 51, 64 supports the southward advection of emissions from the LFPP.

Source diagnostic ratios versus spatial concentration analysis of PAH-3 The critical process determining the relative distribution of PAH-3 is the mode of formation, which is either thermodynamically (geologically formed) or kinetically (combustion) controlled. Variances in combustion conditions are numerous limiting the source discrimination potential of PAH-3. Combustion of biomass is mostly associated with a vaporization or steam distillation phase [225] releasing compounds in their original biological conformation or after minor alteration. Under such conditions a high source recognition potential is given represented by components like retene, 1,7-DMP, 1,8-DMP or 1-MP. This is supported by factor analysis with f4 showing highest loadings for $\text{Re} > 1,7\text{-DMP} > 1,8\text{-DMP} > 1\text{-MP}$ (Table 22). PAH-3 products of near-complete combustion exhibit similar composition limiting discrimination of combustion feedstock based on PAH-3 ratios. The identification of specific combustion sources or feedstocks is improved by mapping PAH-3 concentrations thus unraveling the close spatial relationship between dominant emitters and adjacent receptor sites. In this study the predominant origin of PAH-3 from lignite fueled power plants is evident (Fig. 55a,b). Since the introduction of sulfur concentration regulation for diesel fuels the amount of thioaromatic emissions from mobile PAH-3 sources has decreased dramatically and at present the emissions of DBT dominantly derive from LFPP [124].

PAH-3 that are not released by combustion but via vaporization from petroleum or petroleum products are highly variable in concentration with maximum amounts noted

in the vicinity of petrochemical plants where such emissions are easily recognized by exceptional atmospheric abundance. Compositional variations between thermodynamically or kinetically favored methylphenanthrenes (Fig. 56b) or dimethylphenanthrenes (Fig. 56d) are suitable for identification of petrochemical products. The relationship DBT vs. 2-MP (Fig. 56f) indicates that emissions from petrochemical sites are depleted in sulfur compounds. Given the fairly constant ratio between DBT and MP in raw petroleum, the DBT depletion indicates its removal during petroleum refining to meet regulatory thresholds for low-sulfur diesel.

Terpenoid emissions from vegetation, especially from conifer resins, may form a recognizable fraction of PAH-3 in areas with low impact from combustion sources. Differentiation of biogenic PAH-3 released by natural processes from those emitted via distillation upon wood combustion is hardly possible. In addition the components indicative of such sources are compositionally similar to those emitted by blow-out of thermally immature lignite dust from open pit mines.

4.4.4 Conclusions

Factor analysis in part reflects above discussed source dependencies of PAH-3. Although, the FA is dominated by the physico-chemical properties of the compounds, i.e. degree of alkylation, it reveals source specific loadings as highlighted in Table 22. Factor 1 and 2 describe 70 % of the data set including evaporative PAH from refineries (f1) and combustion PAH from LFPP and high traffic regions (f2). Factors 3 and 4 comprise PAH-3 derived from distillation processes and forest emissions. Second and third place loadings show that a clear separation of one compound to a single source cannot be done. This supports the sense of PAH-3 ratios.

Despite the limitations due to comparable mode of formation PAH-3 offer significant source discrimination potential and due to the high total abundance of this compound class in the atmosphere and the biosphere an inclusion of the full suite of PAH-3 in environmental studies would be beneficial.

4.5 Cologne Conurbation air quality - a synthesis

The aim of this study is to achieve a most detailed differentiation of sources and dispersal routes for various atmospheric pollutants employing biomonitoring methods. Previous studies have successfully demonstrated the potential of biomonitoring methods concentrating on single pollutant groups. Here, the combination of organic, inorganic and enviromagnetic studies is applied for an enhanced understanding of emission sources in areas of multiple, mixed emissions as exemplified by the Greater Cologne Conurbation. This chapter provides a synthesis and attempts an integration of the various atmospheric quality proxies employed in this study to unravel the origin, concentration and distribution of air pollutants.

There are only few investigations published addressing a combination of organic and inorganic data in environmental sample sets [138, 84], inorganic and enviromagnetic data [103, 66], and enviromagnetic and organic data [285, 222], respectively. A previous biomonitoring study conducted in Cologne City showed that organic PAH loads are comparable to enviromagnetic particulate matter (PM) proxies [123].

Here, organic and inorganic compounds, enrichment factors, enviromagnetic proxies and ratios showing highest significance in source characterisation as shown previously in this chapter are used for correlation and following emission discrimination. In addition, the efficiency and plausibility of source characteristic properties of a source marker can be tested by a combined multi-proxy analysis. A total of 13 potential sources could previously be described by factor and spatial analyses of pine needle pollutant loads in the GCC, including emissions of lignite fueled power plants (LFPP), traffic combustion and abrasion and industry (Table 23). Here, more specific source informations are extracted, based on spatial analyses in a high-resolution sampling set ($n = 71$) covering 3600 km² in the Greater Cologne Conurbation.

4.5.1 Sampling and Analysis

Multi-proxy biomonitoring is applied to a data set comprising 71 spatially distributed *Pinus nigra* needle samples in the Greater Cologne Conurbation. Bulk pine needles were subjected to major and trace element analysis and determination of enviromagnetic pollution proxies. PAH concentrations were investigated by GC-MS of aromatic fractions derived from medium-polar needle surface extracts. For PAH molecular structure and synonym abbreviations see Figure 61 and Table 25 in the appendix. Details about sampling, analytical methods and calculation of element enrichment factors (EF) are given by Lehndorff et al. [126], Lehndorff and Schwark [125, 124] and previously in this chapter. Here, the focus has been set on statistical methods which were tested for achieving a most detailed source characterization.

Spearman's rank correlation coefficients and factor analyses were calculated with SPSS 15.0. Factor analysis was performed with principal component extraction and varimax rotation. Spatial interpolation between data points for isopleths map construction was calculated using the ArcGIS Spatial Analyst tool (ESRI) using the inverse distance weighted method, power=1, including 6 nearest neighbours. The colour pattern from green over red to white induces low to high concentrations, ratios, concentrations proxies or element enrichment, respectively (Fig. 58, Fig. 59, Fig. 60).

4.5.2 Results

Compounds and proxies with source indicative character (Table 23) were extracted previously in this chapter and subjected to statistical analyses to find significant relations caused by differences in emission sources.

source	LFPP	biomass burning	industry Cologne-S	MWI	traffic	refinery	industry Cologne-N
formation		combustion			combustion + abrasion	combustion + evaporation	
PAH	DBT, Py, BaA, Bep, Ip	1,7/(1,7+2,6) -DMP, BbjFla, BeP, Ip, Re	CpcdPy	x4(x4+1,8) -DMP, Ip/(Ip+BghiP)	CpcdPy, Py 9/(9+1)-MP, 1,7/(1,7+2,6) -DMP	9/(9+1)-MP, DMP, Ip, Ip/(Ip+BghiP)	Ip, Ip/(Ip+BghiP)
tracer elements			Sr	Cr	Sb, Fe	In, Sn, Mo, Cu	W
enviromagnetic proxy	ARM, IRM				ARM, B _{cr} , SIRM, IRM/ARM		
source	fertilizer application	UCC	lignite dust	basalt dust	ore deposits	carbonaceous accumulation	
formation		blow-out				blow-out + root uptake	
PAH			P, BaA			x4/(x4+1,8)-DMP	
tracer elements	-	REE, Th		Ti	Cd	Ca	
enviromagnetic proxy			B _{cr} s-ratio	SIRM IRM/ARM s-ratio			

Table 23: Compilation of sources and source diagnostic compounds, ratios and enviromagnetic pollution proxies established on pine needles in the Greater Cologne Conurbation.

Statistical analyses Spearman's rank correlation coefficients for organic, inorganic, and enviromagnetic data of 71 spatially distributed pine needle samples taken in the GCC are given in Table 24. Most significant relations were found within pollutant groups as discussed previously in this chapter. Relationships between different pollutant groups were observed for i) PAH versus enviromagnetic proxies with DMP and BaA showing good correlations with ranks about 0.5 to χ and Bcr and with notable dependencies to SIRM and ARM; no relation of the IRM/ARM ratio to PAH was observed; ii) PAH versus element concentrations and element enrichment factors (EF) yielded highest ranks of 0.5 for DMP and BaA against iron concentration, followed by lower ranks for REE, Ca, Cd, and Cr (Table 24). DBT concentrations and Flua/(Flua+Py), Ip/(Ip+BghiP) and x4/(x4+1,8)-DMP ratios reveal dependence to source diagnostic trace elements (Fe, V, W). Traffic marker PAH CpcdPy and ratios of 9/(9+1)-MP and 1,7/(1,7+2,6)-DMP reveal no significant correlation to major and trace element loads or enrichment on pine needles; iii) correlation of enviromagnetic data to absolute major and trace element loads and EFs is higher than 0.5 for χ , SIRM and B_{cr} versus Fe and REE concentration, and also observed for ARM and IRM/ARM to Ca, Cr, Hg, Sb, Ti, V enrichment factors, respectively.

An extraction of factors with source descriptive potential yielded no satisfactory results. Factor analysis is mainly driven by differences between pollution classes, thus, source dependent differences do not contribute significantly to factor extraction.

Bivariance analysis Analysis of coherences between pollutants or pollutant proxies and potential emitters was exercised using bivariance plots. Therefore, a classification of locations was established according to six different pollution type or emission scenarios. These pollution types comprise emissions of lignite fueled power plants (LFPP), industrial areas including refineries, municipal waste incineration (MWI), dust blow out due to open pit lignite mining, mixed urban emissions, and areas that are dominated by forest cultivation and agricultural use (Fig. 57). The classifications were derived from data provided by CORINE landcover [69] and the Emission Register of the Environmental Agency NRW [118].

Comparison of rare earth elements (REE) concentrations on needles to the magnetite concentration indicator SIRM reveals a constant increase of both near LFPP, but higher REE contributions near lignite open pit mines and relatively higher magnetite concentrations in urban and industrial areas (Fig. 57a). ARM that was previously shown to be sensitive for fine dust emissions by LFPP [126] exhibits a good correlation to DBT, which was shown to be almost exclusively emitted by lignite combustion (chapter 4.4). Needles sampled in highly industrialized regions are clustered by high ARM values (Fig. 57b). Vanadium enrichment and DBT correlation reveals three well separated clusters of LFPP, urban and industrial pine needle samples (Fig. 57c).

Plotting indium enrichment versus the organic source diagnostic Ip/(Ip+BghiP) ratio reveals two independent groups of industrial emissions (Fig. 57d). The biplot of iron concentration of *Pinus nigra* needles versus their magnetic susceptibility χ shows a very good correlation with maximum values at urban locations followed by sites close to LFPP and lignite minings (Fig. 57e). Minor deviations to relatively higher Fe concentrations were observed for mining areas and two LFPP samples, where a substantial non-magnetite contribution to iron oxides is inferred. A contribution of

	DBT [ng g ⁻¹]	DMP [ng g ⁻¹]	CpcdPy [ng g ⁻¹]	BaA [ng g ⁻¹]	Flua/ (Flua+Py)	Ip/ (Ip+BghiP)	x4/ (x4+1,8)-DMP
χ		.521(**)		.462(**)			
B _{cr}		.520(**)		.474(**)			
SIRM		.368(**)		.365(**)			
ARM		.318(**)		.237(*)			
s-ratio		-.258(*)					
IRM / ARM							
Fe	.359(**)	.550(**)		.511(**)			
Σ REE		.371(**)		.351(**)			
Ba EF							.343(**)
Ca EF	-.257(*)	-.262(*)		-.399(**)			.244(*)
Cd EF	-.274(*)	-.285(*)				.259(*)	
Cr EF		-.363(**)		-.275(*)			
Fe EF					-.246(*)		.266(*)
Hg EF							.267(*)
Pb EF					-.318(**)		
Sb EF					-.390(**)		
Ti EF							
V EF	.239(*)	.244(*)			-.323(**)		.268(*)
W EF					-.315(**)		.277(*)

	χ [10 ⁻⁸ m ³ kg ⁻¹]	B _{cr} [mT]	SIRM [A m ¹ kg ⁻¹]	ARM [A m ¹ kg ⁻¹]	s-ratio	IRM / ARM
Fe	.830(**)	.773(**)	.747(**)	.589(**)	-.551(**)	
Σ REE	.617(**)	.524(**)	.617(**)	.553(**)	-.384(**)	
Ba EF						
Ca EF	-.366(**)	-.389(**)	-.360(**)	-.282(*)	.383(**)	-.298(*)
Cd EF		-.270(*)				-.295(*)
Cr EF	-.467(**)	-.509(**)	-.394(**)	-.452(**)	.551(**)	
Fe EF						
Hg EF	-.238(*)	-.287(*)	-.271(*)		.267(*)	-.260(*)
Pb EF						-.269(*)
Sb EF	.244(*)	.262(*)				
Ti EF	-.380(**)	-.300(*)	-.270(*)	-.466(**)	.505(**)	
V EF	.360(**)	.427(**)	.266(*)	.279(*)		
W EF						

Table 24: Spearman's rank correlation coefficients of organic, inorganic and enviromagnetic air quality proxies at 0.01(**) and 0.05(*) significance level, respectively.

50 mg g⁻¹ Fe to diamagnetic phases on the needle is derived from intercept of the regression line with the y-axis (Fig. 57e) and in principal represents the biogenic iron component.

Spatial variance analysis Spatial interpolation between sampling locations to construct isopleths maps was used to identify zones of minimal and maximal pollution. A comparison of these zones with emission data provided by the NRW Emission Register [118] served as a base for source allocation. Results of the spatial analysis of PAH, major and trace elements and enviromagnetic proxies were discussed in detail previously in this chapter. Here, similarities and differences between isopleths maps constructed from independent pollutants and pollutant proxies of variable origin, i.e. organic compounds, elements, environmental signals, are discussed. The distribution patterns of Fe concentrations, Fe enrichment factors and magnetic susceptibility χ of bulk pine needles reveal significant maxima or hot-spots. Several of the Fe concentration hot-spots occur in urban areas, especially in Cologne City (Fig. 58a). However, a spatially extended plume in the north-western GCC was not associated with urban fabric. This plume in particular disappears when Fe concentrations are normalized to geogenic dust and thus the Fe-enrichment in this area was attributed to mineral dust blow-out from open pit lignite mines in the area. This interpretation is confirmed by results from pine needle susceptibility measurements (Fig. 58a) that also fail to pick out the dust-related Fe-enrichment due to its low magnetite versus hematite ratio. The maximum in Fe-concentration in this area is located further to the southeast when compared to the

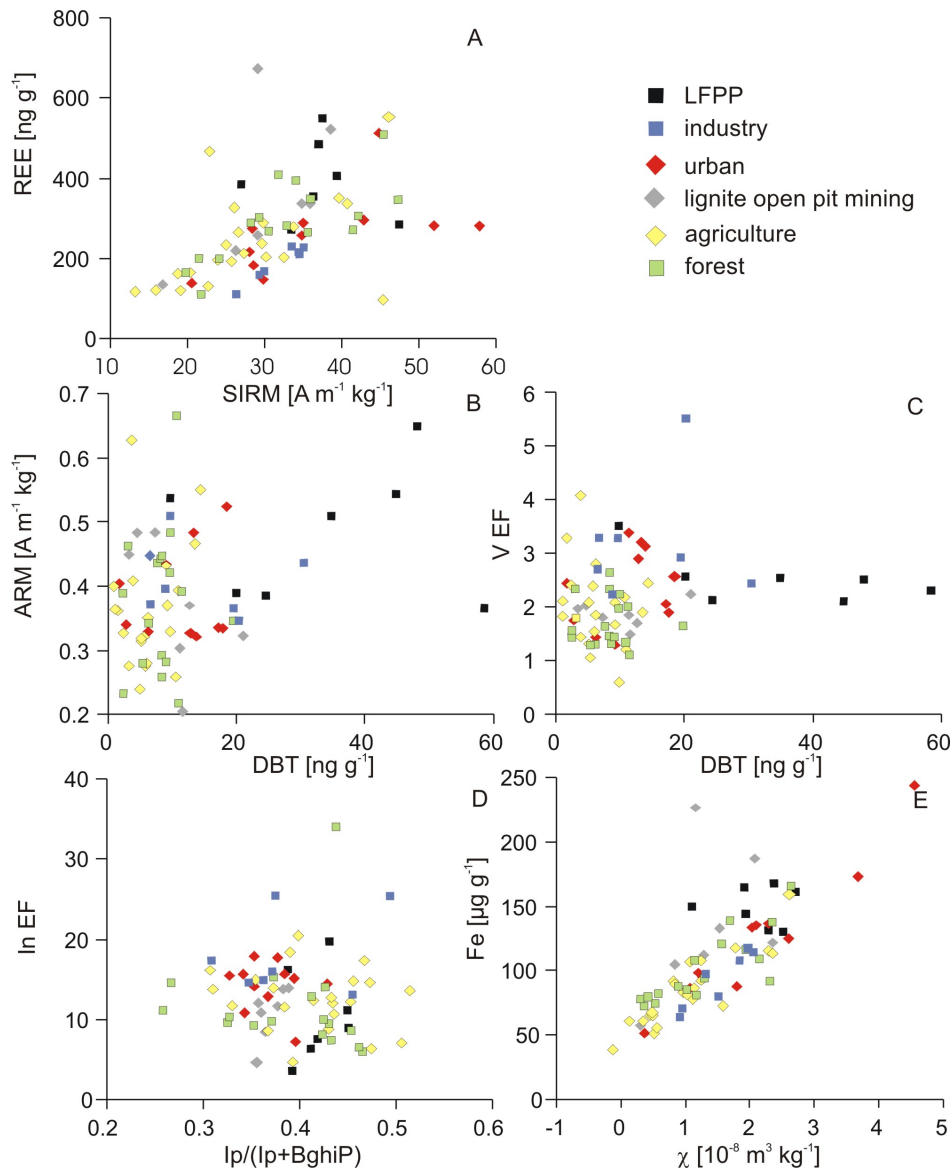


Figure 57: Bivariate plots between PAH, elements and enviromagnetic proxies revealing source characteristic trends and clusters. Sample classification was performed according to dominant land use and emission sources.

moderate plume noted in magnetic susceptibility (Fig. 58a). The former is caused by mining dust the latter is due to combustion derived emission of magnetite spherulites from the LFPP. The combination of various proxies thus allows refinement in source attribution and allocation for Fe-associated atmospheric pollutants.

Urban emission reached its maximum in Cologne City but was also present in the smaller towns of Bonn, Euskirchen and Dueren as shown previously in this chapter (Fig. 58a,b). These emissions were best represented by Fe EF, Sb EF, CpcdPy concentration, 9/(9+1)-methylphenanthrene ratio and magnetic mineral concentration parameters (Fig. 58a,b). Nevertheless, figure 58b shows deviations in spatial distribution with antimony and iron enrichment preferentially in the western part of Cologne City and PAH being more dominant in the eastern part of the city center. The 4-ring

PAH CpcdPy does not appear -or in minute amounts only - in forested areas in the central study area, in the east and the south-west. In contrast, antimony EF and the 9/(9+1)-MP ratio are more prominent in remote areas (Fig. 58b).

Markers for lignite combustion in lignite fueled power plants are presented by isopleths maps in figure 59a. The organic compound dibenzothiophene is almost exclusively found on needles sampled in the north-western GCC, where the major three of four LFPP are located. The fine-dust proxy ARM highlights the LFPP region, the western Cologne City and is found in a open plain area to the southwest that receives wind input from the LFPP region (Fig. 59a). Vanadium enrichment is dominant in the Cologne Conurbation and near adjacent industrial complexes to the south, but reveals notable contribution from sources in the north-west leading to a threefold enrichment versus geogenic dust loads. The north-western maximum shows deviations in distribution induced by varying pollutant loads on needles at locations 1, 2, 12, 14, 15 and 25 (Fig. 59a, loc. 1, 2, 12, 15 high in DBT; loc. 12, 14, 15, 25 high in ARM and loc. 12, 14 with high V EF).

Iron and REE, the magnetic s-ratio and the organic 1,7/(1,7+2,6)-DMP ratio (Fig. 58a, Fig. 59b) were previously described as tracers for lignite dust (chapter 4.1, chapter 4.4). High amounts of Fe and REE co-appeared at locations 15, 25 and 27 situated in the central mining zone (Fig. 58a, Fig. 59b). The s-ratio reflected magnetic mineral changes at locations 25, 26, 27 and the 1,7/(1,7+2,6)-DMP ratio revealed maximum loads at locations 26 and 39 herewith showing a notable deviation to the east when compared to the north-western s-ratio and REE maxima (Fig. 59b).

Chromium and mercury enrichment and enhanced Ip/(Ip+BghiP) ratios showed differential distribution patterns throughout the GCC, but exhibited two maxima in common. These were found in the north of Cologne and in Bonn (Fig. 60a, loc. 10, 61). Tungsten, indium and the methyl-PAH ratio x4/(x4+1,8)-DMP revealed significant enhancement on a larger scale around the northern Cologne City industrial complex. Emissions were highest at location 3 and 10 for Tungsten. Indium and the organic x4/(x4+1,8)-DMP ratio show additional enhancement at locations 11 and 1, respectively (Fig. 60b).

4.5.3 Discussion

An analytical multi-proxy approach at spatial high-resolution allows and requires a discussion of statistical methods which is provided in the first paragraph of the discussion. Statistical results proved to be beneficial for a proper handling of the large data set and guides interpretation in terms of pollutant sources and dispersal, as described in the second part of the discussion.

Statistics in multi-proxy biomonitoring Biomonitoring in general is affected by highly variable natural background concentrations of compounds of interest and challenged by atmospheric mixing of pollutants derived from multiple emission sources. Thus, biomonitoring of air quality is often supported by statistical analytical tools and factor analysis was successfully used for discrimination of either PAH or element sources [51, 5]. In this study a multi-proxy approach employing organic, inorganic pollutants and enviromagnetic properties of pine needles was chosen for detailed source

reconciliation and tested for statistical analysis.

Calculation of correlation coefficients indicated dependencies between the three pollutant groups, revealing minor connections between organics and enviromagnetic parameters (Table 24). This was mainly related to differences in preferred phase of atmospheric residence, being particulate for magnetite and predominantly gaseous for PAH-2, PAH-3 and PAH-4. The estimated dependence between traffic marker CpcdPy and magnetite concentration parameters χ and SIRM was not expressed by calculation of correlation coefficients. Additionally, relations between PAH and elements were low and did not reflect anticipated dependencies: no significant correlation was observed between traffic indicators CpcdPy and 9/(9+1)-MP versus Sb, Fe, Pb, and industrial markers Pb and W showed no co-evolution with DMP, Ip/(IP+BghiP) or x4/(x4+1,8)-DMP. Higher correlation ranks were observed for enviromagnetics versus element enrichment and concentration, due to stronger similarities in emission processes and atmospheric transport fractionation. Nevertheless, extraction of detailed information on diverse pollutant sources proved impossible, if exclusively based on statistical data treatment. In principle, factor analysis tended to group pollution parameters according to analytical methods and thus has to be applied for within individual pollutant groups as shown previously in chapter 4.

The high spatial variability and the input of data derived from independent methodologies required application of alternative routes in spatial analyses. This was met by construction and interpretation of isopleths maps generated for each pollutant. These isopleths maps were analysed for sources and dispersal separately and compared thereafter.

Source recognition via multi-proxy biomonitoring in the Greater Cologne Conurbation Analysis and interpretation of spatial dependencies between independent air quality factors is conducted in the following paragraph by inspection of major sources that were identified previously in the GCC by means of PAH, element and enviromagnetic analyses, respectively.

Traffic indicators Urban emissions revealed substantial amounts of iron and magnetic mineral concentration indicator χ for the inner city of Cologne and neighbouring towns (Fig. 58a). Enrichment factors of elements Fe and Sb complementary highlight the city centers and are known to be primarily derived from abrasive processes in traffic, e.g. brake and tire wear [64]. While particulate magnetite is also derived from combustion processes and subsequent spherulite formation [58], organic tracers CpcdPy and methylated phenanthrenes are emitted from gasoline by incomplete combustion and preferentially appear in the atmosphere in gaseous state [15, 193, 139]. Therewith, differences in spatial dispersal of traffic indicators can be interpreted in terms of emission process and atmospheric transport phenomena.

Antimony bulk concentrations or enrichment factors served as excellent traffic marker in the GCC (Fig. 58b). Maximum concentrations were observed for Cologne City whereas rural areas showed a rapid decline in Sb EF. This was attributed to intensive brake use in areas of high traffic density, characterized by intensive stop and go traffic. Reduced Sb emissions were found associated with continuous traffic flow on highways in the Greater Cologne Conurbation. In contrast, local increase in CpcdPy

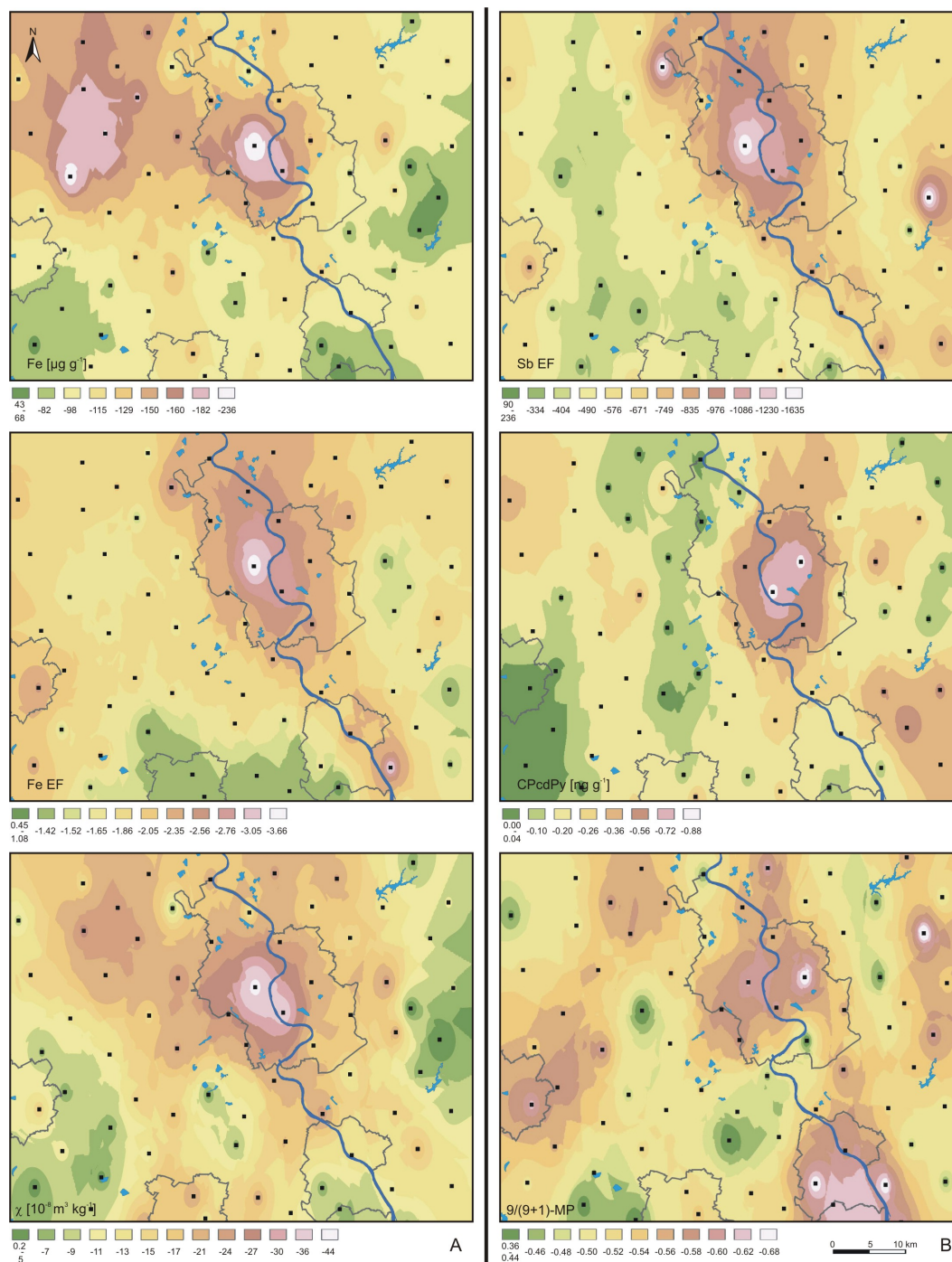


Figure 58: Isopleths maps for source characteristic PAH, elements and enviromagnetic proxies, (A) iron associated pollution, (B) urban and traffic emissions. For orientation sampling locations and outlines of city limits were provided, for more details see overlay transparency in the appendix (Fig. 62).

and the 9/(9+1)-MP ratio was observed in rural areas as well, and here attributed to equivalent amounts of fuel combustion on highways (Fig. 58b). In Cologne City an offset of maximum pollution to the east is observed for organic traffic indicators CpcdPy and 9/(9+1)-MP when compared to enviromagnetic and elemental abrasion indicators

χ , Sb EF and Fe EF (Fig. 58a,b). This offset could be related to phase-dependent fractionation upon pollutant transport as indicated by the spatial distribution of CpcdPy, showing a clear dependence on morphology and surface vegetation cover. CpcdPy was enhanced in non-forested areas with flat topography (Rhine Valley, south-eastern Sieg Valley and south-western Zuelpicher Boerde) and decreased notably in forested zones at higher elevation (central Ville Hills, eastern Bergisches Land, southern Eifel). This observation suggested that distribution of primarily gaseous PAH was not simply controlled by vapour pressure phase partitioning but rather a question of air/plant-capturing mechanisms (Fig. 58b).

More knowledge about the particle fraction in urban emission scenarios is gained by plotting geogenic dust indicator REE against magnetite concentration proxy SIRM (Fig. 57a). In general, a trend of co-variation between non-anthropogenic dust and magnetite is observed. This was indicative for atmospheric magnetite occurring in a grain size range similar to that of geogenic dust and, therefore, being subject to identical transport mechanisms. However, urban sampling sites revealed a significantly higher proportion of magnetite than estimated from geogenic input, thus highlighting traffic as a specific source for magnetite.

LFPP indicators Best proxies for lignite combustion in lignite fueled power plants (LFPP) as determined in previous investigations (chapter 4) and compiled in Table 23 were the sulfur bearing aromatic compound DBT and ultrafine magnetite concentration parameter ARM. Graphical correlation of DBT to ARM revealed a source diagnostic pattern for samples characterized by LFPP emissions through aberrantly high DBT concentrations and elevated ARM signals (Fig. 57b). Interestingly, this indicated a connection between ultrafine particulates $< 0.4 \mu\text{m}$ and DBT, proposing a particle-bound transport for DBT in the atmosphere.

In contrast to enhanced magnetic particle concentration on pine needles northeast of the LFPP, absolute Fe concentrations decreased towards this direction (Fig. 58a). A normalization of Fe on geogenic dust confined Fe enrichment to highly trafficked areas and most of the elemental iron near and in particular southeast of the LFPP was attributed to geogenic dust loads. In turn this supported source differentiation with areas southwest of the LFPP receiving primarily geogenic hematite-enriched dust influx, whereas the zone to the northeast of the LFPP showed enhanced lignite combustion-derived magnetite input. Additional element emissions of LFPP are only observed for vanadium. The expected increase in concentration of mercury, an element often associated with lignite and volatilized upon its combustion, could not be observed (Fig. 60a). The isopleths map of vanadium is dominated by emissions from traffic and industry (Fig. 59a) but correlation of V to DBT in a bivariate plot allowed for a good separation between samples with LFPP versus industrial derived emissions (Fig. 57c).

Lignite mining indicators Open pit lignite mining activities are mainly characterized by a high dust blow-out, due to large outcrops of approximately 100 km^2 in the Greater Cologne Conurbation, requiring constant sprinkling during dry summer month. The geogenic derived dust fraction was previously shown to be best represented by rare earth element loads on pine needles, which perfectly highlighted the lignite mining area

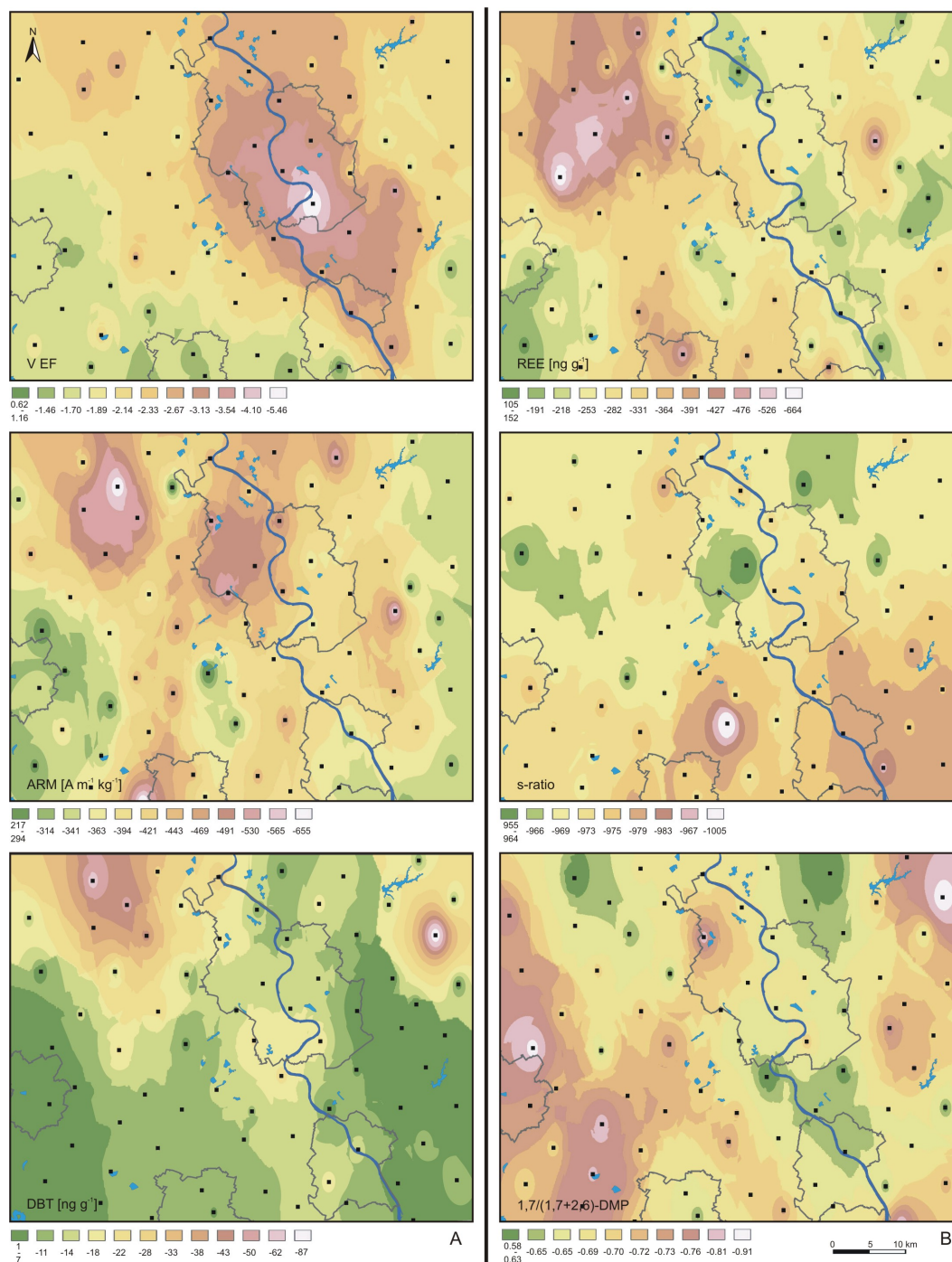


Figure 59: Isopleths maps for source characteristic PAH, elements and environmental proxies, (A) LFPP related pollutants, (B) geogenic dust. For orientation sampling locations and outlines of city limits were provided, for more details see overlay transparency in the appendix (Fig. 62).

in the north-west of the study area (Fig. 59b). A very close relation of REE concentrations to those of iron and susceptibility χ of pine needles is evident from figure 58a. In combination with low remanence signals (SIRM and ARM, Fig. 59a) this indicated the lack of magnetite in the open pit area, but an abundance of non-remnant iron

minerals. As evident from figure 57e, enhanced proportions of non-magnetic iron occurred in samples near lignite mines. Accordingly, iron concentrations in lignite from the Lower Rhine Embayment were related to iron sulfides or oxides/hydroxides. Iron oxide mineral phases can be differentiated based on the enviromagnetic s-ratio, developed as an indicator for a mixing of hematite and magnetite. The low s-ratio of 0.95 was interpreted to indicate contributions of weathered magnetite to the magnetic signal on pine needles in the lignite mining area.

Formed as a diagenetic product of retene, the aromatic diterpenoid 1,7-dimethylphenanthrene (1,7-DMP) in organic geochemistry is commonly used as marker for softwood land plants. The relation of 1,7DMP to petroleum derived 2,6-DMP is in use as a diagnostic ratio for wood combustion and combustion of fossil fuels [14, 139]. In the GCC the ratio reveals especially high values west of open pit lignite minings (Fig. 59b). This hot spot was previously related to lignite blow-out, but comparison with REE, Fe and s-ratio interpolation maps shows little spatial overlapping that can hardly be related to transport differences. In addition, REE distribution reveals a tendency to eastwards transportation from mines (Fig. 59b), which is in agreement with prevalent wind directions in this part of the GCC. Thus, a use of 1,7/(1,7+2,6)-DMP ratio as lignite dust indicator is questionable.

Municipal waste incineration The GCC bears two large municipal waste incinerators (MWI), one in the north of Cologne and one in Bonn city with capacities for 590,000 and 245,000 t a⁻¹ of waste, respectively. The combustion of waste is known to release substantial amounts of trace metals into the atmosphere including mercury and chromium. Enrichment of these elements is observed at the sampling locations close to the Cologne and Bonn MWI (Fig. 60a, loc. 10, 61). The organic source diagnostic ratio of Ip/(Ip+BghiP) is indicative for wood and fossil fuel combustion [287] and reveals a significant hot spot at the Cologne MWI, that is supposed to be related to the associated compost plant.

Markers for industrial emissions In the Greater Cologne Conurbation various industrial emitters are found. According to data from the Emission Register of the Environmental Agency NRW [118], two refinery complexes in the north and south of Cologne and inorganic chemical industry situated in the south-eastern Sieg Valley are dominating emitters of atmospheric pollutants. Maximum concentrations of W and In in the north of Cologne are related to emissions from nearby organic chemical industry. Indium additionally occurs in the southern refinery complex thus pointing towards two different production processes in these plants. Alkylated and low molecular weight PAH as x4-DMP and 1,8-DMP are released by petroleum refinery and wood combustion, respectively. High ratios of x4/(x4+1,8)-DMP thus meet expected values in vicinity of organic chemical production plants in the study area. In general, a source allocation with trace metals W or In is of higher significance due to a local limitation of dispersal and resulting hot spots in the isopleths map (Fig. 60b). Thus, the x4/(x4+1,8)-DMP ratio is of minor importance for a source allocation, but provides essential information about source and emission process.

The relation of indium to the Ip/(Ip+BghiP) ratio is plotted in figure 57d and reveals two clusters for sampling sites with industrial background. Thus, a separation

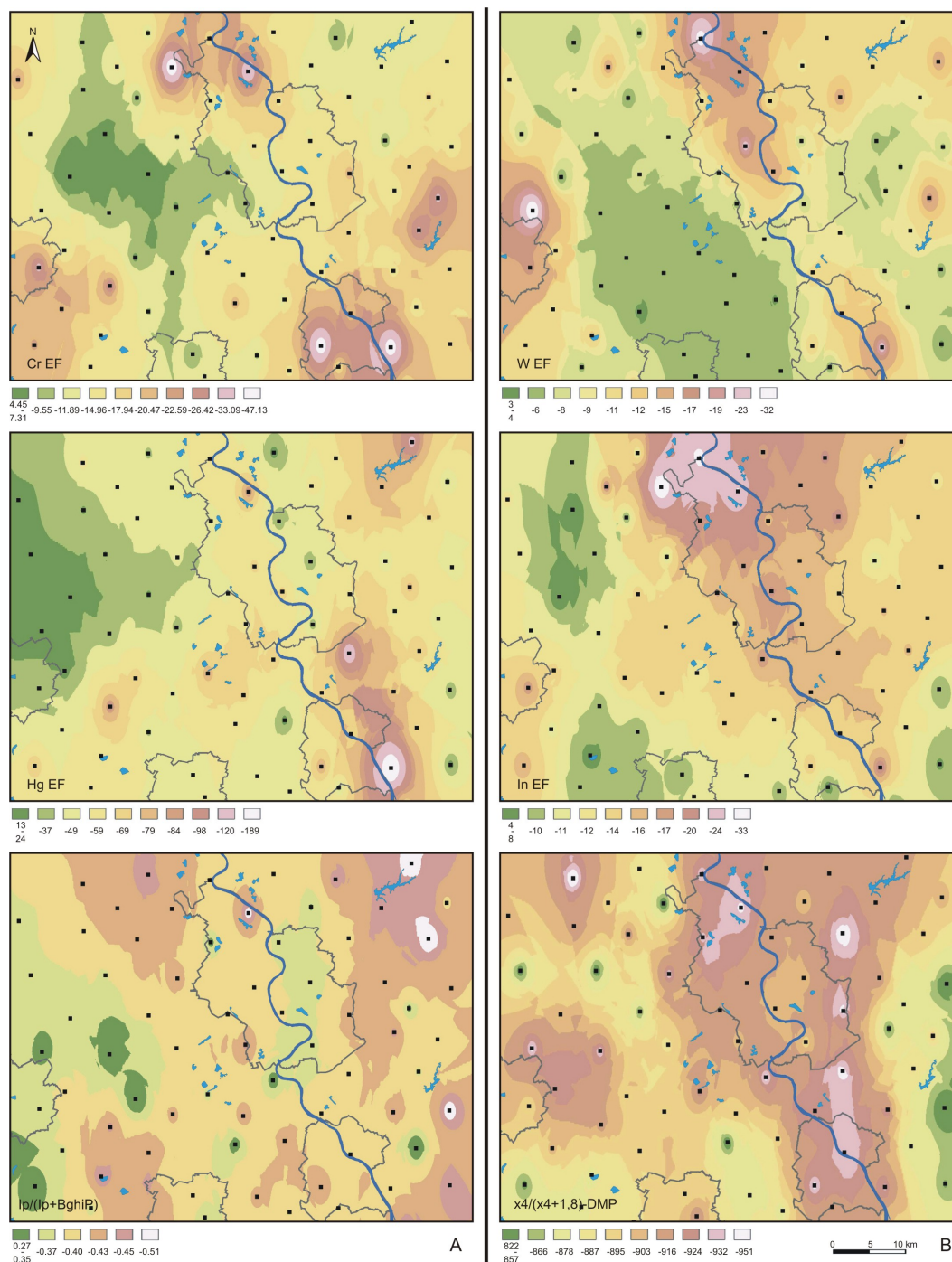


Figure 60: Isopleths maps of source characteristic PAH, elements and enviromagnetic proxies, (A) element enrichment and PAH ratio related to MWI, (B) element enrichment and PAH ratios influenced by industrial emissions. For orientation sampling locations and outlines of city limits were provided, for more details see overlay transparency in the appendix (Fig. 62).

of industrial processes of the Cologne-North area from other industrial complexes is provided.

Biogenic iron concentrations The multi-proxy approach finally allows for an approximation of plant derived iron concentrations. The linear correlation trend between iron concentration in pine needles and bulk susceptibility gives the amount of diamagnetic iron on needles by intercept with the y-axis. This diamagnetic iron is supposed to represent the biological proportion of iron with on average $50 \mu\text{g g}^{-1}$ per needle and thus is in agreement with data given by Bargagli [11] or Giertych et al. [71] for unpolluted pine needles. In contrast, an exception must be made for needles sampled near lignite mining zones (Fig. 57e) that are supposed to be enriched with diamagnetic Fe due to contributions of lignite derived iron sulfides as discussed above.

4.5.4 Conclusion

A spatially high-resolved multi-proxy biomonitoring enables a detailed source characterization for traffic emissions, lignite industry, organic industry and municipal waste incineration in the Greater Cologne Conurbation. A spatial analysis employing isopleths maps of single pollutants and pollutant proxies was shown to lead to best results in source reconciliation. Finally, comparison of organic, enviromagnetic and trace elemental data allows a very detailed differentiation of sources: i) abrasive and combustion products in traffic utilizing Fe, Sb and CpcdPy; ii) a good correlation of aromatic DBT and fine dust proxy ARM from LFPP reveals a preferential appearance and transport of DBT in particle form in the atmosphere; iii) a combination of magnetic properties with elemental Fe and REE concentrations allow a closer look on mineral composition of lignite dust in the study area; iv) emissions from organic industry and municipal waste incineration are predominantly traceable via element loads on *Pinus nigra* needles, but comparison with PAH source diagnostic ratios reveals significant correlation, thus pointing at new applications for these ratios in industrial emission tracing.

Multi-proxy biomonitoring is highly recommended for source recognition, especially where informations about original source composition is vague, because analysis of samples directly at the source is restricted. Thus, for political decision makers a reliable source allocation is of major importance and can be achieved by multi-proxy biomonitoring.

5 Synthesis and outlook

Individual chapters of this thesis have provided summaries on the subject areas covered therein and chapter 4.5 already provided a synthesis of the results obtained for the regional scale study of the Greater Cologne Conurbation. Here a synthesis of all aspects addressed in the thesis is provided, followed by an outlook on future prospects of biomonitoring in atmospheric quality analysis.

The overall goal of the investigation was to evaluate the potential of biomonitoring in atmospheric quality of urbanized regions, and if positive results were obtained, to apply the technique to a case study in the area of Cologne, NW-Germany. Consequently, the reliability of biomonitoring techniques had to be verified first. Methods have been established to investigate air quality by the presence, the distribution and health appearance of indicator plants, in particular lichens. This approach does not allow for discrimination of stressors that have caused the detrimental effects on the indicator plants and thus was discarded. Plants utilized in this study serve as receptors or accumulators of atmospheric pollutants that after a period of exposure can be extracted from the plants and analyzed using appropriate techniques. Various plant types have been utilized in the past for such purposes and large national surveys of air quality have been conducted using mosses. Mosses, however, are difficult to date and in most cases do not allow normalization of pollutant concentration to atmospheric exposure time. Evergreen higher plants do allow for continuous pollutant monitoring over a full growth period and thus are superior to grasses, vegetables or deciduous trees used in previous studies. The Black or Austrian Pine (*Pinus nigra*) was selected as biomonitoring plant for the Greater Cologne Conurbation (GCC) based on excellent availability in the study area, robustness against environmental stress and the fact that up to 5 needle ages could be recovered. This feature allowed studying temporal accumulation trends in pine needle pollutants loads. Proof of systematic accumulation of air pollutants on pine needle surface is a pre-requisite for application in biomonitoring studies.

Feasibility of biomonitoring Chapter 2 of this thesis is devoted to the investigation of accumulation trends of air pollutants on and in pine needles. It outlines that plant physiological factors, e.g. wax or water content, plant substrate, e.g. soil type, climatic and morphological factors, e.g. elevation above sea level, wind stress, precipitation do not notably affect the bioreceptor potential of Black Pine for airborne pollutants. It became obvious though that a dynamic equilibrium between pollutant accumulation on plant surfaces and abrasion or erosion of plant surface waxes exists and that seasonal variation in pollutant loads exists. In order to compensate for such temporal trends, collection of pine needles used for air quality assessment should be done in a short period of days or maximum weeks. If done that way pine needle pollutant concentrations provide very reliable comparison between different sites and thus allow for identification of pollution hot-spots or pollution dispersal routes.

It becomes clear though that until present biomonitoring in the GCC has been restricted to relative assessment of pollution levels between sites whereas conversion of pine needle pollutant concentrations into those expected to occur in surrounding atmosphere (in mg m³ air) could not be achieved. Conversion of relative to abso-

lute pollutant concentrations has to be an ultimate goal in atmospheric biomonitoring but requires much larger efforts in terms of costly active air measurements in parallel to biomonitoring. This subject was clearly beyond the scope of this thesis but will need to be addressed in the future, if biomonitoring is taken to be implemented in environmental legislation.

In contrast to this shortcoming biomonitoring offers substantial advantages over active air filtering for pollutant determination. First of all, the atmosphere and in particular the boundary level represent extremely dynamic systems, where the determination of one factor or property at a given point in time by no means needs to be representative for longer time intervals in the order of weeks, month or years. Active air collection for subsequent analysis in most cases will not allow for continuous monitoring for budgetary and technical reasons. Furthermore, once a severe air pollution event already has taken place, it is extremely difficult or usually impossible to analyze the extent (spatially and intensity) of such an event in retrospect using active air sampling. In that sense all direct measurements will have to be replaced by proxy analyses. Biomonitoring is suitable to address such problems and provides information on temporal trends, if samples are taken in closely spaced time intervals to monitor variation, but also on the time-integrated degree of pollution at a given site. In the Cologne Conurbation, pollution levels predating collection time by up to 5 years were obtained with *Pinus nigra* needles.

Multi-proxy analysis Pine needles acquire a great variety of substances from the environment. Not all of those are regarded as pollutants but in fact may be essential nutrients required for optimum plant growth. If element concentrations of pine needles are determined, it is difficult to differentiate whether these elements have been acquired via root uptake or via atmospheric dry and wet deposition. In order to identify enrichment of a given element in plant needles parallel investigation of water-soluble and chelating element species in soil can be conducted. Particular enrichment of elements in soil can thus be corrected for when interpreting needle concentrations. This approach would have been very demanding in terms of analytical efforts and associated costs and could not be realized in this study. Alternatively, biogenic background values for pines were collected from the literature and pine needle element concentrations were referred to geogenic dusts loads by normalization to Upper Continental Crust (UCC) element composition. Using these two approaches, the anthropogenically derived element enrichment in pine needles could be determined and related to specific emission sources and distribution pathways.

For hydrophobic organic pollutants including the polycyclic aromatic hydrocarbons (PAH) root uptake is negligible and geogenic background values (e.g. due to natural fires or volcanic emissions) are extremely low. Concentration of these compounds in pine needles was thus unaffected by processes playing a dominant role for selected major and trace elements. However, due to the high vapor pressure of low molecular weight PAH their patterns are severely affected by plant/air and particle/air partitioning processes. Highly volatile PAH with molecular weight below 170 Daltons, e.g. fluorene, acenaphthene or acenaphthylene, thus have been excluded from the analyses. For source recognition a variety of PAH compositional patterns or signatures have been established, usually based on canonical ratios of compounds with comparable physico-

chemical properties. The latter is mandatory because fractionation upon transport and deposition dependent on physical properties may otherwise govern the source ratios. In addition, different water solubility, or in general bioavailability, affects PAH once they have accumulated on pine needles. Microbial degradation may thus selectively affect PAH concentration on pine needles, in particular for older needle cohorts with several years of exposure time. For specific PAH photo-oxidation plays an important role and longer term exposure to sunlight may notably affect the PAH composition. Although some of these processes will affect PAH attached to atmospheric particulates, differences between PAH obtained by air filtering and bioaccumulation may be encountered, complicating comparison of results gained from both approaches. PAH accumulation though affected by season trends was proven to be systematic in the GCC as demonstrated in chapter 2 and thus biomonitoring of this important class of atmospheric pollutants is feasible.

PAH are predominantly produced by incomplete combustion processes that in addition to refractory organic residuals will also emit iron-bearing spherulites into the atmosphere. A predominant phase of these iron oxide spherulites is represented by magnetite, a mineral of very strong magnetic susceptibility and characteristic environmental magnetic properties. Magnetite spherulites, their regular shape being evidence for formation from a drop of molten iron-oxide at high temperature combustion processes, were identified on pine needles by electron microscopy coupled to energy dispersive X-ray spectroscopy (REM-EDX). Environmental magnetic analysis of susceptibility and remanence properties provides a very sensitive and reliable technique requiring only small sample amounts as well as preparation and analysis time at simultaneously very low cost. Enviromagnetics are thus a very affordable tool in environmental pollution analyses of compounds that derive from combustion processes. It was shown in chapter 2 that the accumulation trends of PAH, iron and associated combustion derived elements and magnetic properties of needles co-vary. If sufficient calibration measurements of e.g. trace elements or PAH have been conducted for a given case study, enviromagnetics allow for very high spatiotemporal analyses of pollutants, thus enabling analyses of various needle cohorts per site, where otherwise for more costly analyses only average values can be determined.

Spatial analyses of airborne pollutants The atmospheric pollutant groups investigated in this study accumulate in a systematic and predictable process on and in pine needles. Their environmental fate and impact can thus be assessed in a time-integrated manner by biomonitoring at high spatiotemporal resolution. Systematic accumulation of pollutants on pine needles is a prerequisite for constructing isopleths maps of atmospheric pollutants for proper surveying of local or regional pollution maxima, for delineation of rural-urban gradients in atmospheric quality and for identification of dispersal routes from a given emission source.

In concert with known emission sources from environmental data bases or cadastres, it is possible to pinpoint pollution maxima and attribute those to registered emitters or in the case of spatial mismatch identify other, previously unknown or underestimated pollution sources. This approach of spatial matching of potential sources derived from land use data bases proved more efficient than allocation of pollutant distribution patterns to sources via application of statistical procedures. Factor analysis was shown

to be inefficient in differentiation of multiple emission sources that exhibit similar or even quasi-identical compositions in emitted pollutants. This is the case for a variety of combustion processes that all yield a similar spectrum of atmospheric pollutants. Intensive atmospheric mixing of near-ground air masses and variable sorption/desorption-processes of PAH additionally obscure original source patterns in pollutant composition before bioreceptors are able to capture and preserve the components. If at any location variable contributions of the same pollutant (e.g. a PAH or Fe) from more than two or three sources co-occur the factor analyses does not differentiate between the emitters. Factor analysis when carried out for merged sets of element, PAH and enviromagnetics data tended to group parameters according to analytical method applied rather than reflecting emissions sources. Based on the results for merged data sets it had to be concluded that statistical analyses does not reveal the power to provide guidelines for interpretation that are superior to manual inspection of isopleths maps and locations of known emitters. A combination of statistically useful information, bivariance plots of indicator compounds or ratios pre-assigned to emission sources and isopleth maps was successfully applied in source discrimination in particular on the regional scale level. This certainly had to be attributed to a wider range of potential emitters not present or less prominent in the local Cologne City study. Sources including combustion residues from lignite fueled power plants (LFPP), dust blow-out from open pit mines or mine tailings from former ore processing and fertilizer application in agricultural areas simply do not constitute a recognizable fraction of total emissions in central urban areas. On the contrary, differentiation of metal pollution signals derived from industrial processing and traffic could readily be achieved in Cologne City but proved more difficult to demonstrate for the regional study.

Allocation of pollutant sources Within the Greater Cologne Conurbation it became evident that on regional scale the by far dominant PAH source is combustion of lignite in power plants. The three major plants to the west of Cologne city consume on average about 65 million tons of lignite with an average carbon content of 60 % and are known to generate half of all the CO₂ emitted within the state of North Rhine-Westphalia. This study documents that the LFPP also prone to contribute about half of the PAH to the regional atmospheric PAH burden. The introduction of filters in LFPP smoke stacks has significantly reduced the sulfur oxide emissions from these sources and in conjunction with a concomitant reduction of sulfur in petrol and diesel has rendered the acid rain problem a minor issue in NW-Germany. However, the emission of organically bound sulfur, in particular as thioaromatic hydrocarbons like dibenzothiophene or naphthobenzothiophene is not affected by the LFPP filter systems. Due to a comparably low pyrite/marcasite concentration of lignite from the Rhenish lignite mining district, the thioaromatic hydrocarbon emission remain only slightly enhanced but still exceed those determined for inner cities. This example demonstrates that though substantial improvement of air quality due to environmental regulation and legislation of power plant emissions has been achieved, unresolved or potentially even unrecognized problems still exist.

The regional study further revealed that beside combustion related emissions from LFPP large scale detrimental effects of dust blow-out from open pit mines constitute an important environmental issue. Fine dust particulates originating from open pit

mining could be mapped as a plume of some tens of kilometers in diameter. The potential hazardous pollutants associated with these mining dust particles thus will affect the health of the population in an area of some 400 to 800 km².

Regional pollutant mapping unraveled the presence of atmospheric pollutants that are commonly underestimated or neglected in terms of occurrence and influence. The element iron constitutes such an underestimated pollutant and it has only become evident in the most recent time that iron constitutes a major proportion of ultrafine traffic-derived dust collected in tunnels and co-varied with traffic-derived lead, is released as ultrafine particles upon iron and steel processing (e.g. iron foundry operations, drilling and grinding), and in particular uptake of its bioavailable species in epidemiological studies correlates with human diseases. In the GCC study conducted here, substantial enrichment of Fe after normalization to UCC was noted for inner city regions, especially in Cologne. The maximum in Fe concentration correlated well with Sb, a marker for traffic-related brake abrasion, and concentration of cyclopenta[cd]pyrene, a PAH marker diagnostic for traffic emission. This strongly suggests that Fe is at least particularly associated with health-relevant traffic emissions.

Such a conclusion immediately raises the question about the relative contribution of various Fe-sources to the pine needle Fe budget. The multiple analytical approaches used in this study allows to differentiate biogenic iron by its paramagnetic properties and geogenic dust derived component via normalization to UCC, leaving the remaining Fe fraction being released by anthropogenic processes, mainly industrial activities and traffic. The strong correlation of Fe with other traffic indicator proxies points towards a dominantly traffic-associated source for anthropogenic iron. The attribution of pine needle Fe to various sources could only be achieved due to the multiproxy approach exercised in this investigation.

Future investigations Application of several and preferably independent analytical techniques to an environmental problem in general is accompanied by knowledge gain. However, in this study a reliable interpretation of factors controlling atmospheric quality in the Cologne area would have been impossible, if only one out of several analytical approaches would have been chosen. The techniques applied proved to serve well for pollutants occurring in or being adsorbed predominantly to the particulate phase. A number of atmospheric pollutants, however, do occur in the gas phase and due to inherent problems of uptake and revolatilization, biomonitoring of such compounds does not comprise a preferred method of choice in spatiotemporal analyses of air quality. Nevertheless, preliminary investigations of pine needle biomass for its isotopic composition offered promising results. The $\delta^{13}\text{C}$ -composition of needles was depleted in urban areas, where fossil fuel derived CO₂ of light isotopic composition is utilized upon photosynthesis. These results were further supported by reduced levels of ¹⁴C in needle photosynthate, again caused by contributions of ¹⁴C-free fossil fuel derived CO₂. Nitrogen isotopic composition of pine needles was further shown to be affected by traffic-related emission of NO₂ in urban areas. The preliminary results obtained here clearly indicate the high additional resolving power of isotopes for source allocation in polluted urban areas. In addition to the improved differentiation potential derived from gaseous pollutants, first investigations of platinum group element distribution in pine needles offered promising results. In combination with traffic indicators already

established in this study and supplemented by isotope source characterization a constantly improving set of discrimination tools can be developed in biomonitoring studies. The preliminary investigations initiated, though they clearly went beyond the scope of this thesis, should be pursued in future studies to achieve an ultimate refinement of air quality assessment in the Greater Cologne Conurbation.

Acknowledgements

I thank my supervisor Prof. Dr. L. Schwark for suggestion of the topic and for giving me the possibility to learn from his great experience. He supported my work with many ideas, a lot of time for discussions and a never ending enthusiasm. His help in the time of research, writing publications and during writing this thesis deeply encouraged me.

I want to thank Prof. Dr. Y. Shao for reviewing this thesis.

I am very thankful to Dr. Michael Urvat for guiding me through the enviromagnetic parts of my work and a lot of productive discussions.

I thank Ulrich Flenker, Frank Hülsemann (Deutsche Sporthochschule Köln) and Christian Ostertag-Henning (BGR) for measuring N-isotopes, Dr. M. Thönnessen and Oliver Paech for AAS analytics, Prof. Dr. G. Bareth and Dr. Hannes Hamhaber (Geographical Institute, University of Cologne) for support with the geoinformationsssystem, Hanna Ciescynski for operating the REM and Dominik Hetzel for introduction to the mikroprobe.

Special thanks to my colleagues Nicole Juraschek, Guido Lars Bruno Wiesenberg, Birgit Nabbefeld and Oli Paech, who helped me in all the time of the work with stimulating ideas.

My deepest thanks to my family Markus, Judith, and my parents for every-time support and a lot of patience.

References

- [1] Abfallentsorgungs- und Verwertungsgesellschaft, Köln. Emissionswerte. www.avgkoeln.de, 2008.
- [2] J. Aboal, J. Fernandez, and A. Carballeira. Oak leaves and pine needles as biomonitors of airborne trace elements. *Environmental and Experimental Botany*, 51:215–225, 2004.
- [3] H. Aichinger. Introduction - The IPPC Directive. In *The Sevilla process. A driver for Environmental Performance in Industry*. Stuttgart, 2000.
- [4] A. Aksoy. *Eleagnus angustifolia* L. as a biomonitor of trace element pollution. *Turkish Journal of Botany*, 23:83–87, 1999.
- [5] M.G. Alaimo, G. Dongarra, M.R. Melati, F. Monna, and D. Varrica. Recognition of environmental trace metal contamination using pine needles as bioindicators. The urban area of Palermo (Italy). *Environmental Geology*, 39:914–924, 2000.
- [6] M.C.M. Alvim-Ferraz and S.A.V. Afonso. Incineration of different types of medical wastes: emission factors for particulate matter and heavy metals. *Environmental Science and Technology*, 37:3152–3157, 2003.
- [7] J. Bäck, M. Turunen, A. Ferm, and S. Huttunen. Needle structures and epiphytic microflora of Scots pine (*Pinus sylvestris* L.) under heavy ammonia deposition from fur farming. *Water, Air and Soil Pollution*, 100:119–132, 1997.
- [8] S.O. Baek, R.A. Field, M.E. Goldstone, P.W. Kirk, J.N. Lester, and R. Perry. A review of atmospheric polycyclic aromatic hydrocarbons: sources, fate and behaviour. *Water, Air and Soil Pollution*, 60:279–300, 1991.
- [9] M.I. Bakker, J. Tolls, and C. Kollöffel. Deposition of atmospheric semivolatile compounds to vegetation. In R.L. Lipnick, J.L.M. Hermens, K.C. Jones, and D.C.G. Muir, editors, *Persistent, Bioaccumulative and Toxic Chemicals I - Fate and Exposure*, 772, pages 218–236. ACS Symposium, 2001.
- [10] M.I. Bakker, M. Vorenhout, D.T.H.M. Sijm, and C. Kollöffel. Dry deposition of atmospheric polycyclic aromatic hydrocarbons in three *Plantago* species. *Environmental Toxicology and Chemistry*, 18:2289–2294, 1999.
- [11] R. Bargagli. *Trace elements in terrestrial plants - an ecophysiological approach to biomonitoring and biorecovery*. Springer, London, Heidelberg, 1998.
- [12] P. Baumard, H. Budzinski, P. Garrigues, H. Dizer, and P.D. Hansen. Polycyclic aromatic hydrocarbons in recent sediments and mussels (*Mytilus edulis*) from the Western Baltic Sea: occurrence, bioavailability and seasonal variations. *Marine Environmental Research*, 47:17–47, 1999.
- [13] K.P. Beckett, P.H. Freer-Smith, and G. Taylor. Particulate pollution capture by urban trees: effect of species and windspeed. *Global Change*, 6:995–1003, 2000.

- [14] B.A. Benner and G.E. Gordon. Mobile sources of atmospheric polycyclic aromatic hydrocarbons: a roadway tunnel study. *Environmental Science and Technology*, 23:1269–1278, 1989.
- [15] B.A. Benner, S.A. Wise, L.A. Currie, G.A. Klouda, and D.B. Klinedinst. Distinguishing the contributions of residential wood combustion and mobile source emissions using relative concentrations of dimethylphenanthrene isomers. *Environmental Science and Technology*, 29:2382–2389, 1995.
- [16] J. Berlekamp, U. Herpin, M. Matthies, H. Lieth, B. Markert, V. Weckert, B. Wolterbeek, T. Verburg, H.-J. Zinner, and U. Siewers. Geographic classification of trace element concentrations in mosses and stream sediments in the Federal Republic of Germany. *Water, Air and Soil Pollution*, 101:177–195, 1998.
- [17] Berlin Senate Department of Urban Development. *Bioindicators*. Berlin Digital Environmental Atlas, www.stadtentwicklung.berlin.de/umwelt/umweltatlas/, 1991.
- [18] A. Beyer, F. Wania, T. Gouin, D. Mackay, and M. Matthies. Temperature dependence of the characteristic travel distance. *Environmental Science and Technology*, 37:766–771, 2003.
- [19] W. Birmili, A.G. Allen, F. Bary, and R.M. Harrison. Trace metal concentrations and water solubility in size-fractionated atmospheric particles and influence of road traffic. *Environmental Science and Technology*, 40:1144–1153, 2006.
- [20] A. Björseth and T. Ramdahl. Sources and emissions of PAH. In A. Björseth and T. Ramdahl, editors, *Handbook of Polycyclic Aromatic Hydrocarbons*, pages 1–20. Marcel Dekker, New York, 1985.
- [21] J. Bloemendahl, J.W. King, F.R. Hall, and S.-J. Doh. Rock magnetism of late Neogen and Pleistocene deep-sea sediments: Relationship to source, diagenetic processes and sediment lithology. *Journal of Geophysical Research*, 97:4361–4375, 1992.
- [22] Stadtwerke Bonn. MVA Müllverwertungsanlage Bonn. www.stadtwerke-bonn.de, 2006.
- [23] M.L. Bosco, D. Varrica, and G. Dongarra. Case study: Inorganic pollutants associated with particulate matter from an area near a petrochemical plant. *Environmental Research*, 99:18–33, 2005.
- [24] C.E. Boström, P. Gerde, A. Hanberg, B. Jernström, C. Johansson, T. Kyrklund, A. Rannug, M. Törnqvist, K. Victorin, and R. Westerholm. Cancer risk assessment, indicators, and guidelines for polycyclic aromatic hydrocarbons in the ambient air. *Environmental Health Perspectives*, 110, Supplement 3:451–488, 2002.

- [25] R. Bradshaw and R. Thompson. The use of magnetic measurements to investigate the mineralogy of icelandic sediments and to study catchment processes. *Boreas*, 14:203–215, 1985.
- [26] W. Brücher and M. Kerschgens. Simulation of concentration statistics with an Eulerian model - relevance of several factors to quality of results. *Metereologische Zeitschrift*, 10:247–252, 2001.
- [27] H. Budzinski, I. Jones, C. Pierard, and P. Garrigues. Evaluation of sediment contamination by polycyclic aromatic hydrocarbons in the Gironde estuary. *Marine Chemistry*, 58:85–97, 1997.
- [28] A. Bytnerowitz and M. Turunen. Effects of ozone exposures on epicuticular wax of Ponderosa Pine needles. In K.E. Percy, J.N. Cape, R. Jagels, and C.J. Simpson, editors, *Air pollutants and the leaf cuticle*, volume 36 of *Series G, Ecological Sciences*, pages 305–314. NATO ASI, 1994.
- [29] D. Calamari, E. Bacci, S. Focardi, C. Gaggi, M. Morosini, and M. Vighi. Role of plant biomass in the global environmental partitioning of chlorinated hydrocarbons. *Environmental Science and Technology*, 25:1489–1495, 1991.
- [30] E. Callender and K.C. Rice. The urban environmental gradient: anthropogenic influences on the spatial and temporal distributions of lead and zinc in sediments. *Environmental Science and Technology*, 34:232–238, 2000.
- [31] W. Calmano. *Untersuchung und Bewertung von Sedimenten - ökotoxikologische und chemische Testmethoden*. Springer, 2001.
- [32] D. Ceburnis and E. Steinnes. Conifer needles as biomonitors of atmospheric trace element deposition: comparison with mosses and precipitation, role of the canopy. *Atmospheric Environment*, 34:4265–4271, 2000.
- [33] S.N. Chillrud, R.F. Bopp, H.J. Simpson, J.M. Ross, E.L. Shuster, D.A. Chaky, D.C. Walsh, C.C. Choy, L.-R. Tolley, and A. Yarme. Twentieth century atmospheric metal fluxes into Central Park Lake, New York City. *Environmental Science and Technology*, 33:657–662, 1999.
- [34] M. Coskun. Toxic metals in the austrian pine (*Pinus nigra*) bark in the Thrace region, Turkey. *Environmental Monitoring and Assessment*, 121:173–179, 2006.
- [35] T.B. Councell, K.U. Duckenfield, E.R. Landa, and E. Callender. Tire-wear particles as a source of zinc to the environment. *Environmental Science and Technology*, 38:4206–4214, 2004.
- [36] J. Couto, J. Fernandez, J. Aboal, and A. Carballeira. Annual variability in heavy-metal bioconcentration in moss: sampling protocol optimization. *Atmospheric Environment*, 37:3517–3527, 2003.

- [37] L. Culotta, A. Gianguzza, and S. Orecchio. Leaves of *Nerium oleander* L. as bioaccumulators of polycyclic aromatic hydrocarbons (PAH) in the air of Palermo (Italy): extraction and GC-MS analysis, distribution and sources. *Polycyclic Aromatic Compounds*, 25:327–344, 2005.
- [38] D. Cuny, C. van Haluwyn, and R. Pesch. Biomonitoring of trace elements in air and soil compartments along the major motorway in France. *Water, Air and Soil Pollution*, 125:273–289, 2001.
- [39] D.A. Davidson, A.C. Wilkinson, and J.M. Blais. Orographic cold-trapping of persistent organic pollutants by vegetation in mountains of Western Canada. *Environmental Science and Technology*, 37:209–215, 2003.
- [40] B.M. Didyk, B.R.T. Simoneit, L.A. Pezoa, M.L. Riveros, and A.A. Flores. Urban aerosol particles of Santiago, Chile: organic content and molecular characterization. *Atmospheric Environment*, 34:1167–1179, 2000.
- [41] C. Dietl, W. Reifenhäuser, and L. Peichl. Association of antimony with traffic - occurrence in airborne dust, deposition and accumulation in standardized grass cultures. *The Science of the Total Environment*, 205:235–244, 1997.
- [42] M. Dimashki, L.H. Lim, R.M. Harrison, and S. Harrad. Temporal trends, temperature dependence, and relative reactivity of atmospheric polycyclic aromatic hydrocarbons. *Environmental Science and Technology*, 35:2264–2267, 2001.
- [43] DoH. Non-biological particles and health. *The committee on the Medical aspects of Air Pollution*, 1995.
- [44] G. Dongarra, D. Varrica, and G. Sabatino. Occurrence of platinum, palladium and gold in pine needles of *Pinus pinea* L. from the city of Palermo (Italy). *Applied Geochemistry*, 18:109–116, 2003.
- [45] D.L. Dowdy and T.E. McKone. Predicting plant uptake of organic chemicals from soil or air using octanol/water and octanol/air partition ratios and a molecular connectivity index. *Environmental Toxicology and Chemistry*, 16:2448–2456, 1997.
- [46] D.J. Dunlop and Ö. Özdemir. *Rock magnetism - Fundamentals and Frontiers*. Cambridge University Press, Cambridge, 1997.
- [47] G. Eriksson, S. Jensen, H. Kylin, and W. Strachan. The pine needle as a monitor of atmospheric pollution. *Nature*, 341:42–44, 1989.
- [48] W. Esteve, H. Budzinski, and E. Villenave. Relative rate constants for the heterogeneous reactions of NO₂ and OH radicals with polycyclic aromatic hydrocarbons adsorbed on carbonaceous particles. Part 2: PAHs adsorbed on diesel particulate exhaust SRM 1650a. *Atmospheric Environment*, 40:201–211, 2006.
- [49] European Community. EC Directive 1996/92/EC relating to the monitoring and the evaluation of ambient air quality. Brussels, 1996.

- [50] European Community. EC Directive 1999/30/EC relating to limit values for SO₂, NO₂ and NO_x, particulate matter, lead in ambient air. Brussels, 1999.
- [51] G.-C. Fang, Y.-Sh. Wu, C.-N. Chang, and T.-T. Ho. A study of polycyclic aromatic hydrocarbons concentrations and source identifications by methods of diagnostic ratio and principal component analysis at Taichung chemical Harbor near Taiwan Strait. *Chemosphere*, 64:1233–1242, 2006.
- [52] Federal Environmental Agency, Germany. *Environmental Specimen Bank*. www.umweltbundesamt.de, 2004.
- [53] A. Feilberg, M.W.B. Poulsen, T. Nielsen, and H. Skov. Occurrence and sources of particulate nitro-polycyclic aromatic hydrocarbons in ambient air in Denmark. *Atmospheric Environment*, 35:353–366, 2001.
- [54] M.B. Fernandes and P. Brooks. Characterization of carbonaceous combustion residues: II. Nonpolar organic compounds. *Chemosphere*, 53:447–458, 2003.
- [55] J. A. Fernandez and A. Carballeira. A comparison of indigenous mosses and topsoils for use in monitoring atmospheric heavy metal deposition in Galicia (northwest Spain). *Environmental Pollution*, 114:431–441, 2001.
- [56] R. Fertmann, I. Tesseraux, M. Schürmann, and H. Neus. Evaluation of ambient air concentrations of polycyclic aromatic hydrocarbons in Germany from 1990 to 1998. *Journal of Exposure Analysis and Environmental Epidemiology*, 12:115–123, 2002.
- [57] S. Fink. Die Koniferennadel - Strukturelle Aspekte gesunder und geschädigter Nadelblätter. *Naturwissenschaften*, 83:448–458, 1996.
- [58] P.J. Flanders. Identifying fly ash at a distance from fossil fuel power stations. *Environmental Science and Technology*, 33:528–532, 1999.
- [59] V.R. Franceschi and P.A. Nakata. Calcium oxalate in plants: formation and function. *Annual Reviews of Plant Biology*, 56:41–71, 2006.
- [60] J. Franzaring. Temperature and concentration effects in biomonitoring of organic air pollutants. *Environmental Monitoring and Assessment*, 46:209–220, 1997.
- [61] J. Franzaring and L.J.M. van der Erden. Accumulation of airborne persistent organic pollutants (POPs) in plants. *Basic and Applied Ecology*, 1:25–30, 2000.
- [62] P.H. Freer-Smith, K.P. Beckett, and G. Taylor. Deposition velocities to *Sorbus aria*, *Acer campestre*, *Populus deltoides* X *trichocarpa* “beaupre”, *Pinus nigra* and *X Cupressocyparis leylandii* for coarse, fine and ultra-fine particles in the urban environment. *Environmental Pollution*, 133:157–167, 2005.
- [63] A. Galuszka. The chemistry of soils, rocks and plant indicators in three ecosystems of the Holy Cross Mountains, Poland. *Environmental Monitoring and Assessment*, 110:55–70, 2005.

- [64] B.D. Garg, S.H. Cadle, P.A. Mulawa, P.J. Groblicki, C. Laroo, and G.A. Parr. Brake wear particulate matter emissions. *Environmental Science and Technology*, 34:4463–4469, 2000.
- [65] P. Garrigues, H. Budzinski, M.P. Manitz, and S.A. Wise. Pyrolytic and petrogenic inputs in recent sediments: a definitive signature through phenanthrene and chrysene compound distribution. *Polycyclic Aromatic Hydrocarbons*, 7:275–284, 1995.
- [66] P. Gautam, U. Blaha, and E. Appel. Magnetic susceptibility of dust-loaded leaves as a proxy of traffic-related heavy metal pollution in Kathmandu city, Nepal. *Atmospheric Environment*, 39:2201–2211, 2005.
- [67] M.D. Geller, S.B. Sardar, H. Phuleria, P.M. Fine, and C. Sioutas. Measurements of particle number and mass concentrations and size distributions in a tunnel environment. *Environmental Science and Technology*, 39:8653–8663, 2005.
- [68] Geologischer Dienst NRW. Geowissenschaftliche Gemeindebeschreibungen NRW. www.gd.nrw.de, 2008.
- [69] German remote sensing data center. CORINE land cover. www.corine.dfd.dlr.de, 2008.
- [70] M. Giertych, L. De Temmerman, and L. Rachwal. Distribution of elements along the length of Scots pine needles in a heavily polluted and a control environment. *Tree Physiology*, 17:697–703, 1997.
- [71] M.J. Giertych, P. Karolewski, and L.O. de Temmermann. Foliage age and pollution alter content of phenolic compounds and chemical elements in *Pinus nigra* needles. *Water, Air and Soil Pollution*, 110:363–377, 1999.
- [72] C.L. Gigliotti, L.A. Totten, J.H. Offenbergl, J. Dachs, J.R. Reinfelder, E.D. Nelson, T.R. Glenn, and S.J. Eisenreich. Atmospheric concentrations and deposition of polycyclic aromatic hydrocarbons to the mid-atlantic east coast region. *Environmental Science and Technology*, 39:5550–5559, 2005.
- [73] A. I. Gogou, M. Apostolaki, and E.G. Stephanou. Determination of organic molecular markers in marine aerosols and sediments: one-step flash chromatography compound class fractionation and capillary gas chromatographic analysis. *Journal of Chromatography A*, 799:215–231, 1998.
- [74] M.B. Goldhaber, E. Callender, and R. Reynolds. The geochemical and magnetic record of coal-combustion products in West Virginia reservoir sediments and soils. In R.J. Hill, Z. Aizenshtat, M.J. Baedeker, G. Claypool, R. Eganhouse, M. Goldhaber, J. Leventhal, and K. Peters, editors, *Geochemical Investigation in Earth and Space Science*, volume Publication No. 6, pages 159–186. The Geochemical Society, 2004.

- [75] W.S. Gratton, K.K. Nkongolo, and G.A. Spiers. Heavy metal accumulation in soil and Jack Pine (*Pinus banksiana*) needles in Sudbury, Ontario, Canada. *Bulletin of Environmental Contamination and Toxicology*, 64:550–557, 2000.
- [76] J.O. Grimalt, B.L. vanDrooge, A. Ribes Pilar Fernandez, and P. Appleby. Polycyclic aromatic hydrocarbon composition in soils and sediments of high altitude lakes. *Environmental Pollution*, 131:13–24, 2004.
- [77] G. Grimmer, J. Jacob, K.W. Naujack, and G. Dettbarn. Determination of polycyclic aromatic compounds emitted from brown-coal-fired residential stoves by gaschromatography/mass spectrometry. *Analytical Chemistry*, 55:892–900, 1983.
- [78] P.M. Gschwend and R. Hites. Fluxes of the polycyclic aromatic compounds to marine and lacustrine sediments in the northeastern United States. *Geochimica et Cosmochimica Acta*, 45:2359–2367, 1981.
- [79] E.M. Gstoettner and N.S. Fisher. Accumulation of cadmium, chromium and zinc by the moss *Sphagnum papillosum* lindle. *Water, Air and Soil Pollution*, 93:321–330, 1997.
- [80] K.E. Gustafson and R.M. Dickhut. Particle/gas concentrations and distributions of PAHs in the atmosphere of Southern Chesapeake Bay. *Environmental Science and Technology*, 31:140–147, 1997.
- [81] C. Hagner. *Historical review of European gasoline lead content regulations and their impact on German industrial markets*. Geesthacht, GKSS Research Centre, report no. 99/E/30, 1999.
- [82] M. Hanesch, R. Scholger, and D. Rey. Mapping dust distribution around an industrial site by measuring magnetic parameters of tree leaves. *Atmospheric Environment*, 37:5125–5133, 2003.
- [83] H. Harmens, A. Buse, P. Büker, D. Norris, G. Mills, B. Williams, B. Reynolds, T.W. Ashenden, A. Rühling, and E. Steinnes. Heavy metal concentrations in european mosses: 2000/2001 survey. *Journal of Atmospheric Chemistry*, 49:425–436, 2004.
- [84] S. Harrad, S. Hassoun, M.S. Romero, and R.M. Harrison. Characterisation and source attribution of the semi-volatile organic content of atmospheric particles and associated vapour phase in Birmingham, UK. *Atmospheric Environment*, 37:4985–4991, 2003.
- [85] R.M. Harrison, A.R. Deacon, M.R. Jones, and R.S. Appleby. Sources and processes affecting concentrations of PM₁₀ and PM_{2.5} particulate matter in Birmingham (UK). *Atmospheric Environment*, 31:4103–4117, 1997.
- [86] R.M. Harrison, R. Tilling, M.S. Callen Romero, S. Harrad, and K. Jarvis. A study of trace metals and polycyclic aromatic hydrocarbons in the roadside environment. *Atmospheric Environment*, 37:2391–2402, 2003.

- [87] R.M. Harrison and J. Yin. Particulate matter in the atmosphere: which particle properties are important for its effects on health? *The Science of the Total Environment*, 249:85–101, 2000.
- [88] K.L. Hay, J.A. Dearing, S.M.J. Baban, and P. Loveland. A preliminary attempt to identify atmospherically derived pollution particles in English topsoils from magnetic susceptibility measurements. *Physics and Chemistry of the Earth*, 22:207–210, 1997.
- [89] F. Heider, A. Zitzelsberger, and K. Fabian. Magnetic susceptibility and remanent coercive force in grown magnetite crystals from 0.1 μm to 6 mm. *Physics of the earth and Planetary Interiors*, 93:239–256, 1996.
- [90] D. Hjortenkrans, B. Bergbäck, and A. Häggerud. New metal emission patterns in road traffic environments. *Environmental Monitoring and Assessment*, 117:85–98, 2006.
- [91] V. Hoffmann, M. Knab, and E. Appel. Magnetic susceptibility mapping of roadside pollution. *Journal of Geochemical Exploration*, 66:313–326, 1999.
- [92] I. Holoubek, P. Korinek, Z. Seda, E. Schneiderova, I. Holoubkova, A. Pacl and J. Triska, P. Cudlin, and J. Caslavsky. The use of moss and pine needles to detect persistent organic pollutants at local and regional scales. *Environmental Pollution*, 109:283–292, 2000.
- [93] M. Horstmann and M.S. McLachlan. Atmospheric deposition of semivolatile organic compounds to two forest canopies. *Atmospheric Environment*, 32:1799–1809, 1998.
- [94] J. Hovorka and G. Marshall. Determination of As, Cd, and Pb in epicuticular waxes of pine and spruce needles by ETAAS. *Fresenius Journal of Analytical Chemistry*, 358:635–640, 1997.
- [95] X.D. Huang, I. Olmez, N.K. Aras, and G.E. Gordon. Emissions of trace-elements from motor-vehicles - potential marker elements and source composition profile. *Atmospheric Environment*, xx:X.D.1385–1391, 1994.
- [96] H.-M. Hwang, T.L. Wade, and J.L. Sericano. Concentrations and source characterization of polycyclic aromatic hydrocarbons in pine needles from Korea, Mexico, and United States. *Atmospheric Environment*, 37:2259–2267, 2003.
- [97] S.B. Idso, C.D. Idso, and R.C. Balling. An intensive two-week study of an urban CO₂ dome in Phoenix, Arizona, USA. *Atmospheric Environment*, 35:995–1000, 2001.
- [98] S.B. Idso, C.D. Idso, and R.C. Balling. Seasonal and diurnal variations of near-surface atmospheric CO₂ concentration within a residential sector of the urban CO₂ dome of Phoenix, AZ, USA. *Atmospheric Environment*, 36:1655–1660, 2002.

- [99] Intergovernmental Panel on Climate Change IPCC, WMO/UNEP. Climate Change 2007. www.ipcc.ch, 2007.
- [100] J. Jacob, G. Grimmer, and A. Hildebrandt. Long-term decline of atmospheric and marine pollution by polycyclic aromatic hydrocarbons (PAHs) in Germany. *Chemosphere*, 34:2099–2108, 1997.
- [101] L. Järup. Hazards of heavy metal contamination. *British Medical Bulletin*, 68:167–182, 2003.
- [102] S. Jensen, G. Eriksson, H. Kylin, and W. Strachan. Atmospheric pollution by persistent organic compounds: Monitoring with pine needles. *Chemosphere*, 24:229–245, 1992.
- [103] N.V. Jordanova, D.V. Jordanova, L. Veneva, K. Yorova, and E. Petrovsky. Magnetic response of soils and vegetation to heavy metal pollution - a case study. *Environmental Science and Technology*, 37:4417–4424, 2003.
- [104] Y. Kang and D. Lee. Epithermal neutron activation analysis of bark, pine-needle, and moss for environmental pollution monitoring in Pusan and Kyungnam. www.atom.kaeri.re.kr/ndel/NDPE01/yस्कang.pdf, 2001.
- [105] H. Kaupp, M. Blumenstock, and M.S. McLachlan. Retention and mobility of atmospheric particle-associated organic pollutant PCDD/Fs and PAHs in maize leaves. *New Phytology*, 148:473–480, 2000.
- [106] G. Kerstiens. *Plant cuticles - an integrated functional approach*. BIOS, 1996.
- [107] C. Kessler, W. Brücher, M. Memmesheimer, M. Kerschgens, and A. Ebel. Simulation of air pollution with nested models in North Rhine-Westphalia. *Atmospheric Environment*, 35, Supplement No. 1:S3–S12, 2001.
- [108] N. Khalili, P. Scheff, and T. Holsen. PAH source fingerprints for coke ovens, diesel and gasoline engines, highway tunnels and wood combustion emissions. *Atmospheric Environment*, 29:533–542, 1995.
- [109] G. Kletetschka, V. Zila, and P.J. Wasilewski. Magnetic anomalies on the tree trunks. *Studia Geophysica et Geodaetica*, 47:371–379, 2003.
- [110] A. Klumpp, T. Hintemann, J.S. Lima, and E. Kandeler. Bioindication of air pollution effects near a copper smelter in Brazil using mango trees and soil microbiological properties. *Environmental Pollution*, 126:313–321, 2003.
- [111] G.N. Koptsik, S.V. Koptsik, and D. Aamlid. Pine needle chemistry near a large point SO₂ source in Northern Fennoscandia. *Water, Air and Soil Pollution*, 130:929–934, 2001.
- [112] M. Krachler, J. Zheng, R. Koerner, C. Zdanowicz, D. Fisherb, and W. Shotyk. Increasing atmospheric antimony contamination in the northern hemisphere: snow and ice evidence from Devon Island, Arctic Canada. *Journal of Environmental Monitoring*, 7:169–1176, 2005.

- [113] P. Kruiver and H. Passier. Coercitivity analysis of magnetite phases in sapropel S1 related to variations in redox conditions, including an investigation of the S ratio. *Geochemistry, Geophysics, Geosystems*, 2:1525–2027, 2001.
- [114] H. Kylin. *Airborne lipophilic pollutants in pine needles*. PhD thesis, Stockholm University, Sweden, ISBN 91-7153-197-1, 1994.
- [115] H. Kylin and A. Sjödin. Accumulation of airborne hexachlorocyclohexanes and DDT in Pine needles. *Environmental Science and Technology*, 37:2350–2355, 2003.
- [116] H. Kylin, K. Söderkvist, A. Undemann, and R. Franch. Seasonal variation of the terpene content, an overlooked factor in the determination of environmental pollutants in pine needles. *Bulletin of Environmental Contamination and Toxicology*, 68:155–160, 2002.
- [117] Landesumweltamt Nordrhein-Westfalen. *Emissionsbericht 1996/97*. Land Nordrhein-Westfalen, 1997.
- [118] LANUV, Landesamt für Natur, Umwelt und Verbraucherschutz, NRW. Emission Register. www.gis.nrw.de, 2004.
- [119] R.K. Larsen and J.E. Baker. Source apportionment of polycyclic aromatic hydrocarbons in the urban atmosphere: a comparison of three methods. *Environmental Science and Technology*, 37:1873–1881, 2003.
- [120] E.B. Ledesma, M.A. Kalish, P.F. Nelson, M.J. Wornat, and J.C. Mackie. Formation and fate of PAH during the pyrolysis and fuel-rich combustion of coal primary tar. *Fuel*, 79:1801–1814, 2000.
- [121] J.Y. Lee, Y.P. Kim, C.-H. Kang, Y.S. Ghim, and N. Kaneyasu. Temporal trend and long-range transport of particulate polycyclic aromatic hydrocarbons at Gosan in northeast Asia between 2001 and 2004. *Journal of Geophysical Research*, 111:doi:10.1029/2005JD006537, 2006.
- [122] M. Legret, L. Odie, D. Demare, and A. Jullien. Leaching of heavy metals and polycyclic aromatic hydrocarbons from reclaimed asphalt pavement. *Water Research*, 39:3675–3685, 2005.
- [123] E. Lehndorff and L. Schwark. Biomonitoring of air quality in the Cologne Conurbation using pine needles as a passive sampler – Part II: polycyclic aromatic hydrocarbons (PAH). *Atmospheric Environment*, 38:3793–3808, 2004.
- [124] E. Lehndorff and L. Schwark. Accumulation behavior of airborne parent and alkyl three-ring PAH on pine needles. *Environmental Pollution*, in review, 2008.
- [125] E. Lehndorff and L. Schwark. Accumulation histories of major and trace elements on pine needles in the Cologne Conurbation as function of air quality. *Atmospheric Environment*, 42:833–845, 2008.

- [126] E. Lehndorff, M. Urvat, and L Schwark. Accumulation histories of magnetic particles on pine needles as function of air quality. *Atmospheric Environment*, 40:7082–7096, 2006.
- [127] V. Librando, G. Perrini, and M. Tomasello. Biomonitoring of atmospheric PAHs by evergreen plants: correlations and applicability. *Polycyclic Aromatic Compounds*, 22:549–559, 2002.
- [128] H.L. Lim, R.M. Harrison, and S. Harrad. The contribution of traffic to atmospheric concentrations of polycyclic aromatic hydrocarbons. *Environmental Science and Technology*, 33, 3538-3542.
- [129] A.L. Lima, T.I. Eglinton, and C.M. Reddy. High-resolution record of pyrogenic polycyclic aromatic hydrocarbon deposition during the 20th century. *Environmental Science and Technology*, 37:53–61, 2003.
- [130] A. Lindgren. Asphalt wear and pollution transport. *The Science of the Total Environment*, 189/190:281–286, 1996.
- [131] G. Locke and K.K. Bertine. Magnetite in sediments as an indicator of coal combustion. *Applied Geochemistry*, 1:345–356, 1986.
- [132] M. Lodenius. Seasonal variations in cadmium concentrations of plant leaves. *Bulletin of Environmental Contamination and Toxicology*, 69:320–322, 2002.
- [133] M. Lodovici, V. Casalini, C. Zappa, and P. Dolara. Polycyclic aromatic hydrocarbons in *Laurus nobilis* leaves as a measure of air pollution in urban and rural sites of Tuscany. *Chemosphere*, 36:1703–1712, 1998.
- [134] J. Loponen, K. Lempa, V. Ossipov, M.V. Kozlov, A. Girs, K. Hangasmaa, E. Haukioja, and K. Pihlaja. Patterns in content of phenolic compounds in leaves of mountain birches along a strong pollution gradient. *Chemosphere*, 45:291–301, 2001.
- [135] G.C. Lough, J.J. Shauer, J.-S. Park, M.M. Shafer, J.T. Deminter, and J.P. Weinstein. Emissions of metals associated with motor vehicle roadways. *Environmental Science and Technology*, 39:826–836, 2005.
- [136] P. Madejon, T. Maranon, and J.M. Murillo. Biomonitoring of trace elements in the leaves and fruits of wild olive and holm oak trees. *Science of the Total Environment*, 355:187–203, 2006.
- [137] B. Maher, C. Mooreb, and J. Matzka. Spatial variation in vehicle-derived metal pollution identified by magnetic and elemental analysis of roadside tree leaves. *Atmospheric Environment*, 42:364–373, 2008.
- [138] M. Malawska and B. Wilkomirski. An analysis of soil and plant (taraxacum officinale) contamination with heavy metals and polycyclic aromatic hydrocarbons (PAHs) in the area of the railway junction Ilawa Glowna, Poland. *Water, Air and Soil Pollution*, 127:339–349, 2001.

- [139] M. Mandalakis, Ö. Gustafsson, T. Alsberg, A.-L. Egeback, C.M. Reddy, L. Xu, J. Klanova, I. Holoubek, and E.G. Stephanou. Contribution of biomass burning to atmospheric polycyclic aromatic hydrocarbons at three european background sites. *Environmental Science and Technology*, 39:2976–2982, 2005.
- [140] B. Mankovska. Long term effects of pollutants on forest vegetation in Central Spis Region. In G. Spiers, P. Beckett, and H. Conroy, editors, *Mining and the Environment III*. Sudbury, 2003.
- [141] B. Markert. Establishing of ‘reference plant’ for inorganic characterization of different plant species by chemical fingerprinting. *Water, Air and Soil Pollution*, 64:533–538, 1992.
- [142] B. Markert, editor. *Plants as biomonitors - Indicators for heavy metals*. VCH, Weinheim, 1993.
- [143] B. Markert, A.M. Breure, and H.G. Zechmeister. *Bioindicators and biomonitors. Trace metals and other contaminants in the environment*, volume 6. Elsevier, 2003.
- [144] L.C. Marr, T.W. Kirchstetter, R.A. Harley, A.H. Miguel, S.V. Hering, and S.K. Hammond. Characterization of polycyclic aromatic hydrocarbons in motor vehicle fuels and exhaust emissions. *Environmental Science and Technology*, 33:3091–3099, 1999.
- [145] M. Marsili, M. Stracquadiano, C. Trombini, and I. Vassura. The epicuticular wax of *Laurus nobilis* leaves as a passive sampler of polycyclic aromatic hydrocarbons in ambient air. *Fresenius Environmental Bulletin*, 10:26–30, 2001.
- [146] S. Matsuzawa, L. Nasser-Ali, and P. Garrigues. Photolytic behaviour of polycyclic aromatic hydrocarbons in diesel particulate matter deposited on the ground. *Environmental Science and Technology*, 35:3139–3143, 2001.
- [147] J. Matzka and B.A. Maher. Magnetic biomonitoring of roadside tree leaves: identification of spatial and temporal variations in vehicle-derived particulates. *Atmospheric Environment*, 33:4565–4569, 1999.
- [148] G. McIntosh, M. Gómez-Paccard, and M.L. Osete. The magnetic properties of particles deposited on *Platanus x hispanica* leaves in Madrid, Spain, and their temporal and spatial variations. *Science of the Total Environment*, 382:135–146, 2007.
- [149] M.S. McLachlan. Framework for the interpretation of measurements of SOCs in plants. *Environmental Science and Technology*, 33:1799–1804, 1999.
- [150] S.M. McLennan. Relationships between the trace element composition of sedimentary rocks and upper crust. *Geochemistry, Geophysics, Geosystems*, 2(2000GC000109), 2001.

- [151] E. Menichini, F. Monfredini, and F. Merli. The temporal variability of the profile of carcinogenic polycyclic aromatic hydrocarbons in urban air: a study in a medium traffic area in Rome, 1993-1998. *Atmospheric Environment*, 33:3739–3750, 1999.
- [152] W.M. Meylan and P.H. Howard. Estimating octanol-air partition coefficients with octanol-water partition coefficients and Henry’s law constants. *Chemosphere*, 61:640–644, 2005.
- [153] Z.M. Migaszewski. Determining organic compound ratios in soils and vegetation of the Holy Cross Mts., Poland. *Water, Air and Soil Pollution*, 111:123–138, 1999.
- [154] Z.M. Migaszewski, A. Galuszka, A. Swiercz, and J. Kucharzyk. Element concentrations in soils and plant bioindicators in selected habitats of the Holy Cross Mountains, Poland. *Water, Air and Soil Pollution*, 129:369–386, 2001.
- [155] F. Monaci, F. Moni, E. Panciotti, D. Grech, and R. Bargagli. Biomonitoring of airborne metals in urban environments: new tracers of vehicle emission, in place of lead. *Environmental Pollution*, 107:321–327, 2000.
- [156] E. Moreno, L. Sagnotti, J. Dinares-Turell, A. Winkler, and A. Cascella. Biomonitoring of traffic air pollution in Rome using magnetic properties of tree leaves. *Atmospheric Environment*, 37:2967–2977, 2003.
- [157] W.A. Morris, J.K. Versteeg, D.W. Bryant, A.E. Legzdins, B.E. McCarry, and C.H. Marvin. Preliminary comparisons between mutagenicity and magnetic susceptibility of respirable airborne particulate. *Atmospheric Environment*, 29:1352–2310, 1995.
- [158] L. Morselli, P. Olivieri, B. Brusori, and F. Passarini. Soluble and insoluble fractions of heavy metals in wet and dry atmospheric depositions in Bologna. *Environmental Pollution*, 124:457–469, 2003.
- [159] J.F. Müller, D.W. Hawker, M.S. McLachlan, and D.W. Connell. PAHs, PCDD/Fs, PCBs and HCB in leaves from Brisbane, Australia. *Chemosphere*, 43:507–515, 2001.
- [160] A. R. Muxworthy, J. Matzka, and N. Petersen. Comparison of magnetic parameters of urban atmospheric particulate matter with pollution and meteorological data. *Atmospheric Environment*, 35:4379–4386, 2001.
- [161] A. R. Muxworthy, E. Schmidbauer, and N. Petersen. Magnetic properties and Mössbauer spectra of urban atmospheric particulate matter: a case study from Munich, Germany. *Geophysical Journal International*, 150:558–570, 2002.
- [162] A.R. Muxworthy, J. Matzka, A.F. Davila, and N. Petersen. Magnetic signature of daily sampled urban atmospheric particles. *Atmospheric environment*, 37:4163–4169, 2003.

- [163] K.M. Nauss. Critical issues in assessing the carcinogenicity of diesel exhaust: a synthesis of current knowledge. In *Diesel Exhaust: A Critical Analysis of Emissions, Exposure and Health Effects*, pages 11–61. Health Effects Institute: Cambridge, MA, 1995.
- [164] F. De Nicola, G. Maisto, M.V. Prati, and A. Alfani. Temporal variations in PAH concentrations in *Quercus ilex* L. (holm oak) leaves in an urban area. *Chemosphere*, 61:432–440, 2005.
- [165] T. Nielsen. The decay of benzo(a)pyrene and cyclopenteno(cd)pyrene in the atmosphere. *Atmospheric Environment*, 22:2249–2254., 1988.
- [166] T. Nielsen, H.E. Jorgensen, J.C. Larsen, and M. Poulsen. City air pollution of polycyclic aromatic hydrocarbons and other mutagens: occurrence, sources and health effects. *The Science of the Total Environment*, 189/190:41–49, 1996.
- [167] T. Nieminen, J. Derome, and H.-S. Helmisaari. Interactions between precipitation and Scots pine canopies along a heavy-metal pollution gradient. *Environmental Pollution*, 106:129–137, 1999.
- [168] I.C.T. Nisbet and P. K. Lagoy. Toxic Equivalency Factors (TEFs) for Polycyclic Aromatic Hydrocarbons. *Regulatory Toxicology and Pharmacology*, 16:290–300, 1992.
- [169] J.O. Nriagu. A silent epidemic of environmental metal pollution? *Environmental Pollution*, 50:139–161, 1988.
- [170] J.O. Nriagu. A history of global metal pollution. *Science*, 272:223–224, 1996.
- [171] J.O. Nriagu and J.M. Pacyna. Quantitative assessment of worldwide contamination of air, water and soils by trace metals. *Nature*, 333:134–139, 1989.
- [172] G. Oberdörster. Toxicology of ultrafine particles: in vivo studies. *Philosophical Transactions of the Royal Society of London*, A 358:2719–2740, 2000.
- [173] W.A. Ockenden, E. Steinnes, C. Parker, and K.C. Jones. Observations on persistent organic pollutants in plants: implications for their use as passive samplers and for POP cycling. *Environmental Science and Technology*, 32:2721–2726, 1998.
- [174] T. Ohura, T. Amagai, M. Fusaya, and H. Matsushita. Spatial distributions and profiles of atmospheric polycyclic aromatic hydrocarbons in two industrial cities in Japan. *Environmental Science and Technology*, 38:49–55, 2004.
- [175] Organization of Forest Monitoring System. Forest condition in Poland 2002. Annual report, Organization of Forest Monitoring System, Poland, bazy.ibles.waw.pl/bazy/monitor/raport02a/spis.html, 2002.
- [176] R. Orlinski. Multipoint moss passive samplers assessment of urban airborne polycyclic aromatic hydrocarbons: concentrations profile and distribution along Warsaw main streets. *Chemosphere*, 48:181–186, 2002.

- [177] K. Ots. Impact of emission from oil shale fueled power plants on the growth and foliar elemental concentrations of Scots pine in Estonia. *Environmental Monitoring and Assessment*, 85:293–208, 2003.
- [178] J.M. Pacyna and T.E. Graedel. Atmospheric emissions inventories - status and prospects. *Annual Review of Energy and the Environment*, 20:265–300, 1995.
- [179] J.M. Pacyna and E.G. Pacyna. An assessment of global and regional emissions of trace metals to the atmosphere from anthropogenic sources worldwide. *Environmental Reviews*, 9:269–298, 2001.
- [180] J.M. Pacyna, T. Scholtz, and Y.-F. Li. Global budgets of trace metal sources. *Environmental Reviews*, 3:145–159, 1995.
- [181] N. Panichev and R. McCrindle. The application of bio-indicators for the assessment of air pollution. *Journal of Environmental Monitoring*, 6:121–123, 2004.
- [182] B.C. Panther, M.A. Hooper, and N.J. Tapper. A comparison of air particulate matter and associated polycyclic aromatic hydrocarbons in some tropical and temperate urban environments. *Atmospheric Environment*, 33:4087–4099, 1999.
- [183] S. Paterson, D. Mackay, E. Bacci, and D. Calamari. Correlation of the equilibrium and kinetics of leaf-air exchange of hydrophobic organic chemicals. *Environmental Science and Technology*, 25:866–871, 1991.
- [184] J. Pearson, D. Wells, K. Sellers, A. Bennett, A. Soares, J. Woodall, and M. Ingrouille. Traffic exposure increases natural ^{15}N and trace element concentrations in mosses. *New Phytologist*, 147:317–326, 2000.
- [185] K. Peltonen and T. Kuljukka. Air and analysis of polycyclic aromatic hydrocarbons. *Journal of Chromatography*, 710:93–108, 1995.
- [186] K. Percy, J. Cape, R. Nagels, and C. Simpson, editors. *Air pollutants and the leaf cuticle*, volume 36 of *NATO Scientific Affairs Division Series*. Springer, 1993.
- [187] C. Peters and R. Thompson. Magnetic identification of selected natural iron oxides and sulphides. *Journal of Magnetism and Magnetic Materials*, 183:365–374, 1998.
- [188] N. Pirrone, P. Costa, and J.M. Pacyna. Past, current and projected atmospheric emissions of trace elements in the mediterranean region. *Water Science and Technology*, 39:1–7, 1999.
- [189] J. Poikolainen. Sulphur and heavy metal concentrations in Scots pine bark in Northern Finland and the Kola Penninsula. *Water, Air and Soil Pollution*, 93:395–408, 1997.
- [190] C.A. Pope III, R.T. Burnett, M.J. Thun, E.E. Calle, D. Krewski, K. Ito, and G.D. Thurston. Lung cancer, cardiopulmonary mortality, and long-term exposure to fine particulate air pollution. *Journal of the American Medical Association*, 287:1132–1141, 2002.

- [191] C.A. Pope III and D.W. Dockery. Epidemiology of particle effects. In S.T. Holgate, J.M. Samet, H.S. Koren, and R.L. Maynard, editors, *Air Pollution and Health*, pages 673–705. Academic Press, London, 1999.
- [192] C.A. Pope III, M.J. Thun, M. M. Namboodiri, D.W. Dockery, J.S. Evans, F.E. Speizer, and C.W. Heath Jr. Particulate air pollution as a predictor of mortality in a prospective study of U.S. adults. *American Journal of Respiratory and Critical Care Medicine*, 151:669–674, 1995.
- [193] D.L. Poster, B.A. Benner, M. Schantz, L.C. Sander, and S.A. Wise. Determination of methyl-substituted polycyclic aromatic hydrocarbons in diesel particulate-related standard reference material. *Polycyclic Aromatic Compounds*, 23:113–139, 2003.
- [194] D.L. Poster, M.J. Lopez de Alda, S.A. Wise, J.C. Chuang, and J.L. Mumford. Determination of PAHs in combustion-related samples and in SRM 1597, complex mixture of PAHs from coal tar. *Polycyclic Aromatic Compounds*, 20:79–95, 2000.
- [195] M. Prasad and J. Hagemeyer, editors. *Heavy metal stress in plants - from molecules to ecosystems*. Springer, 1999.
- [196] P. Rademacher. Atmospheric trace elements and forest ecosystems. In *Convention on long-range transboundary air pollution - International Co-operative programme on assessment and monitoring of air pollution effects on forests*. Federal Research Centre for Forestry and Forest Products, United Nations Economic Commission, 2001.
- [197] M. Radke. Application of aromatic-compounds as maturity indicators in source rocks and crude oils. *Marine and Petroleum Geology*, 5:224–236, 1988.
- [198] T. Ramdahl. Retene - a molecular marker of wood combustion in ambient air. *Nature*, 306:580–582, 1983.
- [199] P. Rautio, S. Huttunen, E. Kukkola, R. Peura, and J. Lamppu. Deposited particles, element concentrations and needle injuries on Scots pine along an industrial pollution transect in northern Europe. *Environmental Pollution*, 103:81–89, 1998.
- [200] P. Rautio, S. Huttunen, and J. Lamppu. Element concentrations in scots pine needles on radial transects across a subarctic area. *Water, Air and Soil Pollution*, 102:389–405, 1998.
- [201] P.T.A. Reilly, R.A. Gieray, W.B. Whitten, and J.M. Ramsey. Real-time characterization of the organic composition and size of individual diesel engine smoke particles. *Environmental Science and Technology*, 32:2672–2679, 1998.
- [202] M.A. Reis. *Biomonitoring and assessment of atmospheric trace elements in Portugal - methods, response modeling and nuclear analytical techniques*. 230. Delft University Press, 2001.

- [203] M.M. Rhead and S.A. Hardy. The sources of polycyclic aromatic compounds in diesel engine emissions. *Fuel*, 84:385–393, 2003.
- [204] M. Riederer. Estimating partitioning and transport of organic chemicals in the foliage/atmosphere system: discussion of a fugacity-based model. *Environmental Science and Technology*, 24:829–837, 1990.
- [205] W. Rogge, L. Hildemann, M. Mazurek, and G. Cass. Sources of fine organic aerosol. 2. Noncatalyst and catalyst-equipped automobiles and heavy-duty diesel trucks. *Environmental Science and Technology*, 27:636–651, 1993.
- [206] W. Rogge, L. Hildemann, M. Mazurek, and G. Cass. Sources of fine organic aerosol. 3. Road dust, tire debris and organometallic brake lining dust: roads as sources and sinks. *Environmental Science and Technology*, 27:1892–1904, 1993.
- [207] R.A. Root. Lead loading of urban streets by motor vehicle wheel weights. *Environmental Health Perspectives*, 108:937–940, 2000.
- [208] RWE Power. Braunkohle. www.rwe.com, 2008.
- [209] L. Sagnotti, P. Macry, R. Egli, and M. Mondino. Magnetic properties of atmospheric particulate matter from automatic air sampler stations in Latium (Italy): Toward a definition of magnetic fingerprints for natural and anthropogenic PM₁₀ sources. *Journal of Geophysical Research*, 111, 2006.
- [210] I. Salma and W. Maenhaut. Changes in elemental composition and mass of atmospheric aerosol pollution between 1996 and 2002 in a Central European city. *Environmental Pollution*, 143:479–488, 2006.
- [211] J. Sardans and J. Penuelas. Introduction of the factor of partitioning in the lithogenic enrichment factors of trace element bioaccumulation in plant tissues. *Environmental Monitoring and Assessment*, 115:473–498, 2006.
- [212] T. Sawidis, M.K. Chettri, A. Papaioannou, G. Zachariadis, and J. Stratis. A study of metal distribution from lignite fuels using trees as biological monitors. *Ecotoxicology and Environmental Safety*, 48:27–35, 2001.
- [213] C. Schauer, R. Niessner, and U. Pöschl. Polycyclic aromatic hydrocarbons in urban particulate matter: decadal and seasonal trends, chemical degradation and sampling artifacts. *Environmental Science and Technology*, 37:2861–2868, 2003.
- [214] J.J. Schauer, M.J. Kleeman, G.R. Cass, and B.R.T. Simoneit. Measurements of emissions from air pollution sources. 2. C-1 through C-30 organic compounds from medium duty diesel trucks. *Environmental Science and Technology*, 33:1578–1587, 1999.
- [215] J.J. Schauer, M.J. Kleeman, G.R. Cass, and B.R.T. Simoneit. Measurement of emissions from air pollution sources. 3. C1 - C29 organic compounds from fireplace combustion of wood. *Environmental Science and Technology*, 35:1716–1728, 2001.

- [216] P. Schleppei, L. Tobler, J. Bucher, and A. Wyttenbach. Multivariate interpretation of the foliar chemical composition of norway spruce (*Picea abies*). *Plant and Soil*, 219:251–262, 2000.
- [217] Andre Schmitz. Limnogeochemische Untersuchungen eines eutrophierten Fischereisees in einem aufgelassenem Basaltbruch bei Wachtberg, Bonn. Mater thesis, University of Cologne, Germany, 2005.
- [218] J. Schönherr and M. Riederer. Foliar penetration and accumulation of organic chemicals in plant cuticles. *Review of Environmental Contamination and Toxicology*, 108:1–70, 1989.
- [219] H. Schuh. Mär von der sauberen Wärme. *Die Zeit*, 41:www.zeit.de, 2007.
- [220] V.K. Sergey, I.K. Tamara, and S.K. Valery. Study of PAH emission from the solid fuels combustion in residential furnaces. *Environmental Pollution*, 133:383–387, 2005.
- [221] Z. Shams and M. Beg. Lead in particulate deposits and in leaves of roadside plants, Karachi, Pakistan. *The Environmentalist*, 20:63–67, 2000.
- [222] V. Shilton, C. Booth, J. Smith, P. Giess, D. Mitchell, and C. Williams. Magnetic properties of urban street dust and their relationship with organic matter content in the West Midlands, UK. *Atmospheric Environment*, 39:3651–3659, 2005.
- [223] J. Shu, J.A. Dearing, A. Morse, L. Yu, and C. Li. Magnetic properties of daily sampled total suspended particulates in Shanghai. *Environmental Science and Technology*, 34:2393–2400, 2000.
- [224] M.A. Sicre, J.C. Marty, A. Saliot, X. Aparicio, J. Grimalt, and J. Albaiges. Aliphatic and aromatic hydrocarbons in different sized aerosols over the Mediterranean Sea: Occurrence and origin. *Atmospheric Environment*, 21:2247–2259, 1987.
- [225] M.F. Simcik, S.J. Eisenreich, and P.J. Lioy. Source apportionment and source/sink relationships of PAHs in the coastal atmosphere of Chicago and Lake Michigan. *Atmospheric Environment*, 33:5071–5079, 1999.
- [226] R. Simo, J.O. Grimalt, and J. Albaiges. Loss of unburned-fuel hydrocarbons from combustion aerosols during atmospheric transport. *Research Communications, Environmental Science and Technology*, 31:2697–2700, 1997.
- [227] B.R.T. Simoneit. Biomarker PAHs in the environment. In A.H. Neilson, editor, *The Handbook of Environmental Chemistry*, volume 3 of *Part I, PAHs and related compounds*, pages 176–221. Springer, Berlin, 1998.
- [228] B.R.T. Simoneit and V.O. Elias. Organic tracers from biomass burning in atmospheric particulate matter over the ocean. *Marine Chemistry*, 69:301–312, 2000.

- [229] B.R.T. Simoneit and M.A. Mazurek. Organic matter of the troposphere. II - Natural background of biogenic lipid matter in aerosols over the rural western United States. *Atmospheric Environment*, vol. 16, no. 9, 1982, p. 2139-2159, 16:2139–2159, 1982.
- [230] B.R.T. Simoneit and P. Shapiro. Final report: organic tracers of plant classes in biomass combustion and smoke in aerosols. National Center for Environmental Research, Internet, 1998.
- [231] S.L. Simonich and R.A. Hites. Importance of vegetation in removing polycyclic aromatic hydrocarbons from the atmosphere. *Nature*, 370:49–51, 1994.
- [232] S.L. Simonich and R.A. Hites. Vegetation-atmosphere partitioning of polycyclic aromatic hydrocarbons. *Environmental Science and Technology*, 28:939–943, 1994.
- [233] S.L. Simonich and R.A. Hites. Organic pollutant accumulation in vegetation. *Environmental Science and Technology*, 29:2905–2914, 1995.
- [234] M. Sjögren, H. Li, U. Rannug, and R. Westerholm. Multivariate analysis of exhaust emissions from heavy-duty diesel fuels. *Environmental Science and Technology*, 30:38–49, 1996.
- [235] J.F. Slater, L.A. Currie, J.E. Dibb, and B.A. Benner. Distinguishing the relative contribution of fossil fuel and biomass combustion aerosols deposited at Summit, Greenland through isotopic and molecular characterization of insoluble carbon. *Atmospheric Environment*, 36:4463–4477, 2002.
- [236] S.W. Slayden and J.F. Liebman. The energetics of aromatic hydrocarbons: an experimental thermochemical perspective. *Chemical Reviews*, 101:1541–1566, 2001.
- [237] K.E. Smith, G.O. Thomas, and K.C. Jones. Seasonal and species differences in the air-pasture transfer of PAHs. *Environmental Science and Technology*, 35:2156–2165, 2001.
- [238] L. E. Smith, M. F. Denissenko, W. P. Bennett, H. Li, S. Amin, M. Tang, and G.P. Pfeifer. Targeting of lung cancer mutational hotspots by polycyclic aromatic hydrocarbons. *Journal of the National Cancer Institute*, 92:803–811, 2000.
- [239] B. Smodis, M.L. Pignata, M. Saiki, E. Cortes, N. Bangfa, B. Markert, B. Nyarko, J. Arunachalam, J. Garty, M. Vutchkov, H.T. Wolterbeek, E. Steinnes, M.C. Freitas, A. Lucaciu, and M. Frontasyeva. Validation and application of plants as biomonitors of trace element atmospheric pollution - a co-ordinated effort in 14 countries. *Journal of Atmospheric Chemistry*, 49:3–13, 2004.
- [240] H.S. Söderström and P.A. Bergqvist. Polycyclic aromatic hydrocarbons in a semi-aquatic plant and semipermeable membrane devices exposed to air in Thailand. *Environmental Science and Technology*, 37:47–52, 2003.

- [241] E. Steinnes and A.J. Friedland. Metal contamination of natural surface soils from long-range atmospheric transport: Existing and missing knowledge. *Environmental Reviews*, 14:169–186, 2006.
- [242] E. Steinnes, N. Lukina, V. Nikonov, D. Aamlid, and O. Royset. A gradient study of 34 elements in the vicinity of a copper-nickel smelter in the Kola Peninsula. *Environmental Monitoring and Assessment*, 60:71–88, 2000.
- [243] D.I. Stern. Global sulfur emissions from 1850 to 2000. *Chemosphere*, 58:163–175, 2005.
- [244] J. Sternbeck, A. Sjödin, and K. Andreasson. Metal emissions from road traffic and the influence of resuspension – results from two tunnel studies. *Atmospheric Environment*, 36:4735–4744, 2002.
- [245] W.M.J. Strachan, G. Eriksson, H. Kylin, and S. Jensen. Organochlorine compounds in pine needles: methods and trends. *Environmental Toxicology and Chemistry*, 13:443–451, 1994.
- [246] M. Struschka, U. Zuberbühler, A. Dreiseidler, D. Dreizler, and G. Baumbach. Ermittlung und Evaluierung der Feinstaubemissionen aus Kleinf Feuerungsanlagen im Bereich der Haushalte und Kleinverbraucher sowie Ableitung von geeigneten Maßnahmen zur Emissionsminderung. Technical Report (Forschungsbericht) 299 44 140, Umweltforschungsplan des Bundesministeriums für Umwelt, Naturschutz und Reaktorsicherheit, 2003.
- [247] Y. Su, Y.D. Lei, F. Wania, M. Shoeib, and T. Harner. Regressing gas/particle partitioning data for polycyclic aromatic hydrocarbons. *Environmental Science and Technology*, 40:3558–3564, 2006.
- [248] R. Thompson and F. Oldfield. *Environmental Magnetism*. Allen and Unwin, 1986.
- [249] P. Tremolada, V. Burnett, D. Calamari, and K.C. Jones. Spatial distribution of PAHs in the UK atmosphere using pine needles. *Environmental Science and Technology*, 30:3570–3577, 1996.
- [250] P. Trüby. Impact of heavy metals on forest trees from mining areas. In *Proceedings of the 3rd Mining and the Environment Conference, Sudbury (Canada)*, www.ott.wrcc.osmre.gov/library/proceed/sudbury2003/sudbury03/156.pdf, 2003.
- [251] T.M. Tuch, B. Wehner, M. Pitz, J. Cyrus, J. Heinrich, W.G. Kreyling, H.E. Wichmann, and A. Wiedensohler. Long-term measurements of size-segregated ambient aerosol in two German cities located 100 km apart. *Atmospheric Environment*, 37:4687–4700, 2003.
- [252] A.B. Turnbull and R.M. Harrison. Major component contributions to PM₁₀ composition in the UK atmosphere. *Atmospheric Environment*, 24:3129–3137, 2000.

- [253] G. Tyler. Rare earth elements in soil and plant systems - a review. *Plant and Soil*, 267:191–206, 2004.
- [254] N. Tzvetkova and C. Hadjiivanova. Chemical composition and biochemical changes in needles of Scots pine (*Pinus sylvestris* L.) stands at different stages of decline in Bulgaria. *Trees - Structure and Function*, 20:405–409, 2006.
- [255] M. Urbat, E. Lehndorff, and L. Schwark. Biomonitoring of air quality in the Cologne conurbation using pine needles as a passive sampler - Part I: magnetic properties. *Atmospheric Environment*, 38:3781–3792, 2004.
- [256] US-EPA. Air quality criteria for particulate matter, Research Triangle Park, NC, USA, October, 2004.
- [257] P.C. van Metre and B.J. Mahler. The contribution of particles washed from rooftops to contaminant loading to urban streams. *Chemosphere*, 52:1727–1741, 2003.
- [258] D. Varrica, A. Aiuppa, and G. Dongarra. Volcanic and anthropogenic contribution to heavy metal content in lichens from Mt. Etna and Vulcano island (Sicily). *Environmental Pollution*, 108:153–162, 2000.
- [259] H. Veijalainen. The applicability of peat and needle analysis in heavy metal deposition surveys. *Water, Air and Soil Pollution*, 107:367–391, 1998.
- [260] E.-L. Viskari. Epicuticular waxes of norway spruce needles as indicator of traffic pollutant deposition. *Water, Air and Soil Pollution*, 121, 327-337.
- [261] D.M. Wagrowski and R. Hites. Polycyclic aromatic hydrocarbon accumulation in urban, suburban and rural vegetation. *Environmental Science and Technology*, 31:279–282, 1997.
- [262] D.C. Walsh, S.N. Chillrud, H.J. Simpson, and R.F. Bopp. Refuse incinerator particulate emissions and combustion residues for New York City during the 20th Century. *Environmental Science Technology*, 35:2441–2447, 2001.
- [263] D. Wang, J. Chen, Z. Xu, X. Qiao, and L. Huang. Disappearance of polycyclic aromatic hydrocarbons sorbed on surfaces of pine [*Pinus thunbergii*] needles under irradiation of sunlight: volatilization and photolysis. *Atmospheric Environment*, 39:4583–4591, 2005.
- [264] Y.-F. Wang, K.-L. Huang, C.-T. Li, H.-H. Mi, J.-H. Luo, and P.-J. Tsai. Emissions of fuel metals content from a diesel vehicle engine. *Atmospheric Environment*, 37:4637–4643, 2003.
- [265] Z. Wang, M.F. Fingas, Y.Y. Shu, L. Sigouin, M. Landriault, and P. Lambert. Quantitative characterization of PAHs in burn residues and soot samples and differentiation of pyrogenic PAHs from petrogenic PAHs – The 1994 Mobile Burn Study. *Environmental Science and Technology*, 33:3100–3109, 1999.

- [266] F. Wania and M.S. McLachlan. Estimating the influence of forests on the overall fate of semivolatile organic compounds using a multimedia fate model. *Environmental Science and Technology*, 35:582–590, 2001.
- [267] G. Weckwerth. Verification of traffic emitted aerosol components in the ambient air of Cologne (Germany). *Atmospheric Environment*, 35:5525–5536, 2001.
- [268] P. Weiss. Vegetation/soil distribution of semivolatile organic compounds in relation to their physicochemical properties. *Environmental Science and Technology*, 34:1707–1714, 2000.
- [269] L. Weißflog and K.-D. Wenzel. Die Vegetation als Senke und biochemischer Reaktor für luftgetragene Schadstoffe. Final Report (Abschlußbericht), Umweltforschungszentrum Leipzig, 1997.
- [270] K.-D. Wenzel, A. Hubert, M. Manz, L. Weissflog, W. Engewald, and G. Schüürmann. Accelerated solvent extraction of semivolatile organic compounds from biomonitoring samples of pine needles and mosses. *Analytical Chemistry*, 70:4827–4835, 1998.
- [271] K.-D. Wenzel, L. Weissflog, M. Manz, A. Hubert, and G. Schüürmann. Differences in time-dependent accumulation of hydrophobic xenobiotics in pine needles. *Fresenius Environmental Bulletin*, 9:47–55, 2000.
- [272] R. Westerholm and H. Li. A multivariate statistical-analysis of fuel-related polycyclic aromatic hydrocarbon emissions from heavy-duty diesel vehicles. *Environmental Science and Technology*, 28:965–972, 1994.
- [273] J.M. Whitcombe, I.E. Agranovski, and R.D. Braddock. Categorisation of particulate emissions from a fluidised catalytic cracking unit. *Particle and Particle Systems Characterization*, 21:463–472, 2004.
- [274] WHO (World Health Organization). Health aspects of air pollution with particulate matter, ozone and nitrogen dioxide. World Health Organisation, 1-94.
- [275] WHO (World Health Organization). Air quality guidelines for Europe - Second Edition. WHO regional publications, Copenhagen, European Series No. 91, 2000.
- [276] H.E. Wichmann and A. Peters. Epidemiological evidence of the effects of ultrafine particle exposure. *Philosophical Transactions of the Royal Society of London, A* 358:2751–2769, 2000.
- [277] E. Wild, J. Dent, J.L. Barber, G.O. Thomas, and K.C. Jones. A novel analytical approach for visualizing and tracking organic chemicals in plants. *Environmental Science and Technology*, 38:4195–4199, 2004.
- [278] E. Wild, J. Dent, G.O. Thomas, and K.C. Jones. Real-time visualization and quantification of PAH photodegradation on and within plant leaves. *Environmental Science and Technology*, 39:268–273, 2005.

- [279] E. Wild, J. Dent, G.O. Thomas, and K.C. Jones. Visualizing the air-to-leaf transfer and within-leaf movement and distribution of phenanthrene: further studies utilizing two-photon excitation microscopy. *Environmental Science and Technology*, 40:907–916, 2006.
- [280] S.R. Wild and K.C. Jones. Polynuclear aromatic hydrocarbons in the United Kingdom environment: a preliminary source inventory and budget. *Environmental Pollution*, 88:91–108, 1995.
- [281] B. Wolterbeek. Biomonitoring of trace element air pollution: Principles, possibilities and perspectives. *Environmental Pollution*, 120:11–21, 2002.
- [282] A. Wytttenbach, P. Schleppei, J. Bucher, V. Furrer, and L. Tobler. The accumulation of the rare earth elements and of scandium in successive needle age classes of norway spruce. *Biological Trace Element Research*, 41:13–29, 1994.
- [283] A. Wytttenbach, L. Tobler, P. Schleppei, and V. Furrer. Variation of the rare earth element concentrations in the soil, soil extract and in individual plants from the same site. *Journal of Radioanalytical and Nuclear Chemistry*, 231:101–106, 1998.
- [284] D.S. Xia, F.H. Chenb, J. Bloemendal, X.M. Liub, Y. Yua, and L.P. Yang. Magnetic properties of urban dustfall in Lanzhou, China, and its environmental implications. *Atmospheric Environment*, 42:2198–2207, 2008.
- [285] S. Xie, J.A. Dearing, and J. Bloemendal. The organic matter content of street dust in Liverpool, UK, and its association with dust magnetic properties. *Atmospheric Environment*, 34:269–275, 2000.
- [286] S.Y.N. Yang, D.W. Connell, D.W. Hawker, and S.I. Kayal. Polycyclic aromatic hydrocarbons in air, soil and vegetation in the vicinity of an urban roadway. *The Science of the Total Environment*, 102:229–240, 1991.
- [287] M.B. Yunker, R.W. Macdonald, R. Vingarzan, R.H. Mitchell, D. Goyette, and S. Sylvestre. PAHs in the Fraser River basin: a critical appraisal of PAH ratios as indicators of PAH source and composition. *Organic Geochemistry*, 33:489–515, 2002.
- [288] M. Zheng, M. Fang, F. Wang, and K.L. To. Characterization of the solvent extractable organic compounds in PM_{2.5} aerosols in Hong Kong. *Atmospheric Environment* 34, 2691-2702., 34:2691–2702, 2002.

Abbreviations used in this thesis		Polycyclic aromatic hydrocarbons	
AAS	atom adsorption spectroscopy	Fluo	fluorene
ARM	anhysteretic remanence measurements	P	phenanthrene
ASE	accelerated solvent extraction	A	anthracene
B_{cr}	remanence coercitivity	DBT	dibenzothiophene
C_x	concentration of element x	CPP	cylopenta[def]phenanthrene
DCM	dichloromethane	MP	methylphenanthrenes
EA	elemental analyzer	Fla	fluoranthene
EC	European Community	Py	pyrene
EDX	energy dispersive X-ray spectroscopy	DMP	dimethylphenanthrenes
EF	enrichment factor	EP	ethylphenanthrenes
EFSA	European Food Safety Authority	BaFluo	benzo[a]fluorene
EPA	Environmental Pollution Agency (US)	BbcFluo	benzo[b+c]fluorene
ET-AAS	electrothermal graphite-furnace AAS	MFla	methylfluoranthenes
FA	factor analysis	MPy	methylpyrenes
FAAS	flame-AAS	BghiFla	benzo[ghi]fluoranthene
GCC	Greater Cologne Conurbation	CpcdPy	cyclopenta[cd]pyrene
GC-MS	gaschromatography-mass spectrometry	BcP	benzo[c]phenanthrene
GIS	geoinformationsystem	BaA	benz[a]anthracene
Hex	n-hexane	CT	chrysene+triphenylene
HR-ICP-MS	high-resolution inductively coupled plasma mass spectrometer	Re	retene
ICP-AES	inductively coupled plasma - atomic emission spectroscopy	BNT	benzonaphthothiophene
INAA	instrumental neutron activation analysis	BbjFla	benzo[b+j]fluoranthene
IRM	isothermal remanence measurements	BkFla	benzo[k]fluoranthene
k_{oa}	octanol-air partitioning coefficient	BeP	benzo[e]pyrene
k_{ow}	octanol-water partitioning coefficient	BaP	benzo[a]pyrene
loc.	location	Per	berylene
MDM	multi domain magnetite	IP	indeno[1,2,3-cd]pyrene
MPLC	medium pressure liquid chromatography	BghiP	benzo[ghi]perylene
mw	mass weight	DbahA	dibenz[a,h]anthracene
MWI	municipal waste incinerator	Cor	coronene
NAAS	thermal neutron activation analyses		
NRW	Northrhine Westphalia		
PAH	polycyclic aromatic hydrocarbons		
PM	particulate matter		
PSD	pseudo-single domain magnetite		
REE	rare earth elements		
SDM	single domain magnetite		
SEM	scanning electron microscopy		
SIM	selected ion mode		
SIRM	saturation isothermal remanence measurements		
SPM	superparamagnetic magnetite		
TEF	toxidity equivalence factor		
UCC	upper continental crust		
VOC	volatile organic compounds		
XRF	X-ray fluorescence		

Table 25: Abbreviations used in text, figures and tables.

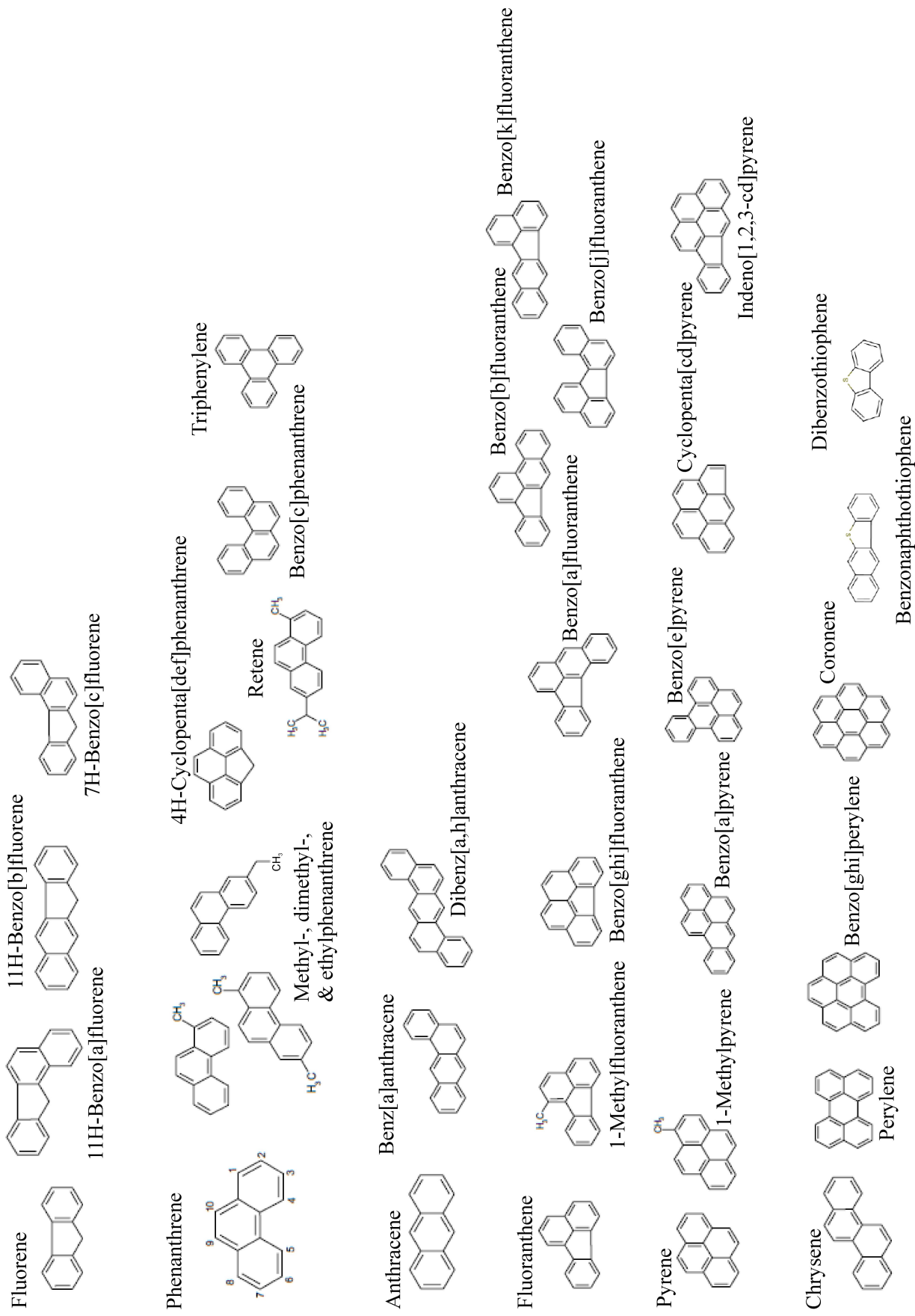


Figure 61: Molecular structure of parent and alkylated polycyclic aromatic hydrocarbons (PAH) analysed on *Pinus nigra* needle surfaces.

sample ID	location	season	tree	needle cohort	exposure [month]	water loss [%]	χ [$10^{-8} \text{ m}^3 \text{ kg}^{-1}$]	SIRM [$\text{A m}^{-1} \text{ kg}^{-1}$]	ARM [$\text{A m}^{-1} \text{ kg}^{-1}$]	B_{err} [mT]	s-ratio
996440	1	W	1	1	8	54	1.24	27.9	0.35	37.4	0.964
996441	1	W	1	2	20	53	2.22	37.4	0.44	48.1	0.965
996442	1	W	1	3	32	52	3.44	50.9	0.60	41.8	0.963
996443	1	W	1	4	44						
996444	1	W	2	1	8	54	1.09	25.6	0.26	46.5	0.974
996445	1	W	2	2	20	52	2.20	36.5	0.44	47.9	0.971
996446	1	W	2	3	32	-	2.47	36.8	0.51	41.9	0.968
996447	1	W	2	4	44	46	3.63	56.4	0.61	28.8	0.974
996448	1	W	3	1	8	49	0.80	23.6	0.30	33.4	0.968
996449	1	W	3	2	20	46	2.12	37.5	0.48	42.3	0.965
996450	1	W	3	3	32	46	3.04	45.6	0.68	38.7	0.963
996451	1	W	3	4	44	48	3.19	49.1	0.67	41.9	0.963
996455	2	W	1	1	8	55	0.35	17.0	0.25	27.7	0.974
996456	2	W	1	2	20	51	0.84	19.8	0.32	48.0	0.966
996457	2	W	1	3	32	53	2.32	31.2	0.49	41.1	0.964
996458	2	W	1	4	44	51	2.37	31.9	0.50	38.9	0.961
996459	2	W	2	1	8	55	0.81	20.7	0.23	32.7	0.969
996460	2	W	2	2	20	52	1.57	26.5	0.39	33.5	0.963
996461	2	W	2	3	32	50	2.60	36.9	0.46	38.3	0.954
996462	2	W	3	1	8	56	0.33	17.3	0.25	28.2	0.972
996463	2	W	3	2	20	54	0.84	20.0	0.35	33.2	0.965
996464	2	W	3	3	32	54	1.69	27.5	0.48	37.6	0.964
996465	2	W	3	4	44	52	2.01	33.7	0.42	36.7	0.961
996514	3	W	1	1	8	55	1.39	26.9	0.33	52.9	0.975
996515	3	W	1	2	20	52	3.09	45.9	0.54	52.4	0.974
996516	3	W	1	3	32	49	4.12	43.2	0.56	42.8	0.970
996517	3	W	2	1	8	55	2.76	40.0	0.53	41.8	0.975
996518	3	W	2	2	20	51	4.35	48.6	0.66	41.5	0.973
996519	3	W	2	3	32	52	5.38	56.3	0.83	42.2	0.971
996520	3	W	3	1	8	54	0.90	22.7	0.30	47.9	0.976
996521	3	W	3	2	20	50	2.43	40.1	0.53	42.3	0.969
996522	3	W	3	3	32	48	3.96	57.7	0.74	43.0	0.968
996523	4	W	1	1	8	53	3.46	47.8	0.42	43.8	0.980
996524	4	W	1	2	20	50	6.41	73.6	0.59	48.5	0.978
996525	4	W	1	3	32	49	8.02	86.4	0.71	52.0	0.977
996526	4	W	1	4	44	51	8.33	96.2	0.69	48.2	0.978
996527	4	W	2	1	8	56	2.17	36.9	0.34	43.4	0.981
996528	4	W	2	2	20	55	5.18	64.5	0.51	47.9	0.980
996529	4	W	2	3	32	54	4.92	56.0	0.43	47.9	0.978
996530	4	W	3	1	8	56	2.69	43.1	0.38	42.3	0.981
996531	4	W	3	2	20	55	3.71	48.9	0.45	47.5	0.978
996532	4	W	3	3	32	47	4.75	58.7	0.54	47.2	0.978
996533	4	W	3	4	44	52	8.18	90.6	0.62	48.3	0.977
996560	5	W	1	1	8	54	0.35	22.7	0.24	28.0	0.978
996561	5	W	1	2	20	51	1.37	32.0	0.37	41.7	0.975
996562	5	W	1	3	32	49	2.10	37.6	0.42	42.1	0.972
996563	5	W	1	4	44	46	1.88	32.6	0.37	42.9	0.969

Table 26: Time-resolved enviromagnetic and physiological parameters determined for 6 locations with different emission characteristics, sheet I.

sample ID	location	season	tree	needle cohort	exposure [month]	water loss [%]	χ [$10^{-8} \text{ m}^3 \text{ kg}^{-1}$]	SIRM [$\text{A m}^{-1} \text{ kg}^{-1}$]	ARM [$\text{A m}^{-1} \text{ kg}^{-1}$]	B_{cr} [mT]	s-ratio
996564	5	W	2	1	8	53	0.64	23.6	0.28	28.2	0.984
996565	5	W	2	2	20	51	1.10	27.1	0.27	38.2	0.975
996566	5	W	2	3	32	52	2.14	39.1	0.40	42.6	0.972
996567	5	W	3	1	8	53	0.82	24.4	0.29	37.7	0.979
996568	5	W	3	2	20	50	1.01	23.9	0.31	37.5	0.971
996569	5	W	3	3	32	50	2.00	36.9	0.40	42.5	0.970
996574	6	W	1	1	8	53	-0.33	11.8	0.19	27.6	0.973
996575	6	W	1	2	20	52	0.06	16.1	0.28	31.9	0.966
996576	6	W	1	3	32	52	0.58	22.7	0.35	38.1	0.960
996577	6	W	1	4	44	45	0.77	22.7	0.35	32.2	0.971
996578	6	W	2	1	8	57	-0.06	18.2	0.24	27.5	0.980
996579	6	W	2	2	20	54	0.17	18.6	0.32	38.0	0.960
996580	6	W	2	3	32	53	0.75	24.7	0.40	33.3	0.963
996581	6	W	2	4	44	49	0.88	25.5	0.40	42.9	0.958
996582	6	W	3	1	8	56	0.21	16.1	0.21	33.8	0.967
996583	6	W	3	2	20	53	0.58	25.0	0.33	42.1	0.961
996584	6	W	3	3	32	52	1.39	35.2	0.45	37.8	0.963
996927	1	S	1	1	3	60	-0.12	13.2	0.09	32.4	0.975
996928	1	S	1	2	14	57	1.91	36.6	0.61	37.6	0.964
996929	1	S	1	3	26	57	3.26	52.2	0.77	42.1	0.964
996930	1	S	1	4	38	57	3.71	55.3	0.88	42.4	0.950
996931	1	S	1	5	50	57	4.75	65.6	0.78	43.0	0.961
996932	1	S	2	1	3	60	-0.27	11.8	0.05	28.2	0.975
996933	1	S	2	2	14	54	1.30	27.9	0.44	37.1	0.968
996934	1	S	2	3	26	53	2.91	44.4	0.49	42.0	0.964
996935	1	S	2	4	38	52	3.37	46.7	0.78	42.5	0.964
996936	1	S	2	5	50	50	3.30	45.3	0.61	41.9	0.964
996937	1	S	3	1	3	-	-0.35	10.5	0.13	28.1	0.955
996938	1	S	3	2	14	56	1.14	26.6	0.45	38.2	0.965
996939	1	S	3	3	26	55	2.15	36.7	0.44	39.0	0.964
996940	1	S	3	4	38	54	2.77	42.0	0.61	40.7	0.963
996941	1	S	3	5	50	53	2.91	42.7	0.54	42.2	0.969
996942	2	S	1	1	3	59	-0.30	9.3	0.15	27.5	0.978
996943	2	S	1	2	14	56	1.13	21.6	0.23	37.7	0.961
996944	2	S	1	3	26	53	1.50	24.2	0.31	38.3	0.959
996945	2	S	1	4	38	53	2.67	34.4	0.56	38.1	0.953
996946	2	S	1	5	50	51	3.17	39.4	0.49	42.1	0.945
996947	2	S	2	1	3	59	-0.34	8.8	0.12	27.0	0.977
996948	2	S	2	2	14	55	1.41	25.3	0.39	37.3	0.956
996949	2	S	2	3	26	53	1.66	28.7	0.42	36.6	0.957
996950	2	S	2	4	38	52	2.32	33.7	0.39	37.7	0.955
996951	2	S	3	1	3	61	-0.54	7.4	0.18	22.7	0.984
996952	2	S	3	2	14	57	0.45	18.5	0.18	31.6	0.965
996953	2	S	3	3	26	57	1.62	30.2	0.32	37.3	0.963
996954	2	S	3	4	38	56	2.52	35.8	0.41	38.5	0.962
996955	3	S	1	1	3	57	-0.37	9.5	0.05	21.6	0.981
996956	3	S	1	2	14	54	1.43	27.3	0.42	37.8	0.968
996957	3	S	1	3	26	54	2.32	34.5	0.42	42.5	0.972

Table 27: Enviromagnetic and physiological parameters, temporal study, II

sample ID	location	season	tree	needle cohort	exposure [month]	water loss [%]	χ [$10^{-8} \text{ m}^3 \text{ kg}^{-1}$]	SIRM [$\text{A m}^{-1} \text{ kg}^{-1}$]	ARM [$\text{A m}^{-1} \text{ kg}^{-1}$]	B_{cr} [mT]	s-ratio
996958	3	S	2	1	3	55	-0.01	11.4	0.14	27.2	0.975
996959	3	S	2	2	14	48	2.55	32.5	0.54	45.5	0.968
996960	3	S	2	3	26	49	3.94	39.3	0.57	42.7	0.971
996961	3	S	3	1	3	59	-0.13	11.5	0.20	26.7	0.978
996962	3	S	3	2	14	-	2.00	32.8	0.44	42.2	0.966
996963	3	S	3	3	26	51	3.46	45.9	0.67	42.1	0.967
996964	3	S	3	4	38	49	3.80	52.9	0.56	42.0	0.962
996965	4	S	1	1	3	61	0.36	18.2	0.17	33.0	0.988
996966	4	S	1	2	14	57	5.09	63.1	0.48	47.8	0.979
996967	4	S	1	3	26	55	7.68	85.6	0.54	48.7	0.980
996968	4	S	1	4	38	52	7.82	82.5	0.61	47.9	0.980
997733	4	S	1	5	50	64	6.74	71.1	0.64	48.4	0.976
996969	4	S	2	1	3	62	0.15	15.1	0.16	28.4	0.982
996970	4	S	2	2	14	57	3.80	48.7	0.35	49.0	0.978
996971	4	S	2	3	26	58	6.17	73.3	0.51	49.3	0.979
996972	4	S	3	1	3	62	0.18	17.0	0.10	34.7	0.989
996973	4	S	3	2	14	60	3.75	50.5	0.52	47.1	0.980
996974	4	S	3	3	26	-	6.61	76.6	0.54	43.4	0.978
996975	4	S	3	4	38	57	6.01	62.3	0.55	48.0	0.977
996976	5	S	1	1	3	-	-0.41	9.9	0.17	27.5	0.965
996977	5	S	1	2	14	50	0.40	18.9	0.24	37.6	0.970
996978	5	S	1	3	26	48	1.50	29.0	0.35	42.1	0.970
996979	5	S	1	4	38	48	1.81	31.3	0.45	43.0	0.970
996980	5	S	1	5	50	44	1.41	26.8	0.36	42.1	0.966
996981	5	S	2	1	3	57	-0.47	8.9	0.06	27.3	0.977
996982	5	S	2	2	14	52	0.57	19.9	0.23	37.2	0.975
996983	5	S	2	3	26	51	1.13	25.7	0.25	41.2	0.971
996984	5	S	2	4	38	51	1.29	26.7	0.29	43.1	0.969
996985	5	S	2	5	50	46	2.77	39.5	0.59	18.0	0.989
996986	5	S	3	1	3	54	-0.39	10.2	0.25	16.1	0.986
996987	5	S	3	2	14	47	0.79	22.1	0.25	37.3	0.978
996988	5	S	3	3	26	50	1.45	27.8	0.37	38.3	0.971
996989	5	S	3	4	38	46	2.62	39.1	0.51	42.7	0.968
996990	5	S	3	5	50	37	2.65	42.8	0.53	27.7	0.979
996991	6	S	1	1	3	59	-0.45	8.6	0.22	26.7	0.971
996992	6	S	1	2	14	54	0.71	23.1	0.34	37.6	0.961
996993	6	S	1	3	26	53	1.08	28.2	0.46	37.2	0.962
996994	6	S	1	4	38	51	1.61	36.4	0.51	38.4	0.961
996995	6	S	1	5	50	49	1.89	37.5	0.60	38.0	0.963
996996	6	S	2	1	3	60	-0.40	11.2	0.11	27.7	0.986
996997	6	S	2	2	14	-	0.49	20.5	0.31	33.4	0.967
996998	6	S	2	3	26	-	1.07	26.9	0.47	37.3	0.960
996999	6	S	2	4	38	51	1.44	31.7	0.49	37.7	0.959
997000	6	S	3	1	3	47	1.26	29.1	0.50	37.5	0.959
997001	6	S	3	2	14	59	-0.29	12.7	0.14	32.4	0.973
997002	6	S	3	3	26	55	1.46	35.3	0.40	37.8	0.961
997003	6	S	3	4	38	54	1.54	34.3	0.57	38.0	0.959
997004	6	S	3	5	50	-	1.86	39.3	0.53	42.1	0.959

Table 28: Enviromagnetic and physiological parameters, temporal study, III

location	season	tree	needle density [%]	water loss [%]	wax [mg g ⁻¹]	χ_c [10 ⁻⁸ m ³ kg ⁻¹]	SIRM [A m ⁻¹ kg ⁻¹]	ARM [A m ⁻¹ kg ⁻¹]	s-ratio	B _{cr} [mT]
1	w	1	85	53.2	14.0	2.03	35.9	0.43	0.965	42.3
1	w	2	90	n.d.	14.0	1.84	32.8	0.38	0.972	45.4
1	w	3	90	n.d.	14.0	2.06	36.6	0.49	0.966	38.6
1	s	1	95	52.8	12.3	2.48	42.3	0.61	0.967	39.4
1	s	2	85	52.4	12.3	1.63	30.7	0.40	0.963	34.4
1	s	3	85	54.6	12.3	1.39	28.5	0.40	0.968	32.4
2	w	1	100	53.1	20.6	1.29	23.6	0.37	0.974	51.3
2	w	2	90	53.2	20.6	1.52	26.8	0.34	0.973	41.7
2	w	3	80	51.4	20.6	0.90	21.4	0.34	0.972	44.7
2	s	1	90	50.6	12.9	1.33	23.1	0.31	0.978	47.9
2	s	2	85	55.4	12.9	1.25	24.0	0.33	0.905	45.6
2	s	3	80	54.0	12.9	0.83	21.4	0.25	0.979	45.5
3	w	1	80	50.7	15.9	2.52	37.6	0.45	0.975	37.3
3	w	2	90	51.9	15.9	3.63	44.9	0.61	0.977	35.9
3	w	3	90	51.5	15.9	2.02	35.5	0.47	0.975	38.5
3	s	1	80	52.3	15.4	1.10	23.5	0.30	0.968	31.4
3	s	2	85	54.3	15.4	2.04	27.1	0.41	0.969	33.3
3	s	3	80	54.1	15.4	1.91	31.5	0.45	0.964	38.1
4	w	1	75	57.6	14.6	6.12	71.3	0.58	0.964	39.1
4	w	2	70	55.2	14.6	3.64	49.9	0.41	0.969	36.7
4	w	3	80	n.d.	14.6	3.93	52.3	0.46	0.961	36.3
4	s	1	80	55.0	13.2	4.51	56.0	0.41	0.963	36.2
4	s	2	80	54.8	13.2	2.63	38.5	0.29	0.961	34.7
4	s	3	90	57.9	13.2	3.41	46.3	0.38	0.970	31.9
5	w	1	95	55.0	16.9	1.27	30.4	0.34	0.974	33.8
5	w	2	100	50.8	16.9	1.21	29.0	0.31	0.971	38.7
5	w	3	n.d.	n.d.	16.9	1.10	26.5	0.32	0.970	37.3
5	s	1	n.d.	57.0	14.5	0.69	21.0	0.28	0.983	43.1
5	s	2	100	59.8	14.5	0.60	19.9	0.21	0.980	39.7
5	s	3	100	n.d.	14.5	0.85	22.3	0.32	0.983	41.9
6	w	1	95	n.d.	18.4	0.03	16.0	0.26	0.968	36.8
6	w	2	100	52.8	18.4	0.26	20.3	0.31	0.974	36.0
6	w	3	90	49.5	18.4	0.59	23.6	0.31	0.978	31.4
6	s	1	100	54.2	17.7	0.72	23.6	0.38	0.964	34.9
6	s	2	100	n.d.	17.7	0.50	20.8	0.32	0.970	33.3
6	s	3	90	n.d.	17.7	1.03	29.0	0.39	0.964	36.8

Table 29: Magnetic properties averaged for each tree (except wax concentration determined on composite samples). Triplicate analyses for summer and winter sampling are given as weighted means of needle cohorts (n = 4 or 5).

location	water loss [%]	wax [mg g ⁻¹]	χ [10 ⁻⁸ m ³ kg ⁻¹]	SIRM [A m ⁻¹ kg ⁻¹]	ARM [A m ⁻¹ kg ⁻¹]	s-ratio	B _{cr} [mT]	
1	median	53.0	13.2	1.93	34.3	0.42	0.966	39.0
2	median	53.1	16.8	1.27	23.4	0.34	0.974	45.6
3	median	52.1	15.7	2.03	33.5	0.45	0.972	36.6
4	median	55.2	13.9	3.78	51.1	0.41	0.963	36.3
5	median	56.0	15.7	0.97	24.4	0.31	0.977	39.2
6	median	52.8	18.1	0.55	22.2	0.31	0.969	35.4
1	mean	53.3	13.2	1.90	34.5	0.45	0.967	38.7
2	mean	53.0	16.8	1.19	23.4	0.32	0.963	46.1
3	mean	52.5	15.7	2.20	33.3	0.45	0.971	35.8
4	mean	56.1	13.9	4.04	52.4	0.42	0.965	35.8
5	mean	55.7	15.7	0.95	24.8	0.29	0.977	39.1
6	mean	52.2	18.1	0.52	22.2	0.33	0.970	34.9
1	std	0.94	1.24	0.38	4.9	0.09	0.003	4.8
2	std	0.95	5.87	0.44	6.5	0.09	0.004	7.0
3	std	0.82	5.87	0.45	6.9	0.10	0.004	6.7
4	std	1.03	5.87	0.53	7.4	0.10	0.004	6.9
5	std	1.40	5.42	0.25	3.6	0.04	0.005	7.5
6	std	1.82	5.42	0.21	2.6	0.03	0.028	6.5
1	cv	0.02	0.09	0.20	0.1	0.19	0.003	0.1
2	cv	0.02	0.35	0.37	0.3	0.29	0.004	0.2
3	cv	0.02	0.37	0.21	0.2	0.22	0.005	0.2
4	cv	0.02	0.42	0.13	0.1	0.24	0.004	0.2
5	cv	0.03	0.35	0.26	0.1	0.12	0.005	0.2
6	cv	0.03	0.30	0.40	0.1	0.10	0.029	0.2

Table 30: Mean, median and standard deviation (std 1 σ) of environmental parameters for each location (n = 3), cv = coefficient of variation.

location	season	needle cohort	exposure [month]	water loss [%]	needle wax [mg g ⁻¹]	χ [10 ⁻⁸ m ³ kg ⁻¹]	STD [A m ⁻¹ kg ⁻¹]	SIRM [A m ⁻¹ kg ⁻¹]	STD [A m ⁻¹ kg ⁻¹]	ARM [A m ⁻¹ kg ⁻¹]	STD [mT]	B _{cr} [mT]	STD	s-ratio	STD
1	w	1	8	52.3	12.4	1.04	0.19	25.7	1.8	0.303	0.03	39.1	5.5	0.969	3.8E-03
1	w	2	20	52.7	15.4	2.18	0.04	37.1	0.5	0.454	0.02	46.1	2.7	0.967	2.8E-03
1	w	3	32	49.3	14.9	4.98	0.40	44.5	5.8	0.596	0.07	40.8	1.5	0.965	2.0E-03
1	w	4	44	47.5	16.4	3.41	0.22	49.1	3.7	0.641	0.03	41.9	6.6	0.968	5.6E-03
2	w	1	8	55.5	11.6	0.50	0.22	18.3	1.7	0.244	0.01	29.5	2.2	0.972	2.2E-03
2	w	2	20	52.3	12.0	1.08	0.34	22.1	3.1	0.354	0.03	38.2	6.9	0.965	1.2E-03
2	w	3	32	52.1	12.5	2.20	0.38	31.8	3.9	0.478	0.01	39.0	1.5	0.960	4.8E-03
2	w	4	44	51.7	13.7	2.19	0.04	32.8	0.9	0.461	0.04	37.8	1.1	0.961	1.2E-04
3	w	1	8	54.6	18.5	1.68	0.79	29.9	7.4	0.384	0.10	47.5	4.6	0.975	5.4E-04
3	w	2	20	51.3	-	3.29	0.80	44.9	3.6	0.577	0.06	45.4	5.0	0.972	2.3E-03
3	w	3	32	49.7	23.4	4.49	0.64	52.4	4.4	0.712	0.11	42.7	0.4	0.970	1.0E-03
4	w	1	8	54.9	12.7	2.77	0.53	42.6	4.4	0.379	0.03	43.2	0.6	0.980	4.6E-04
4	w	2	20	53.5	17.7	1.10	1.10	62.3	10.2	0.517	0.06	48.0	0.4	0.979	1.3E-03
4	w	3	32	49.9	17.6	5.90	1.63	67.0	13.9	0.560	0.09	49.0	2.4	0.978	1.3E-04
4	w	4	44	51.7	-	8.26	0.07	93.4	2.8	0.652	0.03	48.2	0.0	0.977	8.4E-05
5	w	1	8	53.3	13.8	0.60	0.19	23.6	0.7	0.272	0.02	31.3	4.5	0.980	2.7E-03
5	w	2	20	50.3	16.9	1.16	0.16	27.7	1.6	0.317	0.04	39.1	1.8	0.974	1.6E-03
5	w	3	32	50.5	16.9	2.88	0.06	37.9	0.9	0.406	0.01	42.4	0.2	0.971	1.1E-03
5	w	4	44	45.6	-	1.88	-	32.6	-	0.367	-	42.9	-	0.969	-
6	w	1	8	55.4	14.3	-0.06	0.22	15.4	2.7	0.212	0.02	29.6	2.9	0.973	5.5E-03
6	w	2	20	53.1	16.1	0.27	0.23	19.9	3.7	0.311	0.02	37.3	4.2	0.962	2.5E-03
6	w	3	32	52.5	17.2	0.91	0.35	27.5	5.5	0.398	0.04	36.4	2.2	0.962	1.4E-03
6	w	4	44	47.1	13.0	0.82	0.06	24.1	1.4	0.374	0.03	37.6	5.3	0.964	6.5E-03
1	s	1	3	60.2	10.4	-0.25	0.09	11.8	1.1	0.091	0.03	29.6	2.0	0.968	9.3E-03
1	s	2	14	55.6	15.4	1.45	0.33	30.4	4.4	0.498	0.08	37.6	0.5	0.966	1.8E-03
1	s	3	26	54.9	16.2	2.77	0.46	44.4	6.3	0.568	0.15	41.1	1.4	0.964	2.2E-04
1	s	4	38	54.5	15.1	3.28	0.39	48.0	5.5	0.756	0.11	41.8	0.8	0.959	6.4E-03
1	s	5	50	53.4	16.5	3.66	0.79	51.2	10.2	0.645	0.10	42.4	0.4	0.965	3.3E-03
2	s	1	3	59.6	8.8	-0.40	0.11	8.5	0.8	0.149	0.03	25.7	2.2	0.980	3.2E-03
2	s	2	14	56.0	13.1	0.99	0.40	21.8	2.8	0.268	0.09	35.5	2.8	0.961	3.4E-03
2	s	3	26	54.5	14.9	1.59	0.07	27.7	2.5	0.348	0.05	37.4	0.7	0.960	2.7E-03
2	s	4	38	53.6	14.9	2.50	0.14	34.6	0.9	0.456	0.07	38.1	0.3	0.957	3.9E-03
2	s	5	50	51.5	15.3	3.17	-	39.4	-	0.491	-	42.1	-	0.945	-
3	s	1	3	57.1	11.3	-0.17	0.15	10.8	0.9	0.133	0.06	25.1	2.5	0.978	2.5E-03
3	s	2	14	50.8	18.6	1.99	0.46	30.9	2.5	0.467	0.05	41.8	3.2	0.967	1.2E-03
3	s	3	26	51.3	21.2	3.24	0.68	39.9	4.7	0.556	0.10	42.4	0.3	0.970	2.0E-03
3	s	4	38	49.2	24.9	3.80	-	52.9	-	0.563	-	42.0	-	0.962	-
4	s	1	3	61.8	10.0	0.23	0.09	16.8	1.3	0.141	0.03	32.0	2.7	0.986	2.9E-03
4	s	2	14	57.9	15.7	4.21	0.62	54.1	6.4	0.449	0.07	48.0	0.8	0.979	6.8E-04
4	s	3	26	56.7	17.7	6.82	0.63	78.5	5.2	0.530	0.01	47.2	2.6	0.979	7.0E-04
4	s	4	38	54.4	24.1	6.92	0.91	72.4	10.1	0.582	0.03	47.9	0.0	0.979	1.6E-03
4	s	5	50	50.0	-	6.74	-	71.1	-	0.643	-	48.4	-	0.976	-
5	s	1	3	55.5	9.1	-0.42	0.03	9.7	0.5	0.158	0.08	23.6	5.3	0.976	8.5E-03
5	s	2	14	49.5	14.3	1.4	0.16	20.3	1.3	0.238	0.01	37.3	0.2	0.974	3.2E-03
5	s	3	26	53.0	18.3	2.27	0.16	35.6	1.3	0.411	0.05	39.4	1.6	0.970	6.8E-04
5	s	4	38	48.3	16.3	1.91	0.54	32.4	5.1	0.415	0.09	42.9	0.2	0.969	9.5E-04
5	s	5	50	42.4	19.3	2.27	0.62	36.4	6.9	0.495	0.10	29.3	9.9	0.978	9.4E-03
6	s	1	3	59.4	9.7	-0.38	0.07	10.8	1.7	0.158	0.04	28.9	2.5	0.977	6.5E-03
6	s	2	14	54.3	14.5	1.4	0.42	26.3	6.4	0.350	0.04	36.3	2.0	0.963	3.0E-03
6	s	3	26	53.5	15.9	1.23	0.22	29.8	3.2	0.499	0.05	37.5	0.4	0.961	1.3E-03
6	s	4	38	51.0	16.6	1.64	0.17	35.8	3.1	0.510	0.02	39.4	1.9	0.960	1.1E-03
6	s	5	50	48.2	17.6	1.58	0.32	33.3	4.2	0.550	0.05	37.8	0.2	0.961	1.9E-03

Table 31: Averaged mean environmental and physiological parameters for each needle cohort (n = 3), differentiated for winter (w) and summer (s) sampling.

location	needle cohort	season	exposure [months]	Ba [mg kg ⁻¹]	Ca [g kg ⁻¹]	Cd [μg kg ⁻¹]	Fe [mg kg ⁻¹]	Mo [μg kg ⁻¹]	Na [mg kg ⁻¹]	Pb [mg kg ⁻¹]	Sb [μg kg ⁻¹]	Ti [mg kg ⁻¹]	V [μg kg ⁻¹]	Zn [μg kg ⁻¹]	S REE [μg kg ⁻¹]
L1 Do	1	w	8	1.55	3.62	23	86.0	865	99	1.04	141	1.83	160	44	126
	2	w	20	2.30	5.89	21	126	544	174	1.64	200	1.99	232	62	187
	3	w	32	3.04	7.28	22	157	627	203	1.56	307	2.60	297	91	241
	4	w	44	3.75	9.35	23	165	682	476	1.84	316	2.31	334	86	253
L2 B-G1	1	w	8	1.00	3.34	170	74.4	259	16	0.54	106	1.82	129	42	100
	2	w	20	1.61	6.39	151	103	151	14	0.79	154	1.91	154	56	135
	3	w	32	2.30	9.86	117	131	184	33	1.09	209	2.23	282	73	182
	4	w	44	2.78	12.05	116	140	178	46	1.10	253	2.35	275	77	195
L3 Bb	1	w	8	1.99	4.02	187	122	196	8	0.34	95	1.86	308	60	220
	2	w	20	2.89	7.24	233	169	233	11	0.25	278	2.78	432	102	317
	3	w	32	4.46	8.20	255	251	221	29	0.40	374	3.83	626	147	533
	4	w	44	5.25	9.35	255	251	221	29	0.40	374	3.83	626	147	533
L4 Co	1	w	8	1.25	2.79	52	156	429	217	0.77	366	2.14	220	67	134
	2	w	20	1.80	4.41	48	203	408	345	0.97	524	2.36	286	90	169
	3	w	32	2.40	7.26	42	233	414	401	0.48	580	2.85	339	117	204
	4	w	44	3.77	10.51	38	349	439	469	2.09	822	3.79	526	162	340
L5 Bn	1	w	8	1.55	2.06	25	73.9	287	102	0.49	175	1.73	185	49	97
	2	w	20	2.69	4.86	21	92.5	234	93	0.40	118	1.83	211	47	125
	3	w	32	4.12	5.27	14	132	198	112	0.31	228	2.65	272	81	204
	4	w	44	3.88	7.18	6	108	153	81	0.83	207	2.20	286	73	174
L6 Fu	1	w	8	1.01	2.93	44	52.2	94	77	0.19	78	1.27	100	27	81
	2	w	20	1.69	5.43	33	88.8	84	164	0.17	77	1.51	172	37	141
	3	w	32	2.26	7.31	30	109	239	239	0.30	117	1.62	216	44	169
	4	w	44	2.38	8.27	19	87.9	76	241	0.13	112	1.74	167	41	141
L1 Do	1	s	3	0.50	1.45	19	36.9	849	9	0.25	19	1.05	28	15	60
	2	s	14	1.34	3.35	12	93.0	457	76	0.84	108	1.55	126	45	120
	3	s	26	2.02	4.37	8	133	424	113	1.21	172	1.77	202	67	175
	4	s	38	2.37	5.06	9	138	393	59	1.31	238	1.88	270	96	265
	5	s	50	2.74	6.77	8	137	514	58	1.33	285	2.21	239	77	199
L2 B-G1	1	s	3	0.65	2.73	225	43.6	389	8	0.24	37	1.04	33	17	50
	2	s	14	1.57	5.85	222	91.4	113	32	0.52	117	1.49	117	43	131
	3	s	26	2.18	7.76	132	146	154	57	0.90	185	2.02	223	74	244
	4	s	38	2.57	9.22	130	181	195	128	1.18	261	2.74	270	96	265
	5	s	50	3.18	8.25	79	244	238	100	1.82	337	3.36	402	138	361
L3 Bb	1	s	3	0.67	2.18	110	47.1	147	8	0.18	27	1.88	62	41	148
	2	s	14	2.31	6.23	154	139	100	19	0.76	159	3.23	269	101	375
	3	s	26	3.72	9.29	160	203	158	26	1.08	283	4.26	468	149	543
	4	s	38	3.60	9.79	140	207	154	66	1.07	319	4.18	419	144	475
L4 Co	1	s	3	0.48	1.91	65	62.6	522	10	0.20	114	1.66	43	25	46
	2	s	14	1.54	6.07	55	183	310	262	0.87	390	2.53	222	85	137
	3	s	26	2.46	7.56	41	294	392	395	1.46	678	3.48	386	140	227
	4	s	38	2.99	8.13	36	294	377	329	1.65	733	3.45	429	156	233
L5 Bn	1	s	3	0.53	1.69	29	31.6	273	2	0.09	23	1.25	17	20	24
	2	s	14	1.54	3.81	30	71.5	103	8	0.36	116	1.78	95	46	79
	3	s	26	2.32	4.65	27	91.4	131	11	0.53	176	1.97	135	58	110
	4	s	38	4.27	5.87	17	137	159	11	1.01	313	3.11	251	98	208
	5	s	50	2.85	8.74	8	81.0	107	41	0.56	162	1.83	166	54	120
L6 Fu	1	s	3	0.87	3.17	89	39.1	114	46	0.23	28	1.32	38	18	49
	2	s	14	1.97	5.82	61	119	84	180	0.80	135	2.04	168	59	188
	3	s	26	2.38	7.48	46	116	84	157	0.78	147	1.99	166	59	175
	4	s	38	2.51	7.98	28	124	92	269	0.93	160	2.25	193	65	205
	5	s	50	2.66	9.53	11	94.4	68	168	0.91	112	1.82	139	49	150

Table 32: Major and trace element concentrations for 6 locations sampled in winter (w) and summer (s) season for 1 to 5 needle cohorts (n=51).

location	Ba EF	Ca EF	Cd EF	Fe EF	Mo EF	Na EF	Pb EF	Sb EF	Ti EF	V EF	Zn EF
L1 Do	3.41	146	286	2.97	697	4.12	62.7	850	0.74	3.21	0.28
	3.41	160	174	2.93	295	4.91	66.7	814	0.54	3.15	0.27
	3.50	154	140	2.85	264	4.43	49.2	972	0.55	3.13	0.30
	4.10	187	141	2.83	273	9.91	55.3	950	0.46	3.34	0.27
L2 B-G1	2.76	170	2655	3.24	264	0.83	41.1	810	0.92	3.27	0.34
	3.30	240	1521	3.31	113	0.56	44.7	864	0.72	4.01	0.33
	3.49	274	993	3.13	103	0.96	45.7	870	0.62	3.92	0.32
	3.95	313	924	3.12	93	1.24	43.0	988	0.61	3.57	0.31
L3 Bb	2.50	93	1320	2.40	90	0.19	11.9	329	0.43	3.55	0.22
	2.53	116	1144	2.33	56	0.19	5.9	637	0.44	3.46	0.26
	2.32	78	743	2.05	42	0.28	5.8	534	0.36	2.98	0.22
L4 Co	2.58	106	602	5.08	325	8.55	43.9	2081	0.81	4.17	0.40
	2.94	132	445	5.22	245	10.73	43.5	2353	0.71	4.29	0.43
	3.24	180	319	4.95	205	10.33	17.9	2158	0.71	4.20	0.46
	3.07	157	174	4.47	131	7.26	46.9	1839	0.56	3.92	0.38
L5 Bn	4.41	107	403	3.30	300	5.52	38.4	1369	0.90	4.83	0.40
	5.95	197	256	3.22	190	3.92	24.2	720	0.74	4.27	0.30
	5.59	131	110	2.82	99	2.89	11.5	853	0.66	3.39	0.32
	6.17	209	50	2.70	90	2.46	36.5	906	0.64	4.18	0.34
L6 Fu	3.47	184	845	2.81	118	5.02	17.6	730	0.80	3.13	0.27
	3.30	195	858	2.73	61	6.12	9.2	414	0.54	3.08	0.21
	3.70	219	280	2.79	58	7.46	13.6	528	0.49	3.24	0.21
	4.65	297	111	2.70	54	8.98	7.2	604	0.62	2.99	0.23
L1 Do	2.31	123	487	2.69	1442	0.77	31.7	247	0.89	1.18	0.21
	3.08	141	153	3.36	385	3.31	52.9	681	0.65	2.66	0.30
	3.19	126	70	3.30	245	3.39	52.4	748	0.51	2.92	0.31
	3.65	143	76	3.34	222	1.75	55.5	1009	0.53	3.28	0.32
	3.81	173	64	3.00	263	1.55	51.0	1089	0.56	3.05	0.31
L2 B-G1	3.62	278	7029	3.81	794	0.82	36.0	563	1.06	1.68	0.27
	3.31	226	2620	3.03	88	1.30	30.0	763	0.58	2.25	0.26
	2.47	161	838	2.60	64	1.24	28.1	578	0.42	2.32	0.24
	2.69	176	762	2.97	75	2.54	33.8	750	0.52	2.59	0.29
	2.44	116	340	2.93	67	1.46	38.2	711	0.47	2.82	0.30
L3 Bb	1.26	75	1159	1.38	101	0.29	9.3	141	0.65	1.07	0.22
	1.71	84	638	1.61	27	0.27	15.4	324	0.44	1.82	0.22
	1.89	87	457	1.62	30	0.25	15.2	396	0.40	2.18	0.22
	2.10	105	456	1.89	33	0.74	17.1	511	0.45	2.24	0.24
L4 Co	2.87	209	2171	5.87	1142	1.13	32.1	1866	1.81	2.35	0.44
	3.10	225	620	5.79	230	10.05	48.1	2164	0.94	4.10	0.49
	3.00	169	277	5.64	175	9.17	49.0	2270	0.78	4.31	0.49
	3.56	177	239	5.50	164	7.45	54.1	2398	0.75	4.67	0.54
L5 Bn	6.07	353	1864	5.65	1142	0.43	28.2	719	2.61	1.78	0.64
	5.36	243	586	3.91	132	0.50	34.8	1111	1.13	3.04	0.47
	5.86	215	377	3.63	121	0.51	36.9	1224	0.91	3.13	0.42
	5.69	143	130	2.87	77	0.28	37.1	1148	0.76	3.06	0.38
	6.58	370	99	2.94	91	1.79	35.8	1031	0.77	3.51	0.36
L6 Fu	4.90	326	2814	3.45	235	4.93	35.5	437	1.36	1.94	0.29
	2.91	157	503	2.76	46	5.07	32.3	547	0.55	2.28	0.25
	3.76	216	405	2.88	49	4.70	34.0	638	0.58	2.40	0.27
	3.39	198	214	2.63	46	6.92	34.5	596	0.56	2.39	0.26
	4.89	322	111	2.73	46	5.87	45.8	567	0.62	2.35	0.26

Table 33: Enrichment factors (EF) for 6 locations sampled in winter (w) and summer (s) season for 1 to 5 needle cohorts (n=51).

location 6 cohort	needle	season [month]	exposure	P	A	DBT	CPP	3-MP	2-MP	9-MP	1-MP	S MP	2,6-DMP	2,7-DMP	x4-DMP DMP	2,9-, 1,6-	1,7-DMP	1,8-DMP	S DMP + EP	retene
L1 Do	1	w	8	410	nd	20.8	7.96	15.1	26.6	13.3	16.1	71.0	3.12	2.35	9.01	3.88	4.95	0.63	36.85	3.83
	2	w	20	969	nd	33.9	15.7	35.0	58.7	29.0	39.3	161.9	6.01	4.96	19.84	7.58	12.57	1.05	75.12	7.71
	3	w	32	1200	nd	38.9	18.3	45.7	82.3	42.0	48.3	211.2	8.94	8.61	26.53	12.23	19.03	1.97	98.49	9.76
	4	w	44	1120	15.9	41.5	27.0	63.1	127.2	42.0	71.3	416.4	15.2	15.4	37.15	18.44	28.17	3.45	153.87	14.63
L2 B-Gl	1	w	8	93	3.48	4.40	3.04	2.91	2.48	2.55	2.95	10.9	0.30	0.14	1.32	0.66	0.54	0.06	5.36	1.12
	2	w	20	204	nd	6.55	4.86	5.43	4.14	5.01	4.78	19.4	0.48	0.35	2.26	0.76	0.76	0.10	8.37	1.10
	3	w	32	247	nd	7.56	7.27	8.12	6.71	7.50	6.71	29.8	0.65	0.65	3.80	1.54	1.62	0.22	13.19	1.86
	4	w	44	212	7.63	7.18	7.53	8.51	5.92	8.28	8.35	46.0	0.65	0.65	3.59	1.31	1.08	0.24	12.07	1.32
L3 Bb	1	w	8	146	nd	13.5	6.85	8.56	9.38	8.38	6.95	31.2	1.49	0.80	4.55	2.33	2.38	0.63	18.38	3.54
	2	w	20	542	13.7	41.5	17.8	17.9	17.0	12.6	14.1	61.6	1.60	0.63	5.22	2.41	3.66	0.33	19.98	2.24
	3	w	32	1071	27.5	84.2	37.3	39.2	38.9	27.6	32.3	183.0	2.57	1.29	13.00	5.82	4.11	0.97	46.30	5.24
L4 Co	1	w	8	162	nd	7.18	7.18	5.54	6.39	5.86	5.0	22.8	0.94	0.69	3.41	1.65	2.11	0.37	12.95	2.44
	2	w	20	580	19.5	18.2	21.5	19.3	17.6	23.5	15.6	76.0	2.71	2.11	10.46	4.99	6.27	1.00	41.06	5.90
	3	w	32	775	29.9	19.3	27.1	25.4	18.0	36.2	20.8	100.3	3.31	2.10	13.50	5.76	7.12	1.20	46.05	5.97
L5 Bo	1	w	8	161	5.82	10.4	5.70	6.37	6.93	6.70	5.89	25.9	1.03	0.79	4.02	1.80	1.87	0.36	14.84	3.27
	2	w	20	317	16.5	16.2	10.2	10.8	9.05	13.1	10.6	43.5	1.30	0.93	6.64	2.47	2.31	0.53	21.50	3.01
	3	w	32	283	10.7	13.3	9.18	10.4	9.39	11.7	10.4	41.9	1.43	1.07	6.46	2.54	2.59	0.45	21.26	2.91
	4	w	44	536	22.9	19.9	15.8	17.16	4.68	15.3	6.33	33.5	0.88	0.88	4.88	1.08	1.91	0.21	14.94	1.73
L6 Fu	1	w	8	69	2.08	6.41	3.83	1.89	2.48	1.62	1.84	7.83	0.35	0.25	1.48	0.97	1.39	0.20	4.08	1.55
	2	w	20	186	6.46	7.03	5.58	4.79	4.37	4.14	4.62	17.9	0.44	0.27	1.65	0.99	1.54	0.26	8.06	2.57
	3	w	32	268	11.3	12.3	9.34	8.55	9.66	7.50	8.84	34.6	0.76	0.75	3.10	1.76	2.45	0.50	13.68	4.32
	4	w	44	317	5.37	15.4	6.44	8.43	9.45	5.04	8.14	44.7	0.64	0.64	1.86	1.09	2.02	0.28	8.94	2.43
L1 Do	1	s	3	135	1.26	8.40	3.17	5.97	9.71	4.97	4.97	25.6	0.53	0.87	3.74	1.72	1.79	0.20	12.62	1.15
	2	s	14	245	6.63	16.5	5.06	9.78	15.7	6.97	8.97	41.4	1.32	1.65	7.09	2.89	2.77	0.31	27.13	4.03
	3	s	26	360	7.06	17.0	10.1	20.9	34.5	15.4	20.1	90.9	3.38	3.52	11.95	5.74	8.64	1.17	44.66	7.48
	4	s	38	602	14.3	25.9	15.1	30.8	44.4	25.2	32.3	132.6	4.34	4.21	18.04	7.37	10.75	0.92	61.18	8.11
	5	s	50	1232	22.4	47.1	25.6	60.6	108.7	45.0	62.5	340.3	12.6	11.1	32.47	14.48	23.20	2.74	139.27	11.25
L2 B-Gl	1	s	3	45	nd	3.07	0.98	1.58	1.87	1.12	1.22	5.79	0.09	0.10	0.78	0.14	0.14	0.04	3.90	0.30
	2	s	14	71	1.09	2.87	1.61	2.51	1.81	1.91	1.79	8.02	nd	nd	0.94	0.27	0.13	0.02	5.66	0.90
	3	s	26	185	nd	6.41	4.91	7.26	4.81	5.37	5.85	23.3	nd	nd	3.12	0.95	0.65	0.06	17.12	2.19
	4	s	38	301	4.30	7.59	7.15	11.0	7.69	9.0	9.34	37.0	0.60	0.24	3.26	1.20	0.84	0.10	10.56	1.12
	5	s	50	211	4.05	7.97	6.91	10.2	7.32	10.3	7.47	49.4	0.80	0.34	3.57	1.17	0.81	0.00	14.78	0.87
L3 Bb	1	s	3	78	0.80	7.31	2.51	3.52	3.89	2.53	2.60	12.6	0.33	0.15	1.34	0.40	0.40	0.04	5.18	0.43
	2	s	14	418	10.5	32.7	16.5	15.4	12.6	12.0	14.0	54.0	0.80	0.23	4.57	1.55	0.89	0.11	12.66	0.85
	3	s	26	866	25.0	56.7	27.2	20.1	15.1	17.3	14.1	66.6	2.04	2.04	5.39	1.79	0.92	0.17	19.18	0.91
	4	s	38	2113	34.4	136.5	67.8	65.9	52.9	50.8	49.9	257.6	5.30	2.59	15.54	5.70	4.28	0.42	46.64	2.68
L4 Co	1	s	3	129	nd	7.62	4.78	6.18	7.15	4.23	4.15	21.7	0.59	1.17	2.50	1.01	0.77	0.13	8.67	1.21
	2	s	14	384	6.57	13.3	13.9	13.72	10.96	13.8	9.60	48.1	0.83	0.45	5.52	1.55	1.06	0.20	14.71	1.26
	3	s	26	710	nd	14.5	20.7	19.45	13.09	22.6	13.6	68.7	0.75	0.61	6.52	1.91	1.16	0.16	16.96	1.17
	4	s	38	771	nd	6.80	19.5	15.06	8.13	29.3	9.49	98.0	3.10	3.10	9.53	2.40	2.79	0.28	34.50	4.36
L5 Bo	1	s	3	95	1.08	6.57	2.26	4.14	4.23	4.29	3.20	15.9	0.54	0.27	2.31	0.90	0.81	0.15	0.82	0.73
	2	s	14	124	1.61	6.74	3.20	3.91	3.17	4.15	3.30	14.5	0.23	0.10	1.58	0.46	0.30	0.03	0.46	0.35
	3	s	26	354	6.17	13.3	7.44	9.09	5.90	11.6	7.24	33.8	0.50	0.24	3.77	1.08	0.69	0.12	1.82	0.83
	4	s	38	485	nd	15.0	10.8	13.2	8.24	15.8	11.1	48.3	0.75	0.35	6.22	1.49	0.95	0.20	1.93	1.06
	5	s	50	536	13.3	11.1	10.5	9.20	5.16	19.3	7.90	61.3	0.49	0.22	5.21	1.08	0.81	0.15	17.18	1.36
L6 Fu	1	s	3	33	0.72	1.32	0.65	0.88	1.27	0.54	0.66	3.36	nd	0.00	0.29	0.07	0.14	0.00	1.58	0.31
	2	s	14	131	nd	4.75	2.40	2.95	3.38	2.33	2.63	11.3	nd	0.00	0.77	0.11	0.35	0.00	3.69	0.89
	3	s	26	126	nd	3.69	2.92	3.13	3.07	2.34	2.44	10.9	0.08	0.04	0.59	0.11	0.05	0.00	3.05	0.00
	4	s	38	344	7.23	8.86	7.82	8.51	6.95	6.30	7.03	28.8	nd	0.00	1.99	0.68	1.08	0.00	7.47	0.63
	5	s	50	483	nd	12.3	8.73	9.85	9.78	9.35	8.76	47.6	0.44	0.23	2.98	0.76	1.40	0.11	11.33	3.34

Table 34: Concentration data of 3-ring PAH measured on pine needles of six locations and up to 5 consecutive needle age cohorts (n=50).

ID	χ [m ³ kg ⁻¹]	B_{cr} [mT]	SIRM [A m ⁻¹ kg ⁻¹]	ARM [A m ⁻¹ kg ⁻¹]	SIRM / k	kARM / k	s-ratio	IRM / ARM
1	1.09	38.0	26.9	0.37	19.7	0.843	0.965	74
2	1.91	41.9	36.9	0.39	15.5	0.509	0.966	96
3	1.98	42.0	35.1	0.44	15.2	0.603	0.967	82
4	2.36	37.8	41.5	0.46	14.1	0.493	0.966	90
5	2.30	38.5	33.8	0.55	11.7	0.601	0.965	61
6	0.44	33.5	20.3	0.32	37.0	1.836	0.971	63
7	1.06	38.0	29.6	0.32	22.3	0.753	0.966	93
8	1.24	33.7	25.0	0.37	16.1	0.749	0.970	67
9	1.25	37.7	28.1	0.34	17.9	0.672	0.960	84
10	0.92	31.9	26.2	0.40	22.9	1.086	0.976	66
11	0.36	27.1	21.9	0.22	48.2	1.511	0.967	100
12	2.52	42.1	47.6	0.65	15.1	0.647	0.966	73
13	0.83	33.1	26.2	0.30	25.3	0.919	0.971	87
14	2.72	45.9	39.3	0.51	13.0	0.510	0.973	78
15	2.37	37.2	37.5	0.54	12.6	0.576	0.968	69
16	2.11	37.6	35.0	0.52	13.3	0.626	0.966	67
17	2.05	46.8	34.5	0.51	13.5	0.627	0.972	68
18	1.24	35.4	23.9	0.35	20.9	0.988	0.966	68
19	0.97	34.0	25.8	0.34	21.3	0.876	0.969	76
20	0.83	39.6	26.6	0.36	25.8	1.110	0.967	73
21	2.62	42.1	46.2	0.41	14.1	0.392	0.960	113
22	2.02	42.2	34.8	0.33	13.8	0.406	0.972	107
23	4.56	46.4	57.8	0.48	10.8	0.292	0.954	113
24	2.63	38.4	45.4	0.44	13.8	0.416	0.973	104
25	2.09	42.8	38.6	0.48	14.8	0.583	0.964	80
26	1.53	42.0	34.9	0.45	18.3	0.740	0.961	78
27	1.16	41.7	29.1	0.37	20.1	0.803	0.964	79
28	1.28	38.3	29.1	0.32	18.2	0.634	0.971	90
29	2.30	42.1	33.4	0.54	11.7	0.589	0.963	62
30	3.69	42.8	52.0	0.00	11.3	0.000	0.974	0
31	1.58	26.4	32.6	0.40	16.5	0.635	0.975	82
32	-0.13	28.1	13.2	0.24	-80.8	-4.614	0.973	55
33	0.13	33.2	15.9	0.28	99.2	5.495	0.976	57
34	2.35	37.6	40.8	0.63	13.9	0.672	0.967	65
35	1.31	37.9	30.1	0.35	18.4	0.665	0.967	87
36	1.95	41.3	36.4	0.39	14.9	0.502	0.970	93
37	2.36	42.4	35.9	0.48	12.2	0.515	0.968	74
38	1.13	37.5	29.3	0.35	20.7	0.768	0.966	85
39	0.58	32.5	21.5	0.23	29.6	1.010	0.967	92
40	0.42	n.a.	n.a.	0.28	n.a.	1.693	n.a.	n.a.
41	1.56	38.7	32.9	0.44	16.9	0.714	0.961	74
42	0.29	31.5	16.8	0.20	45.7	1.744	0.972	82
43	1.84	38.1	34.5	0.37	15.0	0.499	0.972	94
44	0.94	38.3	29.4	0.37	24.9	0.990	0.979	79
45	0.51	27.3	22.7	0.33	35.7	1.619	0.978	69
46	0.82	32.5	26.2	0.31	25.6	0.966	0.975	83
47	1.52	37.3	33.6	0.45	17.7	0.743	0.976	75
48	2.60	42.2	42.8	0.40	13.2	0.390	0.976	106
49	1.02	34.1	27.4	0.43	21.5	1.069	0.966	63
50	1.69	38.1	36.0	0.48	17.0	0.718	0.965	74
51	0.52	26.4	24.1	0.26	36.8	1.242	0.977	93
52	1.79	31.8	29.9	0.34	13.3	0.477	0.978	88
53	1.17	30.6	30.6	0.39	20.8	0.832	0.974	79
54	1.02	32.5	31.9	0.39	24.9	0.966	0.976	81
55	0.48	36.9	18.8	0.26	31.3	1.358	1.008	73
56	1.78	37.8	39.8	0.47	17.9	0.659	0.968	85
57	1.19	37.2	28.6	0.32	23.5	0.851	0.976	89
58	1.96	37.7	47.3	0.42	19.3	0.541	0.973	112
59	1.29	41.8	42.3	0.28	26.3	0.552	0.978	150
60	1.11	38.1	45.4	0.36	32.6	0.819	0.986	125
61	0.37	26.5	20.5	0.33	44.1	2.249	0.976	62
62	2.14	41.4	34.2	0.45	12.8	0.525	0.966	77
63	2.30	42.8	44.9	0.43	15.6	0.475	0.973	103
64	0.30	34.3	19.9	0.29	17.2	1.290	0.967	68
65	0.33	37.3	19.2	0.28	46.5	2.099	0.970	70
66	0.87	32.5	28.3	0.34	26.0	0.991	0.967	82
67	2.30	33.3	35.5	0.67	12.3	0.726	0.978	53
68	1.08	38.2	28.5	0.33	21.1	0.766	0.969	87
69	1.14	37.2	29.8	0.39	21.0	0.870	0.975	76
70	0.56	32.8	23.0	0.33	32.7	1.473	0.973	70
71	0.49	33.0	30.2	0.28	49.2	1.408	0.976	110

Table 35: Enviromagnetic parameters on pine needles in the Cologne Conurbation (data sheet).

ID	Ag [ng g ⁻¹]	As [ng g ⁻¹]	Au [ng g ⁻¹]	B [μg g ⁻¹]	Ba [μg g ⁻¹]	Bi [ng g ⁻¹]	Ca [%]	Cd [ng g ⁻¹]	Ce [ng g ⁻¹]	Co [ng g ⁻¹]	Cr [ng g ⁻¹]	Cs [ng g ⁻¹]
1	4.05	< 100	< 1	22.87	3.01	10.07	0.48	63.34	110.03	79.16	777.77	15.75
2	10.77	< 100	1.23	17.81	2.91	20.93	0.66	385.37	147.07	387.45	776.07	13.71
3	11.32	< 100	3.87	27.42	2.20	24.22	0.54	22.07	71.44	35.33	784.48	51.55
4	27.04	< 100	1.73	12.95	3.04	21.80	0.46	148.68	73.48	68.30	716.59	9.71
5	52.02	< 100	2.97	23.64	3.58	51.08	0.98	161.26	87.31	72.39	510.20	11.87
6	11.39	< 100	2.46	17.86	1.13	26.08	0.50	70.47	51.17	53.40	404.24	14.38
7	11.46	< 100	5.56	18.55	0.97	13.77	0.34	90.23	72.94	151.02	669.74	9.08
8	43.06	< 100	1.41	16.17	2.01	24.69	0.68	245.00	67.28	82.13	539.34	22.26
9	18.99	< 100	1.41	20.52	1.11	20.66	0.58	67.64	56.34	99.28	540.09	13.55
10	10.31	< 100	1.48	17.21	0.89	21.59	0.36	28.63	33.79	39.94	963.22	6.56
11	6.15	353.68	1.15	9.42	0.50	9.30	0.13	76.62	31.02	44.16	1250.00	14.94
12	21.00	< 100	172.60	14.13	1.65	37.79	0.40	52.76	88.20	87.74	925.39	14.25
13	23.74	122.21	1.52	16.29	1.49	11.86	0.40	65.06	69.74	75.94	1170.15	15.90
14	25.83	285.88	6.11	14.56	2.74	19.89	0.60	216.98	128.76	624.03	846.74	37.18
15	9.50	< 100	< 1	31.38	4.57	12.07	0.60	299.65	164.42	230.60	621.38	19.38
16	20.68	< 100	1.86	23.88	1.99	15.85	0.49	43.37	86.67	66.74	521.55	15.25
17	9.87	< 100	1.54	7.96	1.78	14.51	0.37	158.56	57.18	52.52	680.04	6.38
18	18.69	132.29	1.49	34.44	1.78	18.73	0.72	136.70	59.00	40.48	555.33	13.47
19	20.31	< 100	3.60	11.55	1.13	22.41	0.28	152.01	53.89	62.14	725.23	11.08
20	19.11	< 100	3.22	12.01	1.46	13.91	0.52	225.40	73.00	76.49	581.67	10.00
21	26.79	< 100	1.75	12.63	4.08	36.05	0.85	534.67	155.98	183.70	881.29	23.09
22	9.57	100.31	1.96	26.31	1.89	13.69	0.37	36.09	80.12	53.62	671.75	5.98
23	40.84	235.00	9.39	42.58	2.43	25.94	0.68	44.00	92.91	57.28	929.54	22.77
24	26.66	< 100	< 1	18.66	1.97	12.94	0.29	42.39	156.18	103.93	967.85	10.80
25	21.87	131.17	1.82	24.85	2.56	16.70	0.54	78.50	164.50	107.62	736.40	15.04
26	9.65	< 100	1.28	12.87	1.87	16.93	0.36	86.61	104.35	66.87	775.41	10.81
27	6.00	246.14	1.42	20.06	1.66	8.17	0.34	17.96	214.63	82.93	689.54	18.85
28	11.29	< 100	1.53	11.38	1.23	8.84	0.18	29.25	81.36	77.74	431.45	6.41
29	8.74	< 100	2.23	11.34	1.99	15.87	0.38	24.13	81.25	46.92	477.53	9.65
30	42.64	< 100	103.73	32.85	7.06	19.37	0.79	151.22	85.10	65.48	755.48	27.12
31	9.44	< 100	< 1	22.20	5.98	25.43	0.85	193.44	65.29	282.19	965.05	7.61
32	3.92	< 100	< 1	13.08	0.55	12.46	0.49	146.46	31.68	53.36	441.08	31.80
33	28.54	< 100	1.86	16.18	1.83	7.58	0.49	275.74	31.34	175.40	841.32	16.32
34	2.36	< 100	1.46	15.05	2.23	61.14	0.75	320.13	107.45	99.38	725.51	13.00
35	18.37	< 100	1.90	20.11	1.70	9.23	0.43	81.84	51.15	40.13	540.46	12.36
36	13.36	< 100	1.95	21.89	2.29	15.18	0.49	22.99	111.01	50.61	521.87	6.89
37	14.64	104.51	1.44	8.00	2.10	16.72	0.27	138.95	99.17	447.16	526.27	7.47
38	17.79	< 100	1.70	15.50	1.22	11.15	0.39	48.14	89.42	83.95	512.30	13.92
39	9.91	< 100	2.67	15.30	1.12	10.72	0.28	181.11	63.46	85.55	417.04	5.72
40	27.28	< 100	5.72	16.98	1.46	7.91	0.36	322.37	53.20	75.24	351.72	5.32
41	7.16	< 100	1.43	25.78	3.39	14.83	0.54	48.79	82.83	84.11	348.51	8.09
42	3.35	< 100	< 1	32.74	0.93	6.58	0.36	71.23	35.70	102.51	433.62	9.78
43	15.20	< 100	2.45	33.87	2.93	25.00	0.58	26.85	66.68	46.54	655.02	17.94
44	16.77	< 100	1.21	27.41	2.45	27.93	0.92	84.04	52.13	93.62	590.76	7.82
45	< 1	< 100	2.84	9.03	0.75	20.18	0.39	68.51	41.28	63.83	879.72	5.55
46	9.00	< 100	1.68	19.94	1.83	8.59	0.60	188.99	91.79	79.30	1050.00	12.66
47	4.88	< 100	1.03	13.11	1.76	31.22	0.83	100.58	74.73	114.15	594.63	15.57
48	7.17	< 100	1.95	23.52	3.30	30.85	0.68	44.92	93.85	53.93	825.98	14.45
49	7.41	< 100	1.68	14.52	1.46	9.53	0.43	32.78	60.18	128.19	636.14	5.82
50	22.43	< 100	1.10	16.52	4.07	14.29	0.41	60.13	106.01	115.02	670.90	16.96
51	30.53	< 100	< 1	9.25	1.13	6.32	0.39	23.87	61.09	34.26	1310.00	4.58
52	15.19	< 100	2.55	15.50	1.42	13.29	0.33	27.00	46.55	44.32	1040.00	7.44
53	16.44	< 100	1.06	15.64	3.13	20.38	0.56	247.39	96.29	440.95	1320.00	18.91
54	9.79	< 100	1.08	13.98	1.81	31.62	0.86	237.99	115.44	97.80	821.83	10.68
55	28.15	< 100	4.91	17.71	1.49	26.85	0.44	138.53	53.01	63.75	803.29	5.37
56	26.52	< 100	1.77	16.16	2.58	13.55	0.54	271.25	117.85	340.84	887.16	8.04
57	27.44	< 100	6.07	16.45	2.79	14.23	0.42	19.13	58.60	38.46	708.28	20.42
58	2.67	< 100	2.52	11.03	2.08	32.83	0.47	28.61	116.37	47.65	771.35	10.09
59	13.29	< 100	1.50	12.73	1.93	8.47	0.37	265.86	98.48	469.68	1030.00	12.26
60	< 1	< 100	0.98	26.52	1.13	56.07	0.70	32.32	29.36	47.39	1050.00	10.55
61	4.59	< 100	1.25	17.22	1.71	23.67	0.55	56.34	42.98	38.48	1520.00	12.13
62	6.22	< 100	1.08	20.99	2.12	46.29	0.48	711.72	123.39	466.30	774.02	11.51
63	4.45	< 100	1.60	21.33	2.39	34.02	0.51	24.95	172.96	57.48	926.26	11.98
64	22.00	< 100	17.18	1.56	12.95	0.49	35.70	48.14	31.47	494.93	103.92	10.74
65	13.57	103.39	1.29	15.85	1.06	7.29	0.59	24.49	31.42	24.60	587.37	72.25
66	9.88	191.76	1.12	6.41	2.05	14.37	0.42	16.61	90.55	40.66	712.07	10.74
67	11.83	< 100	3.20	27.23	1.59	26.97	0.42	156.78	87.68	2350.00	692.08	6.72
68	11.66	< 100	1.49	19.84	1.68	42.16	0.48	40.97	96.51	38.57	591.41	6.84
69	14.66	< 100	1.51	21.94	3.29	32.06	0.65	112.06	93.77	64.93	840.95	6.45
70	20.61	< 100	1.43	7.61	2.97	20.05	0.53	189.44	162.31	96.85	1230.00	6.59
71	< 1	< 100	1.37	14.65	2.33	7.51	0.65	41.61	68.16	57.00	634.11	13.45

Table 36: Major and trace element concentrations and enrichment factors (EF) on pine needles in the Cologne Conurbation, I. ID refers to sampling site as indicated on overlay transparency Fig. 62 (data sheet 1-10).

ID	Cu [$\mu\text{g g}^{-1}$]	Dy [ng g^{-1}]	Er [ng g^{-1}]	Eu [ng g^{-1}]	Fe [$\mu\text{g g}^{-1}$]	Ga [ng g^{-1}]	Gd [ng g^{-1}]	Hf [ng g^{-1}]	Hg [ng g^{-1}]	Ho [ng g^{-1}]	In [ng g^{-1}]	K [%]
1	2.05	6.72	3.30	2.81	149.77	19.73	8.44	2.54	57.25	1.20	0.96	0.92
2	2.53	9.56	4.77	3.67	164.97	20.10	11.92	2.71	40.09	1.74	1.42	0.42
3	8.23	3.54	1.80	1.65	117.09	13.02	5.04	2.05	37.25	0.61	1.91	0.43
4	2.88	4.56	2.22	1.98	137.49	16.71	5.58	2.60	7.21	0.77	1.37	0.51
5	2.75	4.76	2.34	2.04	115.72	18.35	6.47	2.64	42.35	0.83	1.60	0.38
6	2.13	2.81	1.41	1.18	65.40	9.99	3.85	1.42	48.20	0.47	0.80	0.44
7	2.39	4.43	2.40	1.58	106.31	12.76	5.65	1.75	17.58	0.81	0.91	0.59
8	2.63	5.40	2.83	1.74	91.90	12.17	6.09	2.62	47.48	0.96	0.93	0.38
9	3.08	3.00	1.57	1.30	95.34	11.57	4.03	2.75	32.34	0.54	1.12	0.52
10	2.83	2.00	0.94	0.83	63.64	9.35	2.35	1.32	28.33	0.33	0.93	0.60
11	4.19	1.76	0.87	0.77	72.08	4.97	2.36	1.04	12.22	0.31	1.24	0.55
12	1.58	4.63	2.23	1.76	129.97	15.55	6.00	2.47	34.93	0.82	1.85	0.50
13	2.73	3.81	1.91	1.57	105.09	11.48	4.99	1.44	9.89	0.67	0.88	0.55
14	3.71	8.96	5.00	3.07	160.93	23.77	9.97	2.71	19.97	1.70	0.48	0.40
15	2.25	9.15	4.71	3.58	167.81	30.11	11.88	3.34	72.59	1.64	1.16	0.71
16	2.64	4.75	2.45	2.09	135.48	16.31	6.41	2.39	24.70	0.86	1.47	0.53
17	2.77	3.82	2.13	1.54	114.40	10.80	4.84	2.61	10.32	0.72	1.02	0.64
18	2.80	3.24	1.65	1.50	107.38	20.13	4.23	1.84	35.89	0.56	1.18	0.43
19	2.64	6.75	4.10	1.85	82.96	10.21	6.81	1.82	31.76	1.36	0.87	0.34
20	2.62	9.40	5.10	2.52	89.63	14.25	9.20	1.89	29.65	1.79	1.09	0.70
21	2.73	13.54	7.71	4.12	158.83	22.46	16.21	3.32	48.56	2.60	1.61	0.46
22	2.40	4.48	2.31	1.89	133.45	13.86	5.80	2.73	19.64	0.81	1.20	0.63
23	8.19	4.22	2.22	2.06	244.21	17.86	6.03	2.85	45.66	0.74	1.46	0.48
24	2.93	8.31	4.03	2.97	166.11	18.82	10.87	3.73	51.41	1.44	1.37	1.22
25	2.68	9.14	4.40	3.59	187.20	28.31	12.38	3.52	30.79	1.60	1.46	0.58
26	3.16	5.50	2.79	2.20	132.91	19.79	7.44	2.33	19.42	0.99	1.29	0.60
27	1.56	13.08	6.43	4.55	226.89	32.01	16.26	3.20	31.20	2.29	1.05	0.57
28	2.72	4.46	2.28	1.77	111.91	11.76	5.67	2.15	14.29	0.79	1.17	0.60
29	2.05	4.15	2.20	1.94	131.26	17.03	5.39	1.95	32.01	0.78	1.46	0.37
30	3.11	4.66	2.40	2.99	172.74	14.71	6.29	3.40	50.13	0.86	1.64	0.41
31	2.43	4.66	2.34	1.97	72.81	8.29	5.64	1.30	31.84	0.86	0.85	0.55
32	3.29	3.26	1.69	0.92	38.53	3.98	3.52	0.60	24.36	0.62	0.45	0.64
33	2.85	3.71	2.52	1.20	60.50	5.80	3.41	1.10	12.11	0.81	0.56	0.63
34	2.58	6.78	3.87	2.24	113.45	18.49	8.30	3.11	39.59	1.31	1.65	0.39
35	2.21	2.36	1.17	1.23	97.37	9.50	3.37	1.91	10.15	0.41	0.83	0.50
36	2.14	5.43	2.76	2.26	143.74	17.19	7.44	2.58	52.78	0.97	1.30	0.55
37	2.46	6.92	3.86	2.50	121.75	18.24	8.13	2.91	26.90	1.31	1.55	0.59
38	2.17	4.73	2.43	1.98	108.04	13.93	6.15	2.30	19.33	0.86	0.96	0.51
39	3.34	3.85	1.98	1.46	82.26	9.45	4.70	1.39	9.65	0.69	0.69	0.50
40	3.53	2.44	1.31	1.12	79.42	7.83	3.58	1.14	6.47	0.45	0.73	0.78
41	1.79	4.69	2.15	1.97	120.68	16.24	5.96	1.75	51.42	0.71	1.36	0.41
42	2.68	2.36	1.27	0.89	57.15	6.62	2.81	1.25	28.23	0.44	0.48	0.70
43	3.04	3.14	1.61	1.77	107.73	11.50	4.59	2.47	41.16	0.57	1.23	0.53
44	2.63	2.91	1.33	1.20	70.86	8.68	3.49	1.26	54.37	0.48	0.84	0.43
45	2.09	2.32	1.14	0.81	50.54	6.82	2.84	1.08	24.70	0.37	0.65	0.55
46	2.97	8.00	4.77	2.32	91.54	11.57	8.68	1.61	25.50	1.59	0.76	0.73
47	2.55	4.49	2.34	1.63	79.77	11.25	5.58	2.18	38.77	0.83	1.00	0.43
48	2.99	4.70	2.36	2.13	124.99	14.83	6.65	2.45	49.50	0.82	1.46	0.46
49	1.94	3.77	1.96	1.62	80.92	11.11	4.93	1.65	34.71	0.68	0.86	0.62
50	2.45	5.41	2.67	2.61	138.85	17.72	7.34	2.77	43.57	0.98	1.61	0.85
51	1.53	3.37	1.64	1.34	74.25	9.67	4.45	1.71	51.17	0.57	0.57	0.79
52	2.98	2.84	1.49	1.21	87.61	9.53	3.40	1.32	12.10	0.52	0.87	0.60
53	2.94	6.64	3.42	2.12	80.54	9.84	7.35	1.53	25.77	1.26	0.86	0.36
54	2.11	11.85	7.12	3.08	84.79	13.10	13.09	2.22	31.21	2.42	1.00	0.33
55	2.21	2.78	1.39	1.23	66.55	8.14	3.57	1.19	24.81	0.49	0.74	0.43
56	2.55	8.02	4.49	2.77	117.75	14.47	9.28	1.83	10.51	1.57	1.23	0.51
57	5.27	2.57	1.34	1.49	98.01	10.74	3.65	1.55	25.39	0.45	0.77	0.44
58	1.99	5.74	2.92	2.30	116.20	16.12	8.03	3.46	50.09	1.03	1.27	0.44
59	3.01	11.81	6.31	3.36	94.14	10.46	11.50	1.61	8.61	2.26	0.66	0.53
60	1.81	1.99	1.10	0.83	77.51	6.85	2.39	1.25	50.18	0.38	0.67	0.72
61	2.28	2.21	1.09	0.98	51.33	6.64	2.88	1.13	32.16	0.36	0.66	0.44
62	2.97	8.86	4.70	2.73	109.04	16.01	10.98	2.49	37.35	1.69	1.31	0.55
63	3.06	8.71	4.24	3.27	136.21	20.19	11.70	4.64	49.41	1.55	1.23	0.49
64	2.38	2.64	1.34	1.18	77.98	22.92	3.41	1.05	21.87	0.46	0.33	0.42
65	2.58	1.65	0.82	0.82	60.34	7.99	2.19	1.33	23.38	0.29	0.64	0.55
66	1.70	4.47	2.18	1.81	87.68	12.39	6.47	2.01	41.02	0.75	0.88	0.29
67	2.41	4.59	2.28	1.79	91.63	11.45	6.27	2.28	35.09	0.82	0.83	0.42
68	2.53	4.06	2.01	1.68	86.11	10.96	5.89	2.39	37.23	0.71	0.98	0.45
69	2.80	5.58	2.29	2.15	86.22	12.34	6.25	2.29	37.06	0.80	0.81	0.49
70	2.15	15.37	9.46	3.68	55.64	8.97	14.68	0.97	31.41	3.14	0.73	0.34
71	2.01	3.59	1.72	1.78	64.55	9.61	4.82	1.91	31.03	0.63	0.43	0.50

Table 37: Major and trace elements in the Cologne Comurbation, II

ID	La [ng g ⁻¹]	Li [ng g ⁻¹]	Lu [ng g ⁻¹]	Mg [%]	Mn [μg g ⁻¹]	Mo [ng g ⁻¹]	Nb [ng g ⁻¹]	Nd [ng g ⁻¹]	Na [μg g ⁻¹]	Ni [μg g ⁻¹]	Pb [μg g ⁻¹]	Pr [ng g ⁻¹]
1	57.60	469.42	1.35	0.11	151.81	111.50	12.11	49.11	92.67	0.58	0.64	12.36
2	88.68	258.51	1.55	0.11	427.65	224.53	17.00	65.48	185.81	0.78	0.98	17.21
3	43.25	78.07	0.72	0.15	14.46	697.37	12.09	28.61	163.30	0.40	1.39	7.66
4	47.01	142.51	0.59	0.12	156.75	184.35	18.72	32.55	107.80	0.63	0.98	8.57
5	55.47	640.05	1.37	0.13	198.69	246.14	12.72	35.86	432.87	0.51	1.04	9.84
6	30.79	23.74	1.20	0.11	84.57	116.66	7.50	22.33	25.25	0.29	0.47	5.89
7	50.80	40.07	0.76	0.11	59.68	167.76	10.28	34.31	58.09	0.56	0.66	9.08
8	47.77	38.71	1.44	0.12	278.27	86.45	9.80	34.00	74.54	0.80	0.61	9.05
9	35.65	133.27	0.63	0.15	116.85	141.46	14.77	23.95	93.51	0.46	0.73	6.56
10	19.09	78.81	1.03	0.09	42.14	272.18	8.86	14.42	94.85	0.50	0.58	3.78
11	21.30	20.22	0.59	0.10	48.99	241.48	5.08	13.82	145.81	1.29	0.44	3.65
12	47.32	118.07	1.12	0.12	106.23	274.33	15.32	36.48	104.60	0.77	1.32	9.51
13	42.44	339.84	0.69	0.13	56.02	114.13	8.60	30.40	255.09	0.62	0.59	8.07
14	58.81	694.26	1.09	0.13	773.89	189.25	13.99	54.47	12.32	2.47	0.31	13.67
15	82.84	220.49	1.15	0.16	671.02	108.34	19.03	69.93	193.79	0.63	1.02	18.06
16	52.35	124.14	0.86	0.16	131.67	218.84	13.62	37.41	112.86	0.44	0.95	9.80
17	37.44	67.35	0.80	0.09	261.30	199.91	13.45	27.20	58.06	1.03	0.84	7.06
18	34.28	137.14	0.71	0.20	48.92	192.85	9.22	24.38	24.01	0.41	0.84	6.67
19	34.85	29.67	1.52	0.08	378.05	71.41	8.62	28.45	123.45	1.20	0.63	7.14
20	47.45	41.23	1.20	0.11	314.33	111.08	10.05	38.57	23.02	1.39	0.70	9.65
21	103.41	84.30	2.12	0.10	412.28	215.08	24.62	78.81	144.50	1.55	0.98	20.93
22	46.00	135.96	0.82	0.13	50.10	287.39	19.18	34.11	59.52	0.66	0.91	9.03
23	52.35	393.01	0.65	0.12	25.44	419.77	19.10	35.59	382.01	0.97	1.04	9.92
24	83.10	153.54	0.81	0.10	117.88	184.71	26.39	68.20	90.91	0.83	1.00	17.64
25	80.24	314.36	1.21	0.13	115.07	179.06	15.91	68.77	160.05	0.61	1.05	17.78
26	64.27	175.45	0.86	0.11	45.54	241.89	12.90	43.23	181.11	0.51	1.23	11.40
27	92.85	333.82	1.31	0.11	15.64	495.24	14.74	94.64	198.17	0.51	0.76	23.32
28	43.08	121.32	0.84	0.08	50.67	347.54	13.86	35.14	37.39	0.39	0.59	9.15
29	48.64	96.26	0.83	0.12	54.00	277.36	13.84	32.64	296.21	0.40	1.29	8.72
30	50.34	84.49	1.07	0.19	125.61	229.78	21.04	36.68	151.18	0.74	1.30	9.58
31	40.07	71.20	1.15	0.09	476.31	98.67	7.51	28.65	33.89	0.92	0.52	7.71
32	26.44	12.07	1.00	0.13	125.71	214.78	3.37	18.12	6.22	0.69	0.23	4.74
33	22.66	51.49	0.89	0.12	423.64	67.42	4.48	16.70	30.54	1.97	0.39	4.34
34	69.34	93.40	1.39	0.08	318.88	157.37	14.92	44.73	342.69	1.20	1.34	11.89
35	31.68	248.30	0.72	0.14	123.81	114.68	10.32	21.18	71.36	0.52	0.53	5.80
36	58.63	302.51	0.96	0.14	19.92	292.45	14.99	48.57	18.18	0.50	0.69	12.80
37	54.60	214.45	1.07	0.08	691.59	131.65	17.82	45.15	69.47	1.55	1.26	11.44
38	48.63	210.55	0.85	0.11	105.54	232.77	14.81	39.53	87.57	0.76	0.71	10.13
39	34.45	53.51	0.74	0.14	192.29	150.92	7.75	27.40	42.71	1.03	0.76	6.97
40	33.06	42.98	0.62	0.13	224.61	82.05	5.53	22.62	32.94	1.77	0.79	6.07
41	59.90	172.22	1.07	0.15	147.90	79.63	11.23	33.83	380.94	0.27	1.12	9.34
42	22.57	178.41	0.76	0.11	462.75	130.36	9.08	16.40	31.17	1.04	0.28	4.34
43	39.53	148.84	0.82	0.12	57.57	194.96	15.02	28.21	47.85	0.51	0.76	7.39
44	30.76	702.46	0.99	0.12	209.74	221.52	10.05	22.14	110.34	0.56	0.51	5.84
45	25.74	31.22	0.95	0.09	143.55	80.73	5.49	16.94	24.74	0.65	0.56	4.53
46	57.13	64.87	1.11	0.12	350.04	75.82	12.67	48.76	35.38	2.31	0.60	12.56
47	41.73	83.12	1.04	0.14	316.72	295.56	13.19	31.22	70.72	0.50	1.07	7.81
48	55.61	109.71	1.13	0.20	96.48	153.37	20.88	41.57	27.40	0.52	0.89	10.40
49	40.62	135.63	0.79	0.10	44.11	220.28	10.89	29.33	50.61	0.50	0.54	7.76
50	68.27	174.85	1.01	0.10	52.01	126.84	16.25	42.82	622.67	0.80	1.33	11.71
51	33.69	244.82	1.01	0.11	13.12	147.68	10.00	25.89	48.65	0.61	0.45	6.85
52	28.91	104.15	0.71	0.09	36.88	177.05	6.81	19.94	155.36	0.54	1.08	5.26
53	54.54	45.01	1.29	0.07	837.20	71.30	6.12	35.95	301.27	1.03	0.55	9.57
54	78.21	128.14	1.86	0.12	389.54	66.57	10.69	64.67	137.97	0.98	0.60	16.72
55	31.99	68.15	0.90	0.12	108.24	359.62	8.31	21.46	77.40	0.49	0.44	5.59
56	69.51	53.60	1.06	0.14	330.82	109.44	17.02	50.85	128.92	1.07	0.80	13.78
57	32.90	782.63	0.56	0.12	29.30	234.99	10.47	25.10	99.78	0.74	0.45	6.17
58	64.02	92.86	1.16	0.09	41.26	160.80	27.02	47.23	45.55	0.41	0.87	12.68
59	56.42	79.51	1.32	0.13	871.20	59.21	28.49	48.59	57.54	2.84	0.43	12.60
60	19.61	113.89	0.83	0.09	78.70	476.01	8.36	13.53	21.91	0.99	0.31	3.60
61	28.22	57.91	0.86	0.17	65.13	86.37	6.34	17.92	41.33	1.41	0.34	4.95
62	77.92	335.60	1.22	0.10	1370.00	121.20	14.34	56.00	213.88	4.10	0.83	14.69
63	88.90	211.22	1.16	0.13	26.13	198.22	26.76	69.32	284.62	0.39	1.00	18.80
64	32.75	136.09	0.51	0.18	16.58	89.97	5.63	19.64	147.36	0.43	0.20	5.43
65	22.36	138.19	0.61	0.19	69.65	58.33	5.21	13.53	91.15	0.36	0.41	3.59
66	54.58	293.51	1.24	0.14	26.88	88.79	11.47	36.71	178.60	0.34	0.70	10.00
67	44.05	448.76	1.25	0.10	175.24	123.09	16.34	36.82	137.18	2.42	1.47	9.66
68	50.69	214.16	0.99	0.12	158.65	129.51	11.65	34.89	128.03	0.46	0.68	9.74
69	56.08	216.21	1.06	0.13	295.34	144.33	19.22	39.00	43.36	0.75	0.46	10.32
70	83.77	69.90	1.98	0.12	482.50	77.14	8.24	72.11	33.99	1.57	0.32	19.51
71	37.53	189.55	1.05	0.13	170.98	144.14	23.99	28.55	39.05	1.40	0.22	7.50

Table 38: Major and trace elements in the Cologne Conurbation, III

ID	Pt [ng g ⁻¹]	Rb [μg g ⁻¹]	Re [ng g ⁻¹]	Sb [ng g ⁻¹]	Sc [ng g ⁻¹]	Sm [ng g ⁻¹]	Sn [ng g ⁻¹]	Sr [μg g ⁻¹]	Ta [ng g ⁻¹]	Tb [ng g ⁻¹]	Te [ng g ⁻¹]	Th [ng g ⁻¹]
1	0.23	8.01	1.95	179.26	17.30	10.16	128.12	5.71	< 0.5	2.21	< 5	116.56
2	0.24	3.49	0.84	220.46	17.90	13.01	143.18	10.08	< 0.5	2.81	< 5	113.42
3	0.19	5.20	0.19	200.66		5.41	227.26	8.35		1.29		55.51
4	0.40	3.38	0.14	314.76	14.77	6.27	154.41	6.96	< 0.5	1.14	< 5	85.25
5	0.38	13.20	0.48	275.45	< 10	7.25	213.09	12.59	< 0.5	1.96	8.63	62.31
6	0.25	13.39	< 0.1	100.74	< 10	4.37	95.93	2.96	< 0.5	1.55	< 5	37.79
7	0.34	3.17	0.20	179.72	< 10	6.30	110.34	2.60	< 0.5	1.32	< 5	45.97
8	0.21	15.48	0.19	155.95	< 10	6.39	125.29	4.28	< 0.5	2.00	8.53	47.73
9	0.22	3.24	0.32	157.61	11.18	4.63	135.26	5.74	< 0.5	1.02	< 5	76.49
10	0.11	5.05	1.18	120.78	< 10	2.69	126.29	3.60	< 0.5	1.30	< 5	28.40
11	0.14	1.78	0.17	229.74	< 10	2.67	179.19	0.92	< 0.5	0.85	< 5	30.18
12	0.77	9.11	0.48	222.95	< 10	7.02	192.60	5.81	< 0.5	1.81	< 5	76.01
13	0.24	4.86	0.26	201.41	< 10	5.83	101.17	7.19	< 0.5	1.25	< 5	48.25
14	0.41	2.89	5.09	209.26	23.49	11.34	68.45	7.54		2.24		102.94
15	0.20	6.32	0.65	163.22	22.62	14.25	120.60	8.88	< 0.5	2.32	< 5	161.49
16	0.40	2.09	0.62	213.91	11.32	7.69	158.16	8.64	< 0.5	1.53	5.65	72.64
17	0.21	2.10	1.10	248.08	< 10	5.47	145.99	2.69	< 0.5	1.25	< 5	59.73
18	0.21	2.61	0.42	168.71		4.72	182.30	11.53		1.28		51.28
19	0.13	6.61	0.18	136.81	< 10	6.20	105.90	2.08	< 0.5	2.23	< 5	34.52
20	0.30	2.51	0.31	197.76	< 10	9.14	147.64	5.22	< 0.5	2.27	< 5	51.99
21	0.62	5.70	0.25	301.58	15.47	15.99	224.23	10.50	0.55	3.67	7.58	119.09
22	0.52	1.33	0.52	322.83	10.40	6.63	168.07	3.89	< 0.5	1.45	< 5	63.02
23	0.57	6.20	0.97	599.30		6.38	235.28	7.76		1.36		65.52
24	0.36	7.58	0.25	270.11	18.02	13.59	195.83	4.34	< 0.5	2.04	< 5	137.67
25	0.25	1.67	1.22	247.35	22.13	14.58	146.15	9.23	< 0.5	2.67	< 5	138.13
26	0.56	0.78	0.85	197.21	10.41	8.72	134.54	5.37	< 0.5	1.67	< 5	80.54
27	0.17	3.05	1.23	224.86	26.53	19.69	106.09	4.88	< 0.5	3.27	5.16	174.23
28	0.31	3.59	0.81	173.30	< 10	6.83	138.11	2.47	< 0.5	1.50	< 5	63.22
29	0.27	0.44	0.77	286.96	10.29	6.74	175.13	4.99	< 0.5	1.36	< 5	76.11
30	0.58	4.82	1.06	387.69	12.82	6.86	235.05	14.14	< 0.5	1.50	< 5	70.16
31	2.21	9.61	0.42	141.34	< 10	5.39	116.85	8.23	< 0.5	1.75	8.74	34.60
32	0.93	18.11	< 0.1	45.03	< 10	3.26	56.15	4.61	< 0.5	1.43	5.10	17.83
33	0.20	3.32	0.18	276.57	< 10	3.52	67.76	5.82	< 0.5	1.18	< 5	27.35
34	3.11	4.85	0.28	219.14	10.19	8.54	188.83	5.28	0.51	2.19	< 5	66.77
35	0.17	7.34	0.65	146.38	< 10	3.82	116.87	8.88	< 0.5	1.02	< 5	43.45
36	0.21	1.27	0.65	195.75	12.33	9.32	213.39	9.28	< 0.5	1.74	< 5	91.10
37	0.34	0.60	0.62	231.21	12.97	8.97	188.41	1.78	< 0.5	1.94	< 5	87.50
38	0.14	3.53	0.99	121.33	10.13	7.68	99.93	5.09	< 0.5	1.52	< 5	86.76
39	0.14	0.79	0.88	119.03	< 10	5.59	86.56	2.14	< 0.5	1.28	< 5	47.08
40	0.14	1.08	0.54	121.58	< 10	3.97	76.15	3.77	< 0.5	0.99	< 5	42.32
41	0.24	1.33	0.73	185.18	10.43	6.23	137.91	7.76	< 0.5	1.62	6.28	70.40
42	0.11	12.30	2.12	68.68	< 10	3.04	52.14	3.73	< 0.5	1.05	< 5	42.01
43	0.31	4.52	1.27	237.88	< 10	5.46	160.40	11.47	< 0.5	1.21	< 5	53.27
44	0.12	9.29	2.56	129.24	< 10	3.81	132.93	12.09	< 0.5	1.35	7.94	31.51
45	0.1	6.08	0.14	27.96	< 10	3.06	71.41	1.74	< 0.5	1.25	< 5	28.35
46	0.15	2.91	0.42	201.01	< 10	10.25	96.17	7.25	< 0.5	1.99	< 5	72.97
47	0.27	18.88	0.65	169.34	< 10	5.94	141.97	7.32	< 0.5	1.63	< 5	48.69
48	0.41	6.75	1.01	325.74	< 10	7.53	197.58	9.88	0.70	1.81	7.51	63.87
49	0.13	2.24	0.34	106.53	< 10	5.58	98.82	8.86	< 0.5	1.24	< 5	53.81
50	0.30	3.82	0.40	227.59	13.37	8.08	186.88	5.08	< 0.5	1.73	< 5	85.86
51	0.15	1.43	2.19	76.69	< 10	5.09	66.78	4.20	< 0.5	1.50	< 5	51.63
52	0.13	3.07	0.65	175.96	< 10	4.02	123.11	4.31	< 0.5	1.09	v 5	29.77
53	0.15	14.97	0.46	93.37	< 10	7.14	114.10	3.71	< 0.5	2.18	6.20	37.48
54	< 0.1	3.21	0.65	98.30	< 10	13.70	118.67	4.62	0.50	3.09	10.06	71.61
55	0.23	5.38	1.54	56.84	< 10	3.68	100.88	5.36	< 0.5	1.18	v 5	35.26
56	0.15	1.94	0.69	134.23	10.79	10.02	119.72	5.37	< 0.5	2.02	< 5	55.36
57	0.21	6.57	0.68	174.28		4.04	93.80	9.88		0.96		43.59
58	0.24	5.29	0.58	206.06	12.66	9.02	144.47	9.89	0.75	1.91	8.96	71.82
59	0.19	3.50	0.39	347.82	< 10	11.24	71.35	4.69	< 0.5	2.64	< 5	34.20
60	0.17	11.69	0.35	125.71	< 10	2.24	98.50	3.62	< 0.5	1.05	8.50	20.38
61	0.13	6.32	0.46	76.91	< 10	3.12	80.06	8.41	< 0.5	1.12	< 5	30.13
62	0.26	4.48	3.12	204.99	< 10	11.16	150.06	4.70	0.50	2.42	5.04	74.92
63	0.37	3.77	1.65	274.08	14.19	13.50	189.98	6.06	0.86	2.47	9.49	113.16
64	0.24	6.54	1.13	86.45		3.70	44.14	4.93		0.94		43.10
65	0.29	4.24	0.68	89.93	< 10	2.63	88.10	6.09	< 0.5	0.85	< 5	38.84
66	0.14	2.19	4.06	105.10	< 10	7.08	93.51	3.61	< 0.5	1.87	< 5	69.36
67	0.31	2.35	7.07	223.78	< 10	7.07	109.48	1.93	< 0.5	1.90	< 5	59.49
68	0.25	3.18	1.88	146.66	< 10	6.56	110.93	5.11	0.56	1.58	9.16	57.00
69	0.19	3.67	0.78	218.84	< 10	6.81	111.49	10.62	0.67	1.62	5.81	59.59
70	< 0.1	5.06	0.66	49.34	< 10	15.26	108.58	7.14	< 0.5	3.45	v 5	51.72
71	0.20	7.37	0.52	66.96	< 10	5.43	53.47	6.80	0.62	1.45	8.91	40.48

Table 39: Major and trace elements in the Cologne Conurbation, IV

ID	Ti [$\mu\text{g g}^{-1}$]	Tl [ng g^{-1}]	Tm [ng g^{-1}]	U [ng g^{-1}]	V [ng g^{-1}]	W [ng g^{-1}]	Y [ng g^{-1}]	Yb [ng g^{-1}]	Zn [$\mu\text{g g}^{-1}$]	Zr [ng g^{-1}]	Σ REE [ng g^{-1}]
1	2.48	5.17	0.42	10.37	348.68	20.33	37.47	2.92	27.18	82.70	385.15
2	2.82	30.85	0.61	5.39	405.56	26.04	64.76	4.08	45.06	92.13	485.57
3	2.05	9.24	0.22	7.02	219.01	87.17	18.29	1.51	31.49	61.19	228.27
4	2.10	10.14	0.29	3.38	250.67	44.79	27.86	2.03	39.18	76.99	272.29
5	2.13	8.99	0.31	4.71	270.16	37.01	25.18	2.17	68.74	86.91	280.28
6	1.82	9.62	0.18	1.82	156.87	17.63	14.20	1.23	24.72	42.49	166.21
7	2.14	5.68	0.30	2.22	196.45	47.50	29.23	1.90	21.19	58.60	238.54
8	2.11	11.42	0.37	2.08	154.48	30.64	36.78	2.42	41.56	64.54	235.47
9	1.85	10.77	0.20	5.08	175.76	23.23	18.78	1.48	23.29	63.14	217.37
10	1.57	1.97	0.12	3.83	98.39	25.26	10.37	0.83	31.21	48.33	111.89
11	1.44	1.39	0.12	1.75	87.84	17.83	10.19	0.82	23.47	27.96	111.09
12	2.45	6.24	0.27	5.62	281.06	61.63	23.99	1.90	27.35	83.04	285.08
13	1.92	8.46	0.23	3.82	160.91	24.91	21.89	1.61	24.67	55.15	221.47
14	2.54	14.32	0.64	7.08	407.23	48.17	56.34	4.07	67.54	90.81	406.74
15	3.28	8.64	0.61	7.79	455.38	21.56	49.34	3.94	53.48	108.26	549.96
16	2.38	5.37	0.30	10.24	290.60	25.58	26.88	2.17	27.36	76.73	287.98
17	1.98	2.36	0.28	2.12	273.63	22.97	29.33	1.87	45.25	63.49	211.33
18	2.03	16.62	0.21	3.63	215.79	37.83	18.79	1.42	49.13	59.20	195.13
19	1.93	2.89	0.56	1.70	161.32	20.86	50.12	3.35	46.59	45.85	193.59
20	2.36	4.97	0.68	1.89	221.49	18.24	66.94	4.20	45.63	64.05	266.17
21	3.81	6.50	1.04	3.85	310.79	37.00	97.51	6.66	95.36	119.19	551.88
22	2.78	2.72	0.29	3.00	295.06	24.12	26.68	1.94	38.44	89.79	258.70
23	2.86	36.08	0.27	4.12	355.99	84.17	25.32	1.83	85.06	114.73	282.05
24	3.35	3.41	0.50	6.32	327.78	54.82	43.37	2.99	27.38	112.98	510.35
25	3.37	5.10	0.53	6.69	372.34	49.47	44.76	3.72	38.30	117.96	523.24
26	2.27	5.45	0.34	5.21	260.76	24.68	28.89	2.46	20.23	81.19	336.77
27	2.75	4.15	0.82	7.21	451.20	26.57	61.03	5.30	14.29	103.53	672.65
28	2.52	3.01	0.28	2.63	227.56	24.03	24.55	1.92	24.32	65.64	258.27
29	2.33	5.42	0.28	5.01	377.19	25.85	24.15	1.90	35.26	76.45	272.91
30	2.81	19.88	0.34	3.79	374.26	54.01	30.09	2.55	66.68	97.80	281.37
31	1.81	10.85	0.30	1.82	145.56	17.13	35.04	2.02	77.27	39.96	202.40
32	1.36	1.52	0.22	1.01	59.85	8.66	22.88	1.33	40.45	25.69	116.04
33	1.58	5.76	0.37	1.18	88.71	30.73	31.95	2.27	41.49	34.98	122.27
34	2.67	7.12	0.52	3.93	543.74	26.13	47.18	3.31	52.35	90.62	338.62
35	1.91	2.94	0.15	2.74	366.27	16.11	12.83	1.09	37.09	51.94	168.58
36	2.81	2.47	0.35	4.59	359.23	20.88	27.74	2.36	30.62	79.21	355.68
37	2.80	3.62	0.49	3.57	268.33	24.79	47.50	3.15	41.03	92.17	336.20
38	2.76	4.78	0.30	3.45	197.10	18.20	26.20	2.10	27.44	64.70	303.05
39	1.94	2.00	0.25	2.15	123.56	88.90	23.87	1.64	58.47	47.18	201.55
40	1.60	1.62	0.16	1.60	86.97	17.84	14.36	1.04	51.63	36.45	172.93
41	2.06	5.42	0.26	5.98	294.76	18.97	23.24	1.90	20.65	61.19	282.85
42	1.67	2.68	0.18	1.79	79.03	9.68	15.49	1.09	42.09	31.85	134.93
43	2.72	5.83	0.22	6.91	248.83	21.09	19.40	1.66	19.68	73.35	216.12
44	1.98	4.48	0.17	4.85	207.20	18.33	15.96	1.30	24.09	44.86	159.42
45	1.40	1.23	0.14	1.79	123.72	14.61	13.57	0.98	28.59	29.14	130.69
46	2.53	3.89	0.61	2.42	135.31	23.20	60.00	3.88	27.95	65.87	326.39
47	2.09	8.18	0.28	2.27	245.06	18.13	26.42	1.95	34.93	69.77	229.89
48	2.98	4.50	0.29	3.24	284.18	36.75	24.69	2.15	35.68	105.41	294.88
49	2.25	2.82	0.24	4.28	176.26	18.05	23.25	1.62	18.09	48.93	214.13
50	2.56	5.64	0.34	5.28	306.79	28.18	32.22	2.25	33.64	83.93	347.07
51	1.89	1.87	0.19	4.17	103.42	12.69	16.73	1.56	20.03	42.48	199.88
52	1.71	2.16	0.20	4.13	100.94	32.45	16.53	1.42	26.92	41.70	147.31
53	1.69	5.97	0.43	2.07	150.45	29.55	41.70	2.54	57.27	41.79	268.20
54	2.30	4.48	0.98	2.92	178.72	15.19	83.70	5.94	44.94	59.02	409.79
55	1.67	2.85	0.19	2.21	140.31	11.42	18.45	1.23	47.57	48.38	163.93
56	3.47	6.02	0.59	2.44	260.82	16.26	55.21	3.64	128.72	55.96	350.79
57	2.04	3.06	0.16	4.98	225.23	28.22	14.03	1.17	60.26	58.78	182.74
58	4.86	3.81	0.36	4.00	268.51	25.81	28.71	2.46	18.72	99.39	347.04
59	6.00	2.47	0.85	1.76	174.17	13.57	76.74	5.22	46.27	61.15	306.78
60	1.87	2.59	0.15	1.62	127.47	30.51	13.48	1.06	21.51	37.43	98.51
61	1.55	3.04	0.13	2.76	102.75	20.36	11.87	0.96	33.24	44.58	137.91
62	2.57	6.03	0.59	3.42	225.46	24.18	61.96	3.66	51.97	97.70	394.94
63	3.97	3.82	0.52	13.01	260.68	31.04	42.61	3.26	18.06	130.37	513.53
64	1.45	14.40	0.16	14.25	151.22	27.00	13.02	1.14	50.60	34.57	164.54
65	1.55	4.08	0.10	3.84	84.70	16.11	9.90	0.77	31.63	34.17	120.46
66	2.28	3.60	0.25	6.35	147.46	19.48	20.65	1.78	16.28	60.36	289.11
67	2.84	4.12	0.28	4.50	139.97	34.63	22.19	1.83	67.34	88.19	265.78
68	2.21	2.13	0.25	4.99	154.29	19.49	21.08	1.78	32.75	61.67	274.33
69	2.96	1.87	0.30	2.77	136.76	19.63	26.43	1.97	49.37	84.46	287.59
70	1.75	2.24	1.39	1.61	108.32	24.66	107.91	8.27	68.10	87.58	466.08
71	4.37	3.96	0.22	2.15	122.96	22.41	22.14	1.62	30.92	69.34	204.50

Table 40: Major and trace elements in the Cologne Conurbation, V

ID	Ag EF	As EF	Au EF	B EF	Ba EF	Bi EF	Ca EF	Cd EF	Ce EF	Co EF	Cr EF	Cs EF
1	32.03			602.30	2.16	31.33	63.74	255.35	0.68	3.13	8.78	1.68
2	67.52		0.21	372.11	1.66	51.64	68.84	1232.32	0.72	12.14	6.95	1.16
3	150.90	0.00	1.43	1218.57	2.67	127.13	119.57	150.15	0.74	2.36	14.94	9.29
4	302.28		0.54	482.47	3.09	95.91	85.88	847.84	0.64	3.82	11.44	1.47
5	564.88		0.90	855.69	3.53	218.36	176.63	893.36	0.74	3.93	7.91	1.74
6	208.62		1.25	1089.98	1.88	187.99	152.90	658.36	0.73	4.89	10.57	3.56
7	146.18		1.97	788.88	1.12	69.17	72.08	587.30	0.73	9.63	12.21	1.56
8	556.52		0.51	696.75	2.36	125.65	147.13	1615.62	0.68	5.31	9.96	3.89
9	265.91		0.55	957.77	1.42	113.88	134.18	483.21	0.62	6.95	10.80	2.56
10	280.54		1.12	1560.50	2.20	231.22	162.29	397.35	0.72	5.43	37.43	2.41
11	168.57	322.98	0.87	860.14	1.24	100.35	59.36	1070.95	0.66	6.05	48.92	5.53
12	224.15		51.18	502.95	1.60	158.85	70.28	287.37	0.74	4.68	14.11	2.06
13	326.24	55.98	0.58	746.26	1.87	64.14	92.30	456.18	0.75	5.22	22.97	2.95
14	193.29	71.30	1.27	363.04	1.86	58.60	75.21	828.32	0.75	23.35	9.05	3.76
15	52.54			578.91	2.30	26.29	54.97	846.03	0.71	6.38	4.91	1.45
16	218.51		0.55	841.06	1.92	65.93	86.83	233.84	0.72	3.53	7.87	2.18
17	142.17		0.61	382.01	2.33	82.27	89.05	1165.02	0.64	3.78	13.99	1.24
18	291.43	68.78	0.64	1790.54	2.53	115.04	188.03	1087.80	0.72	3.16	12.37	2.84
19	319.33		1.57	605.35	1.62	138.68	73.89	1219.24	0.66	4.88	16.29	2.35
20	218.45		1.02	457.89	1.52	62.60	98.72	1314.94	0.65	4.37	9.50	1.54
21	147.75		0.27	232.11	2.04	78.27	77.85	1504.33	0.67	5.07	6.94	1.72
22	112.54	39.34	0.64	1031.61	2.02	63.38	71.96	216.63	0.74	3.15	11.29	0.95
23	440.68	84.52	2.81	1531.64	2.39	110.19	121.41	242.21	0.78	3.09	14.33	3.32
24	159.01			370.93	1.07	30.37	29.12	128.98	0.73	3.10	8.25	0.87
25	127.20	25.43	0.29	481.79	1.35	38.23	52.15	232.95	0.75	3.13	6.12	1.18
26	87.18		0.32	387.59	1.54	60.22	54.07	399.35	0.74	3.02	10.01	1.32
27	27.13	37.12	0.18	302.50	0.68	14.56	25.26	41.46	0.76	1.88	4.46	1.15
28	133.03		0.50	446.83	1.32	40.99	36.14	175.88	0.75	4.58	7.26	1.02
29	97.45		0.69	421.40	2.02	69.66	71.00	137.31	0.71	2.62	7.61	1.45
30	461.17		31.17	1184.29	6.94	82.50	141.51	834.52	0.72	3.54	11.67	3.96
31	141.92			1112.72	8.17	150.55	212.27	1484.01	0.77	21.22	20.73	1.55
32	102.89			1143.52	1.32	128.64	213.75	1959.80	0.65	7.00	16.53	11.27
33	710.50		1.29	1342.49	4.14	74.27	204.52	3501.83	0.61	21.83	29.92	5.49
34	21.23		0.36	450.85	1.82	216.32	111.90	1467.96	0.75	4.47	9.32	1.58
35	331.69		0.95	1209.94	2.79	65.61	128.78	753.81	0.72	3.62	13.94	3.01
36	114.29		0.46	624.30	1.79	51.14	69.88	100.35	0.74	2.17	6.38	0.80
37	132.53	31.54	0.36	241.28	1.73	59.57	40.43	641.74	0.70	20.24	6.81	0.91
38	178.64		0.47	519.01	1.11	44.09	64.61	246.66	0.70	4.22	7.35	1.89
39	149.70		1.12	770.22	1.53	63.70	69.21	1395.33	0.75	6.46	9.00	1.17
40	480.10		2.79	996.14	2.34	54.80	104.13	2894.53	0.73	6.62	8.84	1.26
41	77.05		0.43	924.49	3.32	62.81	96.66	267.85	0.70	4.52	5.36	1.18
42	75.58			2461.57	1.90	58.43	135.33	819.73	0.63	11.56	13.97	2.98
43	214.00		0.96	1589.98	3.75	138.61	134.95	192.90	0.73	3.28	13.18	3.41
44	320.22		0.64	1744.46	4.25	209.94	293.04	818.57	0.78	8.94	16.11	2.02
45			1.84	700.88	1.59	184.97	149.43	813.96	0.75	7.43	29.27	1.75
46	83.88		0.44	619.88	1.55	31.54	92.78	899.10	0.67	3.70	13.99	1.59
47	64.54		0.38	578.49	2.11	162.70	183.80	679.32	0.77	7.56	11.25	2.78
48	73.98		0.56	809.11	3.09	125.35	117.31	236.52	0.76	2.78	12.18	2.02
49	105.28		0.66	687.70	1.89	53.35	102.81	237.73	0.67	9.11	12.92	1.12
50	196.68		0.27	482.73	3.25	49.32	60.07	268.99	0.73	5.04	8.40	2.01
51	464.79			469.33	1.57	37.91	98.71	185.40	0.73	2.61	28.49	0.94
52	313.76		1.46	1067.20	2.68	108.07	113.28	284.63	0.75	4.58	30.69	2.08
53	186.53		0.33	591.61	3.23	91.06	105.91	1432.27	0.85	25.02	21.40	2.90
54	72.69		0.22	346.08	1.22	92.45	105.96	901.78	0.67	3.63	8.72	1.07
55	522.63		2.53	1095.87	2.51	196.24	134.91	1312.14	0.77	5.92	21.30	1.35
56	230.06		0.43	467.43	2.03	46.30	77.50	1200.68	0.80	14.79	11.00	0.94
57	456.98	0.00	2.81	913.18	4.22	93.33	117.90	162.58	0.76	3.20	16.85	4.60
58	23.45		0.61	322.41	1.66	113.36	68.99	128.00	0.80	2.09	9.66	1.20
59	131.82		0.41	421.09	1.74	33.08	61.18	1345.64	0.76	23.30	14.60	1.64
60			0.84	2731.04	3.19	682.04	359.93	509.51	0.71	7.32	46.34	4.40
61	101.29		0.76	1266.64	3.42	205.62	202.66	634.34	0.74	4.25	47.92	3.62
62	47.95		0.23	539.13	1.48	140.43	61.78	2798.23	0.74	17.97	8.52	1.20
63	26.38		0.26	421.34	1.29	79.38	50.82	75.44	0.80	1.70	7.84	0.96
64	406.83	0.00	0.00	1059.49	2.62	94.31	151.67	336.91	0.70	2.91	13.08	25.98
65	342.83	87.07	0.91	1334.39	2.44	72.48	248.43	315.70	0.62	3.11	21.20	24.67
66	103.98	67.29	0.33	225.01	1.96	59.56	74.04	89.19	0.74	2.14	10.71	1.53
67	135.48		1.02	1039.53	1.65	121.58	79.78	915.98	0.78	134.55	11.32	1.04
68	129.37		0.46	733.58	1.69	184.13	88.20	231.90	0.84	2.14	9.37	1.03
69	155.11		0.44	773.89	3.16	133.56	114.55	605.05	0.78	3.44	12.71	0.92
70	134.58		0.26	165.69	1.76	51.55	57.30	631.11	0.83	3.16	11.47	0.58
71			0.57	726.83	3.16	44.01	162.21	315.95	0.79	4.24	13.48	2.71

Table 41: Major and trace elements in the Cologne Conurbation, VI

ID	Cu EF	Dy EF	Er EF	Eu EF	Fe EF	Ga EF	Gd EF	Hf EF	Hg EF	Ho EF	In EF	K EF
1	32.34	0.76	0.57	1.26	1.69	0.46	0.88	0.17	56.55	0.59	7.62	130.10
2	31.78	0.86	0.65	1.31	1.48	0.37	0.98	0.15	31.41	0.68	8.90	47.01
3	219.42	0.67	0.52	1.25	2.23	0.51	0.88	0.24	62.08	0.51	25.50	101.41
4	64.44	0.73	0.54	1.26	2.20	0.55	0.82	0.25	10.08	0.54	15.31	101.39
5	59.73	0.74	0.55	1.26	1.80	0.59	0.92	0.25	57.48	0.56	17.40	74.46
6	78.11	0.74	0.56	1.23	1.71	0.54	0.93	0.22	110.33	0.54	14.63	144.53
7	61.02	0.81	0.66	1.14	1.94	0.48	0.95	0.19	28.04	0.65	11.61	135.33
8	68.02	1.00	0.79	1.28	1.70	0.46	1.04	0.29	76.71	0.78	12.06	88.17
9	86.34	0.60	0.48	1.03	1.91	0.48	0.74	0.33	56.60	0.47	15.74	130.26
10	153.76	0.78	0.56	1.28	2.47	0.75	0.84	0.31	96.32	0.56	25.35	289.48
11	229.53	0.69	0.52	1.19	2.82	0.40	0.85	0.24	41.86	0.54	34.05	269.56
12	33.68	0.71	0.52	1.07	1.98	0.49	0.84	0.23	46.62	0.55	19.74	94.56
13	75.12	0.75	0.57	1.23	2.06	0.46	0.90	0.17	16.98	0.58	12.07	134.97
14	55.47	0.96	0.81	1.31	1.72	0.52	0.98	0.17	18.68	0.80	3.58	53.66
15	24.91	0.72	0.57	1.13	1.33	0.49	0.86	0.16	50.21	0.57	6.40	70.56
16	55.90	0.72	0.56	1.26	2.05	0.51	0.89	0.22	32.63	0.57	15.51	100.40
17	79.79	0.78	0.67	1.26	2.35	0.46	0.92	0.32	18.57	0.65	14.63	163.55
18	87.31	0.72	0.56	1.33	2.39	0.92	0.87	0.25	69.97	0.55	18.47	120.49
19	83.02	1.52	1.40	1.66	1.86	0.47	1.41	0.25	62.41	1.34	13.66	96.57
20	59.85	1.54	1.27	1.64	1.46	0.48	1.38	0.19	42.38	1.28	12.43	143.13
21	30.16	1.07	0.92	1.29	1.25	0.36	1.18	0.16	33.48	0.90	8.88	44.90
22	56.56	0.75	0.59	1.27	2.24	0.48	0.90	0.28	28.88	0.60	14.15	132.98
23	176.83	0.65	0.52	1.26	3.76	0.57	0.86	0.27	61.58	0.50	15.71	92.69
24	34.94	0.71	0.52	1.01	1.42	0.33	0.85	0.19	38.32	0.54	8.19	129.92
25	31.15	0.76	0.56	1.19	1.56	0.48	0.95	0.18	22.38	0.58	8.50	59.83
26	57.15	0.71	0.55	1.13	1.72	0.53	0.88	0.18	21.94	0.56	11.66	96.83
27	14.15	0.85	0.63	1.17	1.47	0.43	0.97	0.12	17.65	0.65	4.76	45.81
28	64.14	0.75	0.58	1.19	1.88	0.41	0.88	0.22	21.05	0.58	13.80	125.41
29	45.77	0.66	0.53	1.23	2.09	0.56	0.79	0.19	44.62	0.54	16.23	73.68
30	67.31	0.72	0.57	1.84	2.67	0.47	0.89	0.32	67.77	0.58	17.76	79.19
31	73.14	1.00	0.76	1.69	1.56	0.37	1.12	0.17	59.85	0.81	12.78	146.61
32	172.42	1.22	0.96	1.37	1.44	0.31	1.22	0.14	79.85	1.01	11.78	299.73
33	141.70	1.32	1.36	1.69	2.15	0.42	1.12	0.24	37.67	1.26	14.01	281.36
34	46.38	0.87	0.76	1.15	1.46	0.49	0.98	0.24	44.48	0.74	14.85	62.91
35	79.94	0.61	0.46	1.26	2.51	0.50	0.80	0.30	22.91	0.46	14.93	160.22
36	36.58	0.66	0.51	1.10	1.76	0.43	0.84	0.19	56.45	0.52	11.15	83.27
37	44.60	0.90	0.76	1.29	1.57	0.49	0.97	0.23	30.44	0.74	14.04	94.73
38	43.58	0.68	0.53	1.13	1.55	0.41	0.81	0.20	24.26	0.54	9.63	91.46
39	100.84	0.83	0.65	1.25	1.77	0.42	0.93	0.18	18.21	0.65	10.37	133.48
40	124.19	0.61	0.50	1.12	2.00	0.41	0.83	0.17	14.24	0.49	12.85	244.50
41	38.55	0.72	0.50	1.21	1.85	0.51	0.84	0.16	69.16	0.47	14.59	78.78
42	120.74	0.76	0.62	1.14	1.84	0.44	0.84	0.24	79.60	0.62	10.89	282.74
43	85.67	0.63	0.49	1.42	2.17	0.48	0.85	0.30	72.44	0.50	17.38	132.52
44	100.35	0.79	0.55	1.30	1.93	0.49	0.88	0.21	129.73	0.57	16.04	145.91
45	97.37	0.77	0.58	1.08	1.68	0.47	0.87	0.22	71.91	0.53	15.02	227.05
46	55.44	1.07	0.97	1.23	1.22	0.32	1.06	0.13	29.72	0.93	7.08	122.22
47	67.52	0.85	0.67	1.22	1.51	0.44	0.97	0.25	64.15	0.69	13.17	102.60
48	61.72	0.69	0.53	1.25	1.84	0.45	0.90	0.22	63.86	0.53	15.11	85.15
49	55.08	0.77	0.60	1.31	1.64	0.46	0.92	0.20	61.67	0.60	12.22	157.36
50	42.97	0.68	0.51	1.30	1.74	0.46	0.85	0.21	47.76	0.54	14.09	133.10
51	46.49	0.73	0.54	1.16	1.62	0.43	0.89	0.22	97.38	0.55	8.71	214.79
52	122.98	0.84	0.67	1.42	2.59	0.58	0.92	0.23	31.24	0.67	17.95	219.51
53	66.68	1.08	0.84	1.37	1.31	0.33	1.10	0.15	36.55	0.89	9.76	73.35
54	31.38	1.26	1.15	1.30	0.90	0.29	1.28	0.14	28.98	1.12	7.44	44.03
55	81.89	0.74	0.56	1.30	1.77	0.44	0.87	0.19	57.58	0.56	13.78	143.22
56	44.23	0.99	0.85	1.37	1.46	0.37	1.06	0.14	11.39	0.85	10.67	79.32
57	175.50	0.61	0.48	1.41	2.33	0.53	0.80	0.22	52.85	0.46	12.90	130.31
58	34.85	0.72	0.56	1.15	1.46	0.42	0.93	0.26	54.91	0.57	11.16	68.90
59	59.68	1.67	1.36	1.89	1.33	0.31	1.50	0.14	10.67	1.40	6.55	93.89
60	111.79	0.88	0.74	1.46	3.42	0.62	0.97	0.33	193.80	0.73	20.55	395.02
61	100.63	0.70	0.52	1.23	1.62	0.43	0.84	0.21	88.72	0.50	14.48	174.18
62	45.82	0.98	0.79	1.20	1.20	0.36	1.11	0.17	35.98	0.81	10.09	76.23
63	36.31	0.74	0.55	1.10	1.15	0.35	0.91	0.24	36.60	0.57	7.28	51.65
64	88.17	0.70	0.54	1.24	2.06	1.25	0.83	0.17	50.57	0.53	6.02	138.30
65	130.37	0.59	0.45	1.18	2.18	0.59	0.73	0.29	73.84	0.46	16.19	247.68
66	35.69	0.67	0.50	1.08	1.32	0.38	0.90	0.18	53.97	0.49	9.27	54.14
67	55.22	0.75	0.57	1.16	1.50	0.39	0.94	0.22	50.22	0.59	9.54	85.88
68	56.10	0.64	0.48	1.06	1.36	0.36	0.86	0.23	51.62	0.50	10.83	89.15
69	59.22	0.84	0.53	1.29	1.30	0.38	0.87	0.21	49.02	0.53	8.61	92.60
70	28.08	1.43	1.34	1.37	0.52	0.17	1.26	0.05	25.64	1.28	4.75	40.11
71	59.76	0.76	0.55	1.51	1.37	0.42	0.94	0.25	57.72	0.59	6.32	132.34

Table 42: Major and trace elements in the Cologne Conurbation, VII

ID	La EF	Lu EF	Mg EF	Mn EF	Mo EF	Nb EF	Nd EF	Na EF	Ni EF	Pb EF	Pr EF	Rb EF
1	0.76	1.66	33.27	99.96	29.37	0.19	0.75	1.27	11.53	16.91	0.69	28.24
2	0.93	1.52	26.15	223.36	46.91	0.21	0.79	2.01	12.18	20.45	0.76	9.76
3	0.96	1.50	77.08	16.07	309.91	0.32	0.73	3.77	13.39	61.67	0.72	30.96
4	0.88	1.03	50.00	146.00	68.69	0.42	0.70	2.08	17.63	36.47	0.67	16.89
5	1.00	2.33	52.25	179.79	89.09	0.28	0.75	8.13	13.90	37.48	0.75	63.98
6	0.94	3.42	72.97	129.05	71.21	0.27	0.79	0.80	13.50	28.87	0.76	109.47
7	1.08	1.51	50.36	63.45	71.35	0.26	0.84	1.28	17.94	28.25	0.82	18.05
8	1.03	2.91	58.31	299.71	37.24	0.25	0.84	1.67	25.91	26.09	0.82	89.30
9	0.83	1.37	77.90	136.33	66.02	0.41	0.64	2.27	16.03	34.21	0.65	20.22
10	0.87	4.36	95.10	95.51	246.77	0.48	0.75	4.46	33.86	52.42	0.72	61.37
11	0.97	2.50	106.08	111.84	220.52	0.28	0.73	6.91	88.61	40.50	0.70	21.81
12	0.84	1.87	46.56	94.51	97.62	0.33	0.75	1.93	20.58	47.12	0.71	43.44
13	0.97	1.48	66.64	64.16	52.28	0.24	0.80	6.06	21.22	27.22	0.78	29.83
14	0.73	1.28	36.82	482.55	47.20	0.21	0.78	0.16	46.30	7.71	0.72	9.67
15	0.76	0.99	33.29	309.44	19.98	0.21	0.74	1.86	8.74	18.89	0.70	15.61
16	0.92	1.42	62.77	115.95	77.09	0.29	0.76	2.06	11.61	33.49	0.73	9.84
17	0.90	1.81	46.56	313.59	95.96	0.39	0.75	1.45	37.24	40.54	0.72	13.50
18	0.89	1.73	114.92	63.58	100.26	0.29	0.73	0.65	16.00	43.76	0.73	18.15
19	0.91	3.74	48.46	495.27	37.42	0.27	0.86	3.36	47.13	33.17	0.79	46.38
20	0.90	2.15	45.99	299.51	42.34	0.23	0.85	0.46	39.86	26.74	0.78	12.79
21	0.95	1.83	21.35	189.47	39.54	0.27	0.84	1.38	21.43	18.04	0.81	14.04
22	0.90	1.50	57.05	49.12	112.70	0.45	0.77	1.21	19.32	35.82	0.75	6.99
23	0.94	1.09	47.39	22.87	150.98	0.41	0.74	7.13	26.06	37.28	0.75	29.86
24	0.83	0.75	22.19	58.58	36.72	0.31	0.78	0.94	12.41	19.81	0.74	20.19
25	0.78	1.10	28.21	55.77	34.72	0.19	0.77	1.61	8.85	20.31	0.73	4.34
26	0.97	1.22	37.71	34.30	72.87	0.23	0.75	2.83	11.61	37.01	0.73	3.17
27	0.70	0.93	18.71	5.90	74.69	0.13	0.82	1.55	5.77	11.42	0.74	6.16
28	0.85	1.54	36.33	49.75	136.51	0.33	0.80	0.76	11.44	23.26	0.76	18.89
29	0.90	1.45	48.21	50.19	103.10	0.31	0.70	5.71	11.19	47.81	0.68	2.18
30	0.91	1.82	76.45	113.22	82.85	0.46	0.76	2.83	19.92	46.80	0.73	23.29
31	1.00	2.70	51.44	596.84	49.46	0.23	0.83	0.88	34.55	26.01	0.82	64.53
32	1.16	4.10	123.25	274.74	187.76	0.18	0.91	0.28	45.13	20.34	0.87	212.01
33	0.94	3.47	109.48	878.74	55.94	0.22	0.80	1.32	122.47	32.05	0.76	36.90
34	1.04	1.95	27.37	238.83	47.14	0.27	0.77	5.33	27.04	40.23	0.75	19.46
35	0.95	2.04	91.62	186.27	69.01	0.37	0.74	2.23	23.51	31.84	0.74	59.16
36	0.84	1.28	45.04	14.20	83.41	0.26	0.80	0.27	10.69	19.71	0.77	4.83
37	0.82	1.52	28.25	521.71	39.72	0.32	0.79	1.09	35.17	37.99	0.73	2.44
38	0.81	1.34	40.77	88.32	77.92	0.30	0.76	1.52	19.06	23.74	0.72	15.83
39	0.87	1.75	77.20	241.97	75.96	0.23	0.80	1.12	38.74	38.09	0.74	5.32
40	0.97	1.71	88.66	329.41	48.13	0.19	0.77	1.00	77.92	46.36	0.75	8.49
41	1.07	1.79	59.87	132.62	28.56	0.24	0.70	7.09	7.21	40.27	0.71	6.40
42	0.85	2.68	95.82	869.77	98.01	0.41	0.71	1.22	58.69	21.40	0.69	123.87
43	0.93	1.81	65.64	67.55	91.51	0.42	0.76	1.17	17.80	35.58	0.73	28.40
44	0.98	2.94	87.56	333.67	140.96	0.38	0.81	3.64	26.50	32.34	0.79	79.21
45	1.00	3.44	76.17	278.58	62.67	0.26	0.76	1.00	37.91	43.31	0.74	63.25
46	0.89	1.62	42.06	271.99	23.57	0.24	0.87	0.57	53.89	18.61	0.82	12.11
47	0.92	2.16	67.69	349.41	130.43	0.35	0.79	1.62	16.52	47.02	0.73	111.58
48	0.96	1.83	76.05	82.98	52.76	0.43	0.83	0.49	13.43	30.50	0.76	31.10
49	0.96	1.76	53.43	52.24	104.36	0.31	0.80	1.24	17.59	25.51	0.78	14.20
50	1.00	1.38	31.32	38.00	37.07	0.28	0.72	9.45	17.51	38.87	0.72	14.96
51	0.86	2.41	60.10	16.64	74.95	0.30	0.76	1.28	23.29	22.67	0.73	9.69
52	1.00	2.28	72.23	63.49	121.93	0.28	0.79	5.55	28.05	74.52	0.77	28.31
53	1.03	2.29	28.58	791.67	26.97	0.14	0.78	5.91	29.31	20.75	0.76	75.85
54	0.97	2.15	32.11	241.09	16.48	0.16	0.92	1.77	18.27	14.88	0.87	10.64
55	0.99	2.61	86.55	167.46	222.55	0.31	0.77	2.49	22.77	26.99	0.73	44.63
56	1.01	1.44	46.97	239.18	31.65	0.30	0.85	1.94	23.17	23.16	0.84	7.50
57	0.91	1.45	75.10	40.67	130.45	0.35	0.80	2.88	30.82	24.83	0.72	48.87
58	0.94	1.59	29.01	30.15	47.00	0.47	0.80	0.69	8.95	25.43	0.78	20.69
59	0.93	2.04	46.62	720.22	19.58	0.57	0.93	0.99	70.41	14.26	0.88	15.49
60	1.01	4.00	104.53	202.64	490.22	0.52	0.80	1.17	76.44	31.57	0.78	161.19
61	1.04	2.97	137.72	119.77	63.54	0.28	0.76	1.58	77.96	24.77	0.77	62.23
62	1.00	1.47	29.26	879.77	31.13	0.22	0.83	2.85	78.97	21.23	0.80	15.41
63	0.88	1.07	28.30	12.90	39.16	0.32	0.79	2.92	5.85	19.72	0.78	9.97
64	1.01	1.47	123.70	25.55	55.47	0.21	0.70	4.72	19.69	12.38	0.71	53.98
65	0.94	2.41	177.61	146.65	49.12	0.26	0.66	3.98	22.61	34.86	0.64	47.79
66	0.96	2.04	56.99	23.58	31.15	0.24	0.74	3.25	8.87	24.39	0.74	10.27
67	0.84	2.23	41.76	167.22	46.98	0.37	0.81	2.72	69.23	56.11	0.78	12.01
68	0.94	1.71	48.80	146.67	47.89	0.26	0.74	2.46	12.80	25.08	0.76	15.75
69	0.99	1.75	52.91	260.45	50.91	0.41	0.79	0.79	19.75	16.16	0.77	17.34
70	0.91	2.02	28.97	262.55	16.79	0.11	0.91	0.38	25.63	7.05	0.90	14.76
71	0.93	2.43	71.05	212.04	71.51	0.71	0.82	1.01	51.96	10.90	0.79	48.94

Table 43: Major and trace elements in the Cologne Conurbation, VIII

ID	Re EF	Sb EF	Sc EF	Sm EF	Sn EF	Sr EF	Ta EF	Tb EF	Th EF	Ti EF	Tm EF	U EF
1	1540.85	354.12	0.62	0.89	9.20	6.44		1.36	4.30	0.33	0.50	1.46
2	527.73	345.45	0.51	0.91	8.16	9.03		1.38	3.32	0.29	0.58	0.60
3	257.98	668.81	0.00	0.80	27.54	15.90	0.00	1.35	3.46	0.46	0.45	1.67
4	152.01	879.52	0.75	0.78	15.69	11.12		0.99	4.45	0.39	0.49	0.67
5	525.55	747.74		0.87	21.04	19.52		1.66	3.16	0.39	0.51	0.91
6		461.16		0.89	15.97	7.73		2.21	3.23	0.55	0.49	0.59
7	250.06	573.24		0.89	12.80	4.74		1.31	2.74	0.46	0.58	0.51
8	245.57	503.90		0.92	14.72	7.90		2.02	2.88	0.45	0.73	0.48
9	448.03	551.68	0.71	0.72	17.22	11.47		1.11	5.00	0.43	0.42	1.27
10	3195.99	821.30		0.81	31.23	13.99		2.76	3.61	0.71	0.49	1.86
11	452.03	1573.49		0.81	44.63	3.61		1.82	3.86	0.66	0.49	0.85
12	514.57	595.04		0.83	18.69	8.86		1.51	3.79	0.44	0.44	1.07
13	361.41	691.95		0.89	12.64	14.12		1.34	3.10	0.44	0.49	0.94
14	3805.06	391.45	0.80	0.94	4.66	8.06	0.00	1.31	3.60	0.32	0.73	0.95
15	359.70	225.81	0.57	0.88	6.07	7.02		1.00	4.18	0.30	0.51	0.77
16	657.33	565.14	0.54	0.90	15.19	13.04		1.26	3.59	0.42	0.49	1.93
17	1589.87	893.15		0.88	19.11	5.54		1.41	4.02	0.47	0.61	0.55
18	658.45	657.85	0.00	0.82	25.85	25.69	0.00	1.56	3.74	0.53	0.50	1.01
19	278.26	537.69		1.08	15.14	4.66		2.73	2.54	0.51	1.33	0.48
20	359.04	565.32		1.16	15.35	8.53		2.03	2.78	0.45	1.17	0.39
21	137.31	415.77	0.39	0.98	11.24	8.27	0.07	1.58	3.07	0.35	0.87	0.38
22	616.45	949.48	0.56	0.87	17.97	6.53		1.34	3.46	0.54	0.51	0.63
23	1051.48	1616.64	0.00	0.77	23.08	11.97	0.00	1.14	3.30	0.51	0.45	0.79
24	148.49	402.69	0.49	0.90	10.62	3.69		0.95	3.84	0.33	0.46	0.67
25	709.61	359.68	0.59	0.94	7.73	7.67		1.21	3.75	0.33	0.47	0.69
26	770.86	445.56	0.43	0.88	11.05	6.93		1.18	3.40	0.34	0.46	0.84
27	556.51	254.35	0.55	0.99	4.36	3.15		1.16	3.68	0.21	0.56	0.58
28	952.14	510.55		0.89	14.80	4.17		1.38	3.48	0.50	0.49	0.55
29	854.21	800.03	0.52	0.83	17.75	7.96		1.18	3.97	0.43	0.48	1.00
30	1147.62	1048.35	0.63	0.82	23.11	21.85		1.27	3.55	0.51	0.55	0.73
31	634.54	531.30		0.90	15.97	17.67		2.06	2.43	0.45	0.68	0.49
32		295.23		0.95	13.39	17.26		2.93	2.19	0.59	0.88	0.47
33	448.04	1721.02		0.97	15.33	20.70		2.29	3.18	0.65	1.40	0.53
34	249.86	492.39	0.42	0.85	15.43	6.78	0.10	1.53	2.80	0.40	0.70	0.63
35	1168.05	660.64		0.77	19.18	22.89		1.44	3.67	0.58	0.42	0.88
36	558.75	418.73	0.48	0.89	16.60	11.35		1.17	3.64	0.40	0.45	0.70
37	557.63	523.25	0.53	0.90	15.51	2.30		1.37	3.70	0.42	0.67	0.58
38	998.23	304.61	0.46	0.86	9.12	7.31		1.19	4.07	0.46	0.46	0.62
39	1328.83	449.36		0.94	11.88	4.61		1.51	3.32	0.49	0.58	0.58
40	950.34	534.91		0.78	12.18	9.48		1.36	3.48	0.47	0.42	0.50
41	788.69	498.11	0.51	0.74	13.49	11.93		1.36	3.54	0.37	0.42	1.15
42	4783.93	387.28		0.76	10.69	12.00		1.85	4.43	0.63	0.62	0.72
43	1788.39	837.46		0.85	20.53	23.07		1.33	3.51	0.64	0.47	1.74
44	4881.43	616.80		0.81	23.07	32.97		2.01	2.81	0.63	0.49	1.65
45	314.38	162.77		0.79	15.12	5.80		2.27	3.09	0.54	0.49	0.75
46	390.69	468.57		1.06	8.15	9.66		1.45	3.18	0.39	0.86	0.40
47	855.21	560.47		0.87	17.09	13.83		1.68	3.01	0.46	0.57	0.54
48	1041.38	840.48		0.86	18.54	14.57	0.16	1.46	3.08	0.51	0.46	0.60
49	483.24	378.53		0.88	12.77	17.99		1.37	3.57	0.53	0.52	1.09
50	349.87	498.92	0.53	0.79	14.90	6.36		1.19	3.52	0.37	0.45	0.83
51	3331.43	291.92		0.86	9.24	9.13		1.78	3.67	0.48	0.45	1.13
52	1347.02	908.84		0.92	23.12	12.72		1.76	2.87	0.59	0.62	1.52
53	520.85	264.89		0.90	11.77	6.01		1.93	1.99	0.32	0.74	0.42
54	480.51	182.52		1.13	8.01	4.90	0.08	1.79	2.49	0.28	1.11	0.39
55	2849.78	263.80		0.76	17.03	14.22		1.71	3.06	0.52	0.52	0.73
56	594.29	291.14	0.43	0.97	9.44	6.65		1.37	2.24	0.50	0.77	0.38
57	1133.79	725.62	0.00	0.75	14.20	23.50	0.00	1.25	3.39	0.57	0.41	1.48
58	508.64	451.77	0.50	0.88	11.52	12.39	0.15	1.31	2.94	0.71	0.47	0.63
59	389.87	862.61		1.24	6.43	6.65		2.05	1.59	0.99	1.27	0.31
60	1068.99	970.98		0.77	27.67	15.96		2.53	2.94	0.96	0.69	0.89
61	1008.51	424.30		0.76	16.06	26.51		1.93	3.11	0.57	0.45	1.09
62	2407.35	394.92		0.96	10.51	5.17	0.09	1.46	2.70	0.33	0.69	0.47
63	980.24	406.08	0.38	0.89	10.24	5.13	0.12	1.14	3.13	0.39	0.46	1.38
64	2095.99	399.77	0.00	0.76	7.42	13.03	0.00	1.35	3.73	0.45	0.46	4.71
65	1715.42	567.98		0.74	20.24	21.97		1.67	4.59	0.65	0.39	1.73
66	4269.71	276.58		0.83	8.95	5.42		1.54	3.41	0.40	0.40	1.19
67	8099.32	640.62		0.90	11.40	3.16		1.70	3.18	0.54	0.48	0.92
68	2085.65	406.74		0.81	11.19	8.10	0.14	1.37	2.96	0.41	0.43	0.99
69	822.25	578.96		0.80	10.73	16.06	0.16	1.34	2.95	0.52	0.48	0.52
70	427.70	80.54		1.11	6.45	6.66		1.76	1.58	0.19	1.38	0.19
71	766.42	249.12		0.90	7.23	14.45	0.21	1.68	2.81	1.08	0.48	0.57

Table 44: Major and trace elements in the Cologne Conurbation, IX

ID	V EF	W EF	Y EF	Yb EF	Zn EF	Zr EF
1	2.30	4.02	0.67	0.52	151.26	0.17
2	2.12	4.08	0.92	0.58	198.89	0.15
3	2.43	29.05	0.55	0.46	295.61	0.21
4	2.33	12.52	0.71	0.52	308.36	0.23
5	2.44	10.05	0.62	0.54	525.66	0.25
6	2.39	8.07	0.59	0.51	318.77	0.20
7	2.09	15.15	0.85	0.55	190.42	0.20
8	1.66	9.90	1.08	0.71	378.26	0.22
9	2.05	8.13	0.60	0.47	229.66	0.23
10	2.23	17.17	0.64	0.51	597.88	0.35
11	2.01	12.21	0.63	0.51	452.75	0.20
12	2.50	16.45	0.58	0.46	205.61	0.23
13	1.84	8.56	0.68	0.50	238.75	0.20
14	2.54	9.01	0.96	0.69	355.88	0.18
15	2.10	2.98	0.62	0.50	208.42	0.16
16	2.56	6.76	0.65	0.52	203.64	0.21
17	3.28	8.27	0.96	0.61	458.95	0.24
18	2.80	14.75	0.67	0.50	539.67	0.24
19	2.11	8.20	1.79	1.20	515.76	0.19
20	2.11	5.21	1.74	1.09	367.43	0.19
21	1.43	5.10	1.22	0.83	370.33	0.17
22	2.89	7.09	0.71	0.52	318.48	0.28
23	3.20	22.71	0.62	0.45	646.38	0.33
24	1.63	8.17	0.59	0.41	114.97	0.18
25	1.80	7.19	0.59	0.49	156.89	0.18
26	1.96	5.57	0.59	0.51	128.77	0.19
27	1.70	3.01	0.63	0.54	45.52	0.12
28	2.23	7.08	0.66	0.52	201.79	0.20
29	3.51	7.21	0.61	0.48	276.87	0.22
30	3.37	14.61	0.74	0.63	507.91	0.28
31	1.82	6.44	1.20	0.69	818.20	0.16
32	1.31	5.68	1.36	0.79	747.03	0.18
33	1.84	19.12	1.81	1.28	727.34	0.23
34	4.07	5.87	0.96	0.68	331.31	0.21
35	5.51	7.27	0.53	0.45	471.50	0.25
36	2.56	4.47	0.54	0.46	184.49	0.18
37	2.02	5.61	0.98	0.65	261.57	0.22
38	1.65	4.57	0.60	0.48	194.04	0.17
39	1.55	33.56	0.82	0.56	621.74	0.19
40	1.28	7.85	0.57	0.42	639.88	0.17
41	2.64	5.10	0.57	0.46	156.48	0.17
42	1.49	5.46	0.79	0.56	668.49	0.19
43	2.92	7.42	0.62	0.53	195.12	0.27
44	3.30	8.75	0.69	0.56	323.85	0.23
45	2.40	8.51	0.72	0.52	468.90	0.18
46	1.05	5.41	1.27	0.82	183.54	0.16
47	2.70	6.00	0.79	0.59	325.69	0.24
48	2.44	9.48	0.58	0.50	259.36	0.29
49	2.09	6.42	0.75	0.52	181.10	0.18
50	2.24	6.18	0.64	0.45	207.76	0.19
51	1.31	4.83	0.58	0.54	214.77	0.17
52	1.74	16.76	0.78	0.66	391.64	0.23
53	1.42	8.38	1.08	0.66	457.68	0.12
54	1.11	2.82	1.41	1.00	235.04	0.12
55	2.17	5.30	0.78	0.52	621.94	0.24
56	1.89	3.53	1.09	0.72	786.47	0.13
57	3.13	11.75	0.53	0.44	706.80	0.26
58	1.96	5.66	0.57	0.49	115.61	0.23
59	1.44	3.36	1.73	1.18	323.25	0.16
60	3.28	23.56	0.95	0.75	468.02	0.30
61	1.89	11.23	0.60	0.48	516.50	0.26
62	1.45	4.66	1.09	0.64	282.03	0.20
63	1.29	4.60	0.57	0.44	75.38	0.20
64	2.33	12.49	0.55	0.48	659.09	0.17
65	1.78	10.18	0.57	0.44	562.78	0.23
66	1.29	5.13	0.49	0.43	120.66	0.17
67	1.34	9.91	0.58	0.48	543.06	0.27
68	1.43	5.41	0.53	0.45	255.87	0.18
69	1.21	5.19	0.64	0.47	367.93	0.24
70	0.59	4.03	1.60	1.23	313.16	0.06
71	1.52	8.34	0.75	0.55	324.01	0.27

Table 45: Major and trace elements in the Cologne Conurbation, X

loc.	seas.	exp. [month]	Fluo	P	A	DBT	CPP	Fla	Py	BaFluo	BbcFluo	EghiFla	CPedPY	BcP	BaA
1	w	8	46.96	409		20.75	7.96	163	97.52	1.49	1.18	5.20		2.81	2.87
1	w	20	70.07	369		33.94	15.68	386	211.89	2.18	1.40	10.86		5.38	4.11
1	w	32	70.00	1199		38.87	18.30	465	252.25	3.83	2.81	14.32		7.24	5.69
1	w	44	48.73	1119	15.91	41.54	26.97	590	339.09	7.14	7.52	15.24		8.65	6.75
2	w	8	15.04	93	3.48	4.40	3.04	51	27.85	0.79	0.44	2.73		1.04	0.78
2	w	20	19.08	146	6.55	4.86	86	44.12	1.01	0.79	2.93	0.066		1.25	0.72
2	w	32	21.42	204	7.56	7.27	1.35	63.37	1.97	1.31	5.08	0.141		2.02	1.42
2	w	44	23.24	211	7.63	7.18	7.53	133	60.77	1.35	0.83	4.49	0.136	1.77	0.70
3	w	8	14.99	145		13.48	6.85	106	66.16	5.03	3.86	12.39	0.250	6.25	5.36
3	w	20	85.67	541	13.71	41.51	17.77	176	89.11	3.49	3.03	6.40	0.158	2.87	2.96
3	w	32	201.14	1071	27.46	84.19	37.30	414	213.42	7.42	5.78	11.31		6.36	4.16
4	w	8	18.52	162	0.00	7.18	7.18	89	60.02	2.73	2.03	8.52	0.190	3.36	3.83
4	w	20	42.46	580	19.54	18.19	21.48	328	197.23	9.58	6.86	28.26	0.698	9.63	12.26
4	w	32	70.67	775	29.93	19.29	27.07	496	260.28	12.92	10.13	29.03	0.781	10.89	11.46
4	w	44	20.80	239		7.21	9.46	167	81.06	2.15	2.14	7.17	0.133	2.62	1.29
5	w	8	22.60	160	5.82	10.37	5.70	102	62.02	2.68	1.72	9.33		5.36	4.39
5	w	20	35.05	316	16.52	16.22	10.20	191	105.75	3.96	2.67	11.77	0.249	6.36	5.08
5	w	32	25.68	283	10.66	13.26	9.18	198	111.50	4.11	2.92	12.70	0.213	6.88	5.52
5	w	44	38.27	535	22.86	19.91	15.79	386	191.13	2.18	1.23	9.72	0.695	4.97	34.57
6	w	8	10.09	69	2.08	6.41	3.83	35	20.83	1.49	1.06	3.78	0.074	1.27	1.92
6	w	20	15.27	185	6.46	7.03	5.58	97	55.27	2.97	2.09	6.17	0.148	2.16	2.51
6	w	32	24.93	268	11.31	12.26	9.34	134	79.04	4.51	3.26	8.96	0.213	3.75	4.05
6	w	44	31.50	317	5.37	15.42	6.44	91	50.44	2.92	3.47	13.37	0.091	1.92	2.40
1	s	3	13.02	134	1.26	8.40	3.17	63	28.68	0.61	0.46	1.22	0.063	0.86	1.32
1	s	14	9.18	244	6.63	16.48	5.06	124	69.60	2.00	1.47	2.99	0.108	1.71	3.10
1	s	26	11.53	359	7.06	16.98	10.14	272	181.88	3.70	2.94	5.47		3.28	4.52
1	s	38	22.06	601	14.27	25.87	15.08	366	198.89	4.29	3.47	13.37	0.264	8.07	7.94
1	s	50	47.06	1232	22.43	47.10	25.62	510	277.87	3.19	3.88	11.13	0.260	5.77	4.41
2	s	3	6.50	45		3.07	0.98	27	11.16	0.21	0.21	0.52	0.062	0.38	1.38
2	s	14	5.20	71	1.09	2.87	1.61	50	20.99	0.21	0.19	0.97	0.043	0.42	0.63
2	s	26	9.91	184		6.41	4.91	62	59.33	1.15	0.85	3.58	0.112	1.72	2.32
2	s	38	17.86	301	4.30	7.59	7.15	167	74.67	0.71	0.61	3.47	0.128	1.79	1.72
2	s	50	18.61	210	4.05	7.97	6.91	165	59.25	0.45	0.67	2.90		1.24	0.49
3	s	3	9.63	77	0.80	7.31	2.51	47	20.41	0.50	0.42	0.91	0.036	0.58	0.93
3	s	14	52.25	418	10.48	32.69	16.47	172	80.44	2.72	2.16	2.72	0.101	1.74	1.57
3	s	26	132.60	866	25.03	56.69	27.23	272	124.64	2.23	1.53	3.16		1.99	5.82
3	s	38	395.94	2112	34.40	136.54	67.84	708	311.93	6.33	3.54	8.04		5.23	1.33
4	s	3	7.92	129		7.62	4.78	135	35.93	0.74	0.47	2.18	0.057	1.39	2.12
4	s	14	18.19	384	6.57	13.27	13.93	218	107.07	2.49	1.63	6.35	0.191	3.01	3.02
4	s	26	37.49	710	14.48	20.67	20.67	324	168.79	1.68	0.83	6.64	0.319	2.64	1.21
4	s	38	18.83	770		6.80	19.52	328	269.64	3.62	1.93	17.43	0.232	8.79	4.90
5	s	3	10.18	95	1.08	6.57	2.26	75	21.58	0.43	0.28	0.08		0.07	0.04
5	s	14	14.66	124	1.61	6.74	3.20	76	26.53	0.47	0.32	0.06		0.04	
5	s	26	30.60	354	6.17	13.35	7.44	184	89.50	0.97	0.46	0.40		0.33	0.12
5	s	38	34.23	485	0.00	15.00	10.79	284	128.59	2.26	1.19	0.53		0.38	0.18
5	s	50	27.72	536	13.32	11.07	10.53	370	174.92	1.90	0.79	7.99	0.120	5.93	4.08
6	s	3	4.05	33	0.72	1.32	0.65	9	3.59	0.02	0.02	0.08	0.019	0.05	0.32
6	s	14	12.95	130		4.75	2.40	43	18.49	0.14	0.12	0.67	0.070	0.43	1.27
6	s	26	9.19	126		3.69	2.92	48	22.41	0.09	0.16	0.85	0.038	0.46	0.23
6	s	38	13.97	343	7.23	8.86	7.82	136	66.84	1.00	0.28	1.66		1.24	4.39
6	s	50	31.26	483		12.26	8.73	171	77.60	1.52	0.61	2.97		2.12	1.15

Table 46: Parent PAH on pine needles of different age needle age in ng g^{-1} dry weight, sheet I.

loc.	seas.	exp. [month]	TRI	CHR	retene	BNT	BbJFLA	BkFLA	BeP	BaP	Per	Ip	BghiP	DbahA	coronene
1	w	8	10.27	27.10	3.83	3.31	7.10	2.14	2.40	2.40		0.86	1.650	0.092	0.336
1	w	20	17.88	47.02	7.71	5.37	12.84	5.05	4.98	4.98		1.57	2.820		0.369
1	w	32	25.06	58.48	9.76	9.16	17.79	4.36	6.22	0.734		2.38	3.599		0.360
1	w	44	23.20	55.31	14.63	10.27	23.37	7.42	9.72	2.119		3.48	4.920	0.091	0.375
2	w	8	2.16	6.67	1.12	0.56	2.43	1.20	1.17			0.52	0.730		0.070
2	w	20	3.07	6.51	1.10	0.55	2.53	0.91	1.13	0.359		0.62	0.918	0.039	0.082
2	w	32	4.05	9.21	1.86	0.71	3.72	1.41	2.07	0.562		0.92	1.543	0.079	0.107
2	w	44	3.28	8.33	1.32	0.40	3.44	1.30	1.60	0.566		0.69	1.212		0.126
3	w	8	8.89	34.15	3.54	7.66	12.82	4.18	4.55	1.288	0.226	2.05	3.104	0.337	0.617
3	w	20	5.70	16.17	2.24	3.41	5.22	1.37	1.65	0.340	0.113	0.72	1.082		0.071
3	w	32	10.77	39.34	5.24	7.05	11.75	4.70	4.70	1.208		1.70	2.790	0.094	0.306
4	w	8	7.58	21.26	2.44	2.73	10.54	3.82	3.62	0.874		1.54	2.378	0.058	0.334
4	w	20	18.21	63.54	5.90	10.77	20.45	7.00	7.22	1.856	1.060	1.96	3.226	0.054	0.419
4	w	32	19.96	49.41	5.97	9.97	16.24	6.50	7.73	2.054	0.346	2.08	3.428	0.116	0.309
4	w	44	3.59	9.21	1.08	1.62	1.54	1.11	0.78	0.178		0.28	0.245		0.069
5	w	8	24.04	48.82	3.27	12.41	13.06	4.93	2.97	0.697		0.54	0.882		0.056
5	w	20	23.22	49.28	3.01	13.19	11.19	4.93	4.04	1.293	0.336	0.80	1.387	0.083	0.138
5	w	32	26.76	48.94	2.91	13.17	12.08	4.76	4.15	1.072		0.81	1.509	0.096	0.096
5	w	44	47.47		1.73	4.56	6.83	2.40	1.74			0.65	1.010	0.463	0.122
6	w	8	2.74	11.53	1.55	1.18	4.16	0.98	0.89	0.207		0.39	0.513	0.016	0.024
6	w	20	4.33	16.10	2.57	1.66	4.61	1.58	1.15	0.215		0.67	0.635		0.035
6	w	32	8.48	26.79	4.32	4.07	6.45	2.99	1.87	0.595	0.669	0.69	0.878	0.039	0.072
6	w	44	3.64	11.32	2.43	1.70	2.88	0.95	0.85	0.235		0.25	0.344		0.021
1	s	3	2.94	7.33	1.15	1.20	4.53	1.22	1.89	0.736	0.116	0.87	1.223	0.070	0.073
1	s	14	8.14	24.97	4.03	2.71	9.05	1.95	3.67	1.065		1.26	3.097	0.129	0.899
1	s	26	18.81	34.08	7.48	4.88	19.29	3.83	7.51	1.772	0.105	2.86	4.460	0.194	0.426
1	s	38	29.27	53.42	8.11	10.00	34.83	9.51	18.16	5.098	0.800	7.03	9.084	0.537	0.800
1	s	50	15.28	35.64	11.25	4.49	14.36	4.03	5.43	1.188		1.87	3.083	0.040	0.177
2	s	3	1.96	5.42	0.30	0.47	2.48	0.70	0.82	0.245		0.49	0.716		0.027
2	s	14	2.50	4.54	0.94	0.44	2.75	0.63	0.93	0.327		0.58	0.759	0.025	0.079
2	s	26	6.55	13.80	2.19	1.80	9.22	2.16	3.57	0.966	0.166	1.75	2.393	0.123	0.227
2	s	38	6.08	8.60	1.12	1.02	5.75	1.62	2.21	0.702		1.00	1.403		0.143
2	s	50	4.90	7.30	0.87	0.67	5.15	1.41	1.97			0.51	0.740		
3	s	3	2.45	6.50	0.43	1.81	5.06	1.22	2.23	0.576	0.087	0.89	0.992	0.115	0.079
3	s	14	6.25	14.05	0.85	3.02	6.40	1.47	2.55	0.923	0.082	1.48	1.946	0.140	0.280
3	s	26	11.67	22.89	0.91	2.69	3.40	1.56	0.49	1.740	0.505	0.82	1.138		
3	s	38	13.01	28.57	2.68	4.97	13.12	5.00	5.99	1.643	0.588	1.85	2.914		
4	s	3	4.50	12.36	1.21	2.69	12.07	2.89	5.90	1.522		1.40	1.367	0.168	0.128
4	s	14	9.55	21.14	1.26	2.78	14.31	4.27	5.62	2.106	0.278	3.92	4.447	0.457	0.652
4	s	26	10.94	14.46	1.17	1.18	7.29	2.73	2.74	0.731		1.26	2.169	0.170	0.170
4	s	38	27.97	54.79	4.36	6.13	30.59	8.59	10.60	3.207		6.17	7.327	0.573	0.779
5	s	3	0.63	0.74	0.73	2.42	0.30	0.14	0.12			0.03	0.031		
5	s	14	0.41	0.42	0.35	1.49	0.16	0.07	0.08			0.01	0.017		
5	s	26	2.82	3.52	0.83	3.98	1.01	0.36	0.34			0.11	0.169		
5	s	38	2.93	3.91	1.06	6.11	1.20	0.40	0.35			0.10	0.168		
5	s	50	38.41	34.16	0.75	5.80	13.12	2.38	3.61	0.914		0.97	1.324		
6	s	3	0.45	0.20	0.31	0.47	0.14	0.07	0.03	0.046					
6	s	14	0.97	1.01	0.89	0.19	0.64	0.45	0.12	0.295	0.026	0.20	0.226		
6	s	26	1.44	2.35	0.00	0.75	0.21	0.45	0.22	0.330		0.14	0.204		
6	s	38	3.26	3.59	2.63	0.87	0.76	1.22	0.39						
6	s	50	4.42	10.07	3.34	3.49	2.80	1.06	1.06			0.38	0.539		

Table 47: Parent PAH on pine needles of different age needle age in ng g^{-1} dry weight, sheet II.

ID	Fluo	P	A	DBT	CPP	Fla	Py	BaFluo	BbcFluo	BghiFla	CPcdPy	BcP	BaA
1	90.7	992	31.5	58.5	47.26	491	242	5.77	5.68	11.29	0.239	5.41	5.08
2	50.2	677		24.5	17.54	507	305	12.36	8.63	31.40		16.68	18.90
3	59.5	810	1.2	30.4	14.09	332	185	2.61	2.06	9.68		5.00	4.14
4	10.8	193		3.0	5.10	157	89	3.14	1.82	8.10	0.263	2.79	2.94
5	31.0	335	6.6	14.4	8.43	176	97	4.50	3.00	11.52	0.370	4.43	5.05
6	23.6	157	5.0	5.8	4.50	92	55	2.68	1.54	4.19		1.91	6.12
7	24.5	218		5.2	7.34	158	91	4.66	2.79	1.83		1.13	0.38
8	23.1	201	4.3	9.3	5.01	94	51	2.03	1.21	6.79	0.125	2.63	2.72
9	40.8	386		17.2	11.69	200	101	3.92	1.99	7.21	0.260	2.94	2.98
10	20.0	227		8.8	5.27	90	53	3.04	2.09	6.23		3.33	2.79
11	47.5	345	4.5	11.1	6.41	151	81	3.33	2.03	8.64	0.321	3.23	4.73
12	88.2	1304		48.1	22.26	701	374	7.62	5.16	18.77		13.15	11.77
13	22.3	240	7.2	11.3	4.38	96	61	2.79	1.82	7.03	0.344	2.51	3.49
14	70.0	439	9.5	34.9	15.57	177	95	4.67	3.75	9.65	0.177	4.80	4.16
15	125.0	1220		44.8	29.50	407	201	5.26	3.44	9.82		4.03	2.54
16	38.0	447		18.5	10.74	252	135	3.45	0.90	13.37		4.86	4.63
17	20.0	249	7.2	9.7	6.87	152	97	4.71	3.77	14.57	0.284	5.09	7.50
18	19.0	153	2.3	6.2	5.24	94	46	1.20	0.80	3.58	0.073	1.44	0.89
19	196.5	1730	23.3	91.8	76.74	592	312	9.09	7.50	13.36	0.316	6.04	9.05
20	6.8	59		1.1	11.84	44	20	0.65	0.26	2.50		0.98	1.01
21	8.4	140	7.9	3.9	7.79	193	104	6.77	5.78	16.55	0.454	6.71	9.26
22	56.0	559	18.7	12.8	21.47	319	201	8.02	5.32	27.27	0.887	7.53	10.96
23	36.6	429	12.3	13.3	16.08	256	147	6.93	5.22	19.09	0.471	6.87	7.93
24	21.9	237		7.8	5.52	196	103	3.96	2.04	17.36		5.59	7.52
25	15.8	289		7.3	7.40	172	95	3.62	1.70	8.72	0.308	3.09	2.84
26	9.7	136	5.0	3.4	4.13	142	81	6.05	4.25	14.14	0.255	5.18	9.81
27	36.2	294	5.9	12.6	8.65	166	90	5.13	2.99	13.30		4.86	4.91
28	58.2	427	13.9	21.0	13.28	205	112	6.28	5.12	15.84	0.342	6.24	9.48
29	30.2	371	9.0	9.8	8.97	176	106	4.14	3.15	12.26	0.138	4.04	4.19
30	35.3	420	9.0	11.4	15.95	279	178	6.95	4.10	22.74	0.869	7.34	11.68
31	3.0	40	0.6	1.0	1.08	23	12	0.33	0.13	0.91		0.40	0.20
32	23.4	158		5.1	4.18	74	38	2.22	1.21	4.11	0.245	2.14	1.41
33	36.2	233	6.7	6.2	6.30	93	53	1.69	0.75	4.87		1.75	1.86
34	6.8	205		3.8	8.22	175	127	8.65	7.64	26.28		11.07	11.45
35	39.0	486	14.1	20.4	12.74	230	130	4.59	3.79	11.23	0.438	4.58	4.70
36	76.1	472	10.5	20.1	11.46	174	96	3.12	1.92	8.21	0.295	3.05	3.22
37	12.5	170	3.7	4.7	6.50	159	91	4.29	2.95	13.34		5.15	4.95
38	83.6	533	12.1	19.6	14.19	187	100	3.02	2.37	7.78	0.189	2.88	2.15
39	8.2	81	3.2	2.5	1.94	47	29	1.24	1.08	5.65	0.179	1.94	3.61
40	19.3	182		5.4	3.91	89	46	1.16	0.79	4.40		1.67	1.65
41	17.7	196		8.3	3.74	84	43	1.67	1.37	4.50	0.215	1.90	1.67
42	33.4	315		11.6	7.07	160	84	3.76	2.32	10.47		3.81	3.74
43	42.7	370	10.4	19.5	10.20	127	79	2.74	2.66	7.98	0.176	3.34	3.50
44	35.8	224	6.0	6.7	8.31	104	63	2.47	1.78	5.36	0.142	2.13	1.78
45	16.1	68	1.6	2.4	1.78	45	25	1.27	0.79	2.98	0.134	1.11	0.99
46	25.1	133	5.1	5.3	3.43	75	43	3.13	2.99	11.08	0.402	3.35	7.44
47	22.5	192	3.6	6.5	7.18	120	78	3.06	2.09	8.69	0.415	3.52	3.57
48	5.5	105	0.0	1.8	3.77	102	68	2.86	2.11	10.56	0.181	4.14	3.07
49	21.8	209	5.9	9.1	6.25	124	67	3.76	3.29	8.01	0.177	3.94	4.66
50	28.3	291		9.8	5.62	112	57	3.31	2.12	8.02		3.32	3.62
51	23.5	213	6.2	8.5	5.45	80	44	1.90	1.29	4.18	0.154	1.75	2.16
52	9.5	98		2.8	2.44	45	27	1.43	1.09	5.08		1.76	2.59
53	10.5	68		2.5	1.65	25	12	0.62	0.22	1.80		0.76	0.22
54	28.3	195	2.1	11.4	5.48	75	37	2.38	1.73	4.74	0.123	1.87	2.08
55	44.5	310		10.6	10.29	162	92	4.25	3.54	10.63	0.167	4.60	4.83
56	27.5	244		13.6	6.52	134	54	2.87	1.87	6.93	0.284	2.67	2.42
57	28.9	277	12.1	13.9	17.36	182	101	3.34	2.23	10.88	0.200	6.04	8.09
58	23.5	296	4.7	9.8	7.84	163	102	3.75	2.15	12.55	0.519	5.66	5.82
59	19.4	152	4.1	9.1	5.35	70	34	2.32	1.82	5.36	0.287	1.88	2.97
60	5.1	77		1.6	2.97	62	37	0.76	0.40	4.64		1.81	1.37
61	61.2	438		17.7	13.76	134	76	2.61	1.72	6.32	0.140	2.56	2.31
62	16.6	248		8.4	7.69	148	85	4.15	3.13	12.48		4.66	4.61
63	32.5	411		9.2	11.48	263	160	5.15	3.82	23.45		8.31	8.37
64	16.4	167	5.6	8.4	5.69	80	46	2.69	1.94	5.64	0.128	2.11	2.57
65	8.8	105		3.3	1.89	54	22	0.75	0.30	3.07		1.21	1.01
66	13.7	188		6.3	4.14	97	48	1.87	1.06	6.64		3.01	2.42
67	34.8	276	5.8	10.8	9.83	136	81	4.37	3.48	7.62	0.249	4.20	4.52
68	19.4	262		6.3	6.18	161	92	3.30	2.38	11.21	0.327	3.81	4.89
69	38.6	417		11.0	11.90	218	129	5.36	4.86	18.19	0.262	6.89	7.37
70	23.7	245		9.8	6.51	103	51	1.60	0.87	5.51		2.48	1.80
71	32.9	235		6.0	6.36	92	52	2.12	1.33	6.73	0.110	3.02	2.17

Table 48: Parent PAH in *Pinus nigra* needles of the Cologne Conurbation in ng g⁻¹ dry weight; ID according to Fig. 62, sheet I

ID	Tri	Chr	retene	BNT	BbjFLA	BkFLA	BeP	BaP	Per	Ip	BghiP	DBahA	coronene
1	15.1	38.3	6.08	7.06	12.81	3.98	4.84	0.985		1.70	2.36		0.362
2	41.3	123.5	8.63	28.88	60.17	15.35	21.57	6.309		8.03	9.75	0.923	1.832
3	16.7	42.2	7.14	5.68	12.39	3.98	4.59	0.304		1.60	2.68	0.043	0.355
4	7.1	20.8	2.34	2.41	8.33	2.62	3.06	0.838		1.41	2.36		0.269
5	11.3	34.4	3.59	4.14	11.72	3.46	3.71	0.832		2.59	2.95		0.744
6	4.7	17.7	0.62	1.61	17.48	5.36	7.97	5.482	1.322	8.45	9.41	0.913	1.665
7	3.9	5.8	12.12	1.52	6.61	2.34	2.76	0.820		0.70	1.13		0.292
8	5.0	20.2	4.24	1.46	7.61	2.17	2.68	0.647		1.86	2.42	0.364	0.715
9	6.3	17.1	4.85	2.03	6.00	2.21	2.59	1.080		0.99	1.91		0.313
10	7.5	17.6	1.66	2.73	9.14	2.73	3.18	1.072		2.96	3.03	0.363	0.744
11	11.8	29.3	2.71	5.42	10.28	3.44	3.72	1.205		1.75	2.24		0.224
12	53.6	112.3	3.04	26.55	89.22	19.59	42.18	8.484		8.48	11.18	0.810	0.742
13	7.7	19.5	6.87	2.55	7.33	2.78	2.65	0.999		1.26	2.27		0.190
14	7.8	27.0	3.20	5.73	9.38	3.03	3.31	0.865	0.147	1.43	2.21	0.159	0.339
15	9.7	28.0	3.04	4.27	6.69	2.44	2.56	0.000		0.93	1.32		
16	12.9	36.8	3.40	5.53	8.74	2.83	2.91	0.000		1.04	2.13		0.262
17	9.7	32.4	3.56	4.99	9.99	2.75	3.23	0.767		1.23	2.31		0.516
18	3.0	7.4	1.31	0.57	2.90	1.17	1.42	0.324		0.67	1.04	0.030	0.091
19	10.8	41.8	2.15	4.31	17.01	5.32	5.27	1.595		3.64	3.43	0.348	0.756
20	2.6	6.3	1.84	0.39	2.38	0.93	0.85	0.000		0.57	0.80		0.093
21	10.8	35.1	7.68	4.70	28.02	6.68	12.53	5.613	0.793	6.99	9.28	1.120	1.865
22	18.9	42.7	4.50	4.95	22.32	6.11	8.82	2.222		3.20	5.87		1.197
23	13.2	40.1	4.16	6.26	14.13	5.14	5.16	1.361	0.440	1.65	2.64	0.061	0.331
24	15.1	46.9	2.90	5.74	19.14	4.49	6.79	1.246		2.51	3.41	0.299	0.531
25	8.9	21.4	2.59	2.88	4.35	1.81	1.52	0.000		0.62	1.09		
26	13.5	41.1	4.73	7.35	8.50	2.50	3.06	1.104		1.17	1.94	0.077	0.283
27	11.6	32.0	3.59	6.05	8.84	2.33	2.54	0.814		1.16	2.10	0.061	0.511
28	9.5	41.0	16.78	3.89	10.78	3.18	3.31	1.048		1.44	2.31	0.121	0.300
29	11.8	32.9	3.65	0.29	8.12	2.68	2.75	0.000		1.14	1.80		0.466
30	15.2	46.0	4.70	5.53	15.90	4.82	5.49	1.662		2.51	4.13	0.293	1.202
31	0.6	2.0	0.33	0.21	1.10	0.30	0.38	0.000		0.15	0.19		
32	4.1	12.5	2.13	1.12	5.20	1.29	2.73	0.555		1.11	2.25		0.274
33	3.3	8.9	2.30	0.61	2.17	0.94	0.91	0.458		0.56	0.95		0.000
34	19.9	72.9	10.66	8.79	27.30	7.90	8.65	1.919		4.52	5.40	0.372	0.957
35	9.3	22.9	11.35	2.59	5.29	1.84	2.03	0.583		0.85	1.49		0.450
36	8.6	25.8	2.95	2.64	5.34	2.34	2.00	0.470		1.12	1.37	0.114	0.500
37	8.8	37.9	6.19	4.15	9.71	3.05	2.74	0.551		0.93	1.47		0.118
38	6.9	15.9	2.04	1.67	4.98	1.66	1.86	0.743		0.81	1.68		0.410
39	4.5	16.7	1.68	1.43	5.01	1.42	1.83	0.623		0.51	1.05		0.248
40	6.2	17.0	1.31	0.91	1.75	0.00	1.75	0.000		0.89	1.27	0.161	0.261
41	4.8	19.8	1.94	2.46	5.85	1.48	1.99	0.469		0.67	1.85		0.247
42	8.2	26.6	4.39	3.43	27.09	12.54	4.19	1.074		1.48	2.64		0.441
43	7.8	22.0	3.00	1.82	6.09	1.95	1.86	0.475		0.69	1.55		0.454
44	3.5	11.5	1.90	1.04	3.06	0.97	1.14	0.248		0.39	0.65		
45	2.0	7.1	1.17	0.74	2.20	0.60	1.11	0.224		0.28	0.50		
46	5.1	18.9	5.03	1.66	8.24	2.28	2.43	0.689	0.102	1.15	1.13	0.053	0.114
47	7.1	16.4	5.21	1.87	6.61	1.86	1.79	0.363		1.35	1.63		0.430
48	9.8	33.6	2.98	2.95	10.96	2.68	3.54	0.405		1.44	2.21		0.606
49	6.7	19.4	6.35	4.08	5.84	1.53	1.83	0.623	0.143	0.98	1.18	0.048	0.099
50	8.4	26.9	2.83	3.68	9.20	2.34	3.43	0.894		1.53	2.05	0.166	0.413
51	3.5	14.1	0.90	1.01	4.39	1.02	1.37	0.382		0.48	0.57		0.076
52	5.2	16.7	1.67	1.25	3.79	1.58	1.33	0.000		0.57	1.04		0.112
53	3.0	5.9	0.82	0.43	2.98	1.15	1.32	0.350		0.53	0.89		
54	5.7	15.9	1.63	2.04	6.28	1.93	0.59	0.000		0.78	1.02	0.058	0.095
55	9.1	30.5	12.03	2.74	5.72	1.91	1.86	0.000		0.70	1.54		0.335
56	6.8	16.7	2.43	2.62	6.00	1.64	2.14	0.762		1.27	1.65		0.283
57	26.9	43.8	2.95	9.29	11.58	4.62	3.43	0.894	0.108	0.69	1.19	0.076	0.098
58	13.1	40.7	12.05	4.57	13.48	3.19	5.20	0.907		1.54	4.41	0.000	0.738
59	3.4	8.4	3.18	1.15	4.40	1.29	1.49	0.595	0.051	0.85	0.99	0.081	0.069
60	5.9	11.5	0.87	2.10	5.54	1.23	1.74	0.221		0.59	0.88		0.095
61	5.1	17.7	1.90	1.89	5.03	1.44	1.74	0.682		1.00	1.33		0.200
62	12.6	46.8	3.68	4.43	17.40	4.69	4.52	0.415		1.74	2.36	0.079	0.513
63	25.9	73.7	5.61	5.95	28.24	8.14	6.77	1.108		2.63	4.00		0.774
64	4.5	16.0	0.88	1.70	4.66	1.57	1.17	0.287		0.53	0.61	0.014	0.025
65	3.2	8.1	1.34	0.59	2.43	1.23	1.08	0.000		0.35	0.78		
66	8.3	30.3	5.65	2.45	6.68	1.78	2.48	0.608		1.02	1.87		0.329
67	5.4	26.2	8.87	1.61	5.36	0.00	1.70	1.472		1.03	1.36		0.207
68	10.4	28.4	2.60	1.94	8.38	2.92	2.62	0.633		0.99	1.90		0.280
69	16.9	44.2	6.81	2.83	13.75	4.18	3.54	1.049		1.35	2.32		0.570
70	6.5	17.8	1.61	1.65	4.88	1.02	1.67	0.165		0.43	0.66		0.033
71	12.3	27.1	1.78	2.54	10.18	2.46	2.32	0.480		0.93	1.04		0.282

Table 49: Parent PAH in *Pinus nigra* needles of the Cologne Conurbation in ng g⁻¹ dry weight; ID according to Fig. 62, sheet II.

ID	location	em. sc.	P	A	DBT	CPP	3-MP	2-MP	9-MP	1-MP
1	Grevenbroich	1	992	31.51	58.48	47.26	34.52	52.15	28.80	30.79
2	Broich	1	677	n.d.	24.52	17.54	13.90	15.48	13.52	11.01
3	Dormagen	2	810	1.22	30.40	14.09	31.53	56.14	25.11	34.56
4	Leverkusen-Reusrath	7	193	n.d.	3.01	5.10	4.01	3.23	6.66	4.08
5	Burscheid	6	335	6.63	14.44	8.43	15.68	17.92	11.64	13.33
6	Dhuenn-Neuenhaus	6	157	5.00	5.75	4.50	2.30	2.73	3.40	2.56
7	Ommernborn	6	218	n.d.	5.15	7.34	6.47	7.91	8.83	10.46
8	Bechen	6	201	4.32	9.26	5.01	9.05	12.42	7.25	9.96
9	Steinbuechel	5	386	n.d.	17.16	11.69	12.89	11.69	12.13	12.98
10	Cologne-Langel	2	227	n.d.	8.80	5.27	5.28	4.38	6.21	4.96
11	Stommeler Busch	7	345	4.46	11.05	6.41	4.03	4.39	5.12	3.88
12	Sinsteden	1	1304	n.d.	48.08	22.26	15.38	13.32	15.33	10.80
13	Jackerath	4	240	7.21	11.32	4.38	9.71	17.93	7.04	9.52
14	Bedburg	1	439	9.54	34.89	15.57	16.61	16.56	11.84	13.36
15	Rheidt	1	1220	n.d.	44.79	29.50	19.03	16.36	20.44	15.92
16	Cologne-Auweiler	5	447	n.d.	18.54	10.74	16.18	17.26	13.53	14.78
17	Cologne-Flittard	2	249	7.22	9.70	6.87	6.70	8.53	8.09	7.18
18	Bergisch-Gladbach	6	153	2.28	6.20	5.24	5.71	4.46	5.30	5.28
19	Ebbinghausen	6	1730	23.28	91.77	76.74	23.53	15.82	21.15	9.51
20	Linde	6	59	n.d.	1.10	11.84	2.07	2.26	2.03	1.91
21	Untereschbach	6	140	7.86	3.95	7.79	13.42	15.15	8.26	11.55
22	Cologne-Merheim	5	559	18.65	12.83	21.47	12.96	11.06	23.44	11.40
23	Cologne city	5	429	12.33	13.28	16.08	14.36	12.33	18.46	11.94
24	Brauweiler	7	237	n.d.	7.82	5.52	8.98	7.68	9.79	8.49
25	Bergheim	4	289	n.d.	7.29	7.40	5.92	5.84	7.06	6.05
26	Bettenhoven	4	136	5.00	3.37	4.13	4.36	4.86	5.11	4.78
27	Etzweiler	4	294	5.88	12.64	8.65	8.97	10.60	10.34	8.86
28	Horrem	4	427	13.88	20.99	13.28	25.19	41.63	15.69	28.16
29	Efferen	1	371	8.95	9.80	8.97	7.62	8.04	11.04	8.02
30	Cologne-Poll	5	420	8.97	11.38	15.95	12.67	11.29	17.88	12.56
31	Cologne-Koenigsforst	6	40	0.62	0.99	1.08	1.54	1.09	1.52	1.21
32	Stoecken	6	158	n.d.	5.10	4.18	4.06	3.83	5.77	5.00
33	Seelscheid	6	233	6.70	6.18	6.30	3.28	3.19	4.48	2.87
34	Muchensiefen	6	205	n.d.	3.80	8.22	8.73	12.75	8.59	10.03
35	Cologne-Zuendorf	3	486	14.06	20.44	12.74	27.24	39.02	17.06	27.56
36	Huerth	1	472	10.54	20.05	11.46	8.86	7.89	9.95	7.14
37	Tuernich	4	170	3.65	4.67	6.50	8.02	8.65	8.47	8.36
38	Blatzweiler	7	533	12.11	19.62	14.19	7.04	6.46	9.86	6.27
39	Ellen	7	81	3.16	2.54	1.94	1.78	1.96	2.04	1.86
40	Girbelsrath	7	182	n.d.	5.38	3.91	4.28	3.28	4.82	3.66
41	Pingsheim	7	196	n.d.	8.30	3.74	5.92	6.50	5.79	7.20
42	Erfstadt	4	315	n.d.	11.60	7.07	9.82	10.89	9.19	8.80
43	Cologne-Wesseling	2	370	10.35	19.51	10.20	13.96	13.53	9.91	12.22
44	Spich	3	224	6.01	6.74	8.31	8.11	5.52	8.45	5.74
45	Birk	6	68	1.61	2.45	1.78	3.66	3.84	4.52	3.94
46	Altenboedingen	6	133	5.15	5.33	3.43	3.56	4.08	3.16	3.26
47	Niederpleis	3	192	3.60	6.54	7.18	9.49	9.18	8.99	8.72
48	Mondorf	5	105	n.d.	1.83	3.77	4.82	4.68	4.81	4.19
49	Merten	6	209	5.93	9.13	6.25	9.34	10.17	7.00	7.71
50	Ahrem	7	291	n.d.	9.78	5.62	4.40	4.37	4.22	4.19
51	Gladbach	7	213	6.23	8.50	5.45	3.51	2.33	4.37	3.98
52	Dueren	5	98	n.d.	2.80	2.44	2.33	2.52	2.67	1.65
53	Soller	7	68	n.d.	2.49	1.65	1.77	1.91	3.02	2.44
54	Haus Boulich	7	195	2.13	11.37	5.48	5.40	5.80	5.66	5.21
55	Metternich	6	310	n.d.	10.62	10.29	14.39	27.52	10.06	17.28
56	Alfter	6	244	n.d.	13.57	6.52	8.27	8.58	4.60	5.35
57	Bonn	5	277	12.13	13.89	17.36	8.74	7.90	10.75	8.41
58	Uthweiler	7	296	4.68	9.78	7.84	14.03	17.73	10.81	13.17
59	Rostingen	7	152	4.12	9.09	5.35	6.09	9.65	4.18	5.36
60	Koenigswinter	6	77	n.d.	1.63	2.97	2.38	2.00	3.85	2.05
61	Roettgen	5	438	n.d.	17.67	13.76	6.84	4.79	10.54	5.39
62	Miel	7	248	n.d.	8.36	7.69	6.32	7.68	5.95	5.22
63	Erlenhof	5	411	n.d.	9.17	11.48	13.98	16.06	13.75	13.04
64	Fuessenich	7	167	5.62	8.44	5.69	4.68	5.05	3.89	4.63
65	Nideggen	6	105	n.d.	3.26	1.89	1.97	1.49	1.75	1.81
66	Buervenich	7	188	n.d.	6.30	4.14	6.96	15.47	6.62	9.41
67	Obergartzem	7	276	5.83	10.84	9.83	14.94	18.04	9.10	13.28
68	Kuchenheim	5	262	n.d.	6.28	6.18	5.42	5.80	6.00	4.89
69	Lueftelberg	6	417	n.d.	10.97	11.90	12.00	13.66	11.23	11.60
70	Pech	6	245	n.d.	9.78	6.51	5.14	4.71	6.57	4.12
71	Bad Honnef	6	235	n.d.	5.97	6.36	3.94	3.77	5.83	3.86

Table 50: Alkylated and parent three-ring PAH in *Pinus nigra* needles of the Cologne Conurbation in ng g⁻¹ dry weight, I; n.d. = not detectable; emission scenarios (em.sc.) : (1) lignite fueled power plant, (2,3) industry, (4) lignite open pit mining, (5) urban, (6) forest, (7) agriculture; ID according to Fig. 62.

ID	2,6-DMP	2,7-DMP	x4-DMP	2,9+1,6-DMP	1,7-DMP	1,8-DMP	Σ DMP+EP	retene
1	3.01	1.72	9.65	5.03	4.40	0.47	35.29	6.08
2	2.41	1.61	6.18	3.33	5.56	0.86	32.02	8.63
3	6.17	5.47	18.30	7.89	12.08	1.25	70.96	7.14
4	0.73	0.53	2.46	1.06	1.38	0.23	11.48	2.34
5	1.67	1.35	6.69	3.10	2.23	0.63	27.49	3.59
6	0.20	0.15	1.12	0.45	0.60	0.11	7.33	0.62
7	0.38	0.49	2.63	1.09	4.09	0.28	17.74	12.12
8	1.15	0.35	4.75	2.20	2.88	0.50	19.25	4.24
9	1.41	0.98	5.14	2.61	2.57	0.62	22.64	4.85
10	0.65	0.47	3.56	1.40	1.42	0.24	12.75	1.66
11	0.74	0.58	1.99	1.03	1.57	0.41	9.55	2.71
12	1.41	0.96	4.54	2.01	2.50	0.58	22.58	3.04
13	1.28	1.27	4.02	2.19	4.09	0.45	25.32	6.87
14	1.68	0.79	5.94	2.82	3.25	0.54	22.72	3.20
15	1.68	1.03	4.95	2.33	2.86	0.43	22.45	3.04
16	0.67	0.83	6.17	1.30	2.74	0.47	25.18	3.40
17	1.38	1.11	4.91	2.24	2.62	0.53	19.75	3.56
18	0.51	0.37	2.51	1.01	0.93	0.13	9.06	1.31
19	1.20	0.75	3.66	1.47	2.05	0.41	14.49	2.15
20	1.50	1.16	4.53	2.67	3.37	0.97	20.35	1.84
21	2.61	1.58	6.81	3.90	5.42	0.66	33.01	7.68
22	2.43	1.60	9.33	4.03	4.99	1.10	36.54	4.50
23	1.96	1.42	7.80	3.53	4.40	0.73	28.79	4.16
24	1.26	0.82	4.83	1.67	2.01	0.32	20.51	2.90
25	1.12	0.74	2.91	1.86	2.66	0.56	15.02	2.59
26	1.02	0.87	2.85	1.65	2.62	0.53	16.31	4.73
27	1.70	1.29	5.27	2.63	3.77	0.61	22.21	3.59
28	6.68	4.21	13.21	7.76	16.69	2.32	71.70	16.78
29	1.63	1.18	5.92	2.46	3.59	0.58	23.54	3.65
30	2.00	1.66	8.03	3.72	3.93	0.92	35.26	4.70
31	0.18	0.14	0.60	0.26	0.32	0.04	2.77	0.33
32	0.75	0.52	2.97	1.34	1.83	0.43	14.27	2.13
33	0.44		1.61	0.58	1.03	0.18	9.56	2.30
34	2.50	2.02	8.10	4.69	7.73	1.52	38.13	10.66
35	4.42	4.26	13.67	7.90	11.24	1.78	63.10	11.35
36	0.97	0.78	4.47	1.68	1.76	0.52	16.63	2.95
37	1.42	1.13	5.22	2.97	4.19	0.70	21.62	6.19
38	0.90	0.49	3.58	1.38	1.51	0.24	15.20	2.04
39	0.14	0.16	1.04	0.56	0.97	0.07	6.34	1.68
40	0.34	0.25	2.21	0.85	0.82	0.18	10.18	1.31
41	0.74	0.45	3.19	1.61	1.90	0.40	14.49	1.94
42	1.12	0.71	4.17	2.01	2.41	0.32	18.15	4.39
43	1.40	0.76	5.98	2.68	2.02	0.36	19.88	3.00
44	0.76	0.39	3.80	1.29	1.22	0.24	12.84	1.90
45	0.54	0.27	2.98	1.50	1.45	0.36	10.72	1.17
46	1.28	0.39	1.79	1.04	2.09	0.40	10.57	5.03
47	1.10	0.86	4.05	1.79	2.24	0.35	16.52	5.21
48	1.35	0.81	4.26	2.04	2.34	0.36	16.71	2.98
49	1.00	0.68	3.58	1.92	2.48	0.43	13.71	6.35
50	0.68	0.61	2.00	1.18	1.69	0.26	10.25	2.83
51	0.13	0.03	1.29	0.62	0.54	0.13	6.33	0.90
52	0.76	0.67	3.32	1.76	2.04	0.44	14.23	1.67
53	0.60	0.51	2.83	1.55	1.30	0.30	11.21	0.82
54	0.72	0.53	2.57	1.39	1.62	0.33	10.67	1.63
55	2.63	2.22	5.90	3.57	7.39	1.15	35.08	12.03
56	0.99	0.91	2.32	1.30	1.91	0.29	11.85	2.43
57	1.19	0.87	5.48	2.10	2.17	0.42	18.37	2.95
58	3.54	1.92	8.72	4.31	6.93	1.37	39.18	12.05
59	0.87	0.68	2.01	1.15	2.18	0.35	9.18	3.18
60	0.37	0.22	1.56	0.60	0.61	0.12	4.89	0.87
61	0.79	0.57	3.28	1.22	1.55	0.21	13.09	1.90
62	1.36	1.15	3.28	1.81	3.03	0.50	17.26	3.68
63	2.37	1.35	7.24	3.33	4.35	0.90	33.14	5.61
64	0.49	0.37	1.88	1.14	1.70	0.28	7.68	0.88
65	1.01	0.85	3.06	1.73	2.15	0.55	13.78	1.34
66	1.51	1.20	4.19	2.30	4.78	0.63	22.30	5.65
67	2.35	1.62	6.56	3.08	5.28	0.86	29.99	8.87
68	3.42	2.81	9.50	4.56	5.79	0.77	38.75	2.60
69	1.78	1.61	6.17	3.09	4.85	0.92	28.16	6.81
70	0.54	0.39	1.88	0.89	1.05	0.20	7.97	1.61
71	0.28	0.19	1.81	0.32	1.28	0.23	8.58	1.78

Table 51: Alkylated and parent three-ring PAH in *Pinus nigra* needles of the Cologne Conurbation in ng g⁻¹ dry weight, II; n.d. = not detectable; emission scenarios (em.sc.) : (1) lignite fueled power plant, (2,3) industry, (4) lignite open pit mining, (5) urban, (6) forest, (7) agriculture; ID according to Fig. 62.

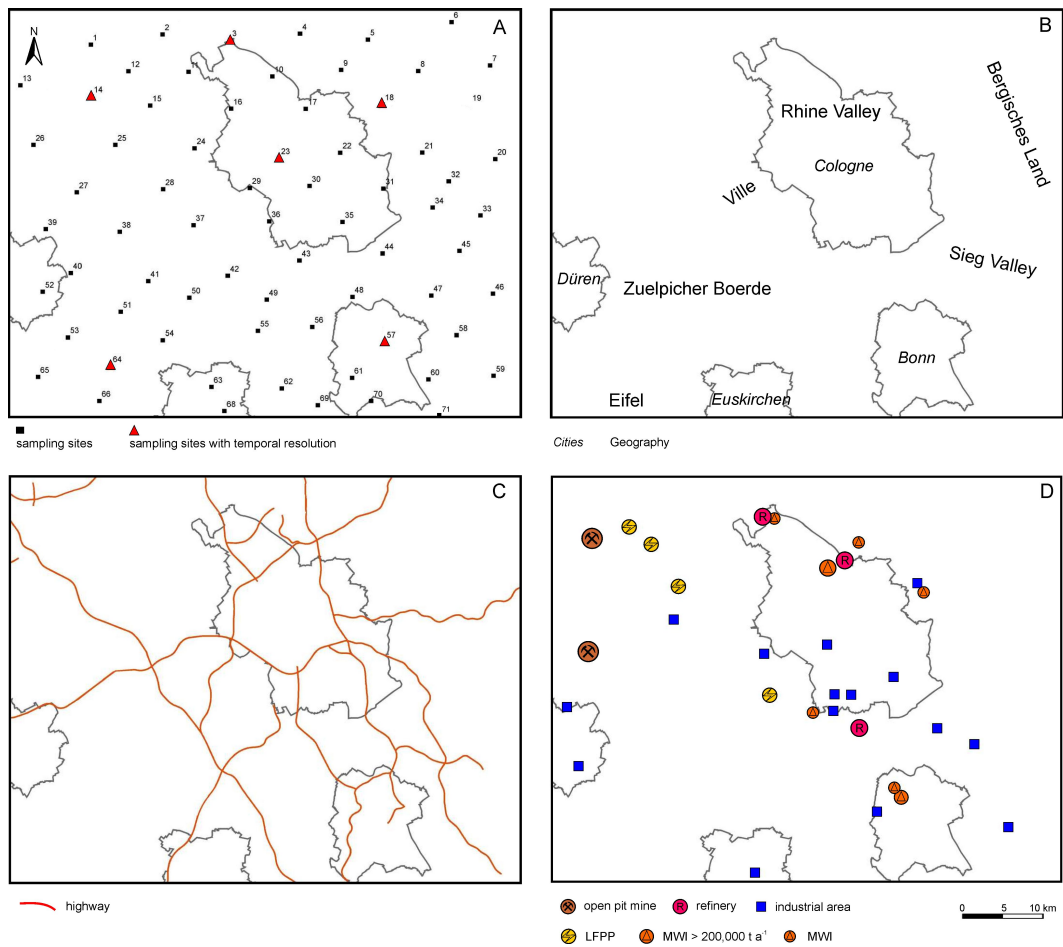


Figure 62: a) sampling locations of regional-scale biomonitoring, temporally resolved sites are given in red, b) cities and local designations in the Cologne Conurbation, c) highways, d) most significant emitters in the Cologne Conurbation according to the NRW Emission Register [118], figure available as overlay transparency inside the back.

Erklärung

Ich versichere, dass ich die von mir vorgelegte Dissertation selbstständig angefertigt, die benutzten Quellen und Hilfsmittel vollständig angegeben und die Stellen der Arbeit - einschliesslich Tabellen, Karten und Abbildungen -, die anderen Werken im Wortlaut oder dem Sinn nach entnommen sind, in jedem Einzelfall als Entlehnung kenntlich gemacht habe; dass diese Dissertation noch keiner anderen Fakultät oder Universität zur Prüfung vorgelegen hat; dass sie - abgesehen von unten angegebenen Teilpublikationen - noch nicht veröffentlicht worden ist sowie, dass ich eine solche Veröffentlichung vor Abschluss des Promotionsverfahrens nicht vornehmen werde. Die Bestimmungen der Promotionsordnung sind mir bekannt. Die von mir vorgelegte Dissertation ist von Prof. Dr. L. Schwark betreut worden.

Publications in peer-reviewed journals

M. Urbat and E. Lehndorff and L. Schwark, 2004. Biomonitoring of air quality in the Cologne Conurbation using pine needles as a passive sampler - Part I: magnetic properties. *Atmospheric Environment* 38, 3781-3792.

E. Lehndorff and L. Schwark, 2004. Biomonitoring of air quality in the Cologne Conurbation using pine needles as a passive sampler - Part II: polycyclic aromatic hydrocarbons (PAH). *Atmospheric Environment* 38, 3793-3808.

E. Lehndorff and M. Urbat and L. Schwark, 2006. Accumulation histories of magnetic particles on pine needles as function of air quality. *Atmospheric Environment* 40, 7082-7096.

E. Lehndorff and L. Schwark, 2008. Accumulation histories of major and trace elements on pine needles in the Cologne Conurbation as function of air quality. *Atmospheric Environment* 42, 833-845.

E. Lehndorff and L. Schwark, 2008. Accumulation behavior of airborne parent and alkyl three-ring PAH on pine needles. *Atmospheric Environment*, in review.

Lebenslauf

Angaben zur Person

Name Eva Lehndorff
Adresse Wahlenstr. 9
50823 Köln
Staatsangehörigkeit deutsch
Geburtsdatum 22 .11.1976

Studium und Schulbildung

seit 01 / 2004 **Promotionsstudium** am Institut für Geologie
und Mineralogie der Universität zu Köln
Thema: *Air quality in the Cologne Conurbation –
high-resolution spatiotemporal biomonitoring*
05 / 2003 **Diplom** in Geologie, Universität zu Köln
Thema: *Verteilungsmuster luftgetragener
Schadstoffe im Ballungsgebiet Köln*
Gesamtnote: sehr gut
10 / 1996 Studium der Geologie/Paläontologie,
Universität zu Köln
1996 **Abitur**, Dreikönigsgymnasium Köln
1987 – 1996 Gymnasium, Konstanz / Köln
1983 – 1987 Grundschule, Konstanz

Beruflicher Werdegang

seit 06 / 2007 Mutterschutz und Elternzeit
06 / 2003 – 04 / 2007 **Wissenschaftliche Mitarbeiterin** am Institut
für Geologie und Mineralogie der Universität zu Köln
09 / 2004 – 12 / 2006 **Vertretung von PD Dr. L. Schwark**,
Institut für Geologie und Mineralogie der
Universität zu Köln
03 / 2002 Praktikum in der Gerling Consulting Gruppe,
Abteilung "Liability Risk Service"
10 / 1999 – 05 / 2003 Studentische Hilfskraft am Institut für Geologie
und Mineralogie der Universität zu Köln
Betreuung und Wartung von Analysengeräten,
Nasschemie
05 – 06 / 1996 Praktikum bei Dipl. Geol. P. Fülling, Wuppertal
Gutachter

Köln, den 01.04.2008

